STATIC STRUCTURAL SYSTEM IDENTIFICATION USING OBSERVABILITY METHOD

By

Jun LEI

A Doctoral Thesis Submitted to

DEPARTMENT OF CIVIL ENGINEERING
TONGJI UNIVERSITY

and

DEPARTAMENT D'ENGINYERIA CIVIL I AMBIENTAL
UNIVERSITAT POLITÈCNICA DE CATALUNYA

Supervisors:

Prof. Dong XU (Tongji University)

Prof. José Turmo Coderque (Universitat Politècnica de Catalunya)

Shanghai

June 2018

UNIVERSITAT POLITÈCNICA
DE CATALUNYA
BARCELONATECH

Static structural system identification using observability method

by
Jun LEI

Doctoral
Thesis

JUN
LEI

STATIC STRUCTURAL SYSTEM IDENTIFICATION USING OBSERVABILITY METHOD

June
2018

Abstract

During the construction and operation stages of many civil structures and infrastructures, various factors lead to irreversible degradation that could affect the normal use and the public safety of these structures. In recent years, it has been common in civil engineering to carry out condition assessment of existing structures using Structural System Identification (SSI) methods. These methods provide the decision-making basis for the follow-up treatment measures (repair, rehabilitation, demolition).

SSI is essentially the application of parameter estimation in structural system. Prior to the estimation, one key issue is to guarantee the observability of the parameters to be estimated. This was already addressed by the SSI by original Observability Method (OM) using static tests. However, a systematic analysis of the effect of measurement and simulation errors for this method is lacking. A ramification of this analysis is the effective strategies to use redundant measurements to tackle measurement errors. Meanwhile, the linearization of unknowns in the SSI by original OM might lead to the omission of potentially observable unknowns.

This PhD thesis presents a unified SSI method under the framework of OM for 2D structures modelled by beam elements with loads in the plane. Extensive research has focused on the dynamic SSI methods and much less attention has been paid to the static case. The proposed method is based on the static information (external loads, measured deflections and rotations) obtained during non-destructive static tests. With this aim, this work gathers six methodological contributions conceived to (1) extract as much information as possible from measurements to ensure the observability of target parameters in SSI; (2) analyze the effect of measurement errors and simulation errors on the estimation results; (3) propose different strategies to use redundant measurements to alleviate the adverse effect of measurement errors regarding the accuracy of the SSI results.; (4) place the sensors in an optimal configuration so that robust estimations are obtained for the target parameters.

Firstly, the basic procedure of the SSI by original OM is presented and validated by error-free measurement data in a beam-like structure. Then the effects of measurement errors and simulation errors on the accuracy of estimation result is analyzed for the minimum measurement sets that ensure the observability of all parameters. The studied factors include single measurement errors, random measurement errors, error levels and loading cases. The influence of the recursive process of SSI by OM is also discussed. In order to solve the problem of misjudging the minimum measurement sets caused by the linearization of the unknowns in the SSI by original OM, the SSI by constrained OM is proposed. The nonlinear constraints are reintroduced by optimizations after the completion of the original method when necessary. The method is validated by the examples of a simply supported beam and a high-rise frame.

As demonstrated by the unsatisfactory SSI results from the SSI by OM using minimum measurement sets, the necessity of using redundant measurements is emphasized. Three ways of using redundant measurements are proposed. The SSI by compatible OM derives the compatibility conditions in beam-like structures. The incompatibility in the displacements due to measurement errors are reduced by imposing these conditions. In the second method, the theoretical advantage of using rotations in SSI is justified by a statistical analysis based on the analytical expression of the target parameters together with the inverse distribution theory. Then four strategies to use redundant rotation measurements are proposed and compared. The model averaging method using only rotations is proposed. As the SSI by compatible OM and the model averaging method are subjected to the limit of structure type or measurement type, the SSI by Measurement Error-Minimizing Observability Method (MEMOM) is proposed. In this method, the measurement error terms are separated from the coefficient matrix of the observability equations and the final estimations are obtained by minimizing the square sum of the ratios between the error terms and the measurements using optimization technique. The performance of the method is investigated in detail with respect to factors including loading cases, parameterization of FEM, measurement types and constraint types. The Optimal Sensor Placement (OSP) problem for static SSI is also addressed in this thesis. The OSP problem is formulated as maximizing the determinant of the Fisher Information Matrix (FIM) using genetic algorithm. Meanwhile, the identifiability of the structural parameters is evaluated according to the diagonal elements of the inversed FIM.

Resumen de la Tesis

Durante las etapas de construcción y operación de muchas estructuras e infraestructuras civiles, se puede producir una degradación de las mismas debido a diversos factores. Esto puede afectar a su uso normal y a la seguridad pública. En los últimos años, la evaluación de las condiciones de las estructuras existentes utilizando los métodos de Identificación de Sistemas Estructurales (SSI, por sus siglas en inglés) se ha convertido en un tema candente en la ingeniería civil. Estos métodos proporcionan la base de la toma de decisiones de mantenimiento (reparación, rehabilitación, demolición).

La SSI es esencialmente la aplicación de la estimación de parámetros en un sistema estructural. Antes de esta estimación, sin embargo, una cuestión clave es garantizar si, dado un conjunto de medidas, unos determinados parámetros se podrán estimar. Esto ya fue abordado por el SSI mediante el Método de Observabilidad (MA) usando ensayos estáticos. Sin embargo, aún falta un análisis sistemático del efecto de los errores de medición y simulación para este método. Además, no hay estrategias efectivas para usar mediciones redundantes para disminuir los efectos de los errores de medición en las estimaciones. Mientras tanto, la linearización de incógnitas que se usaba en el SSI por OM original podría conducir a la omisión de incógnitas observables.

Esta tesis doctoral presenta un método SSI unificado en el marco de OM para las estructuras 2D modeladas por elementos tipo viga con cargas contenidas en el plano. Una amplia investigación se ha centrado en los métodos dinámicos de SSI y se ha prestado mucha menos atención al caso estático. Este método se basa en la información estática (cargas externas y desplazamientos medidos) obtenida durante ensayos estáticos no destructivos. Con este objetivo, este trabajo reúne seis contribuciones metodológicas concebidas para (1) extraer tanta información como sea posible de las mediciones para garantizar la observabilidad de los parámetros objetivo en SSI; (2) analizar el efecto de errores de medición; (3) proponer estrategias diferentes para usar mediciones redundantes para aliviar el efecto adverso de los errores de medición con respecto a la precisión de los resultados de SSI; (4) ubicación de los sensores en una configuración óptima para que se obtengan estimaciones robustas para los parámetros objetivo.

En primer lugar, el procedimiento básico del SSI por OM original se presenta y valida con datos de medición sin errores en una estructura tipo viga. A continuación, se analizan los efectos de los errores de medición y simulación sobre la precisión del resultado de la estimación para los conjuntos mínimos de medición que garantizan la observabilidad de todos los parámetros. Los factores estudiados incluyen errores de medición únicos, errores de medición aleatorios, distintos niveles de error y distintos casos de carga. También se discute la influencia del proceso recursivo de SSI por OM. Con el fin de resolver el efecto de la linearización de las incógnitas en el SSI por OM original, se propone el SSI por OM restringido. Las restricciones no lineales son

reintroducidas como requisitos que ha de satisfacer la solución, pasando la resolución del problema a ser un proceso de optimización. El método está validado con ejemplos de vigas y de un pórtico de gran altura.

El uso de conjuntos mínimos de medidas con errores conduce a resultados poco satisfactorios. Se impone el uso de conjuntos de medidas redundantes. Las formas de minimizar el error en la estimación usando medidas redundantes se estudian en tres apartados. 1) El SSI por OM compatible deriva la expresión matemática de las condiciones de compatibilidad de los distintos desplazamientos de los nodos en estructuras tipo viga. La incompatibilidad en los desplazamientos debidos a errores de medición se reduce al imponer estas condiciones. 2) La ventaja teórica de usar rotaciones en SSI se justifica mediante un análisis estadístico basado en la expresión analítica de los parámetros objetivo junto con la teoría de distribución inversa. Luego, se proponen y comparan cuatro estrategias para usar mediciones de rotación redundantes. Se propone el método de promediado del modelo estimado utilizando solo rotaciones. 3) Como el SSI por OM compatible y el método de promediado del modelo están sujetos al límite de tipo de estructura o tipo de medida, se propone el SSI mediante el Método de Observación de Minimización de Errores de Medición (MEMOM). En este método, los términos de error de medición se separan de la matriz de coeficientes de las ecuaciones de observabilidad y las estimaciones finales se obtienen minimizando la suma cuadrada de las relaciones entre los términos de error y las mediciones utilizando la técnica de optimización. El rendimiento de los distintos métodos se investiga en detalle con respecto a factores que incluyen casos de carga, parametrización de FEM, tipos de medición y tipos de restricciones. El problema de ubicación óptima del sensor (OSP) para SSI estático también se aborda en esta tesis. El problema OSP está formulado para maximizar el determinante de la Matriz de Información de Fisher (FIM) usando un algoritmo genético. La identificabilidad de los parámetros estructurales se evalúa de acuerdo con los elementos diagonales de la FIM inversa.

Acknowledgement

First of all, I want to express my most sincere gratitude to my supervisors, Prof. Dong XU and Prof. Jose Turmo, for their support, advice and encouragement during my PhD study. Without their great help, the completion of this thesis would not have been possible. They have always been role models for me not only in the field of research but also in daily life. They are really hard-working people with rigorous attitude towards research. They have spent so much time in enlightening me, revising and improving my work, and training me to present my work in a better way. It is truly a very pleasant experience to work with them during my PhD stage.

I am honored to have spent my undergraduate and most of my doctorate in Tongji University. Specially, I have to express my thanks to Prof. Chao LIU, Dr. Yu ZHAO, Dr. Fangyuan XU, Dr. Yingsheng NI, Dr. Yu ZHANG, Wei Wang, Lijun SUN, Tong ZHOU and all my colleagues in the division of Concrete Bridges for their warm companionship and selfless help.

I spent two years in Universitat Politècnica de Catalunya (UPC), Barcelona, as an academic exchange student in my secondary institute. It is a great honor to work with all the professors and members in the construction engineering group of Universitat Politècnica de Catalunya. I want to thank Prof. Gonzalo Ramos for those on-going engineering project visits, Prof. Joan Ramon Casas and Prof. Michel Ghosn for their precious comments during those seminars. Meanwhile, I want to thank Prof. Lozano Galant and Prof. Maria Nogal for all the discussions and suggestions that give me new ideas on my work. Thanks to my colleagues and friends in UPC, Daniel Tomas, Ahmed Elkherbawy, Seyyed Behrad Emadi, Behnam Mobaraki, Irene Josa. Also, to my roommates in Barcelona, Han Yang, Yuyang Wang, Langjing Shi. I appreciate their companionship, which makes my life in Spain more colorful.

Thanks to my girlfriend Yanrong for your support and unwavering belief in me when I am trying to get my PhD

Specially, I want to thank my beloved family for their unselfish and unreserved love during all these years.

This work is funded by the Ministerio de Economia y Competitividad (MINECO) and the FEDER fund through the grant project (BIA2013-47290-R) directed by Jose Turmo. Also, funding has been provided to the author by MINECO through the FPI grant (BES-2014-07022).

Content

List of Tables

List of Figures

1. Introduction

1.1 Motivation

The expected service life of civil structures is normally more than 50 years. During the construction and operation stages, due to the steel corrosion, the carbonation, the cracking, the spalling or the freeze-thaw cycle of concrete, overloading and many other factors (Figure 1-1), these structures suffer from irreversible degradation and may not behave as anticipated regarding their serviceability and safety.

Figure 1-1 Common causes of the degradation of structural behavior

For instance, bridges are important components of transportation networks connecting different regions in the transportation system. The occurrence of interruption of the normal operation or even the collapse of bridges might pose serious threat on the regional economy or even public safety. Given the fact that modern bridges have larger spans and are more often crossing over rivers or even seas than those in old times, the consequence of potential bridge failure is even more unacceptable.

Considering the undesirable consequence of the malfunction of structures, it is of primary importance to assess the current condition of these structures. Subsequently, the result of the condition assessment can serve as the decision-making basis for follow-up treatments (repair, retrofit or demolition). Regarding the means of condition

assessment, Structural System Identification (SSI) has become one of the most popular methods. The process of SSI can be presented as the sequence of the preparation of a well-designed test, the collection of experimental data (external excitations and structural response), the data preprocessing, the estimation of the target parameters featuring the structural system. In this process, the estimation of the target parameters is the most important one.

1.2 Classification of SSI methods

Regarding the SSI, the main methods presented in the literature are reviewed and classified.

1.2.1 Intrinsic property of the external excitation

Based on the intrinsic property of the external excitation, the SSI methods can be categorized as dynamic methods and static methods.

(1) Dynamic SSI methods

According to the source of external excitation, dynamic SSI methods are composed of forced (artificial) vibration and ambient vibration. In the former case, the external excitation on the structural can be measured and hence is controllable. The ambient vibration is induced by operation loads such as traffic or wind. The external excitation is unknown and is commonly assumed to satisfy certain statistical property (Brincker & Ventura, 2015). The benefit of SSI methods using ambient vibration is the avoidance of interruption of the operation of structures.

A main classification criterion for the dynamic methods is the data domain where the measurement data is processed. These domains include the time domain and the frequency-domain. The time-domain based methods try to minimize the errors between the simulated and measured responses (time history), including the extended Kalman filter (X. Liu, Escamilla-Ambrosio, & Lieven, 2009), the unscented Kalman filter (Mariani & Ghisi, 2007), the particle filter (Yan, 2014), and the least square estimation (J N Yang, Pan, & Lin, 2007). The frequency-domain methods extract the modal parameters (frequencies, modal shapes and damping) of the structure by analyzing the frequency response function or transfer function. This type of method has a long history and is well developed. With the acquired modal parameters, some methods locate damage by detecting the abnormality in the variation of some dynamic signatures (e.g. frequencies, modal shapes, modal curvatures, frequency response functions). Alternatively, other methods adopt iterative or optimization-based approaches to update the physical parameters (mass, stiffness or damping) of a selected model so that the modal parameters given by this model match those obtained from the experimental modal analysis.

Despite the wide investigations on the dynamic methods, there exist some problems: (1) Many factors affect the dynamic response of structures, including the stiffness, the mass and the damping. However, it is common to assume that no damping exists in the structure and the damage of the structure does not lead to the loss of mass. These assumptions might introduce systematic errors in the SSI (Papadopoulos & Garcia, 1998; X. Wang, Hu, Fukunaga, & Yao, 2001); (2) For stiff structures, it is difficult to obtain clear and accurate modes; (3) In real applications, high accuracy can be achieved for natural frequencies. However, the natural frequencies are not sensitive to the damage of structures (Farrar et al., 1994; Kim, Ryu, Cho, & Stubbs, 2003). The mode shapes, especially those of high orders, are sensitive indicators for structural damage. But mode shapes are hard to measure accurately. (4) The amplitude of the vibration of large structures is not significant, which imposes a basic requirement on the SSI methods to be insensitive to measurement errors.

(2) Static SSI methods

Extensive research on the dynamic SSI methods has been carried out. On the contrary, much less attention was paid to the static SSI methods. In fact, static tests are widely used in civil engineering. Before the opening of new structures or in the proof load test of existing structures, it is common to apply static loads on the structure within the serviceability limit state. In October 2013, a new bridge in Grevenmacher, Germany, was statically loaded by six trucks to verify its structural performance prior to its opening (Nguyen, Schommer, Maas, & Zürbes, 2016). In the full-scale static tests of two prestressed concrete bridges in Florida, the structure was tested to the ultimate live load (Issa & Shahawy, 1993). After twenty three years' operation, a static test was conducted on the Antonio Dovali Jaime cable-stayed bridge in Mexico (Ortiz et al., 2008). No residual deformation of the structure was detected. In the static test of a concrete arch bridge built in the mid-to-late 19th century, two DE24000 diesel locomotives were used to load the structure (Caglayan, Ozakgul, & Tezer, 2012). The load rating results showed that the structure was safe. (Marefat, Ghahremani-Gargary, & Ataei, 2004) used a combination of dynamic load tests and static load tests to assess the condition of a 20m+20m concrete arch. In the static load test, a total weight of 7280 kN was used.

For the static SSI methods, different researchers have done the following work. (Sheena, Unger, & Zalmanovich, 1982) proposed an analytical minimization method based on the deflection of structures under concentrated loads. The theoretical stiffness matrix was established by the Finite Element Model (FEM), and was corrected by the measured deflection. When all the equilibrium equations were satisfied, the structural parameters were estimated by minimizing the difference between the theoretical and the estimated stiffness matrices.

(Masoud Sanayei, 1986) proposed a static parameter identification method using

incomplete measurement data. The geometrical parameters (areas and inertias) were identified by measuring the load and the displacements on some DOFs of the structure. The method was successfully applied on planar truss and frames. The effect of measurement errors was also investigated.

(Hajela & Soeiro, 1990b, 1990a) classified the SSI methods into three categories: (1) equation error; (2) output error; and (3) minimum deviation method. They combined static and modal responses to evaluate the stiffness changes of all elements in the model. For models of many parameters, they proposed substructure methods and techniques for reducing the order of models.

(Banan, Banan, & Hjelmstad, 1994a, 1994b) used an iterative algorithm to solve the least squares problem formulated in the static SSI. The objective function to be minimized was the square sum of the displacement errors and the square sum of the load errors, respectively. In the parameter estimation process, the parameter grouping technique was adopted, and the influence of the initial values for the optimization was studied.

On the basis of Banan's work, (Hjelmstad & Shin, 1997) assumed that the reference values of the structural parameters were known and proposed an adaptive parameter grouping algorithm that used static measurement data to detect and evaluate structural damage. Two indices for describing the bias of estimations were proposed. A criterion to detect the existence of damage was developed based on these indices.

(P. Liu & Chian, 1997) used the static strains to identify the geometrical properties of truss members. He deduced the equilibrium equations of the trusses using the FEM and converted the parameter identification problem into an optimization problem. The objective function to be minimized was the residues of the equilibrium equations. He pointed out that if the axial force of a truss member was always zero in all loading cases, it would be very difficult to identify the axial stiffness of the member accurately. This method can give the global minimum unique solution when the measured data is sufficient and the loading cases can fully excite the mechanical behavior of the structure.

(Abdo, 2012) carried out a parametric study on the relation between the change in displacement curvature and the location of the damage as well as the severity of the damage. The studied structure included a cantilever beam and a continuous beam. The results showed that structural curvature was an effective indicator of structural damage. However, this method cannot determine the extent of damage, and the response of the intact structure is required.

(Brian J. Walsh & González, 2009) proposed a parameter estimation method using cross-entropy to estimate the bending stiffness of a simply supported beam subjected to static loads. This method used the deflections of the structure to estimate the flexural stiffness of the structure under vehicle loads. When analyzing the severity of the damage and the location of the damage, the studied factors include the assumed

distribution of stiffness parameters, the number of measurement points, and the number of samples.

(R. S. He & Hwang, 2006) used the combination of the natural frequencies and the static displacements as the indices to represent the dynamic and static behavior of the structure. The structural parameters were obtained by minimizing these indices predicted by the given model and those obtained from test data. The optimization problem was solved by an adaptive real-coded genetic algorithm with the simulated annealing algorithm. The method was validated by beam-like structures of different boundary conditions and damage scenarios. The results showed that the accuracy of the estimation result with error-free measurements was high while the accuracy of the estimation result in the presence of measurement errors was acceptable.

There are two main problems in static SSI methods: (1) In the case of static SSI, fewer data are available than the data in the case of dynamic SSI. Consequently, it is more difficult to obtain ideal SSI results (Chen et al. 2005); (2) Damage to the structure might be concealed by the load path. If the loading cases do not excite the structural behavior of the damaged part, the damaged part can hardly be identified.

The advantages of the static SSI methods are: (1) The establishment of the equilibrium equations in the static SSI is only related to the stiffness parameters while the formulation of the mathematical equations in dynamic SSI is also involved with the mass and the damping information. Hence, the static SSI methods are much simpler than those dynamic SSI methods; (2) The available measurement devices can obtain accurate static responses of the structure cheaply and quickly. The sensors for the static SSI are cheaper and have higher accuracy than those for the dynamic SSI (Andreaus, Baragatti, Casini, & Iacoviello, 2017; Kourehli, 2017; X. Wang et al., 2001). (3) The static tests provide important information on the deformation (displacement, rotation and strain) of the structure. It is an appropriate alternative and an important supplement to the dynamic tests (Nguyen et al. 2016). Also, compared with the natural frequencies, static response is a more sensitive indicator for damage identification (Jenkins, Kjerengtroen, & Oestensen, 1997). The static response can better reflect the local information of the structure while the dynamic characteristics, especially the natural frequencies, usually reflect the global, distributed information of the structure. (Brownjohn, Fujino, Inaudi, & Wu, 2008) also pointed out that the static methods can be used together with the dynamic methods. The static methods have a more detailed examination of the local response of the structure, while the dynamic method cannot.

Due to these reasons, this thesis will focus on static SSI methods for the purpose of condition assessment.

1.2.2 Parametric and non-parametric methods

According to the mathematical models bridging the structure response and the structural parameters, the SSI methods can be divided into parametric methods (Alves, Cury, Roitman, Magluta, & Cremona, 2015; Au, Ni, Zhang, & Lam, 2012; Y. Chang & Huang, 2014; Doebling, Farrar, Prime, & Shevitz, 1996; Ewins, 1984; P. Liu & Chian, 1997; Masoud Sanayei, 1986; Masoud Sanayei, McClain, Wadia-Fascetti, & Santini, 1999; Masoud Sanayei & Scampoli, 1991; Masound Sanayei, McClain, & Wadia-Fascetti, 1999) and non-parametric methods (American Society of Civil Engineers, 2013; Catbas, Gokce, & Gul, 2012; Lakshmi, Rao, & Gopalakrishnan, 2017; Shahsavari, Chouinard, & Bastien, 2017).

The parametric methods are parameter estimation methods based on models of clear physical meanings. This type of methods is usually based on the FEM of the analyzed structure. The target parameters include modal parameters (Alves et al., 2015; Doebling et al., 1996; Ewins, 1984; Masound Sanayei et al., 1999) or geometrical parameters (Abdo, 2012; American Society of Civil Engineers, 2013; Au et al., 2012; Marefat et al., 2004; Papadopoulos & Garcia, 2001; Masoud Sanayei & Scampoli, 1991). Modal parameter estimation is the most common parameter estimation problem in the field of structural dynamics. In the modal parameter estimation, it is assumed that the dynamic response can be described by the equation of motion (second-order differential equations). This system of equations contains the mass matrix, the damping matrix and the stiffness matrix. The modal parameters of the structure can be estimated from the actual dynamic response using experimental modal analysis.

Geometrical parameter estimation is the process of reconstructing the FEM using the measured response together with optimization techniques. This type of methods uses dynamic or static measurement data to estimate structural parameters at the component level. In the FEM, the structure is discretized into finite number of elements and the parameters of the elements represent the geometrical properties (for instance, areas and inertias) of different regions of the structure. These geometrical parameters provide engineers with intuitive, quantitative and interpretable description of the condition of the structure, which can be easily associated with the extent of structural damage.

The parametric SSI methods have the following advantages: (1) The physical parameters of the structure can be estimated directly, and changes in the condition of the structure can be evaluated from the changes in the physical parameters. The parameters in the parametric methods have a clearer physical meaning and is more interpretable than those in the non-parametric methods; (2) The parameters of the FEM can be updated by the estimated parameters, and the response of the structure under other scenarios can be predicted based on the updated model.

Non-parametric methods are called model-free or data-driven SSI methods (Catbas et al., 2012). In the mathematical model of this type of methods, the input-output relation

of the structural system is linked by a series of equations with no explicit physical meaning and is not related to the mechanical relation of the structural system. Such models include neural network models (Bakhary, Hao, & Deeks, 2007; Catbas et al., 2012; Sahin & Shenoi, 2003), autoregressive moving average (ARMA) models (Lakshmi et al., 2017; Yao & Pakzad, 2012), principal component analysis methods (Bellino, Garibaldi, Marchesiello, & Fasana, 2010; Hà & Golinval, 2010), wavelet analysis (Rucka, 2011; Shahsavari et al., 2017), and correlation analysis(L. Wang, Yang, & Waters, 2010; Muyu Zhang & Schmidt, 2015). These non-parametric methods do not need a traditional mechanical model and the core of these methods is to track the changes of some statistical features of the structure response. Based on the statistical comparison of the response data between the damaged and the intact structure, the measured structural response is analyzed and the intrinsic feature of the structure is dug out to make a structural diagnosis (detection and localization of damage).

The advantages of the non-parametric methods are: (1) The computational efficiency is high, even in the case of large amount of data, which makes them highly suitable for real-time applications. (2) Suitable for the situation where only the detection and the localization of damage is required. The disadvantages of these methods include: (1) It lacks physical interpretability of the result and only the presence or absence of damage and the location of the damage can be known, but not the extent; (2) It cannot provide the prediction of the structural behavior in other scenarios.

1.2.3 Deterministic and statistical methods

Various uncertainties exist in the SSI, such as measurement errors, modelling errors, external loads, and environmental factors. According to the means of treating uncertainties, SSI methods can be divided into deterministic methods and statistical methods.

The deterministic methods (Bakhtiari-Nejad, Rahai, & Esfandiari, 2005; Eskew & Jang, 2017; S. Li & WU, 2005; Monti, Quaranta, & Marano, 2009; Nogal, Lozano-Galant, Turmo, & Castillo, 2015; Masoud Sanayei, Imbaro, McClain, & Brown, 1997) attempt to find a set of optimal parameters to minimize the discrepancy between the response predicted by the parametric model and the measured response. In the deterministic methods, optimization techniques are often applied to minimize the user-defined objective functions. These objective functions can be established from the displacements (Nogal et al., 2015; Masoud Sanayei et al., 1997), the strains (S. Li & WU, 2005; Masoud Sanayei et al., 1997), the external load (Bakhtiari-Nejad et al., 2005), and the acceleration (Monti et al., 2009) , the modes and frequencies (Eskew & Jang, 2017) or maximizing the sensitivity of the frequency response function (Raich & Liszkai, 2012).

The SSI methods combined with probabilistic analysis are expected to be general

methods to make structural diagnosis of large civil structures. (Zong, 2012) pointed out that the basic idea of the probabilistic methods is to establish some statistical models to determine the distribution of the model output based on the distribution of the parameters of the model that represents the mechanical behavior of the structure. Then the uncertainty of the damage in the structure can be detected and quantified by the statistical model under certain confidence levels.

In the case of statistical approach, mainly in the Bayesian method, the distributions of the target parameters are obtained by Bayesian inference (J. L. Beck & Katafygiotis, 1998; James L. Beck & Au, 2002; James L Beck & Yuen, 2004; Cheung & Beck, 2010; Muto & Beck, 2008). This method regards all the parameters to be estimated as random variables, and the initial distribution of structural parameters (prior distribution) based on subjective experience. Assume that a statistical model is used to embed the obtained structural response information into the prior distribution, update the prior distribution of all parameters, and obtain the posterior distribution of all parameters. Then, the parametric uncertainty can be quantified in the form of probability distribution (Ghrib & Li, 2017; Jiang, Mahadevan, & Adeli, 2007).

(Zong, 2012) pointed out that in the Bayesian-based SSI methods, it is generally assumed that the prediction errors satisfy Gaussian white noise with zero mean. This assumption does not always hold, which leads to underestimation of uncertainties in the model. In the case of unobservable parameters, the establishment of the posterior distribution for the structural parameters is often confronted with the intractable large-scale computation. (H. Sun, Feng, Liu, & Feng, 2015; K.-V. Yuen & Kuok, 2011) pointed out that the main challenges of these Bayesian-based SSI methods are: (1) In many cases, it is impossible to obtain the explicit likelihood function to establish the prior distribution and the posterior distribution. (2) Even if there is an implicit likelihood function, the computational cost for solving the model is very large or even infeasible; (3) The computational cost increases exponentially with the number of parameters to be estimated, especially when the structural parameters are not globally observable. (Xin, Guoqiang, & Jing, 2005) pointed out that efficient searching strategies to obtain the posterior distribution of structural parameters is the key to tackle with the computational bottleneck occurred in Bayesian-based SSI methods. The application of Bayesian-based SSI methods in the dynamic case is described in detail by (K.-V. Yuen & Kuok, 2011).

1.3 Observability

The parameters of the system represent the current state of the system. The condition assessment of the system can be converted into the estimations of the system parameters. The SSI problem is essentially the application of parameter estimation in structural systems. The majority of parameter estimation problems ultimately are involved in solving a large system of equations. In parameter estimations (Enrique Castillo, Conejo,

Eva Pruneda, & Solares, 2007), two problems should be addressed:

(1) Compatibility problem: Whether the original equations have any solution (unique or multiple) that can yield the same output as the observed measurements. The compatibility problem depends on the selection of the measurements and the corresponding observations. The system may not have any output that is consistent with the actual observations. This could happen when there are measurement errors in the observations.

(2) Observability problem: This is associated with whether the unknowns in a system of equations can be uniquely determined or not. The focus of the observability problem is the guarantee of the uniqueness of the remaining variables prior to the parameter estimation when some variables are known. When some unknowns in the system of equations can be uniquely determined (despite that other variables are not), these unknowns are observable. In the parameter estimation, the observability of all parameters may not be guaranteed in the case of inappropriate measurement configurations (insufficient measurements or bad placement of sensors).

Observability problem is closely related to parameter estimation problem and is addressed in many fields related with parameter estimation. Many researchers have carried out a lot of work in assessing whether the known information is sufficient to estimate the unknown system parameters, such as hydraulic system (Carpentier & Cohen, 2007; Díaz, González, & Mínguez, 2016; Nagar & Powell, 2000), transportation network (E. Castillo, Jimenez, Menendez, & Conejo, 2008; Enrique Castillo, Conejo, Menéndez, & Jiménez, 2008; Enrique Castillo, Conejo, Pruneda, & Solares, 2005), power system (Caro, Arévalo, García-Martos, & Conejo, 2013; Enrique Castillo et al., 2005). In order to ensure the reliability of the parameter estimation results, the measurement configuration in the system should at least ensure the observability of the system parameters. (Abur & Exposito, 2004) gave the definition of observability as the ability to uniquely determine the current state of the system under given measurement configuration. If there are different states of the system satisfying the observed measurements, the system is called *non-uniquely observable system*. For parameter estimation of *non-uniquely observable systems*, the final estimations of the system parameters depend on the chosen initial values of these parameters. Because there are multiple sets of system parameters that satisfy the observed measurements, the final solution converges to the solution nearest to the chosen initial points. Therefore, regarding parameter estimations in *non-uniquely observable systems* caused by improper measurement configuration, the accuracy and reliability of the obtained solutions are doubtful. For the *fully observable* system, the solution of the system state is unique. No matter what the initial points of the algorithm are, the solution is expected to converge to the exact one. The iterative least-squares method is only applicable to observable systems. When using this type of methods, the observability analysis of the

system parameters is of primary importance. When the least-squares method is used to estimate the system parameters in the power system, if any state variable of the system cannot be observed under the given measurement configuration, all system parameters cannot be estimated. (Díaz et al., 2016) pointed out that when using mathematical programming or heuristic algorithms to minimize the state estimation error, the observability analysis is especially important. This is because these methods always provide estimations of all the parameters even if the system parameters cannot be observed from the given measurement configuration. These parameters might be regarded as the true values of the parameters despite the fact that the estimations of these parameters are meaningless. (Díaz et al., 2016) pointed out that the key factors affecting the parameter estimation result include the full observability of the parameters to be estimated, the measurement accuracy, and the robust state estimation algorithm. (Pruneda, Solares, Conejo, & Castillo, 2010) pointed out that the core step before the estimation of the system parameters is to place a sufficient number and types of measurements in the system to achieve full observability of the system and thus obtain a unique solution to the parameter estimates. This was also agreed by (Carpentier & Cohen, 2007) in the hydraulic system parameter estimation. They carried out the observability analysis to evaluate whether there were enough algebraic relations between the existing information and the system state variables. Hence, the uniqueness of the parameters to be estimated can be determined before the parameter estimation. Meanwhile, their method determines the minimum number of measurements to estimate the status of the hydraulic system. (Pan & Wang, 2005) pointed out that the observability of parameters was very important in the nonlinear state space equations for dynamic SSI, but this problem has not received enough attention. In the continuous-time system, they used the observable rank as a criterion to analyze the single-point or multi-point output system, and demonstrated that the method can determine the observability of the parameters before parameter estimation.

The review of the literature shows the importance of observability analysis on system parameters for accurate and reliable parameter estimation results. In many fields of engineering, the following issues emerge regarding the observability problem:

(1) Under a given measurement configuration, which parameters can be uniquely determined (observed)?

(2) How to design a measurement configuration using a minimum number of measurements that ensures the observability of all system parameters? Or, how to determine the minimum measurement set?

(3) Under a given measurement configuration, which parameters can be observed when additional measurements are provided?

The first question is the most important one. When the first question is tackled, the other two can be addressed smoothly. Regarding the second question, the measurement

configuration can be designed based on experience or generated by the enumeration of all possibilities. Then the minimum sets can be determined from those sets that can ensure the observability of all parameters with the least number of measurements. The effect of adding extra measurements on the observability of system parameters can be obtained by comparing the respective observability before and after the inclusion of these extra measurements while the tool to determine the observability comes from the answer to the first question.

The first question can be answered by Observability Method (OM) (Enrique Castillo et al., 2007). OM uses null spaces as the main tool to solve the observability problem in linear system of equations. In the context of static SSI, the very first application of OM was proposed by (Jose Antonio Lozano-Galant, Nogal, Castillo, & Turmo, 2013). In this method, observability equations are obtained by a series of algebraic operations on the nodal equilibrium equations using direct stiffness method, which makes SSI by OM a parametric static method. The efficacy of this method was verified by its application in the identification of trusses, beams, frame structures (Jose Antonio Lozano-Galant, Nogal, et al., 2013). Also, it was applied in cable-stayed bridges (Jose Antonio Lozano-Galant, Nogal, Paya-Zaforteza, & Turmo, 2014). At that time, the observability of the structural parameters was addressed symbolically. Later, (Nogal et al., 2015) proposed SSI by Numerical OM (NOM) that introduced a numerical approach to determine the values of those observable parameters. However, in all these works, noise-free measurements were considered. Nevertheless, this assumption is far from reality as the data of actual nondestructive tests is always subjected to measurement errors.

1.4 Conclusion

The current gaps for the research on SSI by OM should be pointed out:

(1) The measurement errors and simulation errors are not accounted in SSI by OM yet. This is indispensable for the application of this method in practical SSI. This will be addressed in Section 3.2.1.

(2) Due to the algebraic techniques adopted in SSI by OM, the nonlinear problem is simplified by the linearization of the nonlinear unknowns appearing in the observability equations. A side effect of this simplification is the occasional omission of observable parameters. This will be demonstrated in Section 3.2.3.

(3) When redundant measurement data are available, different strategies of using the measurement data might have different efficiency in acquiring the critical information about the condition of the structure.

(4) Apart from addressing the observability of structural parameters, a systematic sensor placement method dealing with the accuracy of static SSI result is lacking.

2. Objective

The general objective of this thesis is to provide a systematic SSI method for the condition assessment of structures under the framework of OM. To serve this purpose, the detailed objectives of this thesis can be presented as:

Objective 1: To obtain a quantitative recognition of the effect of measurement errors and simulation errors on the estimation of structural parameters using minimum measurement sets.

Objective 2: To enhance the capability of the SSI by original OM to detect minimum measurement sets by introducing the missing nonlinear constraints when necessary.

Objective 3: To smooth the incompatible displacements due to measurement errors by imposing compatibility conditions. These compatible geometric conditions can be obtained by OM in beam-like structures.

Objective 4: To obtain a robust SSI method using rotation measurements. Inclinometers have become popular in real-life applications. The theoretical advantage and detailed strategies of using rotations for SSI are demonstrated and justified.

Objective 5: To propose a versatile SSI method under single loading case, which is applicable for both beam-like structures and frame structures and does not suffer from the limitation of measurement types.

Objective 6: To generalize the method for single loading case to that for multiple loading cases. This generalization provides an efficient solution for the problem in identifying those parameters associated with null curvature zones in the one loading case.

Objective 7: To provide a systematic method to determine the optimal sensor placement (OSP) for the static SSI. The determinant of the Fisher Information Matrix (FIM) is used as the criterion to assess the goodness of a sensor configuration. The OSP is formulated as maximizing the determinant of the FIM with genetic algorithm.

The following chapter presents the methodologies and results associated with these objectives. Specifically, objectives 1~6 are addressed in Section 3.1-3.6, respectively. Meanwhile, objective 7 is attended to in both sections 3.5 and 3.6 for single loading case and multiple loading cases, respectively.

Finally, in Chapter 4, the main conclusions and contributions of this thesis are first summarized. Then, some future research lines are pointed out.

3. Methodologies and results

In this chapter, the six publications that constitute this thesis are presented. Note that three of them have already been accepted and published in the journal of Structural Control and Health Monitoring. For the rest, two manuscripts are currently under peer-review in the Structural Control and Health Monitoring and one is still at draft stage. Relevant dates and general information about each publication are detailed in the corresponding section.

3.1 Analysis of measurement and simulation errors in structural system identification by observability techniques

Title: Analysis of measurement and simulation errors in structural system identification by observability techniques

Authors: Jun Lei, José Antonio Lozano-Galant, María Nogal , Dong Xu, José Turmo

Journal: Structural Control and Health Monitoring

Publication: Technical Paper

Submitted: 18 January, 2016

Accepted: 15 July,2016

DOI: http://dx.doi.org/10.1002/stc.1923

Available at: https://onlinelibrary.wiley.com/doi/abs/10.1002/stc.1923

3.1.1 Summary

During the process of structural system identification, errors are unavoidable. This paper analyzes the effects of measurement and simulation errors in structural system identification based on observability techniques. To illustrate the symbolic approach of this method a simply supported beam is analyzed step−by−step. This analysis provides, for the very first time in the literature, the parametric equations of the estimated parameters. The effects of several factors, such as errors in a particular measurement or in the whole measurement set, load location, measurement location or sign of the errors, on the accuracy of the identification results are also investigated. It is found that error in a particular measurement increases the errors of individual estimations, and this effect can be significantly mitigated by introducing random errors in the whole measurement set. The propagation of simulation errors when using observability techniques is illustrated by two structures with different measurement sets and loading cases. A fluctuation of the observed parameters around the real values is proved to be

a characteristic of this method. Also, it is suggested that a sufficient combination of different loading cases should be utilized to avoid the inaccurate estimation at the location of low curvature zones.

Keyword: structural system identification; stiffness method; observability technique; measurement error; simulation error; observability flow

3.1.2 Introduction

Structural System Identification (SSI) methods enable the estimation of stiffnesses and/or masses of actual structures from the monitored data. A large number of SSI methods have been presented in the literature. In fact, the state of the art of these methods have been reviewed in a number of works (Nogal et al., 2015; Sirca & Adeli, 2012). According to most of these works, system identification methods can be classified as parametric (Garcia-Palencia et al. 2015; Mukhopadhyay, Lus, and Betti 2015; Mukhopadhyay, Lus, and Betti 2014; Sanayei, Khaloo, et al. 2015) and non-parametric (genetic algorithms (Chisari, Bedon, & Amadio, 2015; Jeong, Choi, & Koh, 2013; Trinh & Koh, 2012), evolutionary strategy (Bighamian & Mirdamadi, 2013; Karabeliov, Cuéllar, Baeßler, & Rücker, 2015; R. Li, Mita, & Zhou, 2013; Serhat Erdogan, Necati Catbas, & Gundes Bakir, 2014), neural networks (Facchini, Betti, & Biagini, 2014; Santos, Crémona, Calado, Silveira, & Orcesi, 2015) or least-squares estimation (Feng, Sun, & Feng, 2015; Y. Lei, Liu, & Liu, 2014; Z. Wang & Chen, 2013).

The major difference between these two methods refers to the equations that link the input and output data, as only in the parametric methods equations have a physical meaning. For this reason, parametric methods might be preferred over non-parametric ones.

A major concern for the structural system identification in actual structures refers to the sensitivity of the SSI method to errors. (Masoud Sanayei, Arya, Santini, & Wadia-Fascetti, 2001) summarized the different errors that influence the accuracy of these methods as follows: (1) Measurement errors: independent of the measurement device, error free measurements cannot be obtained in any actual nondestructive test. In this way, when these measurements are introduced into the SSI technique, deviations in the estimates appear. These unbiased errors can be reduced by technological developments but cannot be avoided. (2) Errors in the parameter estimation technique: Every SSI method is characterized by its characteristic simulation error. This error appears even when noise-free measurements are considered as it depends on the technique formulation. Examples of this error refer to the hypotheses of iterative or optimization processes used in the identification method or the loss of numerical accuracy in computer calculation. However, for the very first time in the literature, the explicit analytical solutions of these estimated parameters can be derived from the observability method in a symbolic way. Hence, those errors in parameter estimation might be avoided if noise-free data were used. (3) Modeling errors: These errors are due to

uncertainties in the parameters of the simplified Finite Element Model. Some examples of this error refer to the inaccuracy in material properties, the existence of elements which stiffness was not accounted for, or errors in the boundary conditions.

Significant research has been carried out to study the impact of the different errors on parametric methods. (M Sanayei & Saletnik, 1996b) proposed an error sensitivity analysis to evaluate the effect of noise in measurements. (Masoud Sanayei et al., 1997) compared the results of different error functions to evaluate the errors in the parameter estimation technique in a small scale model. (Masoud Sanayei et al., 2001) studied the effects of modeling errors in frame structures with elastic supports. (K.-V. V. Yuen & Katafygiotis, 2006) studied the effects of noisy measurements in structural system identification. (Caddemi & Greco, 2006) studied the influence of instrumental errors on the static identification of damage parameters for elastic beams. (M Zhang, Beer, & Koh, 2012) used intervals analyses to limit the values for the identified parameters under the effect of modeling errors. (S. Wang, 2014) studied the effects of flexible joints and boundary conditions for model updating. (Masoud Sanayei, Khaloo, et al., 2015) presented an error sensitivity analysis to study each parameter based on the loading cases and measurement locations of the nondestructive tests.

(Jose Antonio Lozano-Galant, Nogal, et al., 2013; Jose Antonio Lozano-Galant et al., 2014) proposed the observability method for structural system identification from static tests. This parametric technique analyzes the stiffness matrix method as a monomial-ratio system of equations and enables the mathematical identification of element stiffnesses of the whole structure or of a portion of it using a subset of deflection and/or rotation measurements. In all these works, noise-free measurements were considered. However, this assumption is far from reality as the data of actual nondestructive tests is always subjected to errors in measurement devices. In order to fill this gap, this paper analyzes the effects of measurement errors in structural identification by observability technique. The simulation errors inherent to this identification method are also studied in detail.

This article is organized as follows. In Section 3.1.3, the application of observability techniques to structural system identification is presented. In Section 3.1.4, a simply supported beam is analyzed to illustrate the different errors appearing in the observability technique. In Section 3.1.5 the measurement error is analyzed in an illustrative structure. Next, in Section 3.1.6 two structures are studied to illustrate the errors inherent to the observability technique. Finally, some conclusions are drawn in Section 3.1.7.

3.1.3 Structural System Identification by observability techniques

Prior to the application of observability techniques, a FEM of the structure should be established based on the topology of the structure to be identified, which is a common preliminary step in many identification methods (Feng et al., 2016; Isidori, Concettoni,

Cristalli, Soria, & Lenci, 2016; Omenzetter & Butt, 2016). With this FEM and the stiffness matrix method, the equilibrium equations together with strength of materials theory might be written in terms of nodal displacements and nodal forces as presented in Equation (3-1).

$$[K] \cdot \{\delta\} = \{f\} \tag{3-1}$$

n which $[K]$ is the stiffness matrix of the structure, $\{\delta\}$, is a vector of nodal displacements and $\{f\}$ is a vector of nodal forces. For 2D analysis, Matrix $[K]$ includes the geometrical and mechanical properties of the beam elements of the structure, such as length, L_j, shear modulus, G_j, Young's modulus, E_j, area, A_j, inertia, I_j, and torsional stiffness, J_j, associated with the j-element.

When the SSI is introduced in the stiffness matrix method, the matrix $[K]$ is partially unknown. Usually, L_j is assumed known while the stiffnesses are traditionally assumed as unknown. The determination of the unknown parameters in $[K]$ leads to a nonlinear problem as these parameters are multiplied by the displacements of the nodes (in 2D, horizontal and vertical deflection and rotation associated with the k-node u_k, v_k and w_k, respectively). This implies that non-linear products of variables, such as $E_jA_ju_k$, $E_jA_jv_k$, $E_jI_ju_k$, $E_jI_jv_k$ and $E_jI_jw_k$, might appear, leading to a polynomial system of equations. Before further discussion, one thing should be kept in mind is that the major interest in structural identification is to assess the structural behavior, e.g. axial stiffnesses, EA, or flexural stiffnesses, EI. In order to reduce the number of parameter, these stiffnesses are, respectively, assimilated into areas, A, and inertias, I, by setting the modulus to an assumed value, e.g. unity or typical values from handbooks. When the identification by observability is completed, the axial stiffnesses and the flexural stiffnesses, respectively, can be recovered by the multiplication of the predefined modulus and the estimated area, $\hat{A}$, and the estimated inertia, $\hat{I}$. This strategy is also followed in (Abdo, 2012; Jose Antonio Lozano-Galant, Nogal, Turmo, & Castillo, 2015).

To solve these equations in a linear-form, Equation (3-1) can be rewritten as:

$$[K^*] \cdot \{\delta^*\} = \{f\} \tag{3-2}$$

in which the products of variables are located in the modified vector of displacements $\{\delta^*\}$ and the modified stiffness matrix $[K^*]$ is a matrix of coefficients with different dimensions from the initial stiffness matrix $[K]$. Depending on the known information, the unknown variables of vector $\{\delta^*\}$ may be the non-linear products presented above, as well as other factors of single variables, such as E_jI_j, E_jA_j, E_j, A_j, I_j or node deflections.

Once the boundary conditions and the applied forces at the nodes during the nondestructive test are introduced, it can be assumed that a subset of increments of deflections δ_1^* of $\{\delta^*\}$ and a subset of forces in nodes $f_1$of $\{f\}$ are known and the remaining subset δ_0^* of $\{\delta^*\}$ and f_0 of $\{f\}$ are not. By the static condensation procedure, the system in (3-2) can be partitioned as follows:

$$[K^*]\{\delta^*\} = \begin{pmatrix} K_{00}^* & K_{01}^* \\ K_{10}^* & K_{11}^* \end{pmatrix} \begin{Bmatrix} \delta_0^* \\ \delta_1^* \end{Bmatrix} = \begin{Bmatrix} f_0 \\ f_1 \end{Bmatrix} = \{f\} \quad (3\text{-}3)$$

where K_{00}^*, K_{01}^*, K_{10}^* and K_{11}^* are partitioned matrices of $[K^*]$and δ_0^*, δ_1^*, f_0 and f_1 are partitioned vectors of $\{\delta^*\}$ and $\{f\}$.

In order to join the unknowns, Equation (3-3) can be written in the equivalent form, as:

$$[B]\{z\} = \begin{pmatrix} K_{10}^* & 0 \\ K_{00}^* & -I \end{pmatrix} \begin{Bmatrix} \delta_0^* \\ f_0 \end{Bmatrix} = \begin{Bmatrix} f_1 - K_{11}^* \times \delta_1^* \\ -K_{01}^* \times \delta_1^* \end{Bmatrix} = \{D\} \quad (3\text{-}4)$$

where 0 and I are the null and the identity matrices, respectively. In this system the vector of unknown variables, $\{z\}$, appears on the left-hand side and the vector of observations, $\{D\}$, on the right-hand side. Both vectors are related by a coefficient matrix$[B]$. For the Equation (3-4) to have a solution, it is sufficient to calculate the null space $[V]$ of $[B]$ and checking that $[V][D] = \{0\}$. Examination of matrix $[V]$ and identification of its null rows leads to identification of the observable variables (subset of variables with a unique solution) of vector $\{z\}$. The number of required deflections can be optimized by using a recursive process that takes advantage of the connectivity of the beams in the stiffness matrix. This connectivity is included in partitioned matrices of $[K^*]$ and therefore, in Equation (3-4). In this way, when in the initial observability analysis any deflection, force or structural parameter is observed, this information might help to observe new parameters in the adjacent beam elements through a recursive process. In this analysis, the observed information in the previous step is successively introduced as input data in the observability simulation.

A detailed step by step application of the observability techniques is presented in (Jose Antonio Lozano-Galant, Nogal, et al., 2013; Jose Antonio Lozano-Galant et al., 2014). The readers are recommended to refer to those papers for a more detailed explanation of the peculiarities of the proposed methodology.

The symbolical SSI algorithm presented above cannot obtain the numerical estimations of the observed parameters. To solve this problem, a numerical development of the observability techniques was presented in (Nogal et al., 2015). This algorithm combines two approaches: a symbolical and a numerical one. On the one hand, the symbolic approach is used for the observability analysis. This analysis reduces the effects of the unavoidable numerical errors during the computation of the null spaces of the system of equations. On the other hand, the second approach enables the numerical estimation of the observed parameters. This mixed algorithm also includes a recursive process, in which the new observed parameters are successively introduced into the analysis. This method has been applied to some large structures, including a 13-storeys frame building (Lozano-Galant, Nogal, et al. 2013) and a cable stayed bridge (Lozano-Galant et al. 2014, 2015). The main time cost of the algorithm is in the computation of the null space, $[V]$, by symbolical approach whereas the time cost by the numeric approach is negligible. However, the computation of the null space by symbolical approach can be carried out efficiently in Matlab subroutine. In the case of the 13-story building, it has

been checked that 396 seconds are needed, on a laptop with a 2.4 GHz i7 processor and a 16 GB memory, to get the null space of a matrix [B] with the dimension of 258×462. Note that the number of rows in the matrix [B] is three times the number of nodes, which is unchanging, while the number of columns in the matrix [B] equals the number of unknowns. Moreover, the number of unknowns decreases with the recursive steps since some of the unknowns have been observed in preceding steps. Thus, the computation of the null space of the matrix [B] will be accelerated during the recursive steps due to the decrease of the scale of [B].

This method has so far been only applied in 2D structures simulated by 1D elements with 3 DOFs per node. Conceptually, as a mathematical tool, the observability technique is expected to be implementable in different formulations of the FEM, including but not limited to 3D structures simulated by 1D elements with 6 DOFs per node or 2D structures simulated by 2D elements with 3DOFs per node (Lozano Galant 2013). However, more work associated with this part needs to be done in future.

To illustrate the application of this process, a simple structure is analyzed in the following section. This example also serves to point out the errors of the observability technique.

3.1.4 Identifying errors in observability techniques

To illustrate the mixed procedure presented above, the simply supported beam presented in Figure 3-1.a is analyzed. This structure is modeled by a simplified Finite Element Model (FEM) composed of 4 nodes and 3 beam elements. The Young's modulus of all elements is assumed as unknown. Nevertheless, this is not the case of the inertias and the areas, as their values are considered different and unknown for the three different beam elements. To estimate the three unknown flexural stiffnesses of the system (EI_1, EI_2 and EI_3), one rotation (w_1) and two vertical deflections (v_2 and v_3) are measured.

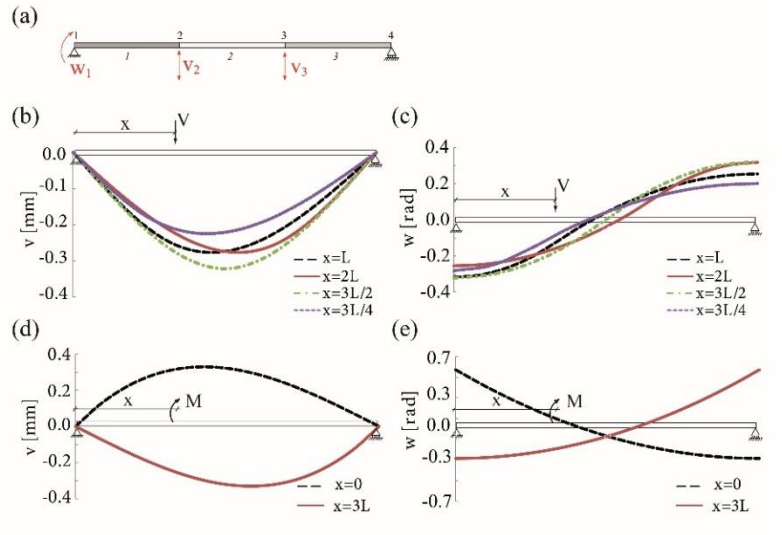

Figure 3-1 (a) Geometry of FEM, (b) vertical deflections, v, throughout the beam for different locations of a concentrated vertical load V, (c) rotations, w, for different locations of V. (D) Vertical deflections, v, for different locations of a concentrated external moment M, and (E) rotations w for different locations of M.

In this structure, the application of Equation (3-4) leads to the following system of equations:

$$\begin{bmatrix}
0 & 0 & 0 & 0 & 0 & 0 & \frac{4w_1}{L}-\frac{6v_2}{L^2} & \frac{2}{L} & 0 & 0 & 0 & 0 & 0 & 0 & 0 & 0 \\
\frac{1}{L} & \frac{1}{L} & -\frac{1}{L} & 0 & 0 & 0 & 0 & 0 & 0 & 0 & 0 & 0 & 0 & 0 & 0 & 0 \\
0 & 0 & 0 & 0 & 0 & 0 & \frac{12v_2}{L^3}-\frac{6w_1}{L^2} & -\frac{6}{L^2} & \frac{12v_2}{L^3}-\frac{12v_3}{L^3} & \frac{6}{L^2} & \frac{6}{L^2} & 0 & 0 & 0 & 0 & 0 \\
0 & 0 & 0 & 0 & 0 & 0 & \frac{2w_1}{L}-\frac{6v_2}{L^2} & \frac{4}{L} & \frac{6v_2}{L^2}-\frac{6v_3}{L^2} & \frac{4}{L} & \frac{2}{L} & 0 & 0 & 0 & 0 & 0 \\
0 & -\frac{1}{L} & \frac{1}{L} & \frac{1}{L} & -\frac{1}{L} & 0 & 0 & 0 & 0 & 0 & 0 & 0 & 0 & 0 & 0 & 0 \\
0 & 0 & 0 & 0 & 0 & 0 & 0 & 0 & \frac{12v_2}{L^3}-\frac{12v_3}{L^3} & -\frac{6}{L^2} & -\frac{6}{L^2} & \frac{12v_2}{L^3} & \frac{6}{L^2} & \frac{6}{L^2} & 0 & 0 \\
0 & 0 & 0 & 0 & 0 & 0 & 0 & 0 & \frac{6v_2}{L^2}-\frac{6v_3}{L^2} & \frac{2}{L} & \frac{4}{L} & \frac{6v_3}{L^3} & \frac{4}{L} & \frac{2}{L} & 0 & 0 \\
0 & 0 & 0 & -\frac{1}{L} & \frac{1}{L} & 0 & 0 & 0 & 0 & 0 & 0 & 0 & 0 & 0 & 0 & 0 \\
0 & 0 & 0 & 0 & 0 & 0 & 0 & 0 & 0 & 0 & 0 & \frac{6v_3}{L^3} & \frac{4}{L} & \frac{2}{L} & 0 & 0 \\
-\frac{1}{L} & 0 & 0 & 0 & 0 & -1 & 0 & 0 & 0 & 0 & 0 & 0 & 0 & 0 & 0 & 0 \\
0 & 0 & 0 & 0 & 0 & 0 & \frac{6w_1}{L^2}-\frac{12v_2}{L^3} & \frac{6}{L^2} & 0 & 0 & 0 & 0 & 0 & 0 & -1 & 0 \\
0 & 0 & 0 & 0 & 0 & 0 & 0 & 0 & 0 & 0 & 0 & \frac{-12v_3}{L^3} & -\frac{6}{L^2} & -\frac{6}{L^2} & 0 & -1
\end{bmatrix} \cdot \begin{Bmatrix}
EA_1u_2 \\ EA_2u_2 \\ EA_2u_3 \\ EA_3u_3 \\ EA_3u_4 \\ H_1 \\ EI_1 \\ EI_1w_2 \\ EI_2 \\ EI_2w_2 \\ EI_2w_3 \\ EI_3 \\ EI_3w_3 \\ EI_3w_4 \\ V_1 \\ V_4
\end{Bmatrix} = \begin{Bmatrix}
M_1 \\ H_2 \\ V_2 \\ M_2 \\ H_3 \\ V_3 \\ M_3 \\ H_4 \\ M_4 \\ 0 \\ 0 \\ 0
\end{Bmatrix} \tag{3-5}$$

In this system, the unknown variables $\{z\}$ include the horizontal reaction, H_1, and vertical reactions, V_1 and V_4, at the boundaries, the inertias, EI_1, EI_2 and EI_3, and nonlinear products of coupled areas and inertias, such as EA_1u_2, EA_2u_2, EA_2u_3, EA_3u_3, EA_3u_4, EI_2w_1, EI_2w_3, EI_3w_3 and EI_3w_4. With $\{p_1\}$, being a vector of coefficients, the general solution of Equation (3-5) can be expressed in terms of a particular solution $\{z_{p1}\}$ and the null space $[V_1]$ of the matrix of the preceding system as follows:

$$\{z_1\} = \{z_{p1}\} + [V_1] \cdot \{p_1\} = \begin{Bmatrix} EA_1u_2 \\ EA_2u_2 \\ EA_2u_3 \\ EA_3u_3 \\ EA_3u_4 \\ \boldsymbol{H_1} \\ \boldsymbol{EI_1} \\ \boldsymbol{EI_1w_2} \\ EI_2 \\ EI_2w_2 \\ EI_2w_3 \\ EI_3 \\ EI_3w_3 \\ EI_3w_4 \\ \boldsymbol{V_1} \\ \boldsymbol{V_4} \end{Bmatrix} = \{z_{p1}\} + \begin{bmatrix} 1 & 0 & 0 & 0 \\ 1 & 0 & 0 & 0 \\ 1 & 0 & 0 & 0 \\ 0 & 1 & 0 & 0 \\ 0 & 1 & 0 & 0 \\ 0 & 0 & 0 & 0 \\ 0 & 0 & 0 & 0 \\ 0 & 0 & 0 & 0 \\ 0 & 0 & \frac{-L}{v_2 - v_3} & 0 \\ 0 & 0 & 1 & 0 \\ 0 & 0 & 1 & 0 \\ 0 & 0 & 0 & \frac{-L}{v_3} \\ 0 & 0 & 0 & 1 \\ 0 & 0 & 0 & 1 \\ 0 & 0 & 0 & 0 \\ 0 & 0 & 0 & 0 \end{bmatrix} \cdot \{p_1\} \quad (3\text{-}6)$$

The analysis of $[V_1]$ illustrates the importance of using a symbolic approach. Otherwise, numerical errors with values very close to zero might appear. This might result in reducing the observed parameters. Those variables whose associated rows of $[V_1]$ are null indicate that their values have a unique solution (that is to say, that is observable and the particular and general solutions are equal). The variables observed in the first step (H_1, EI_1, EI_1w_2, V_1 and V_4) are highlighted in bold in $\{z_1\}$ of Equation (3-6). Obviously, when the value of EI_1 is estimated, w_2 can be deduced from EI_1w_2. The particular solution $\{z_{p1}\}$ of these parameters can be symbolically obtained from Equation (3-5) by the left divide, \, in Matlab (Kroese & Chan, 2014). Similar functions can be found in other commercial packages, e.g. solve function in both Maple (Heal, Hansen, Rickard, & Incorporation, 1998) and Mathematica (Wolfram, 1999). These functions can be used to provide solutions for symbolic systems of equations.

According to the authors' knowledge, such a type of parametric equations cannot be found in the literature for structural system identification. The obtained parametric equations of the estimates $\widehat{EI_1}$, $\hat{V}_1$ and $\hat{V}_4$ are as follows:

$$\widehat{EI_1} = -\frac{(8M_1 - M_2 - M_3 - M_4 + 2V_2L + V_3L)L^2}{18(v_2 - w_1L)} \quad (3\text{-}7)$$

$$\hat{V}_1 = \frac{(M_1 + M_2 + M_3 + M_4 - 2V_4L - V_3L)}{3 \cdot L} \quad (3\text{-}8)$$

$$\hat{V}_4 = \frac{(M_1 + M_2 + M_3 + M_4 + L \cdot V_4 + 2 \cdot L \cdot V_3)}{3 \cdot L} \quad (3\text{-}9)$$

in which M_i and V_i are the bending Moments and the Vertical forces (external loads) applied at the *ith* node of the structure during the nondestructive test and L is the length of the beam elements in the model. In these equations, the super index ^ indicates that the value of the estimate is obtained by observability techniques. Obviously, a different equation would be obtained if either the measurement set or the geometry of the structure were changed. It is noted that the parametric Equation (3-7) might lead to

unrealistic estimation if the denominator tends to zero or is negative when errors are introduced. This is also discussed in detail in section 3.1.5. In order to fill this gap, the researchers are working on an optimization of the measurements which it will be presented in the near future.

The analysis of Equation (3-5) shows that EI_1 depends on the nodal forces applied at the loading case (M_1 to M_4, V_2 and V_3), the length of the beam elements L, and the measured deflection v_2 and rotation w_1. Both v_2 and w_1 are only found in the denominator of the equation. As the structure is simply supported, V_1 and V_4 can be geometrically determined in terms of the geometry and the forces applied in the loading case. For this reason, these parameters do not depend on the measured deflections.

Once the observable parameters are identified, their values can be numerically calculated. To illustrate the results of the method, let's consider a concrete beam of 0.3-m height and 0.2-m width. The inertia and the Young's modulus are 4.5e-4 m^4 and 3.5e7 kN/m^2, respectively. The total length ($3L$) of the beam is 3m. The loading case is assumed as a concentrated load of -55 kN at node 2. This loading case is represented by the following nodal forces: M_1=M_2=M_3=M_4=V_3=0 and V_2=-55 kN. Both the deflections and the rotations obtained throughout the beam for this loading case by FEM program are presented in Figure 3-1.b and c, respectively for a loading location x=L. In this simulation, the shear deformation is neglected.

The numeric values of the estimated $\widehat{EI}_1$, $\hat{w}_2$, $\hat{V}_1$, $\hat{V}_4$ obtained by parametric equations are summarized in the first recursive step of Table 3-1. This table also includes the ratio of deviation between estimated and actual values. As showed in this table, the maximum deviation 0.017% in $\widehat{EI}_1$, which is due to the round-off error, is negligible.

After introducing the parameters observed in the first recursive step, the Equation (3-5) can be rearranged as presented in Equation (3-10). This analysis corresponds with the second recursive step. It is worth noticing that in this system the previously identified parameters (V_1, V_4, EI_1 and w_2) are moved from $\{z\}$ to $[B]$ and $\{D\}$.

Table 3-1 Numerical estimations of the parameters during the recursive steps and the deviations with the actual values obtained from the parametric equations.

Step 1			Step 2			Step 3		
Par.	Est.	Dev.	Par.	Est.	Dev.	Par.	Est.	Dev.
$\widehat{EI}_1$ (kN/m^2)	15753.5	1.7‰	$\widehat{EI}_2$ (kN/m^2)	15750.0	-1.4‰	$\widehat{EI}_3$ (kN/m^2)	15753.6	2‰
$\widehat{w_2}$ (rad)	-1.1e-3	-0.2‰	$\widehat{w_3}$ (rad)	1.3e-3	0.2‰	$\widehat{w_4}$ (rad)	2.1e-3	-0.1‰
$\hat{V}_1$ (kN)	36.7	0.0‰						
$\hat{V}_4$ (kN)	18.3	0.0‰						

Note: Par. for parameter, Est. for estimation, Dev. for deviation.

$$\begin{bmatrix} 0 & 0 & 0 & 0 & 0 & 0 & 0 & 0 & 0 & 0 \\ \frac{1}{L} & \frac{1}{L} & -\frac{1}{L} & 0 & 0 & 0 & 0 & 0 & 0 & 0 \\ 0 & 0 & 0 & 0 & 0 & \frac{12v_2}{L^3}-\frac{12v_3}{L^3}+\frac{6w_2}{L^2} & \frac{6}{L^2} & 0 & 0 & 0 \\ 0 & 0 & 0 & 0 & 0 & \frac{6v_2}{L^2}-\frac{6v_3}{L^2}+\frac{4w_2}{L} & \frac{2}{L} & 0 & 0 & 0 \\ 0 & -\frac{1}{L} & \frac{1}{L} & \frac{1}{L} & -\frac{1}{L} & 0 & 0 & 0 & 0 & 0 \\ 0 & 0 & 0 & 0 & 0 & -\frac{12v_2}{L^3}+\frac{12v_3}{L^3}-\frac{6w_2}{L^2} & -\frac{6}{L^2} & \frac{12v_3}{L^3} & \frac{6}{L^2} & \frac{6}{L^2} \\ 0 & 0 & 0 & 0 & 0 & \frac{6v_2}{L^2}-\frac{6v_3}{L^2}+\frac{2w_2}{L} & \frac{4}{L} & \frac{6v_3}{L^2} & \frac{4}{L} & \frac{2}{L} \\ 0 & 0 & 0 & -\frac{1}{L} & \frac{1}{L} & 0 & 0 & 0 & 0 & 0 \\ 0 & 0 & 0 & 0 & 0 & 0 & 0 & \frac{6v_3}{L^2} & \frac{2}{L} & \frac{4}{L} \\ -\frac{1}{L} & 0 & 0 & 0 & 0 & 0 & 0 & 0 & 0 & 0 \\ 0 & 0 & 0 & 0 & 0 & 0 & 0 & 0 & 0 & 0 \\ 0 & 0 & 0 & 0 & 0 & 0 & 0 & -\frac{12v_3}{L^3} & -\frac{6}{L^2} & -\frac{6}{L^2} \end{bmatrix} \begin{Bmatrix} EA_1u_2 \\ EA_2u_2 \\ EA_2u_3 \\ EA_3u_3 \\ EA_3u_4 \\ EI_2 \\ EI_2w_3 \\ EI_3 \\ EI_3w_3 \\ EI_3w_4 \end{Bmatrix} = \begin{Bmatrix} M_1+\frac{6EI_1v_2}{L^2}-\frac{4EI_1w_1}{L}-\frac{2EI_1w_2}{L} \\ H_2 \\ V_2-\frac{12EI_1v_2}{L^3}+\frac{6EI_1w_1}{L^2}+\frac{6EI_1w_2}{L^2} \\ M_2+\frac{6EI_1v_2}{L^2}-\frac{2EI_1w_1}{L}-\frac{4EI_1w_2}{L} \\ H_3 \\ V_3 \\ M_3 \\ H_4 \\ M_4 \\ H_1 \\ V_1+\frac{12EI_1v_2}{L^3}-\frac{6EI_1w_1}{L^2}-\frac{6EI_1w_2}{L^2} \\ V_4 \end{Bmatrix} \quad (3\text{-}10)$$

With $[V_2]$ being the null space of the matrix $[B]$ in Equation (3-10), $\{p_2\}$ being a vector of coefficients, and $\{z_{p2}\}$ being the particular solution of the system, the general solution $\{z_2\}$ of the second recursive step can be expressed as follows:

$$\{z_2\} = \{z_{p2}\} + [V_2]\cdot\{p_2\} = \begin{Bmatrix} EA_1u_2 \\ EA_2u_2 \\ EA_2u_3 \\ EA_3u_3 \\ EA_3u_4 \\ \boldsymbol{EI_2} \\ \boldsymbol{EI_2w_3} \\ EI_3 \\ EI_3w_3 \\ EI_3w_4 \end{Bmatrix} = \{z_{p2}\} + \begin{bmatrix} 1 & 0 & 0 \\ 1 & 0 & 0 \\ 1 & 0 & 0 \\ 0 & 1 & 0 \\ 0 & 1 & 0 \\ 0 & 0 & 0 \\ 0 & 0 & 0 \\ 0 & 0 & \left(\frac{-L}{v_3}\right) \\ 0 & 0 & 1 \\ 0 & 0 & 1 \end{bmatrix} \cdot \{p_2\} \quad (3\text{-}11)$$

The analysis of $[V_2]$ shows that the only observed parameters are EI_2 and EI_2w_3. From this information the calculation of w_3 is a straightforward task. The observed parameters are highlighted in bold in $\{z_2\}$ of Equation (3-11). The parametric equation of EI_2 is presented in Equation (3-12). This equation shows how EI_2 depends on the values of EI_1 and w_2 estimated in the preceding recursive step. The numerical values of EI_2 and w_3 are summarized in the second recursive step of Table 3-1. As showed in this table, the deviation between the actual value of EI_2 and the estimated one $\widehat{EI}_2$ (-0.014%) is negligible.

$$\widehat{EI}_2 = \frac{2M_2L^2 - M_3L^2 - M_4L^2 - V_4L^3 + 12EI_1v_2 - 4EI_1w_1L - 8EI_1w_2L}{6(v_2 - v_3 + L\cdot w_2)} \quad (3\text{-}12)$$

Finally, in the third recursive step all the parameters observed by the first two steps (V_1, V_4, EI_1, w_2, EI_2 and w_3) are introduced, and the system of Equation (3-10) is updated to:

$$\begin{bmatrix} 0 & 0 & 0 & 0 & 0 & 0 & 0 \\ \frac{1}{L} & \frac{1}{L} & \frac{-1}{L} & 0 & 0 & 0 & 0 \\ 0 & 0 & 0 & 0 & 0 & 0 & 0 \\ 0 & 0 & 0 & 0 & 0 & 0 & 0 \\ 0 & \frac{-1}{L} & \frac{1}{L} & \frac{1}{L} & \frac{1}{L} & 0 & 0 \\ 0 & 0 & 0 & 0 & 0 & \frac{12v_3}{L^3}+\frac{6w_3}{L^2} & \frac{6}{L^2} \\ 0 & 0 & 0 & 0 & 0 & \frac{6v_3}{L^2}+\frac{4w_3}{L} & \frac{2}{L} \\ 0 & 0 & 0 & \frac{-11}{L} & \frac{L}{} & 0 & 0 \\ 0 & 0 & 0 & 0 & 0 & \frac{6v_3}{L^2}+\frac{2w_3}{L} & \frac{4}{L} \\ \frac{-1}{L} & 0 & 0 & 0 & 0 & 0 & 0 \\ 0 & 0 & 0 & 0 & 0 & 0 & 0 \\ 0 & 0 & 0 & 0 & 0 & -\frac{12v_3}{L^3}-\frac{6w_3}{L^2} & -\frac{6}{L^2} \end{bmatrix} \cdot \begin{Bmatrix} EA_2u_2 \\ EA_2u_3 \\ EA_3u_3 \\ EA_3u_4 \\ EI_3 \\ EI_3w_3 \end{Bmatrix} = \begin{Bmatrix} M_1+\frac{6EI_1v_2}{L^2}-\frac{4EI_1w_1}{L}-\frac{2EI_1w_2}{L} \\ H_2 \\ -\frac{12EI_1v_2}{L^3}-\frac{12EI_2v_2}{L^3}+\frac{12EI_2v_3}{L^3}+V_2+\frac{6EI_1w_1}{L^2}+\frac{6EI_1w_2}{L^2}-\frac{6EI_2w_2}{L^2}-\frac{6EI_2w_3}{L^2} \\ M_2+\frac{6EI_1v_2}{L^2}-\frac{6EI_2v_2}{L^2}+\frac{6EI_2v_3}{L^2}-\frac{2EI_1w_1}{L}-\frac{4EI_1w_2}{L}-\frac{4EI_2w_2}{L}-\frac{2EI_2w_3}{L} \\ H_3 \\ \frac{12EI_2v_2}{L^3}-\frac{12EI_2v_3}{L^3}+V_3+\frac{6EI_2w_2}{L^2}+\frac{6EI_2w_3}{L^2} \\ M_3-\frac{6EI_2v_2}{L^2}+\frac{6EI_2v_3}{L^2}-\frac{2EI_2w_2}{L}-\frac{4EI_2w_3}{L} \\ H_4 \\ M_4 \\ H_1 \\ \frac{12EI_1v_2}{L^3}+V_1-\frac{6EI_1w_1}{L^2}-\frac{6EI_1w_2}{L^2} \\ V_4 \end{Bmatrix} \quad (3\text{-}13)$$

With $[V_3]$ being the null space of the matrix $[B]$ in Equation (3-13), $\{p_3\}$ being a vector of coefficients, and $\{z_{p3}\}$ being the particular solution of the system, the general solution $\{z_3\}$ can be expressed as follows:

$$\{z_3\} = \{z_{p3}\} + [V_3] \cdot \{p_3\} = \begin{Bmatrix} EA_1u_2 \\ AE_2u_2 \\ EA_2u_3 \\ EA_3u_3 \\ EA_3u_4 \\ \boldsymbol{EI_3} \\ \boldsymbol{EI_3w_4} \end{Bmatrix} = \{z_{p3}\} + \begin{bmatrix} 1 & 0 \\ 1 & 0 \\ 1 & 0 \\ 0 & 1 \\ 0 & 1 \\ 0 & 0 \\ 0 & 0 \end{bmatrix} \cdot \{p_3\} \qquad (3\text{-}14)$$

The analysis of matrix $[V_3]$ shows that in this step, EI_3 and EI_3w_4 are observed. From this information w_4 can be directly obtained. These parameters are highlighted in bold in Equation (3-14). The parametric equation of EI_3 obtained from the particular solution of Equation (3-13) is presented in Equation (3-14). As in the case of EI_2, this equation depends on the values of parameters (such as $\widehat{EI}_2$ and $\hat{w}_3$) estimated in preceding recursive steps and on measured deflections (v_2 and v_3). The numerical values of $\widehat{EI}_3$ and $\hat{w}_4$ are presented in the third recursive step of Table 3-1. This table shows that the deviation between the actual EI_3 and the estimated $\widehat{EI}_3$ (0.02%) is negligible.

$$\widehat{EI}_3 = \frac{3M_3L^2 - V_3L^3 - 30EI_2v_2 + 30EI_2v_3 - 12EI_2w_2L - 18EI_2w_3L}{6(v_3 + w_3L)} \qquad (3\text{-}15)$$

Evidently, axial stiffness of the beam cannot be estimated due to the fact that the axial resistant mechanism was not excited by the external load. However, this did not impede the bending stiffness to be observable, and henceforth, to be estimated.

The analysis of the parametric equations of EI_1, EI_2 and EI_3 shows their dependence on the measurements and therefore, on their errors (measurement errors). These equations also show that the nature of the recursive process tends to increase the errors throughout the analysis (error associated with the simulation method). The sensitivity of the observability techniques to these two kinds of errors is analyzed in the following sections.

A flow chart of the mixed algorithm of structural identification by observability method is provided in Figure 3-2.

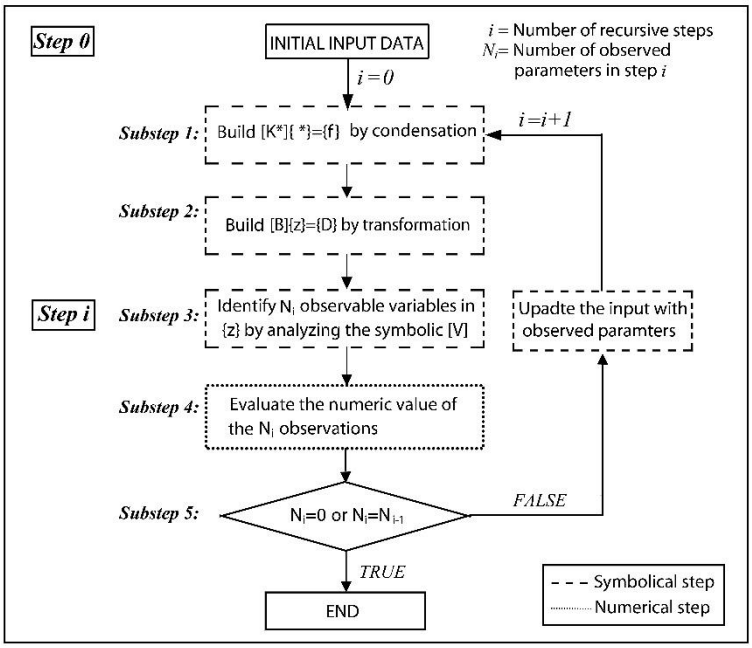

Figure 3-2 Flowchart of the mixed algorithm

All the procedures related with the symbolic approach are enclosed by dashed line whereas the procedures related with the numeric approach are enclosed by dotted line. In *step 0*, input the initial data containing the description of the FEM (nodes, element connectivity, external loads and the unknown set of areas and inertias) and the measurement set. In *substep 1* of step i, absorb the measurements in the matrix $[K^*]$ and collect unknowns in the vector $[\delta^*]$ by static condensation. Next, move the unknowns and the observation, respectively, to the left-hand side and the left-hand side of the system in *substep 2*, by which the system $[B] \cdot \{z\} = \{D\}$ is generated. Then, in *substep 3*, the observability of the unknowns are determined by checking the null row of the symbolic null space, $[V]$, of the matrix $[B]$. The value of the observed parameters will be evaluated by numeric approach in *substep 4*. And, in *substep 5*, it will be examined first whether the number of the observed parameters, N_i, is zero or the same as the number of N_{i-1} from previous step. If so, the identification process is terminated since no more parameter can be observed. Otherwise, the numeric value of the observed parameters from *substep 5* will be used to update the input and regarded as known parameters to initiate the succeeding recursive step.

3.1.5 Measurement errors

This section deals with the role of measurement error in structural system identification by observability techniques. With this aim, two sensitivity analyses of the simply

supported beam in Figure 3-1 are presented. The first simulation analyzes the effects of individual errors in each measurement (deflection or rotation). The deviation in the estimation of $\hat{I}_1$ is also analyzed by means of partial derivatives. Finally, the second sensitivity analysis studies the effect of random errors in all measurements.

Analysis of errors in single measurement

This section analyzes the sensitivity of parametric equations of I_1, I_2 and I_3 obtained from Equations (3-7), (3-12) and (3-15) to errors in one measurement

The measurement set used here is the same as before, one rotation (w_1) and two deflections (v_2 and v_3). The Young's modulus of the three beam elements is assumed as known (2.5e7 kN/m^2).

The ratio between each estimated inertia, $\hat{I}_i$, and the actual one, *I*, with errors from -5% to 5% in v_2, w_1 and v_3 are presented in Figure 3-3.a. This figure shows how the sensitivity to errors in one of the measurements is increased throughout the recursive process. For example, the deviation between the estimated inertia and the actual one for an error of -5% in v_2 changes from -16.7% in I_1 to 47.1% in I_2, and -45.5% in I_3. In this structure, the deviations in I_1 produced by errors in v_2 correspond with those in I_2 for errors in w_1. Generally, the system is more sensitive to errors in deflections than in rotations. This figure also illustrates the importance of the error sign. In fact, the estimations based on the measured deflections are asymmetric. This asymmetry increases throughout the recursive process and is especially significant in the deflections, v.

In Figure 3-3.b, the effect of the errors in measurements on the deviation in the estimation throughout the recursive process is presented. This figure also shows that I_1 is not affected by errors in v_3. This is because the parametric equations of these inertias do not depend on the deflection v_3.

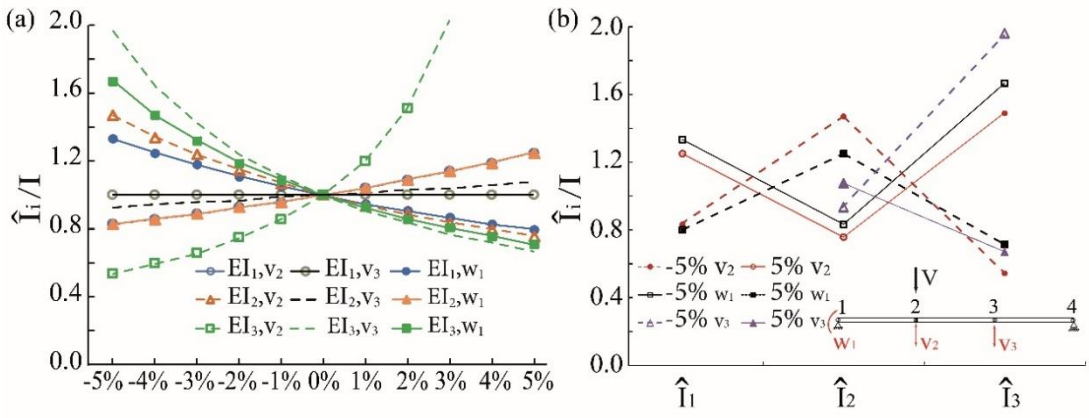

Figure 3-3 (a) Ratio between the estimated inertias, $\hat{I}_i$, and the actual, I, for errors in each measurements v_2, w_1 and v_3. (b) Evolution of the ratio between $\hat{I}_i$ and I

throughout the recursive process for an error of -5% or 5% in measurements v_2, w_1 and v_3.

The effects of the location of two concentrated loads are analyzed in Figure 3-4.a and b, respectively, to clarify the influence of the loading case on the parametric equations of inertias. Loading case one corresponds with a concentrated vertical load V=-55 kN, located at an intermediate node (x=L or x=2L). The second loading case corresponds with a concentrated bending moment, M=100kN·m, located at the beam edge (x=0 or x=3L). These figures present the deviation between the actual inertia, I, and the $\hat{I}_1$ calculated by parametric Equation (3-7) for different errors in v_2 or w_1 and load locations. It should be highlighted that deviations beyond the range of [0,2] do not have physical meaning and thus they are rejected.

Figure 3-4 shows that the loading case is influential in the accuracy of estimated parameters. In Figure 3-4.a, the closer the load to the measurements, the smaller the effect of errors. For example, for an error of -5% in v_2, the deviation of $\hat{I}_1$ increases from -16.6% to -25.9% when V is moved from x=L to x=2L. For the same error level in w_1, moving V from x=L to x=2L increases the deviation of $\hat{I}_1$ from 33.3% to 66.7%. Similar conclusion can be drawn when the effect of bending moment M is analyzed. In this case, for an error of -5% in v_2, the deviation in $\hat{I}_1$ increases from -5.8% to -28.6% when M is moved from x=0 to x=3L. For the same error in w_1, the increment is from 12.7% to 81.2%.

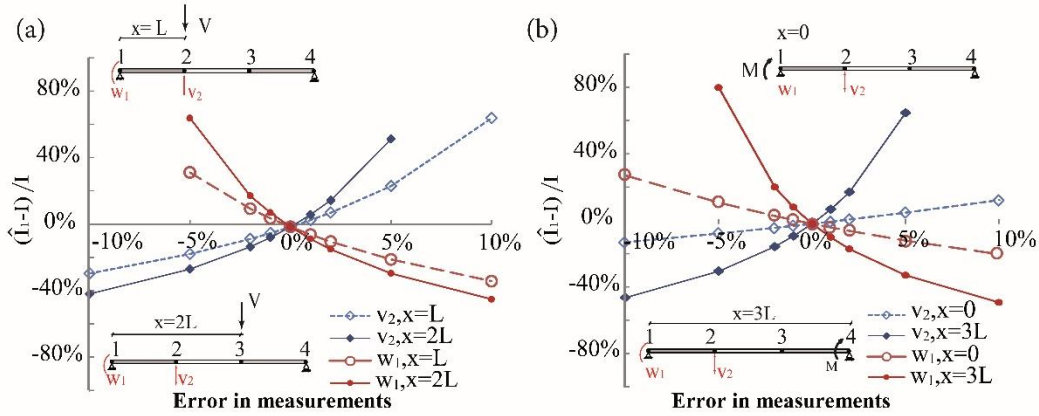

Figure 3-4 Effect of measurement errors in v_2 or w_1 for a loading case of a concentrated vertical force V (a) or bending moment M (b) at different locations x.

In addition, the parametric equations are affected by the location of the measurements. In the observability method, the accuracy of the estimations is highly related to the curvature of the elements where the measurements are performed. Estimates obtained from deflections measured at the low curvatures zone might be more sensitive to errors. For example, in a simply supported beam, the null curvature zones are those adjacent

to the support. The influence of the curvature will be discussed in a more extensive way in the simulation error part.

To clarify the effects of curvatures in the accuracy of the estimates, six FEMs, FEM_2, FEM_3, FEM_4, FEM_6, FEM_8 and FEM_{12}, with the same length, $3L$, but different element numbers were analyzed. The number of elements in these FEMs is indicated by their subscripts. In all these models, only the flexural stiffness of the first element, EI_1, is estimated.

In these models, two measurements are considered, the rotation w_1 at the left support and the deflection v_2 of node 2. Note that the location of the measurement v_2 is and $\{x$=1.5L, L, 0.75L, 0.375L and 0.25L for FEM_2, FEM_3, FEM_4, FEM_6, FEM_8 and FEM_{12}. That is, the measurement v_2 will be located nearer to the null curvature zone in models of more elements.

To analyze the effect of the location of the measurements, the parametric equation of $\widehat{EI}_1$, Equation (3-7), for FEM_3 is analyzed. Similar equations can be obtained for different FEMs by substituting the length of the different elements in each model. The effect of errors ranging from -15% to 15% in w_1 and v_2 is obtained by these equations for each FEM is presented in Figure 3-5. It should be clarified that all these equations are presented as a fraction, in which the numerator indicates information of the loading case while the Denominator, D, indicates information of the measurements.

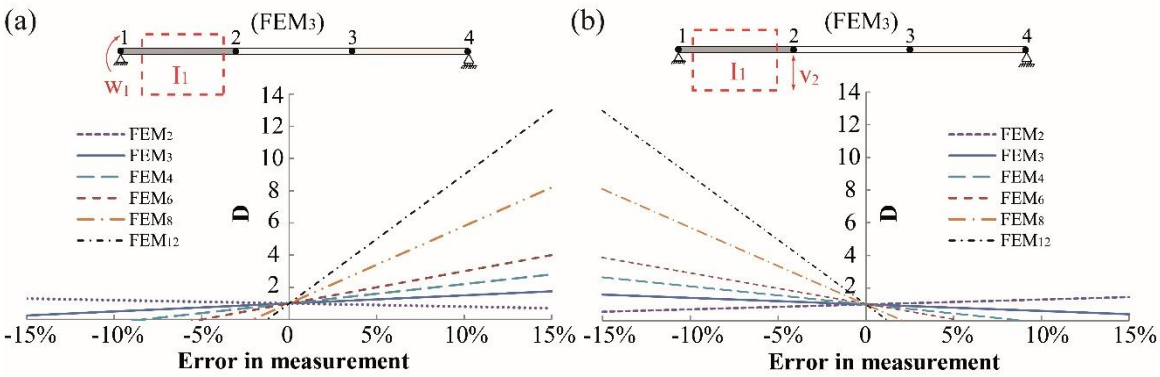

Figure 3-5 Denominator, D, from the parametric equation of $\widehat{EI}_1$, when errors appears in (a) w_1 and (b) v_2

As expected, Figure 3-5 shows that the denominator of the parametric equation of EI_1, D, depends linearly of the error in measurements w_1 and v_2. In the graph, the closer to the null curvature zone the measurement v_2, the higher the inclination of the denominator line. High inclinations of the lines might lead to estimations with no physical meaning as the errors in measurements lead to denominators close to zero or even negative. It is straightforward that the inertia obtained by this value of the denominator would tend to be infinite or negative. In FEM_2, the threshold error level for w_1 and v_2 to render the denominator null is quite high. Nevertheless, the threshold becomes lower with the decrease of the distance between the support and

node 2. Considering the error of w_1, a null denominator is obtained at the following error level: -16.1% (FEM_3), -8.7% (FEM_4), -5.2% (FEM_6), -2.3% (FEM_8) and -1.7% (FEM_{12}). It is suggested to take measurements in the non-null curvature zones to avoid the detrimental effect of the measurement errors on the accuracy of estimations.

Error by partial derivatives

In previous discussion, estimation of $\hat{I}_1$ in FEM_3 depends on errors in v_2 and w_1. With ε being the percentage error in the measurements, the error in $\hat{I}_1$, e_1, due to these two parameters can be calculated by the partial derivatives in Equation (3-16).

$$e_1 = \sqrt{\left(\frac{\partial \hat{I}_1}{\partial v_2}\varepsilon v_2\right)^2 + \left(\frac{\partial \hat{I}_1}{\partial w_1}\varepsilon w_1\right)^2} \tag{3-16}$$

, which can be used to get the deviation in $\hat{I}_1$. Using Equation (3-16), the deviation in $\hat{I}_1$ against error from -5% to 5% is summarized in Figure 3-6.

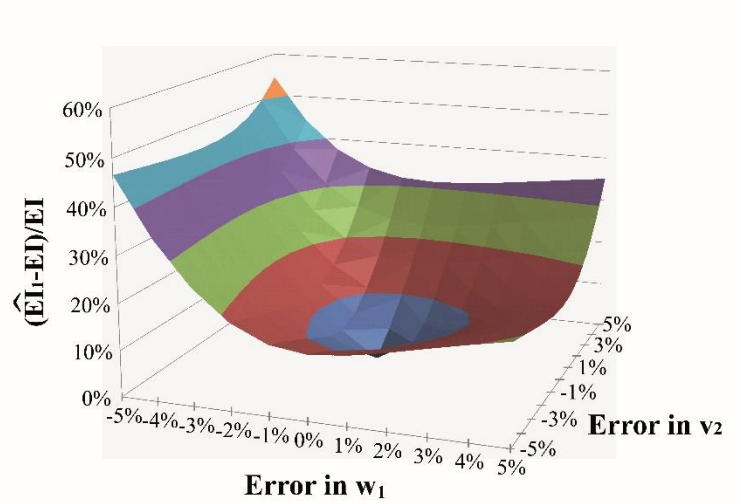

Figure 3-6 Deviation in I_1 calculated by partial derivatives

It can be seen the estimation of $\widehat{EI}_1$ is quite sensitive to errors in v_2 and w_1. Deviation will be magnified if the signs of the error in v_2 and w_1 are opposite. And the maximum deviation, 54.3%, is obtained for an error of +5% in v_2 and -5% in w_1.

Analysis of random errors in all measurements

In practice, measurement errors are inevitable. Furthermore, the actual magnitude of each error is unknown since it depends on a number of parameters including the accuracy of the measurement device. The errors of each measurement are usually assumed to follow a normal distribution. To illustrate the effects of actual errors, an

additional analysis is performed on FEM_3 in Figure 3-1, in which the inertias of the three elements are assumed as different and unknown. Three different measurement sets were analyzed here. The first of these sets (Set 1) is exclusively composed of nodal rotations, w_1, w_2 and w_3. The second set (Set 2) corresponds with that used in preceding sections, one rotation (w_1) and two deflections (v_2 and v_3). Finally, the third set (Set 3) only includes three deflections v_2, v_3 and v_5. As illustrated in Figure 3-7, the measurement of (v_5) corresponds with the vertical deflection at one intermediate node located at the first beam element.

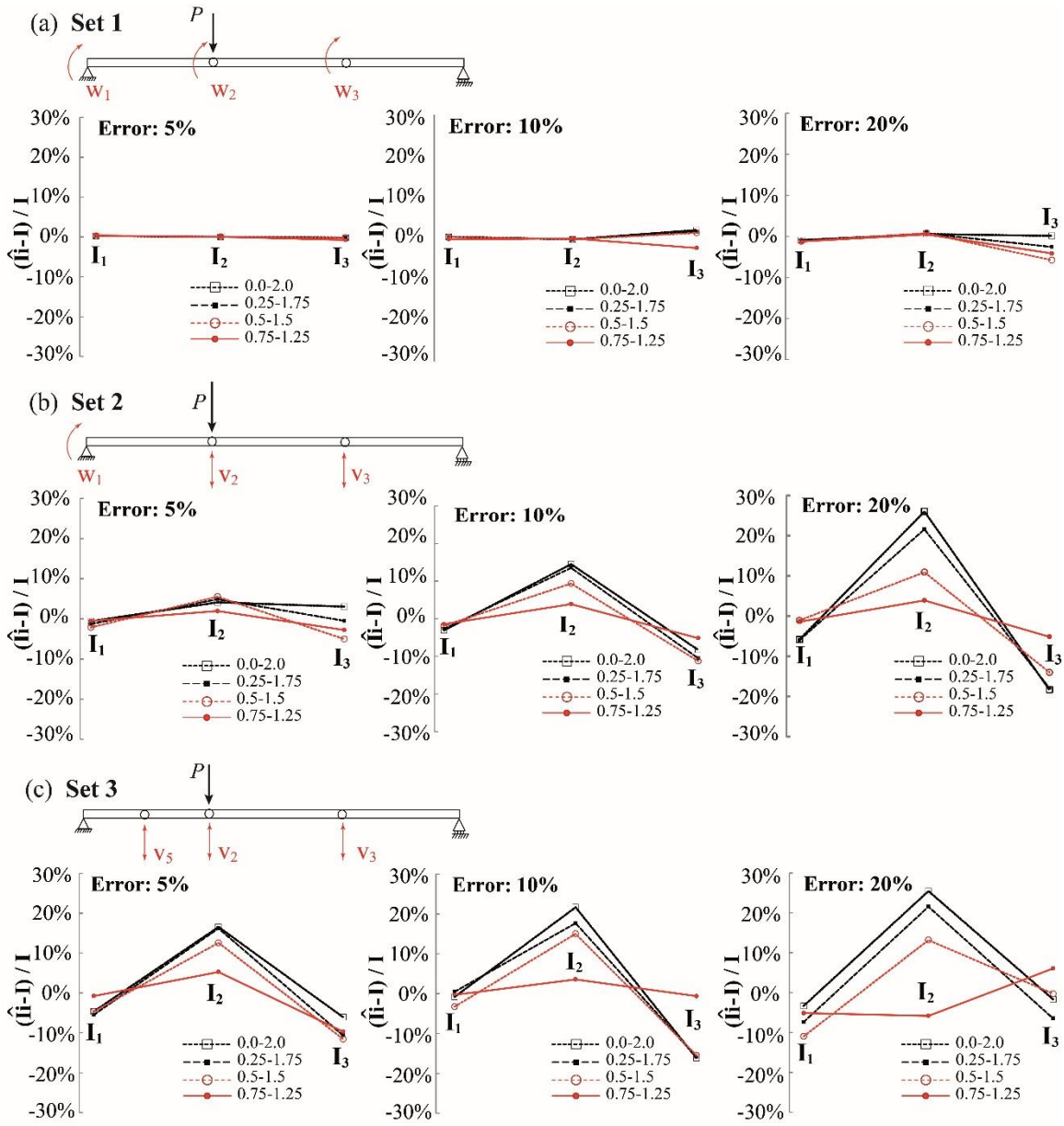

Figure 3-7 Percentage deviations between the estimated inertias, $\hat{I}_i$, and the actual ones, I, for random errors of 5%, 10% and 20% in Set 1(a), Set 2 (b) and Set 3(c), for different physical restrictions on the output. Each analysis is repeated with 200 admissible deformed shapes.

Each measurement sets includes three error levels, e={5%,10% and 20%}, which represent a percentage maximum deviation of the actual value of the measured variable. Equation (3-17) was used to introduce the errors in deflections. The noisy deflection at the i^{th} node, ve_i, is calculated from the error-free deflections, v_i, and the percentage error, e_0, which is the product of the assumed maximum magnitude of the error, e, and a random number, r. The random number r varies between -1.0 and 1.0 according to a truncated normal distribution of null mean and 0.5 standard deviation. A similar equation is used to introduce the errors into the measured rotations we_i.

$$ve_i = v_i + v_i \cdot e_0 = v_i + v_i \cdot r \cdot e \tag{3-17}$$

Random errors in measurements might lead to estimations with no physical meaning since these noisy measurements should satisfy some geometrical constraints. In FEM_3 from Figure 3-1, random errors in measurements might result in deformed shapes where the deflection of the node where the load is applied is not the maximum. In each of these analyses, the physical meaning of the deformed shape is analyzed by checking some geometrical restrictions. For this structure, the restrictions assumed are $ve_2 > ve_3$ and $we_1 < we_2 < we_3 < we_4$. The vertical deflection and rotation at the intermediate node ve_5 and we_5 are limited by those of the adjacent nodes. If any of these restrictions is not satisfied a new set of random measurements is obtained until the 200 admissible deformed shapes are obtained.

The ratios between the estimated inertia, $\hat{I}_i$, of the *ith* beam and the actual one, I, for different random errors in measurements are presented in Figure 3-7. As presented in the preceding section, the errors in measurements might lead to estimations with no physical meaning. This lack of meaning comes from those cases where the denominator of the parametric equation is close to zero. This problem can be avoided by adding some physical restrictions to the solutions of the system of equations. For example, in a damaged structure, the estimated inertias cannot be significantly higher than those of the undamaged elements (that is, estimated inertia cannot be twice as big as the original one). In addition, no negative inertias should be considered. In order to fulfill these restrictions, the results in Figure 3-7 include the average of those analyses where the estimations were bounded by: the 0 and 2 times the original inertia, 0.25 and 1.75 times the original inertia, 0.5 and 1.5 times the original inertia and 0.75 and 1.25 times the original inertia. In this figure, the results are named by the ranges as follows: 0.0-2.0, 0.25-1.75, 0.5-1.5 and 0.75-1.75, respectively. The percentages of analyzed structures satisfying these restrictions are presented in Figure 3-7.a (Set 1), b (Set 2) and c (Set 3).

From Figure 3-7, it is deduced that: 1) As expected, the higher the error in measurements, the higher the deviations in estimated inertias. In Set 2, the maximum errors for an error of 5% and a physical restriction of 0.0-2.0 are increased from 4.1% to 26.1% when the maximum random error in measurements is increased to 20%. 2) It is plausible that the smaller the range of allowable estimated inertias, the more accurate the estimations are. For example, in Set 2 with a random error of 20%, changing the allowed range of estimations from 0.0-2.0 to 0.75-1.25 reduces the deviations from 26.1%

to 2.2%. 3) The estimated parametersis less sensitive to errors in rotations than in deflections. This is appreciable when the results of the different measurement sets are compared. For example, considering a maximum random error of 5% and the physical restriction 0.0-2.0, the maximum errors when only rotations are considered (Set 1 with a deviation of -0.2% in I_3) is significantly lower than the one when w_2 and w_3 are substituted by v_2 and v_3 (Set 2 with a deviation of 3.1% in I_3). These deviations are increased more when only deflections are considered (Set 3 with a deviation of 16.5% in I_2). 4) Deviations in estimations are not increased throughout the recursive process as they fluctuate with the observability flow. In all analyzed sets described in Figure 3-7, the recursive process is initiated at the first beam element, $\hat{I}_1$. This value is used to estimate $\hat{I}_2$ and then, this new inertia is used to estimate $\hat{I}_3$. As illustrated in the Set 3 for an error of 5%, when $\hat{I}_1$ is underestimated, $\hat{I}_2$ is overestimated to compensate the effect of $\hat{I}_1$ into the system of equations. Conversely, the value of $\hat{I}_3$ is slightly underestimated. This fluctuation in the estimation of inertias is a peculiarity of the observability technique which will be analyzed in detail in the following section.

3.1.6 Errors in Parameter Estimation

To clarify the effects of different simulation errors, two examples of increasing complexity are analyzed in this section. The first example corresponds with a cantilever beam. In this example, the errors produced throughout the recursive process are analyzed. To avoid the effect of the curvature, a loading case with a uniform curvature distribution is proposed. In addition, to show the effect of the measurement errors, two different measurement precisions are adopted. The second example corresponds with a statically redundant beam. In this structure, the errors produced by the recursive process for a loading case that produces a uniform distribution of curvatures are studied first. Finally, to illustrate the effect of the curvature, an additional loading case with a non-uniform curvature distribution is simulated.

Analysis of the recursive process

Assume a cantilever beam with a concentrated bending moment, M=100 $kN{\cdot}m$ at the free end. This loading case induces uniform bending moments and curvatures as depicted in Figure 3-8.a. This curvature enables to focus the analysis on the errors produced by the recursive process. For this loading case the maximum deflections (5.11mm) occurs at the beam edge.

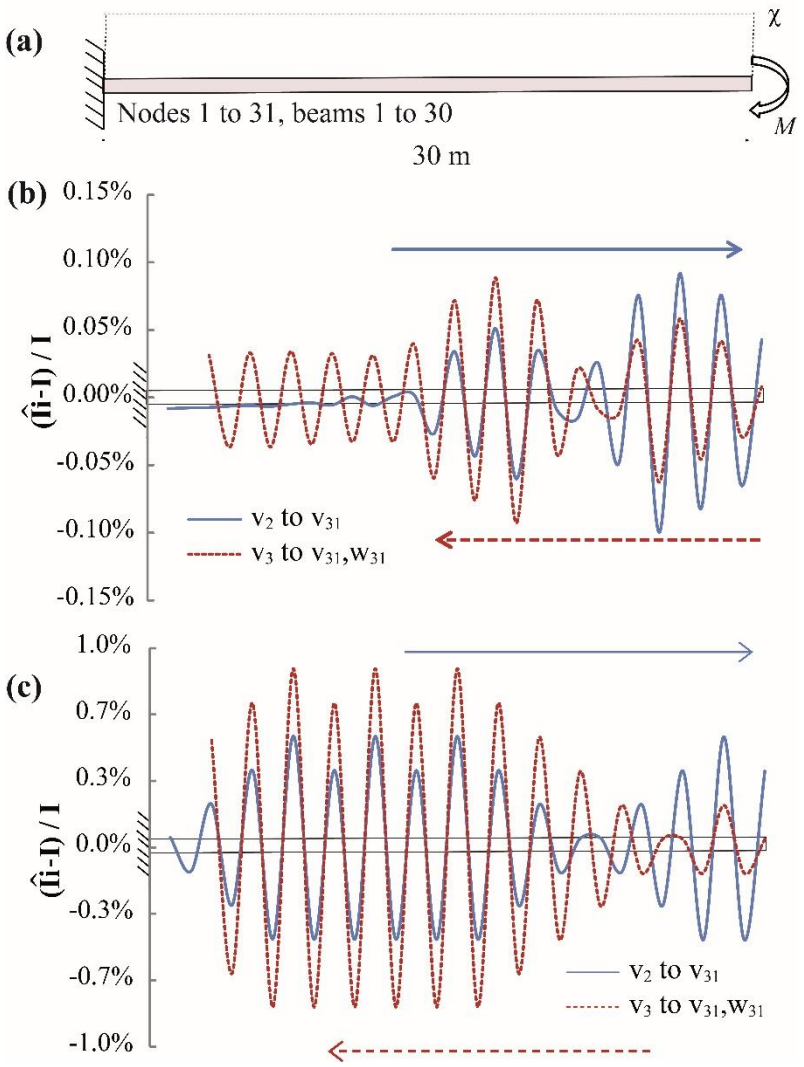

Figure 3-8 Example 1. a) Geometry of the cantilever beam, applied force and curvatures (b) Percentage deviations between the estimated inertias, $\hat{I}_i$, and the actual ones, I, for error free measurements (precision of 1e-9 m in v and 1e-9 rad in w). (c) Percentage deviation between $\hat{I}_i$ and I for traditional measurement errors (1e-5 m in v and 1e-5 rad in w). The arrows represent the direction in which the system of equations is solved (observability flow).

The mechanical properties of the structure correspond with those of the structure presented in (Abdo, 2012). The analyzed beam has a length of 30 m. The area and the inertia of the girder are 0.07 m^2 and 0.04 m^4, respectively and Young's of modulus is E=210 GN/m^2. The simplified FEM of this beam is composed of 31 nodes as presented in Figure 3-8.a. This assumption leads to a number of 30 elements 1m long. As mentioned previously, the flexural stiffnesses can be absorbed in inertias by assuming the Young's modulus as known. Here, these inertias are assumed both different and unknown. As the beam is horizontal, the axial and the flexural mechanisms are uncoupled and can be studied separately. However, only the analysis of the flexural behavior is presented here.

The values of the unknown inertias are estimated by the observability method from two alternative measurement sets derived by the observability trees (Jose Antonio Lozano-Galant et al., 2015). The first set is composed of 30 deflections, from v_2 to v_{31}, while the second one includes 29 deflections, from v_3 to v_{31}, and one rotation w_{31}. Each of these measurement sets solves the equations of the stiffness matrix system in a different sequence (or in other words, by a different observability flow). In the first set the solution of the system of equations starts at the clamped node and flows towards the beam edge in 30 steps. The opposite observability flow is obtained by the second measurement set. The observability flows are illustrated in Figure 3-8.b and c by continuous and dotted arrows, respectively.

Figure 3-8.b and c, respectively, include the percentage differences between the estimated inertia, $\hat{I}_i$, and the actual one, I, based on different error levels in measurement. Figure 3-8.b presents the results for error free measurements (with a precision of 1e-9 m in v and 1e-9 rad in w), while Figure 3-8.c presents the results with the measurement errors found in (precision of 1e-5 m in v (Lü, Liu, Zhang, & Zhao, 2012) and 1e-5 rad in w (Geoffrey & Mark, 2011)).

To solve the system of equations, the recursive process uses information from preceding steps. In this way, the value estimated of a certain rotation or inertia is used in the subsequent steps. It must be emphasized that it is intuitive to think, in the recursive process, that errors will accumulate and propagate, and thus the parameters identified in the final steps will contain significant error. Conversely, this is not the case in the observability techniques. As depicted in Figure 3-8.b, it is shown that for the first set (continuous blue line) the initial error of -0.01% is increased to 0.04% at the end of the beam. A similar phenomenon can be observed for the second set (dotted red line), where the initial deviation of -0.01% is increased to -0.02% at the proximities of the clamped node. In fact, when an estimated inertia is slightly higher than the actual one (i.e. overestimation), the next estimated inertia tends to be slightly underestimated in order to compensate the overestimation in preceding step. This effect leads to the fluctuation of error. However, this fluctuation might produce even higher errors in some middle steps of the recursive process than the one obtained at the final step. For example, in the first flow, the maximum deviation (0.09% in element 26) is 2.14 times higher than the error obtained at the end of the recursive process. The same effect appears in Figure 3-8.c. Nevertheless, in this case, because of the error in measurements, higher fluctuations are obtained. For error free measurements, the maximum deviations are observed at I_7 for the first set (v_3 to v_{31} and w_{31}). The obtained estimation at this point represents the 0.55% of I. This value is 46.1% higher than the value obtained at the end of the recursive process (0.38%).

Analysis of the effects of the curvature

The second structure corresponds with the two-span continuous beam presented in

Figure 3-9.a. This beam has a 60-m length and is evenly divided into 60 elements. The material and mechanical properties are the same as those used in the preceding section. Again, the Young's modulus and the areas are assumed as known whereas the inertias are assumed as different and unknown for each element. This structural system identification problem was presented in (Abdo, 2012). Later, Nogal et al. (Nogal et al., 2015) used this example to illustrate the different simulation errors that might appear in observability techniques. The aim of this example is to extend that study, and to provide a better understanding of the nature and magnitude of the different simulation errors when observability techniques are applied.

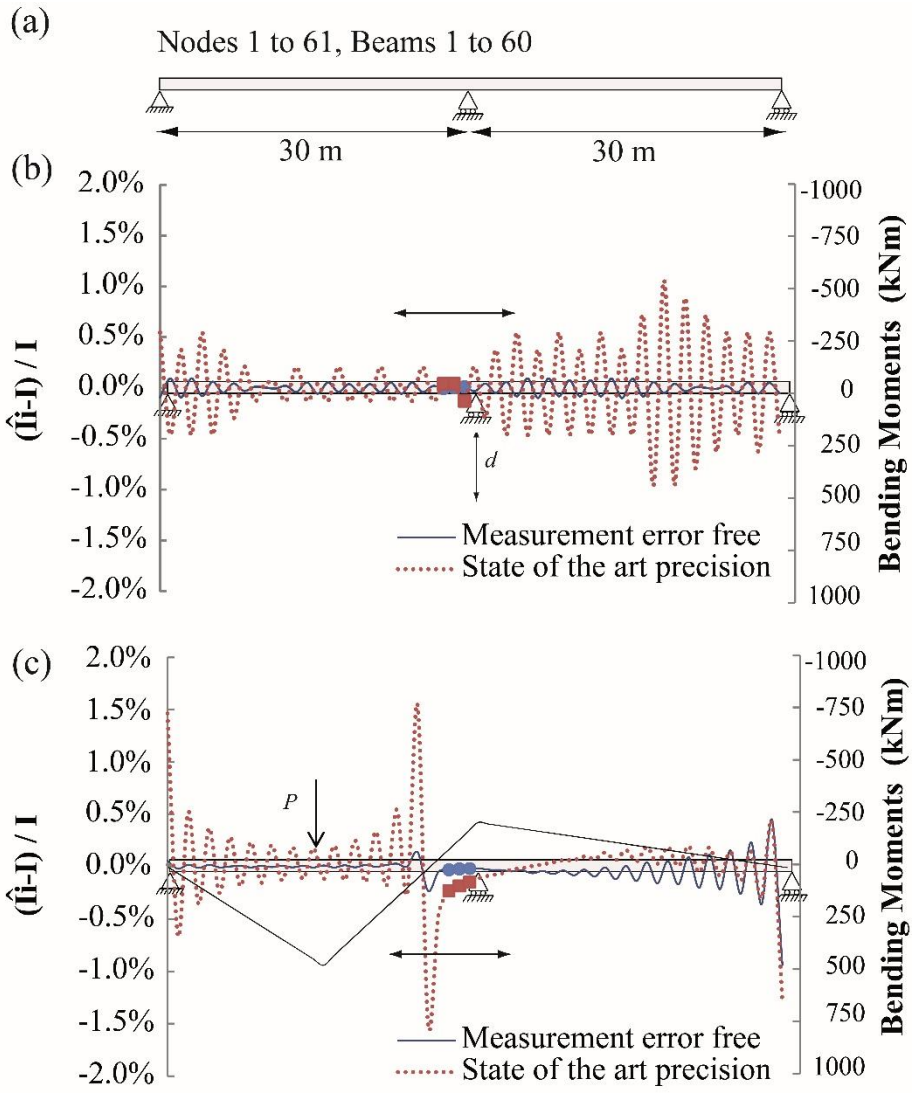

Figure 3-9 Analysis of the effects of the curvature. (a) Geometry of the two-span beam. (b) Loading case 1: Percentage deviations between the estimated inertias, $\hat{I}_i$, and the actual ones, I for different measurement errors. (c) Loading case 2: Percentage deviation between $\hat{I}_i$ and I for different measurement errors. The solid arrows represent the direction in which the system of equations is solved (observability flow).

To estimate the 60 unknown inertias, two different loading cases are studied. The first case includes two concentrated bending moments, M=1000 $kN{\cdot}m$, at the beam edges and a settlement of 5.4 mm at the inner support. This loading case induces, as presented in Figure 3-9.b, a constant bending moment in the structure. The second loading case corresponds with a concentrated vertical load V=-100 kN applied at node 16 as presented in Figure 3-9.c, which produces a linear diagram of bending moments with a maximum (500 $kN{\cdot}m$) at node 16 and a minimum (-250 $kN{\cdot}m$) at node 31 and null values at the vicinity of node 23.

The measurement set in both loading cases is identical and includes 58 deflections (v_1 to v_{30} and v_{32} to v_{60}) and 2 rotations (w_{29} and w_{30}). This measurement set initiates an observability flow at the left hand side of the inner support that is propagated towards both beam edges. The direction of this flow is indicated by the arrows in Figure 3-9.b and c, respectively. In the first recursive step, three inertias ($\hat{I}_{28}$, $\hat{I}_{29}$ and $\hat{I}_{30}$) are observed. The rest of the inertias are successively estimated after 30 steps. The parameters estimated in the first recursive steps are highlighted in these figures by a circle.

The deviations between the actual inertia, I, and the estimated one, $\hat{I}_i$, in each beam element i are summarized in Figure 3-9.b and c. In these figures, the results obtained by the error free measurements (precision 1e-9 m in v and 1e-9 rad in w) and the state of the art errors (1e-5 m in v and 1e-5 rad in w) are presented in different colors.

Figure 3-9.b shows that when a uniform curvature is applied, the errors of the estimations are not increased monotonically throughout the recursive steps. In effect, the deviations from the actual stiffnesses present similar fluctuations to those observed in the cantilever beam. For the error free measurements, the maximum deviation error in the first recursive step (-0.01% in I_{28}) is increased to 0.1% in I_{37} throughout the analysis. In the structures with measurement errors, the fluctuations are slightly more significant since the initial errors (-0.13% in I_{30}) are increased to 1.1% in I_{40}.

Figure 3-9.c illustrates the importance of the curvature in the identification by the observability. In fact, the maximum errors are obtained in those areas with null curvatures (specifically at x=0, x=27 and x=60 m). This effect can be explained by the fact that the bending stiffness is calculated based on the curvature of the beam elements imposed by the loading case. As a result, higher errors appear at those locations with low curvatures. As expected, the maximum deviation (1.52%) is found at x=27 m, which is adjacent to the inflection point of the moment diagram. In this structure, the effects of the magnitude of the curvature are slightly higher than those of the recursive process. To avoid the detrimental effects of the low curvature, adequate loading cases are advised for structural system identification by observability techniques.

3.1.7 Conclusions

This paper analyzes the effects of two unavoidable sources of errors upon the structural system identification by observability techniques. The first of these sources refers to the measurement errors. To simulate this error, the parametric equations of the estimated inertias were analyzed in detail in a simply supported beam. The analysis of this structure shows that: (1) Estimations in subsequent recursive steps depend on the values estimated in preceding steps. As an academic example it is showed that considering an error in single measurement increases the errors in the estimations throughout the recursive process. This effect is significantly mitigated when errors in all measurements are considered. (2) Parametric equations of the estimated parameters can be obtained. These equations are very useful to study the sensitivity of the estimated parameter. In order to make the estimations less sensitive to the errors, it is recommended to use measurements closer to the load location. The numeric analysis shows that the estimations of stiffnesses are less sensitive to errors in rotation measurements than errors in deflection measurements. This parametric approach enables the use of partial derivatives in the error analysis. (3) The loading case is of primary importance. Usually the closer the load location of the concentrated load to the inertia to be estimated the lower the sensitivity of the estimation to measurement errors. This also corresponds to the fact that, for the same loading case, the closer the location of the measurement to the boundary condition, the lower the curvature. (4) The denominator of the parametric equations of the estimated inertia depends, to a large extent, on the measurement errors. Denominators with a value close to zero lead to solutions with no physical meaning. (5) Those estimations based on the measured deflections are asymmetric. Furthermore, the asymmetry in estimates is increased throughout the recursive process. On the other hand, the second analyzed source of error refers to those simulation errors inherent in the observability analysis. To illustrate these effects two structures of growing complexity were analyzed. The simulation of these structures shows that: (1) Fluctuations in the inertias estimated are obtained because of the recursive process. This can be explained by the fact that every time that a certain inertia is underestimated, the next inertia that uses this information will tend to be overestimated to compensate the effect of the preceding one in the system. (2) The curvature of the beam plays an important role in the accuracy of the estimations. In fact, wrong estimations are obtained near points with null curvatures. The effect of the curvature requires an adequate selection of the loading cases for structural system identification by observability techniques.

3.2 Constrained observability method in static structural system identification

Title: Constrained observability method in static structural system identification

Authors: Jun Lei, María Nogal, José Antonio Lozano-Galant, Dong Xu, José Turmo

Journal: Structural Control and Health Monitoring

Publication: Technical Paper

Submitted: 26 July, 2016

Accepted: 21 April, 2017

DOI: http://dx.doi.org/10.1002/stc.2040

Available at: https://onlinelibrary.wiley.com/doi/abs/10.1002/stc.2040

3.2.1 Summary

Identifiability of parameters in Structural System Identification (SSI) is of primary importance in any SSI method. It depends on the number and the location of the measurements, which are linked with sensor configuration. In this paper, under the framework of SSI by Observability Method (OM), the number of necessary measurements to identify all parameters of a structural system was clarified first. Then an example was solved step by step to show the lacking constraints among unknowns in SSI by OM. In a frame example, it was found that no measurement set having as many measurements as the number of unknowns was able to identify all parameters. To further understand this phenomenon, the observability of a simply supported beam was analyzed in an exhaustive way using 252 possible measurement sets. Three quarters of these sets were not able to identify all the parameters. In order to solve this issue, for the very first time, SSI by Constrained Observability Method (COM), which appends the nonlinear constraints to SSI by OM, was proposed. With SSI by COM applied, the observability of structural parameters with respect to the 252 sets was greatly improved. Finally, the efficacy of COM was verified by a 13-storey frame building.

Keyword: structural system identification; stiffness method; observability method; nonlinear constraint; essential set; static

3.2.2 Introduction

Structural System Identification (SSI) has long been an intriguing topic in civil engineering. It can be conceptualized as the process of simulating structural behavior by mathematical models. Based on the type of the excitation, SSI methods are categorized as static (Chisari et al., 2015; Kao & Loh, 2013; Jose Antonio Lozano-Galant et al., 2015; M Sanayei & Saletnik, 1996a; Terlaje & Truman, 2007; Brian J. Walsh & González, 2009) or dynamic (J.P. Amezquita-Sanchez & Adeli, 2016; Breuer,

Chmielewski, Górski, Konopka, & Tarczyński, 2015; Dowling, Obrien, & González, 2012; Z. Li, Park, & Adeli, 2017). The dynamic SSI requires the use of mass, stiffness and damping properties while the static method only requires the use of stiffness properties (Bakhtiari-Nejad et al., 2005). When only the estimation of stiffnesses is targeted, static SSI might be more interesting than dynamic SSI in some cases (Masoud Sanayei et al., 1997). In non-destructive tests of bridges, slow moving loads can be applied as quasi-static loads (Boumechra, 2017; Kim et al., 2003; C. Wang, Huang, & Chen, 2011). Providing that the structure behaves linearly, Maxwell law of reciprocal deflections can be applied to reduce the number of sensors in the structure under moving load (Choi, Lee, Choi, & Cho, 2004; Kim et al., 2003). The irregular variations in curvatures, which are obtained from the displacement influence lines between the damaged and undamaged structures under moving load, can be used to locate the damages (Z. Sun, Nagayama, & Fujino, 2016; C. Wang et al., 2011). (Boumechra, 2017) approximated the inverse of the global stiffness matrix by a Neumann series and used optimization technique to find the optimal correction coefficients of structural parameters such that the predicted response from these parameters are closest to the measured static response under moving loads. This method can accurately localize and quantify the damage with the displacements of selected nodes. (Choi et al., 2004) derived the elastic damage load theorem for statically determinate beam and applied it to locate the damage by checking the variation in the shape of deflection. However, this method is limited to statically determinate structures and cannot quantify the extent of damage.

SSI methods can be also classified as physics-based (e.g. finite element models [FEMs]) or non-physics based models (neural networks models (Jiang et al., 2007; Santos et al., 2015), autoregressive models (Bao, Hao, & Li, 2013; Mei, Mita, & Zhou, 2016) or rational polynomial models (Ku, Tamura, Yoshida, Miyake, & Chou, 2013)). The parameters of physics-based models represent the structural characteristics, e.g. elastic modulus, inertias, mass, while the parameters of the non-parametric models are weight factors of the adopted basis functions, which have no physical meaning and are determined by minimizing the discrepancy between the predicted structural response and the measured response. From a statistical perspective, SSI methods can be categorized as probabilistic methods (Dowling et al., 2012; González, Covián, Casero, & Cooper, 2013; B.J. Walsh, González, & Cantero, 2014; Brian J. Walsh & González, 2009) or deterministic methods (Bakhtiari-Nejad et al., 2005; J. Lei, Lozano-Galant, Nogal, Xu, & Turmo, 2017; Jose Antonio Lozano-Galant, Nogal, et al., 2013). In probabilistic SSI (Dowling et al., 2012; González et al., 2013; B.J. Walsh et al., 2014; Brian J. Walsh & González, 2009), structural parameters are treated as random variables and their distributions can be specified using prior knowledge. Structural parameter sets can be generated by sampling each of these distributions. The goodness of any parameter set is represented by the closeness between the response predicted by that parameter set and the measured response. This goodness is incorporated into the assumed distribution to obtain the distribution of the estimated parameters. The

probabilistic methods not only provide the estimation of the parameters but also a measure of confidence in the estimates. However, their computation cost increases exponentially with the number of parameters due to the combinatorial consideration in sampling distributions. The deterministic methods try to pinpoint a best model yielding the closest response to the measured one. The main drawback of these methods is that the measure of confidence in the estimates is lacking in the theoretical formulation. However, this might be overcome by analyzing the estimates obtained from measurement data generated by Monte-Carlo method.

A vital issue for any SSI method is whether the parameters are identifiable or not given a particular measurement set. This can be addressed by Observability Method (OM) (Enrique Castillo et al., 2007). OM provides the information whether all the unknowns or a subset of the unknowns can be uniquely determined or not. Its application in parameter estimation includes water transport network (Díaz et al., 2016), traffic network (Enrique Castillo, Nogal, Rivas, & Sánchez-Cambronero, 2013) or power systems (Abur & Exposito, 2004). SSI by OM is a deterministic static SSI method first introduced by (Jose Antonio Lozano-Galant, Nogal, et al., 2013), which has the advantage of less computation cost than statistical methods. In this method, the system of equations is derived by algebraic operations on the nodal equilibrium equations using direct stiffness method, which makes SSI by OM a physics-based method. The efficacy of this method was verified by its application in the identification of the structural parameters of trusses, beams, frames (Jose Antonio Lozano-Galant, Nogal, et al., 2013). Also, it was applied in cable-stayed bridges (Jose Antonio Lozano-Galant et al., 2014), wherein the structural audacity and lightness makes these structures sensitive to dynamic and static loading cases in both service and construction stage (Jose Antonio Lozano-Galant, Dong, Payá-Zaforteza, & Turmo, 2013; José Antonio Lozano-Galant & Turmo, 2014). It can also help the decision making during the maintenance of structures (Enrique Castillo, Lozano-Galant, Nogal, & Turmo, 2015).

The identifiability of the structure by any method relies on a good selection of measurements. More measurements are generally desirable for the identifiability of parameters. On the converse, fewer sensors means less instrumental, operational costs and data processing. Considering the extended dimension of structures, the economic reasons and the accessibility, a practical question is how to find the optimal number of measurements and the location of the sensors for successful identifications. A similar issue was addressed in power system using OM (Abur & Exposito, 2004). In a power system specified by n parameters, the question is posed as how to choose measurement sets from m ($m>n$) available measurements to identify the system. If a measurement set of n measurements is able to identify all the n parameters and the drop of any measurement fails to do so, then this set is defined as essential set. Generally, such a set is not unique. The function of OM is twofold: (1) In the preliminary stage, find an essential set to ensure that all parameters can be identified; (2) In the operation stage, determine the observability of these parameters in case of the malfunction of any

measuring device. In the context of SSI, if the number of measurements was less than the number of unknown parameters, the system would become indeterminate (Bakhtiari-Nejad et al., 2005; M Sanayei & Saletnik, 1996a), i.e. only a subset of the parameters might be identified. Moreover, even if the number of measurements equals to the number of unknowns, if those are not properly chosen, the system might still be indeterminate. An increase in measurements or a better placement of sensors can lead to an increase in the number of identified parameters, which is referred as increase of observability in this paper. Eventually, this process will lead to the identification of all parameters, which is referred as full observability.

A wide range of proposals and methods dealing with the placement of sensors in SSI can be found. (Masoud Sanayei, Onipede, Babu, & Babuj, 1992) used a heuristic method to seek near-optimal placement of sensors for structures under non-destructive tests. (M. Chang & Pakzad, 2014) compared several sensor placement strategy including effective influence method, driving point residue kinetic energy method and modified variance method. (H. Jin, Xia, & Wang, 2015) applied an improved harmony search optimization algorithm and the modal assurance criterion to find the optimal sensor placement to identify modal parameters. (Malings & Pozzi, 2016) proposed the sensor placement as an optimization problem with respect to the conditional entropy and the value of information. However, the majority of the existing literature on measurement selection focuses on dynamic SSI. In static SSI by OM, the identifiability of the structural parameters also relies on a proper measurement selection. (Jose Antonio Lozano-Galant et al., 2015) proposed the observability tree method to select measurement set. This method can graphically analyze the sequence of identified parameters during the recursive steps of SSI by OM. It was found that improper selection of the measurement set cuts off the observability flow and thus fails to identify all the unknowns even with more measurements than unknowns. However, the reason for this failure is not clear and the solution was not found at that time. For the aforementioned reasons, the aim of this paper is twofold: (1) to clarify the underlying reason why some measurement sets expected to be able to identify all structural parameters turn out to be incapable of doing so in SSI by OM and (2) to provide a method to alleviate or solve this problem.

The rest of this paper is organized as follows. In section 3.2.3, the essential set is conceptualized first and two examples are used to illustrate the deficiency of SSI by OM. Then the observability of the structural parameters in a simply supported beam is analyzed in an exhaustive way for 252 enumerated measurement sets. From the result, two reasons of the unqualification of some measurement sets to be essential sets are revealed. In the following section, Constrained Observability Method (COM) is proposed as the solution to this problem. The effectiveness and robustness of COM is justified by the improvement of observability on the two examples proposed in section 3.2.3 Next, in section 3.2.5, a 13-storey frame is studied to illustrate the strength of COM. Finally, some conclusions are drawn in section 3.2.6.

3.2.3 Inadequacy of OM

From direct stiffness method, the nodal equilibrium equations for 2D beam models can be expressed as:

$$K \cdot \delta = f \tag{3-18}$$

where the global stiffness matrix K contains the information of flexural stiffness, EI_j, axial stiffness, EA_j, length L_j and the element connectivity. The displacements vector δ contains the horizontal, vertical and rotational displacements of node i, i.e. u_i, v_i and w_i. The external force vector f contains the horizontal forces, vertical forces and moments applied on node i, i.e. H_i, V_i and M_i.

Once the geometry, the boundary conditions and the loading case are specified, then the nodal displacements δ will be uniquely determined by any parameter set. In the case of N_A unknown axial stiffnesses and N_F unknown flexural stiffnesses, this is saying that these N_A+N_F mechanical parameters uniquely specify a set of displacements of the structure. In the inverse analysis, due to the linearity of this system, N_A+N_F measurements are expected to be sufficient to identify all parameters. For simplicity, the ability to identify all parameters of the structure is referred as full observability in this paper. If merely a subset of these parameters are identifiable, then it is referred as partial observability. Hence, in the essential sets (the sets containing the necessary and sufficient number of measurements to achieve full observability), the number of required measurements is N_A+N_F. However, this statement has been verified elsewhere (Jose Antonio Lozano-Galant et al., 2015) and it was found that full observability might not be achieved with $N_A + N_F$ measurements due to improper selection of the measurements, which is related with the placement and type of measuring devices. Previous explanation was that the recursive steps stopped too early without identifying all parameters. However, the underlying cause for this premature end of the recursive steps was not uncovered at that time. This is one of the major interests of this paper, which can also be employed for the sensor placement strategy.

For practical reason, Equation (3-18) can be transformed as:

$$B \cdot z = D \tag{3-19}$$

Equation (3-19) is the result of applying static condensation technique together with the separation of each column, with regard to different unknowns, into several columns and the merger (addition) of those resultant columns related with the same unknowns in the equilibrium equations (Equation (3-18)). After these algebraic operations, all the known quantities are collected in the coefficient matrix B and the vector D. Hence, B and D are known. The unknown vector z is always of two types: (1) monomials of degree one, e.g. $\{EA_j,\ EI_j,\ u_i,\ v_i, V_i$ and $M_i\}$, or (2) monomials of degree two, e.g. $\{EI_j u_i$ and $EA_j v_i\}$. Note that both, EA_j and EI_j are regarded as monomials of degree one. (For more technical details, readers are strongly recommended to review (Jose Antonio Lozano-Galant, Nogal, et al., 2013; Nogal et al., 2015). The occurrence of these

components of the unknown z is due to the fact that Equation (3-19) is essentially established by nodal force equilibrium.

If the vertical deflection, v_i, or the rotation, w_i, appearing in these products, $EI_j v_i$ or $EI_j w_i$, are measured, then the flexural stiffness, EI_j, will be uncoupled and separated from those and the vertical deflection v_i or the rotation w_i will be absorbed in B. Otherwise, these products will appear in z in the form of monomials with degree of two and, as per requirements of OM, be regarded as linear in z. This is to say, even though the physical unknowns for a given problem might be EI_j and w_i. z may contain three different unknowns EI_j, w_i and $EI_j w_i$. Due to the limit of sensor investment, it is not likely to measure all displacements in the structure. Consequently, these products, $EI_j w_i$ or $EI_j v_i$, and the flexural stiffness, EI_j, which is obtained by the uncoupling of these products, all appear in the unknown z. Likewise, the simultaneous occurrence of $EA_j u_i$ and EA_j is ascribed to the nodal equilibrium of axial forces. Furthermore, it is worth mentioning that in frame structures, due to the coupling of the axial displacements and the vertical deflections from different members, the product of axial stiffness and vertical deflection, $EA_j v_i$ and the product of flexural stiffness and axial displacement, $EI_j u_i$, also appear in z. From a mathematical point, if the unknowns of a system are coupled, then they should satisfy certain constraints. Nevertheless, this requirement is not satisfied in SSI by OM and therefore sometimes leads to the failure to identify all parameters (achieve full observability).

In order to clarify this deficiency from the lack of constraints in SSI by OM, a 4-node simply supported beam (Figure 3-10) is studied here. This analysis also sheds light on the peculiarity of this method. For brevity, it is assumed that the flexural stiffnesses of elements 1 and 3, EI_1 and EI_3, the length of element, L, and the external vertical load at node 2, V_2, are known. Since the axial stiffness is not activated by this loading case, hence N_A=0 and the terms associated with axial behavior are removed from the general equation by OM. Thus, the target parameter is the flexural stiffness of the element 2 (in red), EI_2, i.e. N_F=1. Then one measurement suffices to achieve full observability since N_A+N_F=1. Assume the vertical deflection of node 2, v_2, is measured.

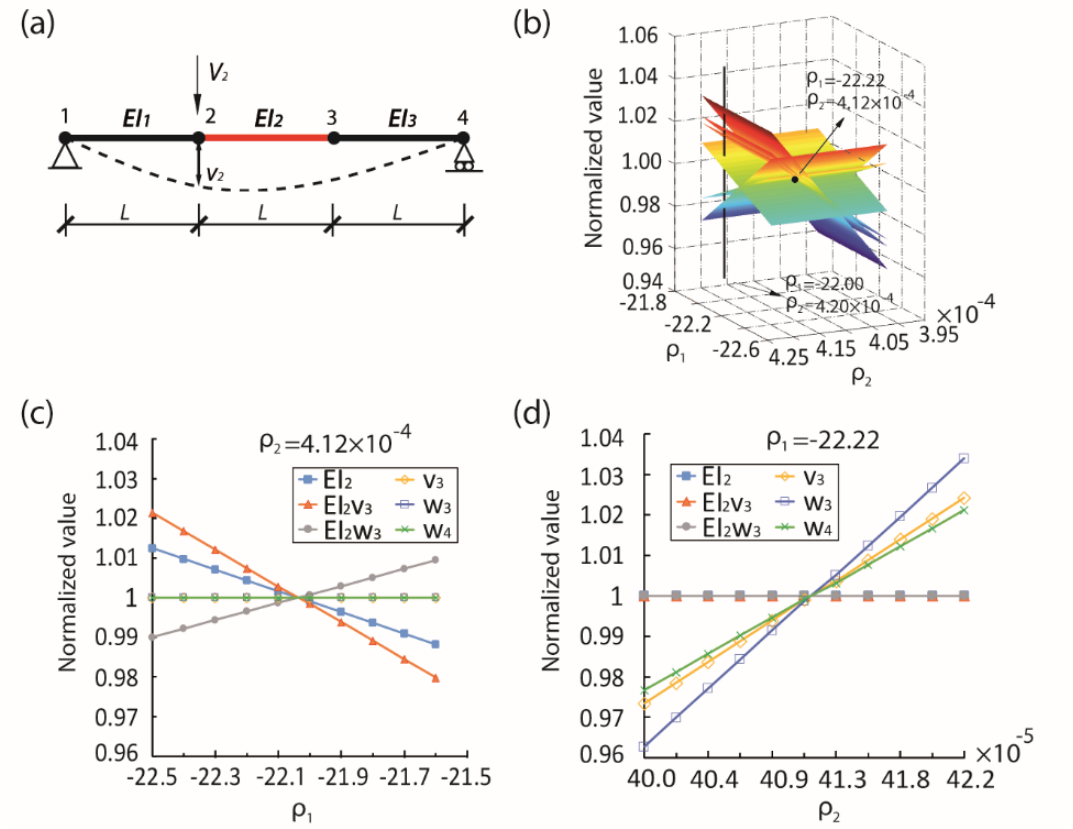

Figure 3-10 (a) FEM of the 4 - node simply supported beam; (b) geometric explanation of the null space; (c) variation of the normalized estimates with the variation of ρ_1 when ρ_2=4.12×10^{-4}; (d) variation of the normalized estimates with the variation of ρ_2 when ρ_1=-22.22.

In the first step, the system of equations given by OM is as follows:

$$B_1 \cdot z_1 = \begin{pmatrix} 0 & 0 & 0 & 0 & 0 & 0 & 0 & \frac{4EI_1}{L} & \frac{2EI_1}{L} & 0 & 0 \\ \frac{12v_2}{L^3} & -\frac{12}{L^3} & \frac{6}{L^2} & \frac{6}{L^2} & 0 & 0 & 0 & -\frac{6EI_1}{L^2} & -\frac{6EI_1}{L^2} & 0 & 0 \\ \frac{6v_2}{L^2} & -\frac{6}{L^2} & \frac{4}{L} & \frac{2}{L} & 0 & 0 & 0 & \frac{2EI_1}{L} & \frac{4EI_1}{L} & 0 & 0 \\ -\frac{12v_2}{L^3} & \frac{12}{L^3} & -\frac{6}{L^2} & -\frac{6}{L^2} & 0 & 0 & \frac{12EI_3}{L^3} & 0 & 0 & \frac{6EI_3}{L^2} & \frac{6EI_3}{L^2} \\ \frac{6v_2}{L^2} & -\frac{6}{L^2} & \frac{2}{L} & \frac{4}{L} & 0 & 0 & \frac{6EI_3}{L^2} & 0 & 0 & \frac{4EI_3}{L} & \frac{2EI_3}{L} \\ 0 & 0 & 0 & 0 & 0 & 0 & \frac{6EI_3}{L^2} & 0 & 0 & \frac{2EI_3}{L} & \frac{4EI_3}{L} \\ 0 & 0 & 0 & 0 & -1 & 0 & 0 & \frac{6EI_1}{L^2} & \frac{6EI_1}{L^2} & 0 & 0 \\ 0 & 0 & 0 & 0 & 0 & -1 & -\frac{12EI_3}{L^3} & 0 & 0 & -\frac{6EI_3}{L^2} & -\frac{6EI_3}{L^2} \end{pmatrix} \cdot \begin{pmatrix} EI_2 \\ EI_2v_3 \\ EI_2w_2 \\ EI_2w_3 \\ V_1 \\ V_4 \\ v_3 \\ w_1 \\ w_2 \\ w_3 \\ w_4 \end{pmatrix} = \begin{pmatrix} M_1 + \frac{6EI_1v_2}{L^2} \\ V_2 - \frac{12EI_1v_2}{L^3} \\ M_2 + \frac{6EI_1v_2}{L^2} \\ V_3 \\ M_3 \\ M_4 \\ 0 \\ \frac{12EI_1v_2}{L^3} \\ 0 \end{pmatrix} = D_1 \quad (3\text{-}20)$$

In Equation (3-20), it is seen that the vertical deflection v_2, flexural stiffnesses EI_1 and EI_3 are absorbed in the matrix B_1 and the vector D_1. The solution of this system can be expressed as the sum of a particular solution z_{p1} and any linear combination of the bases in the null space of B_1 (i.e. V_{n1}),as presented in Equation (3-21).

$$z_1 = z_{p1} + V_{n1} \cdot \boldsymbol{\rho_1} = \begin{pmatrix} EI_2 \\ EI_2 v_3 \\ EI_2 w_2 \\ EI_2 w_3 \\ \boldsymbol{V_1} \\ \boldsymbol{V_4} \\ v_3 \\ \boldsymbol{w_1} \\ \boldsymbol{w_2} \\ w_3 \\ w_4 \end{pmatrix}_{p1} + \begin{pmatrix} 1 & -\frac{L}{v_2} & 0 \\ \frac{1}{v_2} & & \\ 1 & 0 & 0 \\ 0 & 1 & 0 \\ 0 & 1 & 0 \\ \boldsymbol{0} & \boldsymbol{0} & \boldsymbol{0} \\ \boldsymbol{0} & \boldsymbol{0} & \boldsymbol{0} \\ 0 & 0 & -L \\ \boldsymbol{0} & \boldsymbol{0} & \boldsymbol{0} \\ \boldsymbol{0} & \boldsymbol{0} & \boldsymbol{0} \\ 0 & 0 & 1 \\ 0 & 0 & 1 \end{pmatrix} \cdot \begin{pmatrix} \rho_{1,1} \\ \rho_{1,2} \\ \rho_{1,3} \end{pmatrix} \tag{3-21}$$

This particular solution and the bases of the null space can be obtained by many commercial packages, e.g. Matlab and Maple. From Equation (3-21), it is seen in the null space of the matrix B_1 i.e. V_{n1}, the rows associated with $\{V_1,\ V_4,\ w_1$ and $w_2\}$, are all null and their values are not affected by the coefficients $\rho_{1,1},\ \rho_{1,2}$ and $\rho_{1,3}$. Hence they are constant, unique, known and observable. Note that z_1 contains $\{EI_3,\ w_2,\ v_3,\ EI_2 w_2$ and $EI_2 w_3\}$, and these unknowns should satisfy certain nonlinear constraints, e.g. $\{EI_2 v_3 = EI_2 \cdot v_3\}$. However, as linearity is assumed, these constraints are not considered in SSI by OM yet, which leads to the failure of the identification of EI_2.

In the next recursive step, the unknowns observed previously are incorporated into the input of SSI by OM. This is, the new input for this recursive step $\{w_1,\ w_2,\ v_2, V_1$ and $V_4\}$ are regarded as known. Note that this new input will update Equation (3-19) and thus new parameters might be observed. The updated system of equations obtained in the next recursive step is as follows:

$$B_2 \cdot z_2 = \begin{pmatrix} 0 & 0 & 0 & 0 & 0 & 0 \\ \frac{12v_2}{L^3} + \frac{6w_2}{L^2} & -\frac{12}{L^3} & \frac{6}{L^2} & 0 & 0 & 0 \\ \frac{6v_2}{L^2} + \frac{4w_2}{L} & -\frac{6}{L^2} & \frac{2}{L} & 0 & 0 & 0 \\ -\frac{12v_2}{L^3} - \frac{6w_2}{L^2} & \frac{12}{L^3} & -\frac{6}{L^2} & \frac{12EI_3}{L^3} & \frac{6EI_3}{L^2} & \frac{6EI_3}{L^2} \\ \frac{6v_2}{L^2} + \frac{2w_2}{L} & -\frac{6}{L^2} & \frac{4}{L} & \frac{6EI_3}{L^2} & \frac{4EI_3}{L} & \frac{2EI_3}{L} \\ 0 & 0 & 0 & \frac{6EI_3}{L^2} & \frac{2EI_3}{L} & \frac{6EI_3}{L} \\ 0 & 0 & 0 & 0 & 0 & 0 \\ 0 & 0 & 0 & -\frac{12EI_3}{L^3} & -\frac{6EI_3}{L^2} & -\frac{6EI_3}{L^2} \end{pmatrix} \cdot \begin{pmatrix} EI_2 \\ EI_2 v_3 \\ EI_2 w_3 \\ v_3 \\ w_3 \\ w_4 \end{pmatrix} = \begin{pmatrix} M_1 + \frac{6EI_1 v_2}{L^2} - \frac{4EI_1 w_1}{L} - \frac{2EI_1 w_2}{L} \\ V_2 - \frac{12EI_1 v_2}{L^3} + \frac{6EI_1 w_1}{L^2} + \frac{6EI_1 w_2}{L^2} \\ M_2 + \frac{6EI_1 v_2}{L^2} - \frac{2EI_1 w_1}{L} - \frac{4EI_1 w_2}{L} \\ V_3 \\ M_3 \\ M_4 \\ V_1 + \frac{12EI_1 v_2}{L^3} - \frac{6EI_1 w_1}{L^2} - \frac{6EI_1 w_2}{L^2} \\ V_4 \end{pmatrix} = D_2 \tag{3-22}$$

The null space, V_{n2}, of the matrix B_2 and the general solution of Equation (3-22), z_2, are given as:

$$z_2 = z_{p2} + V_{n2} \cdot \boldsymbol{\rho_2} = \begin{pmatrix} EI_2 \\ EI_2 v_3 \\ EI_2 w_3 \\ v_3 \\ w_3 \\ w_4 \end{pmatrix}_{p2} + \begin{pmatrix} \frac{1}{w_2} & 0 \\ \frac{v_2 + w_2 L}{w_2} & 0 \\ 1 & 0 \\ 0 & -L \\ 0 & 1 \\ 0 & 1 \end{pmatrix} \cdot \begin{pmatrix} \rho_{2,1} \\ \rho_{2,2} \end{pmatrix} \tag{3-23}$$

Again, z_2 is the sum of a particular solution, z_{p2}, and any linear combination of the

two bases in the null space, V_{n2}, in which the coefficients are given as $\rho_{2,1}$ and $\rho_{2,2}$. As shown in Equation (3-23), no variable is observable since no null row exists in the null space V_{n2}. In other words, the recursive steps end as per the criterion of null row in the null space. However, the main reason of the premature end of the recursive steps is that the nonlinear constraints, e.g. $EI_2 v_3 = EI_2 \cdot v_3$, are not incorporated into the process.

Figure 3-10.b-d illustrates the effect of the lacking of nonlinear constraints. Providing determined values of $\rho_{2,1}$ and $\rho_{2,2}$, Equation (3-23) specifies a set of solution for z. To present the values of all unknowns in the same range, these values are normalized by their actual values obtained from SAP 2000. The solution of this problem is represented by a point in Figure 3-10.b, where the values of all normalized unknowns are one. If infinite sets of $\rho_{2,1}$ and $\rho_{2,2}$ are provided, all possible normalized values will yield six planes, as shown in Figure 3-10.b. For a given set, the equations $\{\rho_1 = \rho_{2,1}$ and $\rho_2 = \rho_{2,2}\}$ specifies a vertical line and the intersections of this vertical line with the six planes indicate a specific solution of Equation (3-22). For illustration, when $\rho_{2,1}$=-22, $\rho_{2,2}$=4.20E-4, as indicated by the vertical line in Figure 3-10.b, the six solutions are deviated from the solution of the problem. When the parameters are chosen as $\rho_{2,1}$=-22.22, $\rho_{2,2}$=4.12E-4, the six intersections of the vertical line and the six planes will occur at the solution of the problem.

Figure 3-10.c and d illustrate the variation of the normalized solution against $\rho_{2,1}$ with fixed $\rho_{2,2}$ of 4.12E-4 and the variation of the normalized solution against $\rho_{2,2}$ with fixed $\rho_{2,1}$ of -22.22. Evidently, the solution of the problem comes from a particular solution in the general solution. However, SSI by OM is incapable of detecting this solution in the general solution. The reason is that observability treats the coupled unknowns, $EI_2 v_3$, as independent of the corresponding single variables, EI_2 and v_3, though they should satisfy the constraint that $EI_2 v_3 = EI_2 \cdot v_3$ In Figure 3-10.c and d, these constraints are satisfied gradually by adjusting $\rho_{2,1}$ and $\rho_{2,2}$.

Consider the FEM of a one-story, one-bay frame depicted in Figure 3-11. In this frame, each column and each beam are divided into two elements. The end nodes of the columns are clamped. The possible measurements within this structure include 5 horizontal deflections, 5 vertical deflections and 5 rotations. For simplicity, it is assumed that the areas of the columns and the beam are known, and the flexural inertias of the columns are identical. Hence, the two unknowns here are the flexural stiffnesses of the columns and the beam. Due to the requirement of essential set, two measurements should be used and sufficient to identify the two unknown flexural stiffnesses. However, it is found that measuring any two displacements out of the 15 possible measurements (C_{15}^2=105 possible combinations) cannot ensure the identifiability of the two parameters. Half of the possible measurement sets can only identify one flexural stiffnesses and the other half cannot identify any parameter. This means that no essential set exists in this structure. A closer inspection of the general solution for this structure shows that the constraints between the variables are also missing.

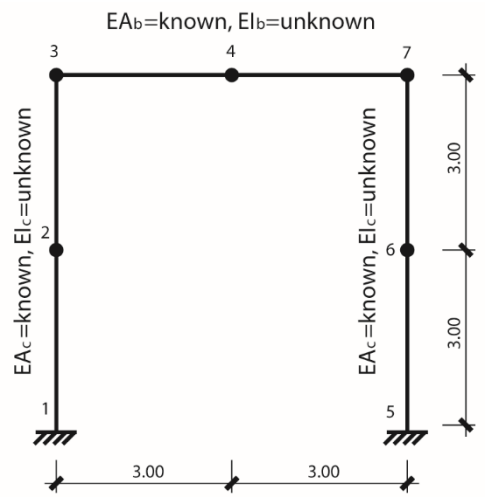

Figure 3-11 A one-story, one-bay frame with two columns and one beam (unit: m)

From the simply supported beam example, an explanation for the observability method being incapable of ensuring identifiability is provided algebraically. The algebraic analysis shows that the nonlinear constraints between the unknowns are neglected in OM. In the graphical illustration of the general solution (Equation (3-23)), it is shown that the exact solution is obtained when the constraints are satisfied. Moreover, the frame example shows that essential set may not exist in some structures due to the same reason.

In order to get more knowledge of this phenomenon, an exhaustive examination of observability of the structural parameters is carried out in the structure depicted in Figure 3-12.a. This is a 15-m simply supported beam with 5 evenly divided elements. A vertical concentrated force is applied at node 3 with a magnitude of 100 kN. The flexural stiffnesses of the five elements are deliberately chosen as different values of 1.5E6 $kN{\cdot}m^2$, 1.2E6 $kN{\cdot}m^2$, 1.1E6 $kN{\cdot}m^2$, 1.4E6 $kN{\cdot}m^2$ and 1.0E6 $kN{\cdot}m^2$. In this structure, potential measurements include six rotations, w_1-w_6, and four vertical deflections, v_2-v_5, i.e. ten in total. All the exact displacements are calculated in SAP2000 and used as the input in SSI by OM. In the identification problem, the five flexural stiffnesses (EI_1-EI_5) are assumed as unknown, i.e. N_F=5, whereas the axial stiffnesses are disregarded due to the loading case, i.e. N_A=0. Therefore, essential set capable of identifying the 5 flexural stiffnesses should have 5 measurements. In order to check the number of essential sets, an exhaustive investigation is carried out on all sets having 5 measurements. Hence SSI by OM is carried out on C_{10}^5=252 combinations of 5 measurements from $\{w_1$-w_6 and v_2-$v_5\}$. Figure 3-12.b illustrates the number of identified flexural stiffnesses by OM, $N_{F,OM}$, for these 252 sets.

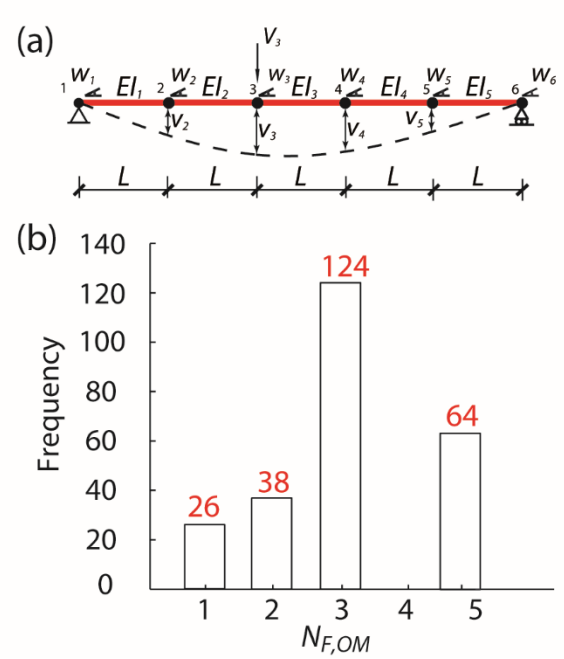

Figure 3-12 (a) FEM of the 6-node simply supported beam; (b) frequency of the occurrence of the number of identified flexural stiffnesses by OM, $N_{F,OM}$

It can be seen that the occurrence of full observability, $N_{F,OM}$=5, occupies 25.4% of the 252 sets whereas the occurrence of partial observability, $N_{F,OM}$ ≤4, occupies 74.6% of the 252 sets. To distinguish among the sets achieving different levels of observability, they are classified into different patterns with regard to the location of the measurements. For instance, in the case of three measurement sets: $\{w_1, v_2, w_2, v_3, w_3\}$, $\{w_1, v_2, v_3, v_4, w_4\}$ and $\{w_1, w_2, w_3, v_4, w_4\}$, they are classified as {1,2,2,3,3}, {1,2,3,4,4} and {1,2,3,4,4}, respectively. In these patterns, the subscript of the measurements (i.e. node number), which indicates the associated locations, will be kept. Also, no distinction is made between measurements of deflections and rotations. If the same node number shows twice in a pattern, it means both the deflection and the rotation of this node are measured. Since the vertical deflection of node 1 and node 6 are null (boundary conditions), v_1 and v_6 will be included to each pattern automatically. Table 3-2 provides the most representative patterns to illustrate the connection between the location of measurements and the number of identified parameters.

All the patterns related with $N_{F,OM}$=5, i.e. full observability, are listed in the first column of Table 3-2. As indicated by the indices of these patterns, the measurements yielding full observability are taken at physically dispersed locations. These patterns, or the distributed placement of sensors, maintain the observability flow and thus the full observability is achieved. If the measurements are taken intensively at local areas, redundancy of measurements will emerge. For instance, in the case of $\{v_3, w_3, v_4, w_4, w_6\}$ (the first pattern related with $N_{F,OM}$=1), all displacements of element 3 are measured and hence EI_3 is identified. Note that the recursive process in

SSI by OM is maintained by continuously providing the displacements of the nodes that are adjacent to the previously identified elements (Jose Antonio Lozano-Galant et al., 2015). The elements adjacent to element 3 are elements 2 and 4. To identify the parameter of element 2 (i.e. EI_2), at least one of v_2 or w_2 is required. However, due to the lack of any information about v_2 or w_2, EI_2 cannot be identified. Similarly, EI_4 cannot be identified due to the lack of any information about v_5 or w_5. The identification of EI_5, which should follow the identification of EI_4, is not executed neither. This renders the measurements v_6 and w_6 unutilized and ineffective. Hence, it can be seen that the effectiveness of a measurement is defined in the context of a particular measurement set and might be different for another set. These unutilized measurements are referred as ineffective measurements and all of them are given in bold in Table 3-2. From this analysis, it can be deduced that one reason for partial observability is that the number of effective measurements is less than the number of unknowns.

Table 3-2. Examples of patterns identifying different number of parameters by OM, and corresponding identified flexural stiffnesses.

Full observability		Partial Observability					
$N_{F,OM}$=5		$N_{F,OM}$=3		$N_{F,OM}$=2		$N_{F,OM}$=1	
Pattern	Observed	Pattern	Identified	Pattern	Identified	Pattern	Identified
1,1,2,3,4,5,6	EI_1~EI_5	1,1,2,3,4,**6,6**	EI_1~EI_3	1,1,2,2,3,3,**6**	EI_1, EI_2	**1**,3,3,4,4,**6,6**	EI_3
1,2,2,3,4,5,6	EI_1~EI_5	**1,1**,3,4,5,6,6	EI_3~EI_5	1,1,2,2,3,**5,6**	EI_1, EI_2	1,1,2,4,4,6,6	EI_1
1,2,3,3,4,5,6	EI_1~EI_5	1,1,2,2,3,4,**6**	EI_1~EI_3	1,1,2,3,3,**5,6**	EI_1, EI_2	**1,1**,3,3,4,4,**6**	EI_3
1,2,3,4,4,5,6	EI_1~EI_5	1,1,2,3,3,4,**6**	EI_1~EI_3	**1,1**,4,5,5,6,6	EI_4, EI_5	**1,1,3**,5,5,6,6	EI_5
1,2,3,4,5,5,6	EI_1~EI_5	1,1,2,3,5,6,6	EI_1, EI_2, EI_5	**1,2**,4,4,5,5,6	EI_4, EI_5	1,1,2,2,**4,6,6**	EI_1
1,2,3,4,5,6,6	EI_1~EI_5	1,1,2,4,5,6,6	EI_1, EI_4, EI_5	1,1,2,2,5,6,6	EI_1, EI_5	**1,3,3**,5,5,6,6	EI_5

However, in the last 2 patterns in the column of $N_{F,OM}$=3, all measurements are involved in the identification but they still lead to partial observability. In fact, the defect of these patterns is not as intuitive as that revealed by ineffective measurements. For the measurement set $\{v_1,w_1,v_2,v_3,v_5,v_6$ and $w_6\}$ (the 5th pattern related with $N_{F,OM}$=3), the identifications of $\{EI_1, w_2\}$ and $\{EI_5, w_5\}$ are, respectively, enabled by the measurements $\{v_1, w_1, v_2\}$ and $\{v_5, v_6, w_6\}$. Likewise, the identification $\{EI_2, w_3\}$ is enabled by the measurements $\{v_2, v_3, w_2\}$. Hence, all known displacements, either measured or estimated, are $\{v_1, w_1, v_2, w_2, v_3, w_3, v_5, w_5, v_6$ and $w_6\}$. However, the lack of any information about v_4 or w_4 terminates the observability flow, and thereby fails the identification of EI_3 and EI_4, despite $\{v_3, w_3, v_5$ and $w_5\}$ are known.

With respect to $N_{F,OM}$=1 and 2, all the patterns yielding partial observability can be categorized as the cases of the ineffective measurements or of the premature end of the recursive steps. Note that the case of $N_{F,OM}$=4 does not exist. The reason is that if $N_{F,OM}$=4, the measured displacements and the displacements which are estimated during the recursive steps, will certainly yield full observability.

3.2.4 SSI by COM

From the first two examples, it is found that the nonlinear constraints among the unknowns are lacking, and the two reasons for the partial observability are: (1) the premature end of the recursive steps and (2) the ineffective measurements due to redundancy in the measurement sets. Since adding nonlinear constraints to SSI by OM is likely to improve the performance of the original method in dealing with partial observability, COM is proposed, which incorporates these constraints into OM. The required nonlinear constraints are imposed through an optimization routine. The following points have to be taken into account when implementing the optimization:

The condition when the optimization should be applied

Whenever possible, appropriate measurement sets have to be chosen in order to avoid optimization. It is less desirable to employ COM than just OM due to the fact that the computation cost is normally higher for the first option. When optimization is required, SSI by OM will be carried out first and then Equation (3-19) from the last recursive step of SSI by OM will be used in COM.

Classification of variables and imposition of constraints

In the optimization, variables will be classified in one of three categories: (1) Coupled variables V_c; (2) Single variables V_{s1}, which already exist in the unknowns z; (3) Single variables V_{s2}, which do not exist in the unknowns z. The final unknown vector z^* will be composed of z and the new single variable V_{s2}, i.e. $z^*=\{z\ V_{s2}\}^T$. For instance, if the unknown z includes $\{EI_2w_2,\ EI_2w_3,\ EI_2v_3$ and $EI_2\}$, coupled unknowns V_c will include $\{EI_2w_2,\ EI_2w_3$ and $EI_2v_3\}$. The single variables from $\{EI_2w_2,\ EI_2w_3$ and $EI_2v_3\}$ are $\{EI_2,\ w_2,\ w_3$ and $v_3\}$. Since EI_2 exists in z, it is categorized as V_{s1} whereas w_2, w_3 and v_3 are categorized as V_{s2}. The new unknown z^* is $\{EI_2w_2,\ EI_2w_3,\ EI_2v_3,\ EI_2,\ w_2,\ w_3$ and $v_3\}$.

After the classification of variables, the variables involved in the constraints are detected. These constraints are ensured by imposing the equality between the coupled unknowns V_c and the product of corresponding single unknowns V_s during the optimization process.

3.3 Objective function

In order to consider the new unknowns V_{s2}, Equation (3-19) is rearranged as:

$$\epsilon = B^* \cdot z^* - D \tag{3-24}$$

where $B^* = [B^{N_{eq} \times N_z} \mid \Omega^{N_{eq} \times N_{s2}}]$. The matrix B, and vectors z and D are obtained from Equation (3-19) in the last recursive step of SSI by OM. B^* is obtained by adding a null matrix Ω to the matrix B. The dimension of this null matrix Ω is N_{eq} times N_{s2}. ϵ is the residual of the equations, which is a column vector having N_{eq} elements. Here, N_{eq} and N_z, respectively, denote the number of equations and the number of unknowns in z. N_{s2} denotes the number of new single unknowns in V_{s2}. The objective function is defined as minimizing the square sum of the residuals in Equation (3-24).

Other remarks

In the optimization, the active-set algorithm (Nocedal & Wright, 2006) is adopted to find the optimal solution to minimize the square sum of the residuals in Equation (3-24) and the optimization toolbox of Matlab is used to implement this program. For better convergence and computational efficiency, the element in row i and column k of the coefficient matrix B^* in Equation (3-24), $B^*_{i,k}$, will be multiplied by the numerical value of the k^{th} unknown obtained from direct stiffness method, $\overline{z_k^*}$, as presented in Equation (3-25):

$$\overline{\overline{B_{i,k}^*}} = B_{i,k}^* \cdot \overline{z_k^*}, \forall i, k = 1,2,\cdots,(N_z + N_{s2}) \tag{3-25}$$

The vector D in Equation (3-24) will remain the same. Consequently, in Equation (3-26), the corresponding value of the solution minimizing the objective function, will be normalized by $\overline{z_k^*}$, and thus the values of the normalized unknowns, $\overline{\overline{z_k^*}}$, are supposed to be around 1.

$$\overline{\overline{z_k^*}} = z_k^* / \overline{z_k^*}, \; k = 1,2,\cdots,(N_z + N_{s2}) \tag{3-26}$$

However, in order to avoid the instability of the solution due to very small or zero values of $\overline{\overline{z_k^*}}$, a threshold z_{th} of 10^{-6} is chosen for $\overline{\overline{z_k^*}}$. If $\overline{\overline{z_k^*}}$ is larger than z_{th}, the original value will be used in Equation (3-26); otherwise, the threshold z_{th} will be used in Equation (3-26).

After the normalization, the initial values for all $\overline{\overline{z^*}}$ are ones. If this normalization is not carried out, the same solution might be attained at a higher cost of time and computation capacity, which is verified later. The lower bound and the upper bound for each element in $\overline{\overline{z^*}}$ are 0.1 and 10, respectively.

Proposed algorithm

This proposed method combines SSI by OM with optimization and thereby includes

the nonlinear constraints in the identification process. The algorithm for SSI by COM is summarized as follows:

Step1: Apply SSI by OM and check whether the full observability is achieved or not. Initiate SSI by OM with the given measurement set. Form the general equation (3-19), and check the null space of coefficient matrix B to see if any parameters are observed. If so, update the input by incorporating observed variables and reinitiate the previous procedure until the end of the recursive process, i.e. no new variable is observable. If not, the OM is ended without estimating any unknown. If full observability is achieved at the end of the recursive process, it is not necessary to perform optimization; otherwise, go to step 2. It is highlighted that several recursive steps can be done in step 1 until no further unknowns are observable by OM;

Step2: Obtain the equation $\boldsymbol{B} \cdot \boldsymbol{z} = \boldsymbol{D}$ (Jose Antonio Lozano-Galant, Nogal, et al., 2013; Nogal et al., 2015). Extract the updated general equation $B \cdot z = D$ from the last step of SSI by OM.

Step3: Analyze the unknowns *z* and generate the new unknowns $\boldsymbol{z}^*$. Divide z into V_c and V_{s1}. Then compare every component of the coupled unknowns V_c with the existing single unknowns V_{s1} and collect the single unknowns V_{s2}, which were not present in z. Generate the new unknowns $z^*=\{z\ V_{s2}\}^T$.

Step4: Form the new matrix $\boldsymbol{B}^*$. Analyze the dimension of matrix B and append the null matrix Ω to contain V_{s2} in the z^* without violating the equations.

Step5: Obtain the normalized unknown $\bar{\bar{z}}^*$. Multiply the column of the matrix B^* with the expected value $\bar{z}^*$ so as to obtain the $\bar{\bar{B}}^*$ and the normalized unknown $\bar{\bar{z}}^*$.

Step6: Store the constraint information. Detect the variables V_c and V_s involved in the nonlinear constraints, and establish the nonlinear constraints.

Step7: Optimization. Choose the initial values of $\bar{\bar{z}}^*$ and set the bounds for the solution. The objective is to minimize the square sum of the residual vector, ϵ. In the optimization process, the nonlinear constraints are imposed by ensuring the equality between the coupled unknowns V_c and the product of corresponding single unknowns V_s.

A summary of the procedure is shown in the flow chart in Figure 3-13.

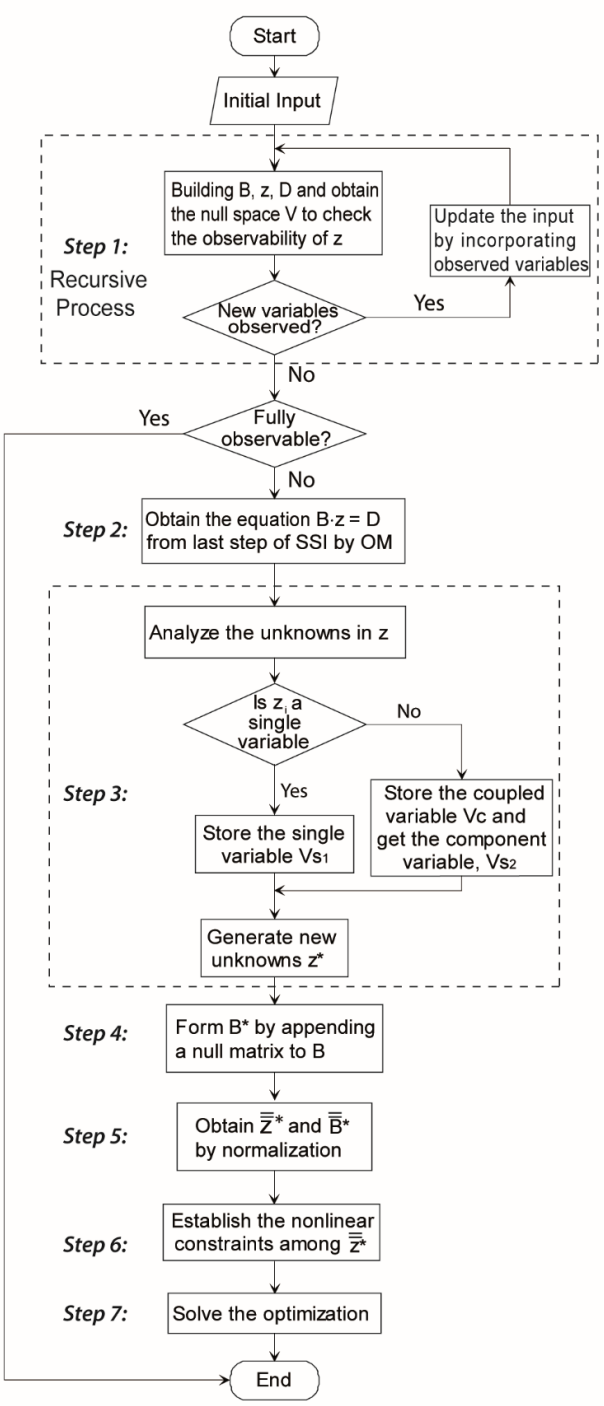

Figure 3-13 Flow chart of structural system identification by constrained observability method

Application of the algorithm

First, both structures depicted in Figure 3-10.a and Figure 3-11 are re-analyzed by COM. As expected, the first example becomes identifiable with the given measurement set. Also, 45 out of the 105 measurement sets becomes capable of identifying all parameters for the frame. However, these structures are far from proving the strength and

robustness of COM. In order to do this, the observability of the structure depicted in Figure 3-12.a is re-analyzed by COM. In this structure, the influence of the normalization and the choice of initial values on the accuracy of the result of the optimization are checked here. Note that the flexural stiffnesses of the five elements are 1.5E6 $kN{\cdot}m^2$,1.2E6 $kN{\cdot}m^2$,1.1E6 $kN{\cdot}m^2$,1.4E6 $kN{\cdot}m^2$ and 1E6 $kN{\cdot}m^2$. Instead of normalizing the columns of the matrix B with the real inertias, these columns are normalized by 1E6 $kN{\cdot}m^2$. Therefore, the normalized estimate of these inertias should be {1.5, 1.2, 1.1, 1.4 and 1}. Meanwhile, instead of using ones as initial values, random numbers generated by uniform distribution on [0.8, 1.2] are used. Note that some of the normalized estimates do not lie in the sampling interval of this distribution. According to the result, the optimization still converges to the same solution as that obtained by using the recommended normalization and initial values but with more iterations. In the following comparison, the normalization factors and the initial values are taken as recommended. The frequency of occurrence of the number of observed flexural stiffnesses by COM, $N_{F,COM}$, is presented in Figure 5.a.

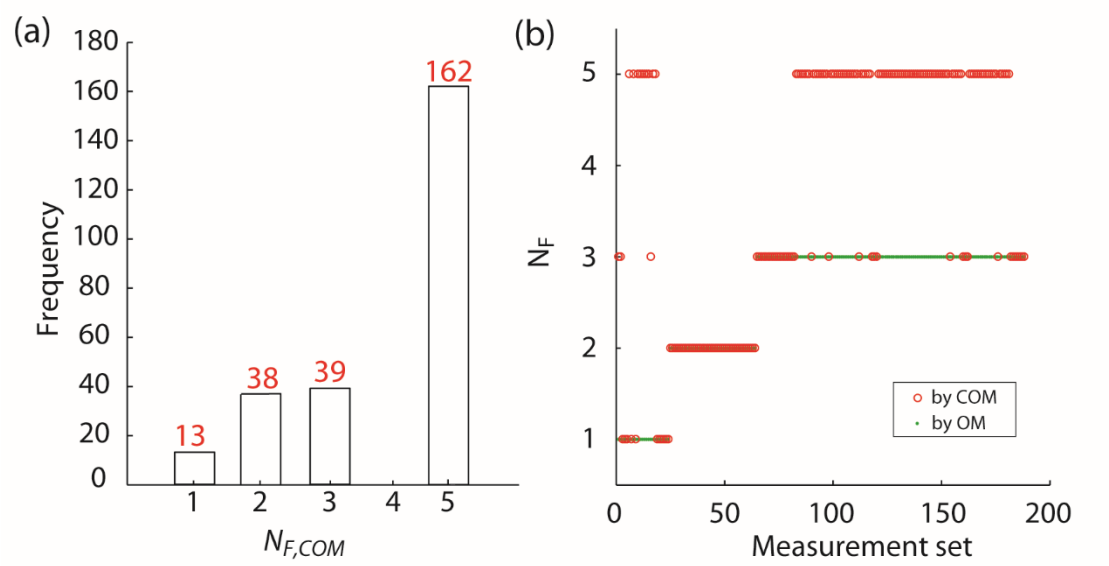

Figure 3-14 (a) Frequency of the occurrence of the number of identified flexural stiffnesses by COM, $N_{F,COM}$; (b) number of observed flexural stiffnesses, N_F, by observability method (OM) and constrained observability method (COM) for the 188 sets with partial observability.

Comparing Figure 3-12.b and Figure 3-14.a, a drastic increase, in the number of the measurement sets yielding full observability, from 64 for SSI by OM to 162 for SSI by COM is seen. In fact, all of the previous 64 sets by OM are contained in the new 162 sets by COM due to the equivalence of the step 1 (recursive process) in SSI by COM and SSI by OM. In other words, the improvement of the observability level occurs in the remaining 188 (=252-64) sets. The numbers of observed flexural stiffness by OM, $N_{F,OM}$, and by COM, $N_{F,COM}$, are plotted in Figure 3-14.b. For better visualization, the

measurement sets are sorted so as to cluster those sets with the same value of $N_{F,OM}$ in an ascending order. In this figure, the number of identified flexural stiffnesses, N_F, for different measurement sets by COM and OM are represented by circles and points, respectively. The abscissa of the markers is the numbering of the sets whereas the ordinate is the number of identified flexural stiffnesses. If an increase in the number of identified parameters is attained by COM, then a position of the circle higher than the one of the dot for that measurement set should be expected. It can be seen that the majority of the sets yielding $N_{F,OM}$=3 by OM, alter to yield $N_{F,COM}$=5 by COM. In these sets, it is found that the discontinuity of the observability flow can be overcome by applying the nonlinear constraints. For instance, in the final step of the observability analysis on the measurement set $\{v_1, w_1, v_2, v_3, v_5, v_6, w_6\}$, the up-to-date information, apart from the original measurements, contains the estimated displacement $\{w_2, w_3, w_5\}$ and flexural stiffnesses $\{EI_1, EI_2, EI_5\}$. Despite the information of $\{v_3, w_3, v_5, w_5\}$, EI_3 and EI_4 cannot be identified due to the lack of any of $\{v_4, w_4\}$. However, these parameters can be identified with the imposition of associated nonlinear constraints. An explanation is that the compatibility requirement of the displacements at the mutual node of elements 3 and 4, i.e. the displacements of the node 4, and the nonlinear constraints force the solution. This deduction can be justified by another case. For measurement set $\{v_1, w_1, v_3, w_3, v_5, w_6, v_6\}$, only the identification of $\{w_5,\ EI_5\}$ is attainable using OM. Note that the condition of the previous deduction is satisfied here for both pairs of elements 1, 2 and elements 3, 4 since all the displacements of nodes 1, 3, 5 are known. As expected, this set yields the full observability by COM, which further verifies the deduction. In effect, each measurement set shifting from partial observability towards full observability, due to the adoption of COM, has been checked in an exhaustive way. It is found that the observability flow of each of these sets are maintained by the same mechanism. Moreover, for the same reason, three measurement sets, though not yielding the full observability, identify more inertias, switching from the case of $N_{F,OM}$=1 to the case of $N_{F,COM}$=3.

For this example, it is seen that if some of the sensors are placed too intensively at a local area, then other sensors will be placed sparsely in the remaining areas in the case of essential sets. This leads to the loss of information in these remaining areas, or leads to the partial observability. A reexamination has been performed on those patterns where no improvement is obtained with COM. For instance, if the information obtained by measurement is considered as a geometric constraint on the deflection shape of the structure, the estimation of the parameters $\{EI_1,\ EI_2,\ EI_3\}$ is not fixed in the pattern $\{1, 1, 4, 4, 5, 6, 6\}$. That is, a relation can be established among them but it is impossible to get a unique estimate of these parameters.

From the comparison of the results obtained by OM and by COM, it can be seen that COM, as an extended version of OM, enhances the performance of the original method. The number of essential sets soars from 64 to 162. Nevertheless, if the sensors are placed too intensively, there still exists possibility of partial observability. Hence,

distributed placement of sensors is strongly recommended.

In the preliminary stage of condition assessment of any structure, the location of the possible measurements can be determined according to the accessibility of the location. The final location of the measurements will be a specific combination of some possible measurements. Prior to instrumentation, the capability of a given measurement set to identify all parameters in the structural system will be examined using the COM. Among all possible measurements sets, the ones more likely to produce full observability are the ones that include at least one measurement for every mechanical property at the location of the element with the unknown parameter to be identified.

3.2.5 Application in a building structure

To test the performance of the proposed method, a large structure (Jose Antonio Lozano-Galant, Nogal, et al., 2013) previously analyzed by OM is re-analyzed by COM. This structure is a 13-storey frame with a height of 39 m and a width of 32 m. This structure is modelled by beam elements with three DOFs per node in SAP2000. The FEM of the structure, sensor and load locations are described in Figure 3-15.a.

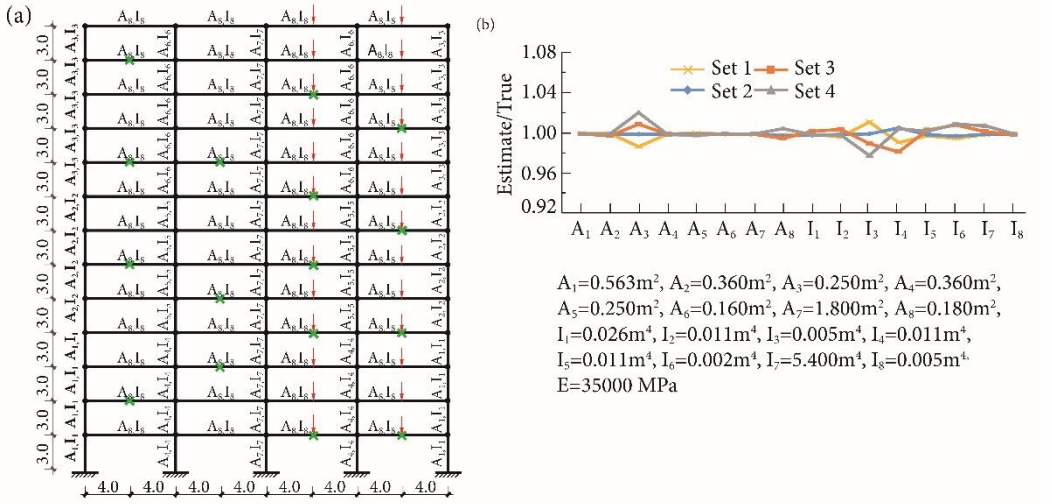

Figure 3-15 (a) FEM of the frame building, sensor locations (indicated by cross), and load locations (indicated by arrows); (b) the ratio between the normalized estimates and the perturbation factors for all parameters (A_1-A_8 and I_1-I_8)

The geometric and material properties are also provided in this figure. In this study, all these 16 mechanical parameters are perturbed by random numbers. In previous study (Jose Antonio Lozano-Galant, Nogal, et al., 2013), 156 vertical deflections were measured while the number of measurements is the same as the number of unknowns in the current analysis. Also, the suggestion of distributed placement of sensors is followed here and the locations of these sensors are indicated by crosses in Figure 3-15.a. To illustrate the robustness of COM, 4 sets of the 16 mechanical parameters are

synthesized by the product of the intact values and random numbers evenly distributed on [0.8,1.2], referred as perturbation factors later. The nodal displacements calculated by SAP2000 using these 4 generated parameter sets are used as the input of SSI by COM. Initial values of all ones are used here. Regarding the results from COM, the estimates of axial stiffnesses (flexural stiffnesses) are normalized by the product of Young's modulus and the intact areas (inertias). In other words, an accurate estimation is characterized by the closeness between these normalized estimates and the perturbation factors. The ratios of the perturbed values and estimated values of the parameters are provided in Figure 3-15.b. In this figure, for each of these parameters, the deviation of the ratio between the estimate and the true value is within 2 percent, which is acceptable. It should be also noted that by OM, no inertia or area can be identified whereas all these parameters are obtainable by COM using this measurement set.

This example shows the applicability of SSI by COM presented in this paper and its ability to identify the mechanical parameters of a large structure using essential sets. In this example, the structural system is defined by 16 structural parameters. One concern is that this assumption will lead to an average estimate of the structural parameters, which might not identify some localized damage appropriately. However, the assumption that the flexural stiffness and the axial stiffness of each element being different in such a structure could be a formidable task for the proposed method to solve. In order to deal with the trade-off between the issue of the number of parameters and the computation cost, it is advisable to use some engineering techniques, e.g. visual inspections, acoustic emission or impact method (hammering), before making modelling assumption with the aim of reducing the unknowns in the model.

3.2.6 Conclusion

One crucial step in SSI is using the adequate number of measurements to achieve full observability of the whole structure. From the formulation of the identification problem by OM, the number of the measurements should be equal to the number of parameters in the structure. However, measurement sets with this number of measurements do not necessarily lead to the identification of all parameters. This is illustrated with a simply supported beam and a frame structure. By the analysis of this structure, the lack of nonlinear constraints, which is essentially induced by the linearity of OM, is presented for the first time.

A thorough examination of the observability of structural parameters in a simply supported beam with more unknowns is carried out using 252 numerated measurement sets. In this analysis, the 252 sets are categorized into 70 patterns by the physical location of the measurements and corresponding identification results are discussed with respect to these patterns. It is found that the reasons of partial observability are: (1) the premature end of the recursive steps and (2) the redundant information due to intensive placement of sensors.

To address the issue of partial observability, SSI by COM, where the lacking nonlinear constraints are appended to SSI by OM through an optimization routine, is proposed with the aim of fully exploiting the information in measurements. In the first step of the proposed method, SSI by OM is performed until no more parameters are observed. If full observability is achieved, then the algorithm returns. Otherwise, the general equation (Equation (3-19)) from the last recursive step will be extracted. The structure of the unknowns in this equation is analyzed first and the relation between variables is identified for the nonlinear constraints used in the optimization. In the last step of the SSI by COM, an optimization is performed on the observability equation with the acquired nonlinear constraints and all the parameters observed in the first step. The efficacy of the proposed method to improve identifiability is justified by reanalyzing the same structure with the 252 enumerated sets. The number of sets achieving full observability via SSI by COM roughly doubles that number via SSI by OM. Nevertheless, it is strongly recommended to place the sensor in a dispersed way since the structure is still not fully observable in case of intensive placement of sensors. The strength and robustness of this method is further testified in a 13-storey building where the real mechanical parameters are perturbed by random numbers. It is seen that the axial stiffnesses and the flexural stiffnesses of all structural members can be estimated accurately.

This method is able to identify mechanical properties for linear systems. For non-linear systems, the load test will induce a deformation increment that will provide the information of secant mechanical properties of different elements. It is highlighted that COM is not suitable to identify structures with geometrical non-linear behavior. As the use of an essential set provides the only possible solution that satisfies the equations, measurement or modelling errors will affect the estimates. These effects are not studied in this paper but it will be addressed in the near future. The importance of this research is that the supplement of the nonlinear constraints to the OM fully exploits the information provided by measurements. In contrast with SSI by OM, the range of the measurement sets qualified to be essential sets are greatly enlarged by adding nonlinear constraints via optimization. Besides, in some other sets, even though full observability is not achieved, number of identified parameters are also increased. Furthermore, the sharp decrease in the number of measurements used in the identification of the mechanical parameters in a 13-storey building also justifies the efficacy of SSI by COM.

3.3 Static structural system identification for beam-like structures using compatibility conditions

Title: Static structural system identification for beam-like structures using compatibility conditions

Authors: Jun Lei, Dong Xu, José Turmo

Journal: Structural Control and Health Monitoring

Publication: Technical Paper

Submitted: 26 July, 2016

Accepted: 21 April, 2017

DOI: http://dx.doi.org/10.1002/stc.2040

Available at: https://onlinelibrary.wiley.com/doi/abs/10.1002/stc.2040

3.3.1 Summary

Due to the inevitable noise existing in the measured responses, Structural System Identification is often a challenging task in terms of the accuracy of the estimations. Structural System Identification by the observability method, which is characterized by the analysis of null spaces, is a powerful tool to determine the observability of structural parameters. However, it did not cope well with measurement errors so far. In this paper, for the first time, functional relations among displacements, denoted by the term compatibility conditions, in beam-like structures are derived by the observability method. Then compatibility conditions are imposed in an optimization procedure to minimize the discrepancy between the measured response and the compatible one. The compatible response obtained by the optimization is used to obtain the final estimations of the parameters. In a simply supported bridge example, the proposed method is thoroughly evaluated with respect to the number of measurements, error levels and loading cases. In an example of a continuous bridge, different loading cases are used to estimate the bending stiffnesses of different zones. The accuracy and the efficacy of the proposed method are verified by the numerical results.

Keyword: beam-like; compatibility conditions; measurement errors; null space; observability; redundant set; static;

3.3.2 Introduction

Research interest in Structural System Identification (SSI) has been increasing over the years due to the growing computation power and the rapid development of various algorithms. Any SSI can be defined as structural parameter estimation using discrete measurements of real-life structural response. A comprehensive description and the associated categories of SSI are provided in the technical report of (American Society

of Civil Engineers, 2013). These categories include static (Bakhtiari-Nejad et al., 2005; S. Li & WU, 2005; Jose Antonio Lozano-Galant, Nogal, et al., 2013; Nogal et al., 2015; Masoud Sanayei et al., 1997; Z. Sun et al., 2016) and dynamic excitations (Juan P Amezquita-Sanchez & Adeli, 2015; Behmanesh & Moaveni, 2015; Brincker & Ventura, 2015; Eskew & Jang, 2017; Habtour et al., 2016; Jiang & Adeli, 2007; Z. Li et al., 2017), parametric (Jose Antonio Lozano-Galant, Nogal, et al., 2013; Masoud Sanayei et al., 1997) and non-parametric models (Jiang & Adeli, 2007; Jiang et al., 2007; Mei et al., 2016; Okada, Nakata, SPENCER Jr, Kasai, & Kim, 2006), deterministic (Bakhtiari-Nejad et al., 2005; Eskew & Jang, 2017; S. Li & WU, 2005; Marano, Quaranta, & Monti, 2011; Nogal et al., 2015; Raich & Liszkai, 2012; Masoud Sanayei et al., 1997) and probabilistic approaches (J. L. Beck & Katafygiotis, 1998; James L. Beck & Au, 2002; Behmanesh & Moaveni, 2015; Ni, Lu, & Lu, 2016; H. Sun & Betti, 2015; F. L. Zhang, Xiong, Shi, & Ou, 2016). For both static and dynamic SSI methods, structural responses have to be measured to provide the necessary information. However, in dynamic methods, the knowledge of the mass and the damping is also required unless full sets of modes are known or the mass scaling factor can be determined by experimental means (Brincker & Ventura, 2015), which is not necessary for static SSI. In addition, dynamic methods require an adequate control of excitation including the elimination of spurious excitation which was essential for precise model-shape measurement, and the resolution of measurements for dynamic response was lower than that for static response (Bakhtiari-Nejad et al., 2005). In certain circumstances, static loading might be more economical than dynamic loading (Masoud Sanayei et al., 1997). Hence, when only stiffness identification is required, static SSI might be more attractive than dynamic SSI. Based on the physical interpretability, SSI methods can be classified as parametric or non-parametric. In parametric methods, parameters correspond with the physical parameters (e.g. elastic moduli, areas, bending/torsional inertias), as they are used in finite element models (FEM). Non-parametric methods use basis functions to regress the response of the structure, e.g. autoregressive models (Mei et al., 2016; W. C. Su et al., 2014) or rational fractional polynomials (Okada et al., 2006).

Concerning probabilistic SSI methods, mainly the Bayesian approach, posterior distributions of parameters are obtained by updating the assumed distributions of those parameters with the measured response. The estimations of the parameters can be obtained by point estimation (e.g. mean, median) or interval estimation (confidence interval) based on these posterior distributions. On the contrary, certainty is assumed for the parameters in deterministic SSI. Generally, deterministic methods try to pinpoint a unique solution of the problem. In both probabilistic and deterministic methods, optimization technique is closely involved. The objective of the optimization might be minimizing the discrepancy between the measured response and the predicted response, e.g. displacements (Nogal et al., 2015; Masoud Sanayei et al., 1997), strains (S. Li & WU, 2005; Masoud Sanayei et al., 1997), loads vector (Bakhtiari-Nejad et al., 2005; Masoud Sanayei et al., 1997), acceleration (Marano et al., 2011), mode shapes and

frequencies (Eskew & Jang, 2017), or maximizing the sensitivity of the frequency response functions (Raich & Liszkai, 2012).

Observability Method (OM) is a mathematical tool dealing with the observability, i.e. the existence and the uniqueness, of the solution of a system of equations (or a subset of it) (Enrique Castillo et al., 2007). It has been applied to many engineering fields, e.g. water distribution systems (Díaz et al., 2016), power systems (Abur & Exposito, 2004), traffic networks(Agarwal, Kachroo, & Contreras, 2016). An algebraic technique to analyze the observability of the solution of a linear system is checking the null space of the coefficient matrix(Enrique Castillo et al., 2007). This technique can be applied to the identification of parameters in physical and engineering problems in which the final systems are in the form of monomial ratio equations (Enrique Castillo, Nogal, Lozano-Galant, & Turmo, 2016). The application of OM has to be tailor-made due to the different characteristics of problems in different fields. The applicability of OM in SSI was verified in a cable-stayed bridge when investigating the measurement set to identify its mechanical properties (Jose Antonio Lozano-Galant et al., 2014). At that time, the method was carried out in a symbolical approach to determine the observability of the parameters and estimations of those observable parameters were lacking. Later, a numerical development of this method was provided to determine the values of those observable parameters (Nogal et al., 2015).

The observability problem in power system (Abur & Exposito, 2004) considers a system with *n* parameters and *m* potential measurements. For the sake of economy and identifiability of the system, it is always desirable to know the least number of sensors required to identify these *n* parameters. In this context, the term essential sets relates to the measurement sets that ensure the identifiability of all *n* parameters while the drop of any measurement fails to do so. In the essential sets, the number of measurements is always the same as the number of parameters in the system. To address the issue of essential set in SSI by OM, observability tree method was proposed to analyze the identification sequence of the parameters (Jose Antonio Lozano-Galant et al., 2015). It was shown that not all measurement sets could lead to global identifiability.

In SSI, there exist three sources of errors (Masoud Sanayei et al., 2001): (1) Errors in measurements. (2) Errors in modeling. (3) Errors in parameter estimation. In most cases, measurement errors are assumed to follow the normal distribution with zero mean (Abdo, 2012; Bakhtiari-Nejad et al., 2005). One way to mitigate the adverse effect of measurement errors is to use weight factors (Masoud Sanayei et al., 1997). Each displacement was measured repeatedly and the variance in those measured values was calculated. Lower weight factors were assigned to displacements having high variances. This idea is similar to the weighted least square method (Abur & Exposito, 2004). Another way to deal with measurement errors is to implement SSI under a Bayesian probabilistic framework. In these methods, many sets of parameters are sampled from prior (assumed) distributions. For each set of sampled parameters, the posterior probability of obtaining the measured response with this parameter set being real is

obtained. The final estimations of the parameters are determined by their posterior (updated) distributions using point or interval estimations. The main drawback of this method is that the intensity of the storage and the computation increase exponentially with the number of parameters. The effect of errors from measurements and parameter estimations was also investigated in SSI by OM for *essential sets* (J. Lei et al., 2017). In the analytical expression of the identified bending stiffness, which is a quotient, it was found that measurement errors might render the sign of the denominator wrong. As a result, the estimations of the parameters might have no physical meaning and their variances are quite high. To deal with measurement errors, an intuitive idea is to measure more displacements. The term *redundant sets* is related with the case when redundant measurements are used in addition to *essential sets* (Abur & Exposito, 2004). These redundant measurements not only maintain the identifiability of the parameters in case of malfunction of sensors but also improve the accuracy of the estimations. However, using redundant measurements can be ineffective for SSI by OM because the denominator of the estimations might still remain close to zero or have a wrong sign. In order to fill this gap, the functional relations among the measured displacements, which are referred to the compatibility conditions, are derived algebraically in beam-like structures using OM for the first time. Then the incompatibility in measured displacements, which is caused by measurement errors, is reduced by an optimization routine with the compatibility conditions imposed. SSI is carried out using the compatible displacements eventually.

In the remaining part of this paper, section 3.3.3 introduces the general idea of SSI by OM. In section 3.3.4, the algorithm of SSI using compatibility conditions is proposed. Each step is detailed by the analysis on a simply supported beam bridge. In section 3.3.5, the accuracy of SSI by OM using redundant sets is provided first to emphasize the necessity of compatibility conditions. Then the performance of the proposed method is investigated regarding the effects of the number of measurements, error levels and loading cases. In addition, the applicability of this method is verified by a continuous bridge example. Finally, some conclusions are drawn.

3.3.3 Structural System Identification by Observability Method

In SSI by OM (Jose Antonio Lozano-Galant, Nogal, et al., 2013), the FEM of the structure has to be defined first. Subsequently, the nodal equilibrium equations are obtained by direct analysis and then transformed into a system of monomial ratio equations. For illustration, assume that we have the following system of equations

$$K \cdot \delta = f \tag{3-27}$$

In Equation (3-27), K, δ and f, respectively, represent the global stiffness matrix, the nodal displacements and the nodal forces. For 2D models with beam elements, the global stiffness matrix K is composed of the characteristics of the beam elements (i.e. length L, elastic moduli E, area A and inertia I). Displacement vector δ includes

horizontal displacements u, vertical deflection v and rotation w whereas force vector f includes horizontal forces H, vertical forces V and moments M.

In direct analysis, every element in the matrix *K* and in the force vector *f* is assumed as known. The displacement vector δ is solved by Equation (3-27). In SSI by OM, which is an inverse analysis, the matrix *K* is partially known. Parameters appearing in the matrix *K* are $\{E, A, I, L\}$. It is generally assumed that the length L is known while elastic moduli, E, areas, A, inertias, I are unknown. Since the main objective of SSI is to assess the condition of the structure, the estimations of axial stiffnesses *EA* and bending stiffnesses *EI* are of primary importance. To reduce unknowns, *EA* and *EI*, instead of being regarded as the product of two unknowns, are treated as one unknown each.

Once the unknowns in the matrix *K*, boundary conditions and measurements are determined, to solve Equation (3-27) in a linearized form, it can be rearranged as:

$$K^* \cdot \delta^* = f \tag{3-28}$$

The operations to linearize Equation (3-27) include: (1) the separation of the columns of matrix *K*, where some entries are the sum of different variables, into several single columns related with different variables, (2) the elimination of duplicated variables, (3) the merge of associated columns and (4) the extraction of the measured displacements from associated products and (5) the multiplication of them with the associated columns in the matrix K^* (Jose Antonio Lozano-Galant, Nogal, et al., 2013). The modified matrix K^* has different dimensions from the matrix *K*. The linearized variables in the modified displacement vector δ^* might be non-linear products of the bending or axial stiffnesses and displacements, e.g. *EAu*, *EIu*, *EIw* and *EIv*, as well as single variables, e.g. *EA*, *EI* or nodal displacements. The variables in δ^* and f can be clustered into groups of known quantities, indicated by subscript *1*, and unknown quantities, indicated by subscript *0*, as shown in Equation (3-29). δ_0^* includes variables associated with measured displacements or boundary conditions while δ_1^* includes variables containing the unknown displacements. Meanwhile, f_1 includes the external loads from the controlled static test while f_0 includes the reactions at the boundary conditions. The modified matrix K^* is partitioned accordingly.

$$\begin{pmatrix} K_{00}^* & K_{01}^* \\ K_{10}^* & K_{11}^* \end{pmatrix} \begin{Bmatrix} \delta_0^* \\ \delta_1^* \end{Bmatrix} = \begin{Bmatrix} f_0 \\ f_1 \end{Bmatrix} \tag{3-29}$$

In order to join the unknowns, Equation (3-29) is transformed into Equation (3-30).

$$B \cdot z = \begin{bmatrix} K_{10} & 0 \\ K_{00} & -I \end{bmatrix} \begin{Bmatrix} \delta_0^* \\ f_0 \end{Bmatrix} = \begin{Bmatrix} f_1 - K_{11}\delta_1^* \\ -K_{01}\delta_1^* \end{Bmatrix} = D \tag{3-30}$$

In Equation (3-30), unknown variables are of two types: (1) Variables containing displacements (*u*, *v* or *w*), or stiffnesses (*EA* or *EI*), or the products of both, (*EAu*, *EAv*, *EAw*, *EIu*, *EIv* or *EIw*); or (2) Reactions at the boundaries, *H*, *V* and *M*. The coefficient matrix *B* is composed of the measured displacements and the length of elements.

Meanwhile, the right-hand side vector D is composed of the external loads f_1 and the equivalent nodal forces ($K_{11}\delta_1$ or $K_{01}\delta_1$). In short, the transformation from Equation (3-29) to Equation (3-30) collects all unknowns in z, and renders both B and D known.

As the observability of the solution of Equation (3-30) are closely related with the concept of null space, its definition is given first. For a matrix $\mathcal{P}$, its null space is the vector space whose vectors v always satisfy Equation (3-31).

$$\mathcal{P} \cdot v = 0 \tag{3-31}$$

From linear algebra, vector v is always a linear combination of basis vectors of the null space of the matrix $\mathcal{P}$. Then the null space matrix N is defined as the matrix whose columns are these basis vectors, this is to say, the columns of the null space matrix N form the basis of the null space. For Equation (3-30) to have a solution, it is sufficient to check that the product of the transpose of the right-hand side vector, D^T, and the null space matrix N^* of the transpose of the matrix B, is a null (zero) vector, i.e. $D^T \cdot N^* = 0$. If this holds, the solution of Equation (3-30) has the structure:

$$z_g = z_p + z_h = \begin{Bmatrix} \delta_0^* \\ f_0 \end{Bmatrix}_p + N \cdot \rho \tag{3-32}$$

where z_p is a particular solution of Equation (3-30). It can be obtained by Moore-Penrose pseudoinverse or least squares methods. z_h is a vector from the null space of matrix B, which is a linear combination of basis vectors of this null space. The columns of the null space matrix N correspond with these basis vectors while the vector ρ is composed of the coefficients of the linear combination.

Null rows in the matrix N render associated elements of $N \cdot \rho$ null. As a result, in the general solution, the variables related to these null rows are equal to their values in the particular solution. In this case, these variables are determined and unique, i.e. observable. This is to say, the inspection of the matrix N and the identification of its null rows lead to the identification of the observable variables. When the product of the transpose of the right-hand side vector, D^T, and the null space matrix N^* of the transpose of the matrix B, is not null , i.e. $D^T \cdot N^* \neq 0$, then Equation (3-30) is not compatible and no solution exists (Enrique Castillo et al., 2007).

When the observability of unknown variables is determined, the values of those observable variables are determined by the particular solution z_p of Equation (3-30). It is to highlight that in SSI by OM, if any deflection, force or structural parameter is observed, this information might help to observe new parameters in the adjacent beam elements through a recursive process. In this analysis, the observed information is successively introduced as new input data in the observability analysis. The peculiarity of this method was illustrated by a detailed step-by-step example in previous studies (Jose Antonio Lozano-Galant, Nogal, et al., 2013; Jose Antonio Lozano-Galant et al., 2014).

3.3.4 SSI for beam-like structures using compatibility conditions

Measurement errors always arise due to uncontrollable factors, e.g. the change in temperature, ambient vibration due to wind. Measured displacements might not be compatible due to these errors. In this section, in order to smooth away the incompatibility among measured displacements, SSI for beam-like structures using compatibility conditions is proposed. The derivation of compatibility conditions among displacements and the procedures for incorporating these conditions into an optimization are illustrated by a simply supported bridge example. A summary of the proposed method is presented at the end.

Example 1

In this section, a simply supported bridge is analyzed. The nine steps required to carry out SSI for beam-like structures using compatibility conditions are exemplified by this structure.

Multi-span simply supported bridge (Figure 3-16.a) is one of the most popular bridge types in practice. Example 1 (Figure 3-16.b) corresponds with an 18-m span of this arrangement. The cross section of the structure is constant and the bending stiffness is $2.3\times10^9\ N\cdot m^2$. A 350 kN vertical load is applied at one-third point of the span. In this example, the targeted parameters are the bending stiffnesses, since the axial behavior is not activated by this loading case.

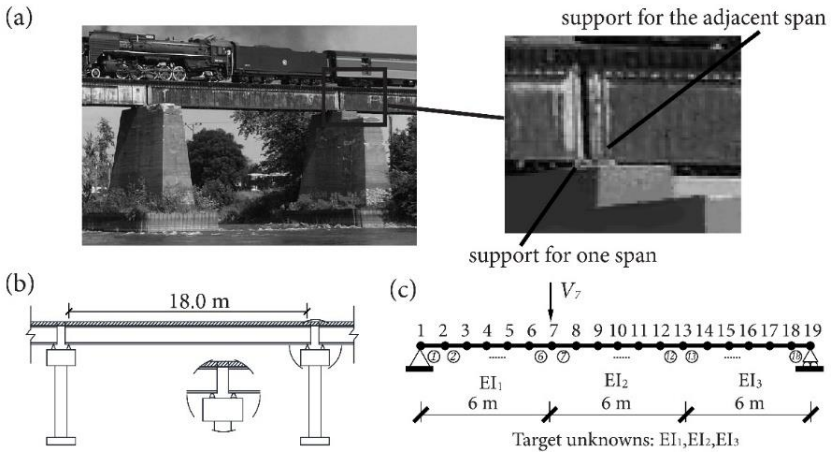

Figure 3-16 (a) Engineering practice of a multi-span simply supported beam; (b) elevation of 18-m span of a simply supported bridge; (c) 19-node beam model for the structure in (b)

Step 1: Introduce the geometry, as well as the known mechanical and geometrical properties and measured node forces to establish a FEM for the beam-like structure.

The FEM associated with Example 1 is shown in Figure 3-16.c. It is composed of 18 one-meter long elements. The bending stiffnesses for elements 1-6, 7-12 and 13-18 are assumed as EI_1, EI_2 and EI_3, respectively. Their real values are $2.3\times10^9\ N\cdot m^2$, that is, $EI_{1,r}=EI_{2,r}=EI_{3,r}=2.3\times10^9\ N\cdot m^2$. An external load is applied at node 7, i.e. V_7=-350 kN.

Step 2: Choose three nodal displacements belonging to elements with the same structural parameter and build Equation (3-30) using these displacements.

Relations among nodal displacements that belong to the elements of the same bending stiffness can be found using OM. For instance, some relations among v_7-v_{13} and w_7-w_{13} exist since elements 7 to 12 have the same bending stiffness EI_2. Without loss of generality, the derivation of these relations is exemplified by the measurement set {w_7, v_{10}, w_{13}}. It is to highlight that a different set (e.g. {v_7, w_8, v_{11}} or {v_9, v_{12}, v_{13}}) does not affect the result. The general equations (Equation (3-30)) corresponding with this FEM and {w_7, v_{10}, w_{13}} is obtained first (not shown here for the sake of brevity). In this equation, the coefficient matrix, the unknown vector and the right-hand side vector are denoted by B_1, z_1 and D_1, respectively.

Step 3: Check the null space matrix N of coefficient matrix B of Equation (3-30) to obtain the observable unknowns.

The null space matrix N_1 of the coefficient matrix B_1 is provided in Equation (3-33).

$$N_1 = \begin{pmatrix} 1/w_7 & 0 & \cdots & EI_1 \\ 1 & 0 & \cdots & EI_1v_2 \\ 2 & 0 & \cdots & EI_1v_3 \\ 3 & 0 & \cdots & EI_1v_4 \\ 4 & 0 & \cdots & EI_1v_5 \\ 5 & 0 & \cdots & EI_1v_6 \\ 6 & 0 & \cdots & EI_1v_7 \\ 1 & 0 & \cdots & EI_1w_1 \\ 1 & 0 & \cdots & EI_1w_2 \\ 1 & 0 & \cdots & EI_1w_3 \\ 1 & 0 & \cdots & EI_1w_4 \\ 1 & 0 & \cdots & EI_1w_5 \\ 1 & 0 & \cdots & EI_1w_6 \\ 0 & 0 & \cdots & EI_2 \\ 0 & 0 & \cdots & EI_2v_7 \\ 0 & 0 & \cdots & EI_2v_8 \\ 0 & 0 & \cdots & EI_2v_9 \\ 0 & 0 & \cdots & EI_2v_{11} \\ 0 & 0 & \cdots & EI_2v_{12} \\ 0 & 0 & \cdots & EI_2v_{13} \\ 0 & 0 & \cdots & EI_2w_8 \\ 0 & 0 & \cdots & EI_2w_9 \\ 0 & 0 & \cdots & EI_2w_{10} \\ 0 & 0 & \cdots & EI_2w_{11} \\ 0 & 0 & \cdots & EI_2w_{12} \\ . & . & \cdots & . \\ . & . & \cdots & . \\ . & . & \cdots & . \\ 0 & 0 & \cdots & V_1 \\ 0 & 0 & \cdots & V_{19} \end{pmatrix} \tag{3-33}$$

It is seen that all the rows related with EI_2, EI_2v_7-EI_2v_{13} and EI_2w_8-EI_2w_{12} are zeros.

Hence, EI_2, EI_2v_7-EI_2v_{13} and EI_2w_8-EI_2w_{12} are observable. Also, reactions, V_1 and V_{19} are observable since this is a statically determinate structure. However, for any row related with EI_1 or associated products (e.g. EI_1v_2, EI_1w_1), at least one element of that row is nonzero. Hence, these unknowns are not observable. Specifically, due to insufficient information of the displacements of nodes 1-7, the first column of N_1 implies a rigid body motion of rotation. That is, the rotations indicated by EI_1w_1-EI_1w_6 are the same while the deflections of these nodes can be calculated by the product of this rotation and the distance between the current node and node 1.

Step 4: Derive the compatibility conditions and analytical expression for the i^{th} structural parameter from those observable unknowns.

Once the observable unknowns are detected, their estimations are specified by the associated values of the particular solution. For instance, the particular solutions for EI_2 and EI_2v_7 are provided in Equations (3-34) and (3-35).

$$\widehat{EI_2} = \frac{18V_7L}{\frac{(w_7 - w_{13})}{L}} \tag{3-34}$$

$$\widehat{EI_2v_7} = -\frac{3V_7L^3(25w_7 - 12v_{10} + 11w_{13})}{2(w_7 - w_{13})} \tag{3-35}$$

The hat, ^, denotes an estimation of the unknown. The physical meaning of the analytical expression of EI_2, Equation (3-34), can be interpreted as the ratio of a moment expressed by the product of force and length and a curvature expressed by the displacements within elements of EI_2.

Rearranging the quotient between Equations (3-35) and (3-34) leads to the compatibility condition among $\{v_7,v_{10},w_7,w_{13}\}$, as presented in Equation (3-36).

$$12v_7 - 12v_{10} + 25w_7 + 11w_{13} = 0 \tag{3-36}$$

The compatibility conditions linking $\{w_7, v_{10}$ and $w_{13}\}$ and each of $\{v_7$-v_{13} and w_8-$w_{12}\}$ are found in the same way for elements of EI_2. It should be pointed out that regardless of the selected measurement set, the derivation of compatibility conditions always leads to identical mathematical equations.

Step 5: Repeat steps 2-4, until compatibility conditions and analytical expressions have been obtained for all parameters

Similarly, compatibility conditions among $\{v_2$-v_7,w_1-$w_7\}$ for EI_1 and those among $\{v_{13}$-v_{18},w_{13}-$w_{19}\}$ for EI_2 as well as the analytical expressions for EI_1 and EI_2 are obtained.

It is pointed out that for one given bending stiffness, the functional relations among the nodal displacements belonging to elements with this stiffness are obtained by the repetition of steps 2-4.

Step 6: Form an underdetermined system by combining all compatibility conditions

It is seen that displacements for beam elements with the same stiffness (EI_1, EI_2 or EI_3) are dependent on three displacements within these elements (being aware that boundary conditions can reduce this number). In a more general case, a set of 7(=2+3+2) adequate displacements is needed to specify every displacement in this structure. Assume {w_1, w_3}, {w_8, v_9, w_{11}} and {w_{15}, w_{19}} are chosen for EI_1-EI_3, respectively. Note that the displacements of joint nodes for elements with different parameters, e.g. v_7 for EI_1 and EI_2, determined by different compatibility conditions should be equal to each other. Hence, 4 more equations can be imposed, i.e. $v_7(w_1, w_3) = v_7(w_8, v_9, w_{11})$, $w_7(w_1, w_3) = w_7(w_8, w_{11})$, $v_{13}(w_8, v_9, w_{11}) = v_{13}(w_{15}, w_{19})$ and $w_{13}(w_8, w_{11}) = w_{13}(w_{15}, w_{19})$. This forms an underdetermined system with 4 equations and 7 unknowns ({w_1, w_3, w_8, v_9, w_{11}, w_{15} and w_{19}}). Hence, 3 out of the 7 adequate displacements are independent due to the 4 additional equations.

It is pointed out that all the compatibility conditions are related together by the displacements of those joint nodes between elements with different stiffnesses. From the resulting underdetermined system, a set of independent displacements can be obtained

Step 7: Choose a set of independent displacements in Step 6 as a condensed set $\hat{\delta}_c$. Express all compatible displacements $\hat{\delta}$ and structural parameters θ as functions of $\hat{\delta}_c$. That is, derive the functional relations $\hat{\delta}_i = f_i(\hat{\delta}_c)$ and $\theta_j = g_j(\hat{\delta}_c)$.

After steps 5 and 6, the relations among the nodal displacements belonging to elements with same stiffnesses as well as those associated with different stiffnesses are obtained. The displacements satisfy all these relations are referred as the compatible ones, $\hat{\delta}$. Note that all these displacements $\hat{\delta}$ are functions of a condensed set $\hat{\delta}_c$ (the independent displacements obtained in step 6). Specifically, $f_i(\hat{\delta}_c)$ is the functional form of the i^{th} compatible displacement $\hat{\delta}_i$ while $g_j(\hat{\delta}_c)$ is the functional form of the j^{th} parameter θ_j.

Without loss of generality, $\hat{\delta}_c$ is selected as {w_1, v_9 and w_{19}} since three displacements among {w_1, w_3, w_8, v_9, w_{11}, w_{15} and w_{19}} are independent (step 6). In this case, the functional relations $f_i(\hat{\delta}_c)$ for {w_3,w_8,w_{11} and w_{15}} are presented in Equations (3-37)-(3-40).

$$w_3 = 2(54v_9 + 1189w_1L + 17w_{19}L)/3123L \quad (3\text{-}37)$$

$$w_8 = -(2356w_1L - 519v_9 + 280w_{19}L)/2776L \quad (3\text{-}38)$$

$$w_{11} = -2(21v_9 + 19w_1L + 103w_{19}L)/347L \quad (3\text{-}39)$$

$$w_{15} = (352w_1L - 378v_9 + 575w_{19}L)/3123L \quad (3\text{-}40)$$

Regarding the functional form for bending stiffness, for instance, $\widehat{EI}_2$ can be determined by w_7 and w_{13} from Equation (3-34). As these two rotations are functions of $\hat{\delta}_c$, the functional form for $\widehat{EI}_2$ in terms of $\hat{\delta}_c$ is also available.

Step 8: Find the optimal $\hat{\delta}_c$ by minimizing the square sum of the proportional deviation of the compatible displacements, $\hat{\delta}$, from the measured displacements, $\tilde{\delta}$, as

indicated by Equation (3-41).

To smooth away the incompatibility in the measured displacements, the square sum of the proportional deviation of the i^{th} compatible displacement, $\hat{\delta}_i$, from the i^{th} measured displacement, $\tilde{\delta}_i$, is minimized, as indicated by Equation (3-41).

$$F(\hat{\delta}_c) = \sum_{i=1}^{N_m} \left(\frac{\hat{\delta}_i}{\tilde{\delta}_i} - 1 \right)^2 = \sum_{i=1}^{N_m} \left(\frac{f_i(\hat{\delta}_c)}{\tilde{\delta}_i} - 1 \right)^2 \tag{3-41}$$

in which N_m is the number of measured displacements.

Step 9: Evaluate the structural parameters by providing the optimal $\hat{\delta}_c$ to SSI by OM.

The best estimations of the bending stiffnesses are determined by providing the optimal $\hat{\delta}_c$ to SSI by OM.

Algorithm for SSI using compatibility conditions

All the necessary procedures to implement SSI for beam-like structures using compatibility conditions are presented in Figure 3-17 and summarized as follows.

Step 1: Introduce the geometry, as well as the known mechanical and geometrical properties and measured node forces to establish a FEM for the beam-like structure.

Step 2: Choose three nodal displacements belonging to elements with the same structural parameter and build Equation (3-30) using these displacements.

Step 3: Check the null space matrix N of coefficient matrix B of Equation (3-30) to obtain the observable unknowns.

Step 4: Derive the compatibility conditions and analytical expression for the i^{th} structural parameter from those observable unknowns.

Step 5: Repeat steps 2-4, until compatibility conditions and analytical expressions have been obtained for all parameters

Step 6: Form an underdetermined system by combining all compatibility conditions

Step 7: Choose a set of independent displacements in Step 6 as a condensed set $\hat{\delta}_c$. Express all compatible displacements $\hat{\delta}$ and structural parameters θ as functions of $\hat{\delta}_c$.

That is, derive the functional relations $\hat{\delta}_i = f_i(\hat{\delta}_c)$ and $\theta_j = g_j(\hat{\delta}_c)$.

Step 8: Find the optimal $\hat{\delta}_c$ by minimizing the square sum of the proportional deviation of the compatible displacements, $\hat{\delta}$, from the measured displacements, $\tilde{\delta}$, as indicated by Equation (3-41).

Step 9: Evaluate the structural parameters by providing the optimal $\hat{\delta}_c$ to SSI by OM.

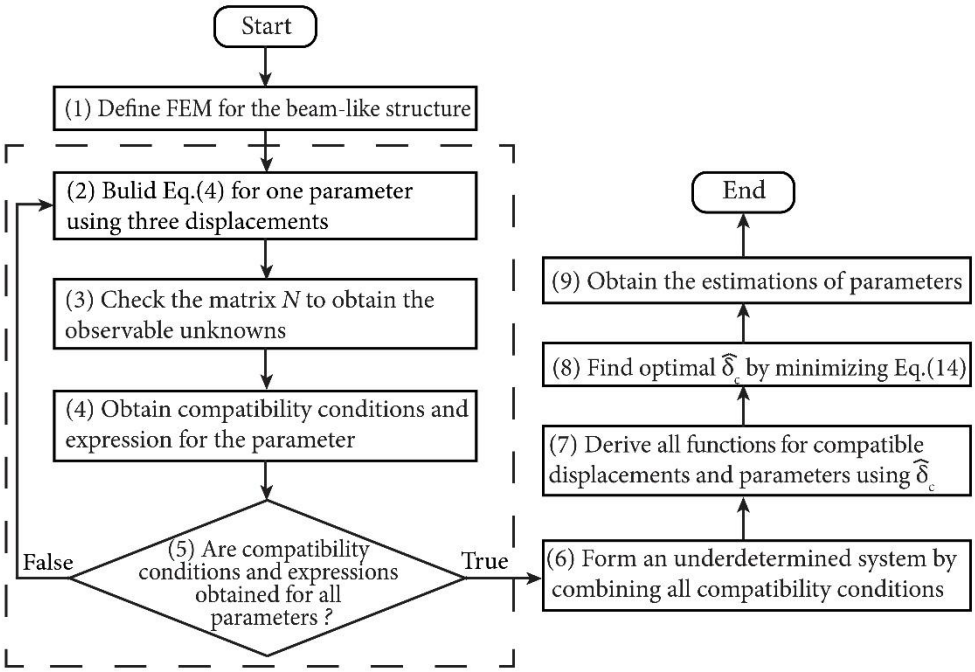

Figure 3-17 Flowchart for structural system identification for beam-like structures using compatibility conditions.

3.3.5 Application of the compatibility conditions

In this section, the accuracy of SSI by OM using redundant measurements without imposing compatibility conditions is presented first. Then the performance of the proposed method is investigated in a simply supported beam with respect to the number of measurements, N_m, error levels, E_{level}, and loading cases. At the end of this section, the applicability of this method is verified in a continuous beam.

Example 1 without compatibility conditions

The redundant set $\{v_3, v_5, v_7, v_9, v_{11}, v_{13}, v_{15}, v_{17}\}$($N_m$=8) is studied first. The measured displacements, $\tilde{\delta}$, are simulated by adding proportional noise to the real displacements, δ_r, as presented in Equation (3-42). This proportional noise is the product of a specified error level, E_{level}, and a random number, χ. This random number χ follows a normal distribution with zero mean and standard deviation of 0.5, and it is truncated by the interval [-1,1].

$$\tilde{\delta} = \delta_r \cdot (1 + E_{level} \cdot \chi) \tag{3-42}$$

2000 numerical simulations of the identification of bending stiffnesses using error levels from 1% to 8% were carried out without imposing compatibility conditions (Nogal et al., 2015). As the number of equations exceeds the number of unknowns, the ill-posed problem was solved using the Penrose inverse subroutine provided by Matlab.

To normalize the estimations, all the estimations are divided by their real values, which are denoted by a hat and the subscript *r*, i.e. $\hat{\ }_r$. This normalization is followed in the rest of the paper. Unless otherwise stated, estimations always refer to those normalized ones.

Without imposing some restrictions to the estimations, the method is useless due to the existence of extreme values (J. Lei et al., 2017). Thus, the average is taken for those estimations falling into the range of [0.5, 1.5]. Table 3-3 presents the mean of the estimations of associated parameters under different error levels using 8 measurements.

Table 3-3 Mean of the estimations for different bending stiffnesses by SSI by OM without compatibility conditions

Error level	$\widehat{EI}_{1,r}$	$\widehat{EI}_{2,r}$	$\widehat{EI}_{3,r}$
1%	0.85	0.79	0.88
2%	0.76	0.70	0.80
3%	0.73	0.68	0.76
4%	0.72	0.67	0.72
5%	0.72	0.68	0.71
6%	0.74	0.65	0.68
7%	0.70	0.62	0.64
8%	0.70	0.62	0.66

From this table, it can be concluded that, when compatibility conditions are not imposed: (1) Regardless of the error level, great bias exists despite redundant measurements are used; (2) The bias is sensitive to the error levels; (3) Using redundant measurements fails to improve the accuracy of the estimation via SSI by OM.

Example 1 with compatibility conditions: Effect of the number of measurements

To investigate the effect of the number of measurements, three measurement sets are studied here. Apart from the set N_m=8, the other two sets are {v_3-v_5, v_7, v_9-v_{11}, v_{13}, v_{15}-v_{17}} (N_m=11) and {v_2-v_{18}} (N_m=17). Note that the locations of measurements in both sets, set N_m=8 and set N_m=11, are included in the locations of measurements in set N_m=17. 2000 samples of measured displacements associated with set N_m=17 are generated with an error level of 4%. Then the samples for sets N_m=8 and N_m=11 are generated by taking the corresponding measurements in set N_m=17.

Figure 3-18 compares the accuracy of the estimations using these three sets. The accuracy of the proposed method is evaluated by the mean of the estimations while the robustness and confidence of the method are evaluated by the coefficient of variation (COV) in the estimations. Small COV of the estimations indicates a low dispersion.

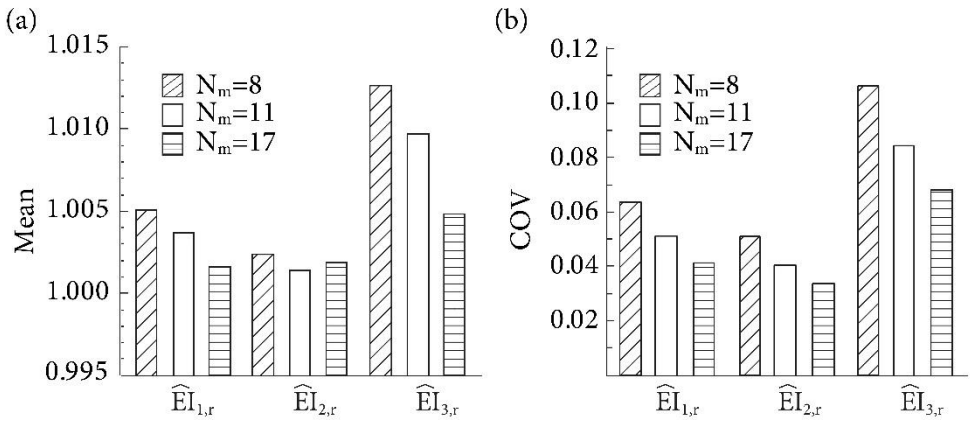

Figure 3-18 Using N_m = 8, 11, 17 measurements under error level of 4%: (a) mean of the estimations; (b) the coefficient of variation (COV) of the estimations

In Figure 3-18.a and b, it is seen that 8 measurements are sufficient to estimate $\widehat{EI}_{1,r}$ and $\widehat{EI}_{2,r}$ accurately with a low dispersion of the estimations. In the case of $\widehat{EI}_{3,r}$, a slight overestimation of 1.3% is observed, which is acceptable. However, the COV of the estimations in $\widehat{EI}_{3,r}$ is 0.112, which might not be negligible. When the number of measurements increases, the mean and the COVs of the estimations of the stiffnesses get closer to one and decrease, respectively. In addition, the improvement in $\widehat{EI}_{3,r}$ is relatively large when compared with the improvements in $\widehat{EI}_{1,r}$ and $\widehat{EI}_{2,r}$. In Figure 3-18.b, the drop of COV for $\widehat{EI}_{3,r}$ is roughly twice the drop of COV in $\widehat{EI}_{1,r}$ and $\widehat{EI}_{2,r}$ when the number of measurements increases. However, despite the fact that using more measurements reduces the extent of dispersion, the COV of the estimations of $\widehat{EI}_{3,r}$ using 17 measurements is still higher than the COV of the estimations of $\widehat{EI}_{1,r}$ or $\widehat{EI}_{2,r}$ using 8 measurements. The improvements of the results can be noticed when compared with those in Table 3-3, where for 8 measurements and a 4% error the results were far from acceptable. The worse accuracy observed in $\widehat{EI}_{3,r}$ compared with those results of $\widehat{EI}_{1,r}$ and $\widehat{EI}_{2,r}$ are in accordance with a previous study (J. Lei et al., 2017). In fact, for a given load test, the lowest the curvature in a given area of the structure, the worst the accuracy of the estimated parameters in that zone.

The analysis of the effect of the number of measurements shows that: (1) For zones where curvature is excited, small number of measurements is sufficient to achieve reasonable accuracy. (2) The more the measurements, the less the deviation and the dispersion of the estimations. (3) Greater improvement in the accuracy of the estimations is seen for parameters in low curvature zones than those in high curvature zones. (4) The curvature level is more important than the number of measurements.

Example 1 with compatibility conditions: Effect of error levels

The effect of error levels is investigated here using the set N_m=8. The studied error levels range from 1% to 8%. For each error level, 2000 samples are generated by Equation (3-42). The mean and COV of the estimations under different error levels are summarized in Figure 3-19. In Figure 3-19.a, the mean of the estimations increases slightly with the error level. However, the sensitivity of the structural parameters to the error levels is quite different. When E_{level} increases from 1% to 8%, the changes in the mean of $\widehat{EI}_{2,r}$ and $\widehat{EI}_{1,r}$ are 1.06% and 1.96% respectively, which are negligible. However, in the case of $\widehat{EI}_{3,r}$, the associated change is 5.26%, which is comparatively large. The order of sensitivity to error levels for these parameters is $\widehat{EI}_{3,r} > \widehat{EI}_{1,r} > \widehat{EI}_{2,r}$. In addition, overestimation can be observed for all parameters. The extent of the overestimation follows the same order. In Figure 3-19.b, COV for all parameters grows linearly with the error levels. Again, the COV of $\widehat{EI}_{3,r}$ is much higher than those of $\widehat{EI}_{1,r}$ and $\widehat{EI}_{2,r}$.

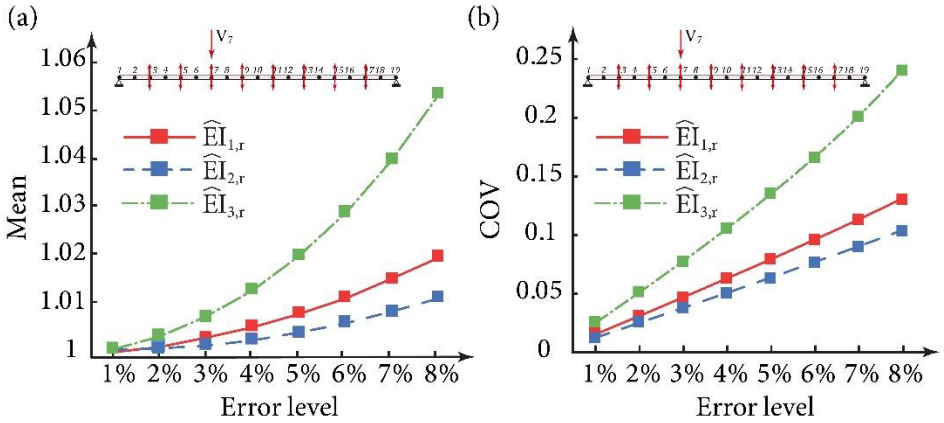

Figure 3-19 Using N_m = 8 measurements under error levels of 1% – 8%: (a) mean of the estimations; (b) the coefficients of variation (COV) of the estimations

Hence, it can be concluded that: (1) For zones where curvature is excited, the deviation in the mean of the estimation is not sensitive to the error levels; (2) The level of dispersion (COV) increases linearly with the error levels; (3) The increase of deviation and dispersion is much faster in low curvature zones.

Example 1 with compatibility conditions: Effect of loading cases

In previous analyses, slight overestimation and large dispersion are observed in low curvature zones. To investigate the influence of curvature, the external load is moved gradually from the left support (node 2) to the center of the structure (node 10), which adds up to 9 loading cases, as indicated in Figure 3-20.a. The measurement set N_m=8 (indicated by double arrows) is used here. 2000 samples are generated for both error levels of 4% and 8% by Equation (3-42). Mean and COV of the estimations of bending

stiffnesses under different loading cases and different error levels are summarized in Figure 3-20.b and c.

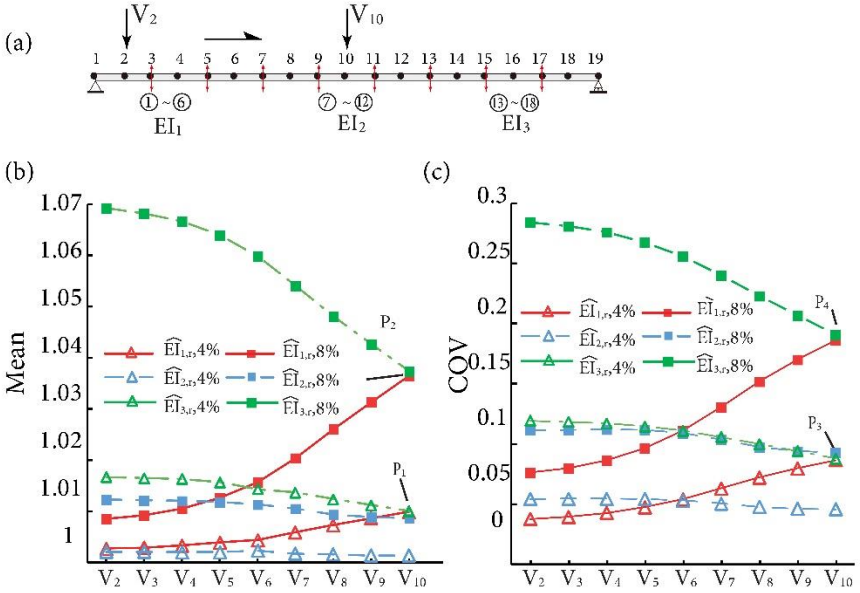

Figure 3-20 (a) Different loading cases (V_2 – V_{10}) and measurements (indicated by double arrows); (b) mean of the estimations under different loading cases with Errors of 4% and 8%; (c) the coefficient of variation (COV) of the estimations under different loading cases with Errors of 4% and 8%

When the load is applied at node 2, the bending behavior of elements of EI_1, i.e. elements 1-6, is quite activated. The associated mean for $\widehat{EI}_{1,r}$ is 1.003 (E_{level}=4%) and 1.009 (E_{level}=8%), which is insensitive to errors. However, in the case of EI_3, a higher overestimation can be observed when higher errors exist in the measurements. The associated mean for $\widehat{EI}_{3,r}$ is 1.017 (E_{level}=4%) and 1.069 (E_{level}=8%).

When the load moves from node 2 to node 10, the curvature of the elements of EI_1 decreases while the curvature of the elements of EI_3 increases. Correspondingly, an overestimation of $\widehat{EI}_{1,r}$ arises and escalates while the overestimation of $\widehat{EI}_{3,r}$ becomes less severe. Similar variation is found in the COV of $\widehat{EI}_{1,r}$ and $\widehat{EI}_{3,r}$. In a symmetric loading case (V_{10}), the mean of $\widehat{EI}_{1,r}$ and $\widehat{EI}_{3,r}$ are the same, marked by the intersection P_1 and P_2 (Figure 3-20.b). This is the same case for associated COV, marked by the intersection P_3 and P_4 (Figure 3-20.c). Note that the bending behavior for elements of EI_2 is quite activated under each loading case. When the load moves from node 2 to node 10, the curvature of these elements becomes even higher. As a result, a small but perceptible improvement is seen in both the mean and the COV of $\widehat{EI}_{2,r}$.

The analysis of Figure 3-20 implies that: (1) In the same loading case, the deviation and the dispersion of the estimations are much higher in zones of lower curvature. (2) When the curvature increases due to the change of loading case, the deviation and dispersion of the estimations decrease correspondingly.(3) it is advisable to apply different loading

cases to study different zones of the beam. For instance, to identify EI_1, the location of the load at node 2 is the best choice.

Example 2: Continuous beam bridge

This section illustrates the application of SSI using compatibility conditions to a 30 m+30 m continuous bridge and the applicability of using different loading cases to study different zones of this structure.

The variation of the sectional properties is simulated by different values of the bending stiffnesses in different zones. The FEM for this structure and the structural parameters are depicted in Figure 3-21.a. It is assumed that $EI_{1,r}$=$EI_{8,r}$=1.5×10^6 $kN \cdot m^2$, $EI_{2,r}$=$EI_{7,r}$=1.8×10^6 $kN \cdot m^2$, $EI_{3,r}$=$EI_{6,r}$=2.1×10^6 $kN \cdot m^2$, $EI_{4,r}$=$EI_{5,r}$=2.5×10^6 $kN \cdot m^2$. In this study, {v_2-v_{12} and v_{14}-v_{24}} are measured and a point load is positioned along the deck to provide different static loading cases. For each loading case, measurements are generated 2000 times by Equation (3-42) using an error level of 4%. The mean and COV of the estimations are summarized in Figure 3-21.b and c. Due to the symmetry of the structure, only the results for half of the structure is provided.

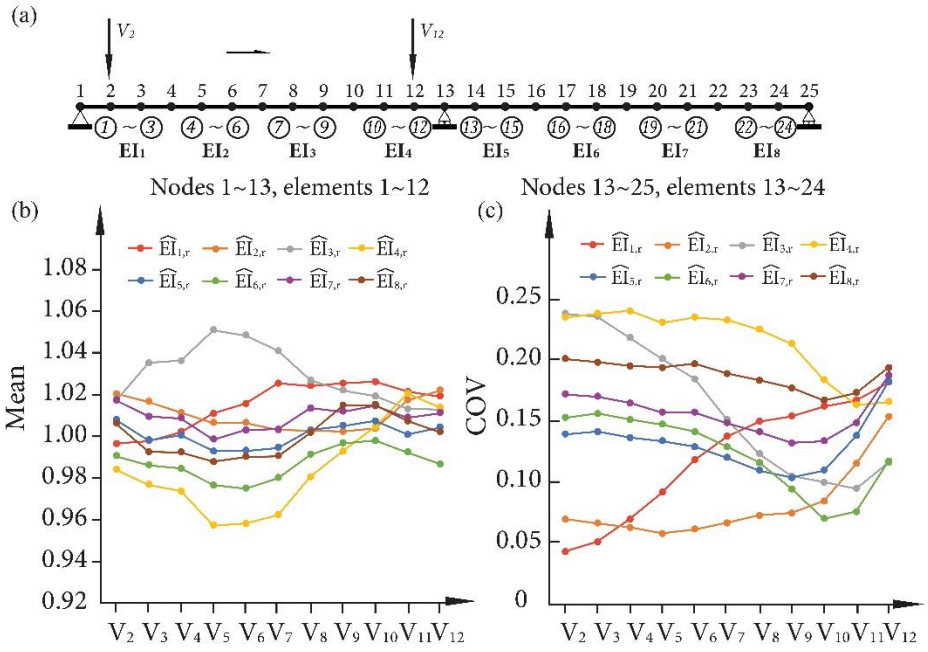

Figure 3-21 (a) Different loading cases (V_2 – V_{12}) and measured deflections (v_2-v_{12},v_{14}-v_{24}); (b) mean of the estimations under different loading cases with Error = 4%; (c) the coefficient of variation (COV) of the estimations under different loading cases with Error = 4%

In Figure 3-21.b, the bias in the mean of the estimations is generally within 2%. The largest bias is seen in $\widehat{EI}_{3,r}$ and $\widehat{EI}_{4,r}$ with a magnitude of around 5% when the

loading case is V_5. When the load is applied at zones associated with EI_3 and EI_4, i.e. from V_7 to V_{12}, associated bias decreases greatly, In Figure 3-21.c, when the load is moved from V_2 to V_{10}, the curvatures of zones related with EI_1 and EI_2 always decrease. Consequently, the COVs for $\widehat{EI}_{1,r}$and $\widehat{EI}_{2,r}$ generally increase. In the case of $\widehat{EI}_{3,r}$ and $\widehat{EI}_{4,r}$, their COVs decrease first due to the increase of curvatures in associated zones. However, when the load is quite close to the middle support, a high proportion of the load is borne by the middle support and insignificant bending behavior is induced in the structure. As a result, a sharp increase of COV is observed in Figure 3-21.c when the loading cases vary from V_{10} to V_{12}.

Since the mean of the estimations is generally around one, the best loading case for a targeted bending stiffness is selected as the loading case leading to the lowest dispersion of associated estimations. Figure 3-21.c shows that the variation of COV largely depends on the loading cases. The lowest COVs for EI_1 and EI_2 are 0.044 (V_2) and 0.058 (V_5), respectively. They increases to 0.182 and 0.154, respectively, when the load is positioned at V_{12}. The best loading case for estimating EI_3 seems to be V_{11}. However, note that the COV curve for $\widehat{EI}_{6,r}$ is always lower than the COV curve for $\widehat{EI}_{3,r}$ in all loading cases. Due to the symmetry of the structure, the estimation of EI_6 using a load in the first span is the same as the estimation of EI_3 using the associated symmetric load in the second span. Hence, the optimal loading case for estimating EI_3 is symmetric to the loading case having the lowest COV of $\widehat{EI}_{6,r}$ (i.e. V_{10}). Due to the symmetry between V_{10} and V_{16}, the loading case V_{16} yields the best estimation of EI_3. The associated COVs for EI_3 are 0.070 (V_{11}) and 0.095 (V_{16}), indicating a decrease of 26.3%. Similarly, the lowest COV of $\widehat{EI}_{5,r}$ occurs at V_9. Concerning the symmetry between EI_4 and EI_5 as well as the symmetry between V_9 and V_{17}, the loading case V_{17} yields the best estimation of EI_4. The best mean, COVs and the load locations for $\widehat{EI}_{1,r}$-$\widehat{EI}_{4,r}$ are listed in Table 3-4. Due to the symmetry, the results for $\widehat{EI}_{5,r}$-$\widehat{EI}_{8,r}$ are not included.

Table 3-4 The best mean, COVs and the associated loading cases for the estimations, $\widehat{EI}_{1,r}$-$\widehat{EI}_{4,r}$.

	$\widehat{EI}_{1,r}$	$\widehat{EI}_{2,r}$	$\widehat{EI}_{3,r}$	$\widehat{EI}_{4,r}$
Mean	0.996	1.006	0.998	1.005
COV	0.044	0.058	0.070	0.104
Best loading case	V_2	V_5	V_{16}	V_{17}

It should be mentioned that, Maxwell-Betti reciprocal theorem can be exploited to reduce the number of sensors while still getting dense measurements (Z. Sun et al., 2016; C. Wang et al., 2011), providing that the response induced by the excitation is still in elastic range. When one sensor is fixed and a point load is positioned at different locations, the readings of the sensor represent the deflections of the structure at the various locations of the load when applying the load at the location of the sensor. This

is to say, when the load is positioned at different locations, the placement of one sensor is the same as adding one loading case. This can be achieved by positioning a truck with calibrated weight at various locations along the bridges (Bell, Lefebvre, & Sanayei, 2013). Hence, in order to get accurate and robust estimations of EI_1-EI_8, it is recommended to place sensors at nodes 2, 5, 16, 17, 9, 10, 21 and 24 together with a load positioned at various locations on the structure.

This example shows the applicability of using different loading cases to obtain reliable estimations of the bending stiffnesses for different zones in a continuous beam. The best loading case for a targeted bending stiffness is selected as the one leading to the lowest dispersion of associated estimations.

3.3.6 Conclusions

This paper proposes a novel approach for identifying compatibility conditions, the relations among displacements, in beam-like structure using observability method. By solving an underdetermined system of equations formulated by compatibility conditions, it is shown that all displacements in a beam-like structure are functions of a subset of these displacements. Then an optimization procedure is introduced to reduce the measurement errors by minimizing the square sum of the proportional deviation of the measured displacements and those compatible displacements. In the numerical simulation, it is shown that when compatibility conditions are not imposed: (1) Regardless of the error level, great bias exists in the estimations though redundant measurements are used. (2) The bias is sensitive to the error levels. (3) Using redundant measurements fails to improve the accuracy of the estimation via SSI by OM. After the imposition of compatibility conditions by optimization, the performance of the proposed method is investigated regarding the number of measurements, error levels and loading cases. It is concluded that: (1) The accuracy and robustness of the estimations are significantly improved when compatibility conditions are imposed. (2) The curvature of the zones where parameters are estimated is of vital importance: In the same loading case, the deviation and dispersion of the estimations are much higher in zones of lower curvature. Also, the deviation and dispersion of the estimations increase faster with error levels in these zones than in zones of higher curvature. (3) The improvement of the estimation due to the increase of measurements is more significant in low curvature zone. (4) For zones where curvature is excited, small number of measurements is sufficient to achieve reasonable accuracy. In addition, the deviation in the mean of the estimation is not sensitive to the error levels in these zones. (5) Different loading cases can be applied to achieve reliable estimations of parameters for different zones.

The overall performance of the proposed algorithm illustrates its potential application in the SSI for beam-like structures. A possible direction of the future research could be the optimal sensor placement for various types of structures and the experimental verification for the proposed method.

3.4 Robust Static Structural System Identification Using Rotations

Title: Robust Static Structural System Identification Using Rotations

Authors: Jun Lei, José Antonio Lozano-Galant, María Nogal, Dong Xu, José Turmo

Journal: Structural Control and Health Monitoring

Publication: Technical Paper

Submitted: 06-Dec-2017

State: Under review

DOI: -

Available at:-

3.4.1 Summary

Deflections are commonly measured in the static structural system identification of structures. Comparatively less attention has been paid to the possibility of measuring rotations. In addition to the advantages of using inclinometers, such as high-resolution and reference-free; although some works using rotations can be found in the literature, this paper, for the very first time, proposes a statistical analysis that justifies the theoretical advantage of measuring rotations. To do so, the analytical expressions for the target parameters are obtained via static structural system identification by constrained observability method first. Combined with the inverse distribution theory, the probability density function of the estimations of the target parameters are obtained. The comparative studies on a simply supported bridge and a frame structure demonstrate the strength of measuring rotations regarding the unbiasedness and the extent of variation in the estimations. In order to tackle with redundant measurements and achieve robust estimations of the parameters, four strategies are proposed and compared. Numerical verifications on a bridge structure and a high-rise building have shown promising results.

3.4.1 Introduction

Motivation

Potential catastrophic events due to the failure of civil infrastructure (e.g. bridges, high-rise buildings, dams) might claim people's lives and cause substantial economic losses. It is vital to know the current condition of structures. For this reason, structural health monitoring and structural system identification (SSI) have attracted much attention in the past decades (Khuc & Catbas, 2017; H. Sun & Büyüköztürk, 2015; Z. Sun, Zou, &

Zhang, 2017). A basic assumption in SSI is that the deterioration or the damage of structures is reflected in the change of structural parameters (such as bending stiffnesses, axial stiffnesses). These parameters can be estimated by various SSI methods using measured response from structures under external excitations. These methods not only validate the accuracy of computational models for the design but also help engineers to better understand the condition of the structures.

SSI methods can be categorized as static or dynamic. The vast majority of these methods are dynamic ones. Depending on the source of excitation, dynamic SSI methods are categorized as input-output methods and output-only methods. The input-output methods were developed in early periods. In these methods, both the external excitation and the response are measured (Atamturktur, Hemez, & Laman, 2012; Cheung & Beck, 2010; Jiang & Adeli, 2005; H. Sun & Betti, 2015). Atamturktur applied model calibration and validation to historic masonry monuments excited by an impact hammer at multiple locations (Atamturktur et al., 2012). (Cheung & Beck, 2010) applied Bayesian model class assessment and averaging to a dynamic system. (Jiang & Adeli, 2005) proposed Levenberg-Marquardt least-square method to train the dynamic fuzzy wavelet neural network model using the seismic records and measured data. (H. Sun & Betti, 2015) applied the Bayesian inference and a hybrid optimization algorithm to model updating. On the other hand, many studies are devoted to the output-only methods, where only ambient (e.g. wind-induced, traffic-induced) vibrations are measured (Juan P Amezquita-Sanchez & Adeli, 2015; Foti, Gattulli, & Potenza, 2014; H. Sun et al., 2015; F.-L. Zhang, Ni, & Lam, 2017). These methods are desirable because there is no need for measuring excitation and interrupting the operation of the structure. (F.-L. Zhang et al., 2017) develops a Bayesian model updating method incorporating modal identification information in multiple setups for structures under ambient excitations. (Foti et al., 2014) implemented the output-only identification for a seismically damaged structure. (Juan P Amezquita-Sanchez & Adeli, 2015) detected, located and quantified damages in a high-rise building without knowing the input. (H. Sun et al., 2015) applied a damped Gauss-Newton method to identify structural parameters with incomplete measurements.

Compared with dynamic methods, static SSI methods are much less developed. (Masoud Sanayei & Scampoli, 1991) identified the plate-bending stiffness of a reinforced concrete pier deck using incomplete static test data. However, this method requires accurate force and displacement measurements. Later, (M Sanayei & Saletnik, 1996a) used optimization techniques to minimize the discrepancy between the measured and the predicted static strains to identify the structural parameters for trusses and frames. A good selection of noise-tolerant measurements and forces was necessary and was achieved by pretest simulations. (Banan et al., 1994a) posed SSI as a constrained nonlinear least-squares problem by minimizing the discrepancies between the measured and the predicted displacements or forces. (Hjelmstad & Shin, 1997) incorporated an adaptive parameter grouping strategy with the work from Banan. The

proposed method can locate and assess damage even under sparse and noisy measurements. (Choi et al., 2004) derived elastic damage load theorem for statically determinate structure and validated the proposed method with a simply supported beam with single damage using deflections. (Z. Sun et al., 2016) approximated the curvatures of the studied beams by the second-order difference of deflections. The damages were located by the abnormality in the curvature curves. However, many deflections were required and the magnitude of damage was not quantifiable. (Q. Yang & Sun, 2010) applied flexibility disassembly technique in stiffness equilibrium equations to locate and quantify damages in structures. The efficacy of this method was validated by a cantilever beam and two trusses. However, an existing model of the healthy structure and measurements of all displacements are required. (Jose Antonio Lozano-Galant, Nogal, et al., 2013) applied the observability method (OM) to determine the identifiability of structural parameters in 2D beam models symbolically with any given static measurements. In this method, the nonlinearity due to the coupling of unknown variables was avoided by treating the products of several unknowns as single linearized variables. Later, the numerical development of this method, SSI by numerical OM (NOM), was proposed by (Nogal et al., 2015). The effects of measurement errors and simulation errors on the estimation accuracy were studied by (J. Lei et al., 2017). Later, (J. Lei, Xu, & Turmo, 2018) derived the compatibility conditions that the displacements of beam-like structures should satisfy using OM. These conditions were exploited to reduce the adverse effect of measurement errors on the estimation accuracy. However, this method is only applicable in beam-like structures.

Existing static SSI methods largely measure deflections rather than rotations (Choi et al., 2004; Z. Sun et al., 2016; Q. Yang & Sun, 2010). However, inclinometers have been well developed and widely applied in many industries, e.g. automotive, electronics and aviation industries (Ha, Park, Choi, & Kim, 2013). In the context of civil engineering, they have been applied in the long term monitoring of structures. For instance, stadiums *Design Plaza Building* (Park, Shin, Choi, & Kim, 2013), high-rise buildings, *Tianjin 117* (597 m) (T. Liu, Yang, & Zhang, 2017), *Shanghai Tower* (632 m) (J. Z. Su et al., 2013) and bridges, *Lutrive Bridge* (Robert-Nicoud, Raphael, Burdet, & Smith, 2005). Specially, the main application of inclinometers in bridges is to reconstruct the deflected shape due to the difficulty in measuring deflection directly. However, systematic errors might be introduced into the approximated deflections due to the assumption made in the basis functions (e.g. precalculated deflected shapes (Robert-Nicoud et al., 2005), polynomials (X. He, Yang, & Zhao, 2014)). Hence, the direct use of rotations might be preferred. Zhang estimated the deflections accurately via partial least square method from an Finite Element Model (FEM) without using basis functions (W. Zhang, Sun, & Sun, 2017). In this work, the possibility of locating damage using inclinometers was also investigated. In fact, inclinometers have some merits that make them advantageous for SSI: (1) Reference-free. No need for reference points from which relative movements are measured for contact-based deflection measurement methods. On the other hand, inclinometers do not suffer from those limitations in

noncontact-based deflection measurement methods, like the illumination condition, the background disturbance and the movement of the cameras (Feng et al., 2016). (2) High resolution. The reported resolution of inclinometers is $9.7\times10^{-7}\ rad$ (Lee, Ho, & Lee, 2012). A table of the technical specifications of several commercial inclinometers is also provided. Due to this high accuracy, it is easy for inclinometers to detect small deformations of the structure. (3) Compactness and lightweight. This makes the installation convenient, even in hard-to-reach locations. (4) Robustness. Each inclinometer is independent of others, and thus the malfunction of any does not affect the rest. (5) Recyclable and economical. Inclinometers are inexpensive and easy to operate (Robert-Nicoud et al., 2005; W. Zhang et al., 2017). They can be dissembled and reused easily. (6) Inclinometers can be incorporated into wireless sensor network to achieve remote and real-time monitoring (Ha et al., 2013).

In previous study, it was demonstrated that the estimations of bending stiffnesses were more sensitive to the measurement errors in deflections than those in rotations for beam-like structures (J. Lei et al., 2017). However, among all those work related to use inclinometers, no theoretical advantage of using rotations can be found. In addition, the comparison between the accuracy of estimations using rotations and using deflections is lacking for SSI in frame structures. Furthermore, when more displacements are measured, the estimations should be improved. However, the result of using more measurements was still biased (J. Lei, Xu, et al., 2018).

Contribution

To have a better understanding of the static SSI problem, the contributions of this paper are:

(1) To provide an original and systematic methodology to obtain the analytical expressions for structural parameters θ in static SSI.

(2) To provide statistical analysis of the distribution of the estimations using the analytical expressions and inverse distribution theory (Johnson, Kotz, & Balakrishnan, 1994).

(3) To justify the theoretical advantage of using rotations than using deflections regarding the unbiasedness and the extent of variation in the estimations.

(4) To provide several strategies to use redundant measurements in order to improve the accuracy of the estimations.

Scope

The remainder of this paper is organized as follows. Section 3.4.3 describes the algorithm for SSI by constrained OM, which obtains the analytical expressions as well as the numerical estimations for the parameters. In addition, the procedure to carry out

statistical analysis with the resulting expression is also presented in this section. Section 3.4.4 provides two illustrative examples to justify the theoretical advantages of using rotations over using deflections. Section 3.4.5 investigates the effectiveness of four strategies to make use of available measurements in a high-rise building. Finally, some conclusions are presented in section 3.4.6.

3.4.2 Methodology

SSI by Constrained observability method

In the first application of OM in SSI, the identifiability of structural parameters was determined symbolically by checking the null space (see ***Definition 1***) of the coefficient matrix of a system of equations that was adapted from equilibrium equations in stiffness matrix method (Jose Antonio Lozano-Galant, Nogal, et al., 2013). This technique was also applied in the identification of structural parameters for cable-stayed bridges (Jose Antonio Lozano-Galant et al., 2014). (Nogal et al., 2015) proposed the SSI by Numerical OM (NOM) where a symbolical approach, which determined the observability of parameters, and a numerical approach, which evaluated the estimations, were combined.

Definition 1(Null space and Null space matrix)*:* The null space for a $m \times n$ matrix $[A]$ is the vector space whose vectors satisfy Equation (3-43), which is a homogeneous equation.

$$[A]\{x\} = \{0\} \tag{3-43}$$

Hence, the null space for matrix $[A]$ is defined in Equation (3-44).

$$Null([A]) = \{\{x\} \in R^n | [A]\{x\} = 0\} \tag{3-44}$$

The null space matrix $[N]$ for the matrix $[A]$ is a matrix whose columns form a basis of the null space $Null([A])$, which can be computed by Gaussian elimination. In fact, any vector in the null space is a linear combination of the basis vectors for $Null([A])$, i.e. columns of the matrix $[N]$.

In both SSI by OM and by NOM, it is pointed out that:(1) The identification of structural parameters is a recursive process in which the parameters identified in the last recursive step are incorporated into the input of the current recursive step to enable the identification of other parameters. (2) In each recursive step, the coupled variables appearing in the system of equations are treated as linearized ones.

However, it was found that the assumption of linearity might reduce the number of observable parameters with given measurement sets(J. Lei, Nogal, Lozano-Galant, Xu, & Turmo, 2018). Then, a two-stage SSI by constrained OM (COM) was proposed: (1) **Stage 1**: SSI by NOM is implemented until no more parameters are observable. (2) **Stage 2**: The system of equations from the last recursive step in **Stage 1** is reformulated

as a constrained optimization problem minimizing the square sum of the residuals of this system.

The 7 steps to carry out SSI by COM are described below. The **Stage 1** is related to **Steps 2-5** while the **Stage 2** is related to **Step 7**.

Step 1: Define an initial FEM using 2D beam elements for the structure to be analyzed. Generate the system of equilibrium equations at all nodes for this FEM, as shown by Equation (3-45).

$$[K]\{\delta\} = \{f\} \tag{3-45}$$

The matrix $[K]$ is the global stiffness matrix that includes the information of length L_j, elastic moduli E_j, area A_j and inertia I_j of element j ($j=1, 2 \ldots N_e$). The displacement vector $\{\delta\}$ comprises horizontal deflection u_i, vertical deflection v_i, rotation w_i of node i ($i=1, 2 \ldots N_n$). The force vector $\{f\}$ comprises horizontal force H_i, vertical force V_i and moment M_i applied on node i ($i=1, 2 \ldots N_n$). The numbers of elements and nodes in the FEM are denoted by N_e and N_n.

Step 2: Introduce the boundary conditions and values of the increments of displacements and forces during the static test to obtain the observability equations.

The entries in the matrix $[K]$ are sums of monomial ratios, which are the ratios between axial or bending stiffnesses and the square (or cubic) of the length, i.e. $\frac{E_j A_j}{L_j}$, $\frac{E_j I_j}{L_j^2}$ or $\frac{E_j I_j}{L_j^3}$.

In direct analysis, the mechanical properties, E_j, A_j, I_j and the geometrical properties, L_j, are known and hence the matrix $[K]$ is known. This is not true when the SSI is introduced. Generally, it is assumed that L_j is still known and E_j, A_j, I_j are unknown parameters to be estimated. Note that E_j, A_j, I_j and L_j from different elements might appear in the same entry due to the element connectivity. To separate these parameters, each column of matrix $[K]$ is divided into multiple columns such that any resulting column is uniquely related to one monomial (stiffness) E_jA_j or E_jI_j. Meanwhile, the displacement vector $\{\delta\}$ is expanded correspondingly. Then, these stiffnesses are extracted from the matrix $[K]$ and the expanded displacement vector is multiplied by them. Hence, a (constant) modified matrix $[K^*]$ and a modified vector $\{\delta^*\}$ composed of nonlinear products, e.g. $E_jA_ju_i$, $E_jI_jw_i$, $E_jI_jv_i$, are obtained, as shown in Equation (3-46).

$$[K^*] \cdot \{\delta^*\} = \{f\} \tag{3-46}$$

Once the boundary conditions and the forces applied in the non-destructive static test have been defined, it is assumed that a subset of increments of deflections $\{\delta_1^*\}$ of $\{\delta^*\}$ is known and a subset of forces $\{f_1\}$ are known while the remaining part $\{\delta_0^*\}$ and $\{f_0\}$ are unknown. By static condensation procedure, Equation (3-46) can be partitioned as Equation (3-47).

$$[K^*]\{\delta^*\} = \begin{bmatrix} K_{00}^* & K_{01}^* \\ K_{10}^* & K_{11}^* \end{bmatrix} \begin{Bmatrix} \delta_0^* \\ \delta_1^* \end{Bmatrix} = \begin{Bmatrix} f_0 \\ f_1 \end{Bmatrix} = \{f\} \tag{3-47}$$

To cluster the unknowns $\{\delta_0^*\}$ and $\{f_0\}$, Equation (3-47) can be rewritten equivalently as the observability equations, Equation (3-48).

$$[B]\{z\} = \begin{bmatrix} K_{10}^* & 0 \\ K_{00}^* & -I \end{bmatrix} \begin{Bmatrix} \delta_0^* \\ f_0 \end{Bmatrix} = \begin{Bmatrix} f_1 - K_{11}^* \delta_1^* \\ -K_{01}^* \delta_1^* \end{Bmatrix} = \{D\} \tag{3-48}$$

in which *0* and *I* are the null and the identity matrices, respectively.

Step 3: Check the null space matrix $[N]$ of the coefficient matrix $[B]$ to determine the observability of unknowns in $\{z\}$ and obtain the numerical estimations for observable variables. For Equation (3-48) to have at least one solution, the product of the transpose of the right-hand side vector, $\{D^T\}$ and the null space of the transpose of the matrix $[B]$, $Null([B^T])$, should satisfy that $[D^T]\cdot Null([B^T])=0$. If this holds, the structure of the general solution $\{z_g\}$ to Equation (3-48) is given by Equation (3-49)

$$\{z_g\} = \{z_p\} + \{z_h\} = \begin{Bmatrix} \delta_0^* \\ f_0 \end{Bmatrix}_p + [N] \cdot \{\rho\} \tag{3-49}$$

where $\{z_p\}$ is a particular solution to Equation (3-48) and $\{z_h\}$ is a solution to the homogeneous version of Equation (3-48) (i.e. the vector $[D]$ is replaced by zeros). From ***Definition 1***, $\{z_h\}$ is a vector in $Null([B])$, as well as a linear combination of the columns of the matrix $[N]$. The coefficients of the linear combination are denoted by the vector $\{\rho\}$. The observability of unknowns in the vector $\{z\}$ is determined by checking null rows in the matrix $[N]$. If any row in the matrix $[N]$ is null, then the same row of $\{z_h\}$ is also null. Then the associated variable in $\{z_g\}$ is determined by its particular solution $\{z_p\}$. This means that this variable is uniquely determined and observable. The calculation of the null space matrix $[N]$ should be carried out symbolically to avoid omitting observable variables because close to zero values from numerical calculations might appear in those null rows. The numerical values of the observable variables are obtained from the particular solution of Equation (3-48) using least squares or Moore-Penrose pseudo-inverse methods. All of these algorithms are available in many packages, e.g. *Matlab* or *Mathematica*.

Step 4: Check whether new variables in the unknown vector $\{z\}$ were identified or not. If identified, go to **Step 5**. Otherwise, go to **Step 6**.

Step 5: Any identified variables will be incorporated into the preceding input to form the subsequent input and initiate a new recursive step. This may enable the identification of other unknowns in $\{z\}$. **Steps 2-4** are repeated until no more variables can be identified.

Step 6: Check whether all variables are identified or not. If all the parameters are identified, then SSI by COM is finished. Otherwise, go to **Step 7**.

Step 7: Obtain the estimations of parameters by solving the constrained optimization

problem that is adapted from the observability equations in the last recursive step. Since the linearization of the unknowns leads to the reduction of observable unknowns, the nonlinearity in SSI is regained by means of solving an optimization problem with the constraints that the linearized products are equal to the product of associated single variables, e.g. $EI_2v_2=EI_2\cdot v_2$.

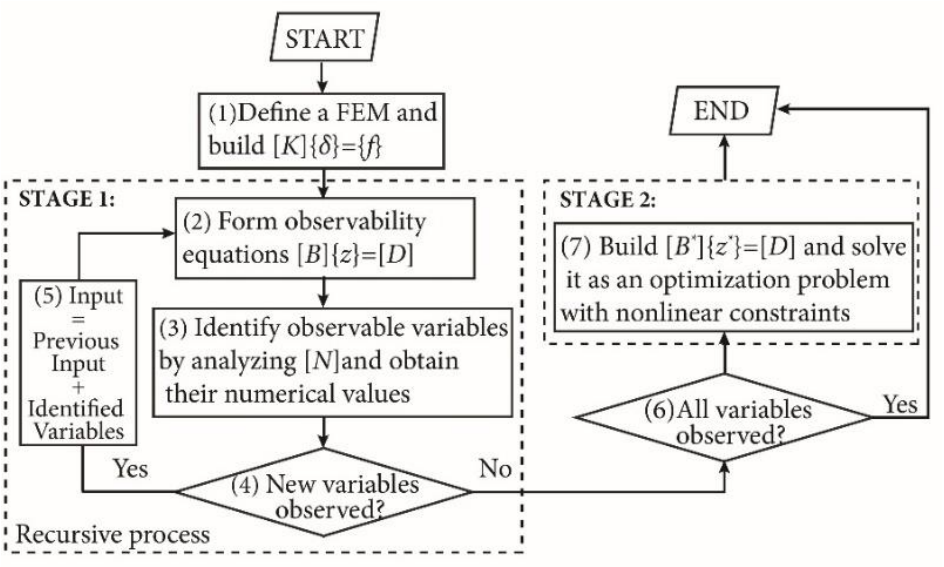

Figure 3-22 Flowchart of the algorithm for SSI by COM

However, some single variables $\{z_s\}$ may not appear in the unknown vector $\{z\}$ of Equation (3-48). A new unknown vector $\{z^*\}$ is obtained by adding $\{z_s\}$ in $\{z\}$. A null matrix $[\Omega]$ is introduced into the coefficient matrix so that the equations are not violated, as shown in Equation (3-50).

$$[B^*]\cdot\{z^*\}=[B\ \Omega]\begin{Bmatrix}z\\z_s\end{Bmatrix}=\{D\} \tag{3-50}$$

The objective function of the optimization is to minimize the square sum of the residuals of Equation (3-50), as shown in Equation (3-51).

$$f(z^*)=\sum_{i=1}^{3N_n}\epsilon_i^2 \tag{3-51}$$

where ϵ_i is the residual of the i^{th} equation in Equation (3-50).

Remark 1: In **Step 2**, the observability equations (Equation (3-48)) are adapted from equilibrium equations. Each equation is related to the equilibrium at one node. In addition, the residuals appearing in Equation (3-51) are those unbalanced nodal forces. The objective function (Equation (3-51)) is essentially the square sum of all unbalanced nodal forces.

Remark 2: In **Step 3**, instead of obtaining numerical estimations, the analytical expressions of the variables can be obtained symbolically using Gaussian elimination, which is essential for the statistical analysis presented in following section.

Remark 3: In stage 1 (**Steps 2-5**), the observability equations are treated linearly such that the computation is much reduced when compared with nonlinear methods. All the steps in stage 1 are the same as those in SSI by NOM.

Remark 4: In stage 2 (**Step 7)**, the ignored nonlinearity is resolved by imposing constraints via optimization with the aim of identifying more parameters. Since some parameters have been identified in stage 1, the solution space for the optimization algorithm to explore in stage 2 is much reduced, which eases the computation and convergence issues. In addition, the magnitudes of the variables in $\{z^*\}$ might be wildly different. Hence, numerical scaling is recommended prior to solve the optimization for faster convergence and better computation efficiency.

Inverse distribution

The definition of inverse distribution is given here.

***Definition 2 (Inverse distribution)**:* Let X be a random variable and the random variable Y is the inverse of X, i.e. $Y=1/X$. Then the distribution of Y is called the inverse distribution of X. In this paper, it is assumed that measurement errors follow a normal distribution. Random errors are added to theoretical displacements in a proportional manner, as indicated by Equation (3-52).

$$\tilde{\delta} = \delta_r \cdot (1 + E_{level} \cdot \xi) \tag{3-52}$$

δ_r is the displacement obtained from finite element analysis and E_{level} is the error level. ξ is a random number that follows the normal distribution with zero mean and standard deviation 0.5, i.e. $N(0, 0.5^2)$. Some important properties about the inverse distribution of normal random variables (Johnson et al., 1994) are provided here. If a random variable X follows the normal distribution with the mean μ and the standard deviation σ, i.e. $X \sim N(\mu,\sigma^2)$, the probability density function of the random variable $Y=1/X$ (or the inverse distribution of X) is given by:

$$p_Y(y|\mu,\sigma) = \frac{1}{\sqrt{2\pi}\sigma y^2} e^{-\frac{\left[\left(\frac{1}{y}\right)-\mu\right]^2}{2\sigma^2}} \tag{3-53}$$

The distribution of Y is bimodal and it has a negative mode at y_1 and a positive mode at y_2.

$$y_1 = -\frac{\mu + \sqrt{\mu^2 + 8\sigma^2}}{4\sigma^2} \tag{3-54}$$

$$y_2 = \frac{-\mu + \sqrt{\mu^2 + 8\sigma^2}}{4\sigma^2} \tag{3-55}$$

The mean and the standard deviation for the distribution of Y on a specified interval can be calculated by associated integrations of the probability density function p_Y. These formulas can be found in classic statistic books (Johnson et al., 1994).

Procedure for the statistical analysis of the distribution of estimations

Step 1: Define a FEM for the structure to be analyzed according to the aimed accuracy of estimations.

Step 2: Choose a measurement set to obtain the analytical expression for the target parameter θ using SSI by COM. Instead of obtaining the particular solution numerically (see **Step 3** in Figure 3-22), the solution is obtained symbolically. Rewrite this expression for θ as the reciprocal of an expression denoted by D_{denom}, i.e. $\theta=1/D_{denom}$.

Step 3: Calculate the theoretical displacements of the structure using the finite element method.

Step 4: Analyze the distribution of D_{denom} using Equation (3-52) and the theoretical values obtained in **Step 3**.

Step 5: Analyze the distribution of $\theta=1/D_{denom}$ using Equations (3-53)-(3-55).

Remark 1: The availability of analytical expressions depends on the number and the type of the measurements in **Step 2**. When less than required measurements are used, the target parameter is not observable (Jose Antonio Lozano-Galant et al., 2015). Hence, neither analytical expressions nor numerical estimations can be obtained. When more than required measurements are used, the target parameters are observable and can be numerically evaluated. However, the analytical expressions are not obtainable. The required measurements can be determined by trial and error methods, i.e. adding one measurement each time until the analytical expressions are obtained. For ease of discussion, the measurement sets that are capable of deriving the analytical expressions for the target parameters θ are referred as minimum sets of parameters θ.

Remark 2: D_{denom} is a linear transformation of the chosen measurements in **Step 2**. Since the measurements follow normal distribution, the distribution of D_{denom} can be obtained from linear transformation of these normal distributions.

3.4.3 Theoretical Motivation Of Measuring Rotations

Advantages of using rotations are not limited to the practical issues mentioned in section 3.4.1. In this section, two illustrative examples using statistical analysis are provided to emphasize the theoretical motivation of measuring rotations rather than deflections. Example 1 corresponds to a simply supported bridge while example 2 corresponds with a two-story one-bay frame.

Example 1: Statistical analysis on a simply supported bridge

In this section, statistical analysis is carried out for a simply supported bridge using different measurement sets. The statistical analysis is validated by a Monte-Carlo simulation first and then a comparative study between different measurement sets is carried out to justify the advantage of using rotations. Example 1 is a simply supported bridge 3L long. Its FEM is discretized into 12 elements and is parameterized by three bending stiffnesses (EI_1–EI_3) (Figure 3-23). Assume the target parameter is EI_2. OM indicates that any two rotations or one rotation plus two deflections, or three deflections in nodes 5-9 are qualified to identify EI_2. Without loss of generality, three sets, set 1 (v_5, v_7, v_9), set 2 (v_5, v_7, w_9) and set 3 (w_5, w_9), are studied.

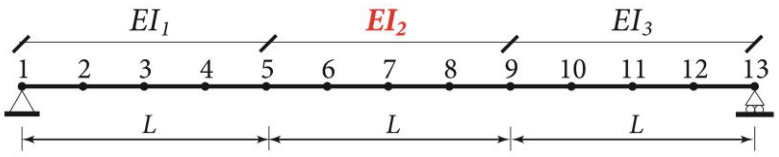

Figure 3-23 FEM for a simply supported bridge

The analytical expression of EI_2 in terms of set 3 (w_5, w_9) is given by Equation (3-56).

$$EI_2^{set3} = \frac{\{16\sum_{i=1}^{5}(M_i - M_{14-i}) + 8M_6 - 8M_8 + 4L\sum_{i=2}^{5}[(i-1)V_i + (i-1)V_{14-i}] + 19V_6L + 20V_7L + 19V_8L\}}{\frac{32(w_5 - w_9)}{L}} \quad (3\text{-}56)$$

In Equation (3-56), the external loads are collected in the numerator while the measurements (w_5, w_9) are collected in the denominator. The estimation of EI_2 only depends on the loading case and the measured displacements, not related with EI_1 or EI_3. Assume L=3 m, the depth and width of the cross section are 0.5 m and 0.3 m. The inertia and the elastic modulus are 3.125×10^{-3} m^4 and 3.5×10^7 kN/m^2. A static test is considered as a vertical concentrated load V_5=100 kN applied at the one-third point. The ratio of the maximum deflection to the span is 1/760. The increments of the measured displacements are listed in Table 3-5. Since V_5=-100 kN and all the other loads are null, Equation (3-56) can be simplified as Equation (3-57).

$$EI_2^{\text{set3}} = \frac{V_5L^2}{2(w_5 - w_9)} = \frac{1}{\frac{2(w_5 - w_9)}{V_5L^2}} \quad (3\text{-}57)$$

Table 3-5 Increments of deformations for example 1 due to the concentrated load V_5=-100 kN

Deformations	Values	Unit
v_5	-0.010971	m
v_7	-0.011829	m
v_9	-0.009600	m
w_5	-0.001829	rad
w_9	0.002286	rad

With Table 3-5 and Equations (3-53)-(3-55), the distributions of w_5−w_9 and $\frac{2(w_5-w_9)}{V_5L^2}$ as well as EI_2^{set3} can be obtained. The distributions for EI_2^{set1}(v_5, v_7 and v_9) and EI_2^{set2}(v_5, v_7 and w_9) are obtained in the same way. To validate the statistical analysis, 2000 samples of measurement set (v_5, v_7 and v_9) are generated by Equation (3-52) with an error level of 5%. 2000 estimations of EI_2 are obtained from these samples. In this paper, unless otherwise stated, all estimations are normalized by their nominal values. The probability density of the 2000 estimations is obtained using kernel density estimation, which is done by the *ksdensity* command in *Matlab*. In Figure 3-24.a, the validity of the proposed statistical analysis is justified by the complete agreement between the estimated probability density curve (red dashed line) and the theoretical one (green solid line) using Equation (3-53). Note that the distribution of EI_2 using set 1 (v_5, v_7 and v_9) is severely right skewed, characterized by the fact that the right tail is much longer than the left one. With low error levels, for all sets, the positive mode occurs close to one and its associated probability density is high. When error levels increase, this is no longer true. Figure 3-24.b and c provide the probability density curves for the estimations of EI_2 using set 1 and set 3 with 20% error. For set 1, the biased positive mode x=0.535 is related with a small density of 0.971. In addition, the negative mode x=-1.152 is not negligible. On the contrary, for set 3, the positive mode x=0.990 is related with a much higher probability density of 5.664 while the negative mode x=-99.771 is negligible and hence not shown. This implies that for high error levels the estimation using deflections leads to underestimations, in fact, even negative estimations, which is not the case for the estimations using rotations. In addition, from the severe right skewness of the probability density curve for set 1, it is expected that the variation in the estimation for set 1 is much higher than that for set 3.

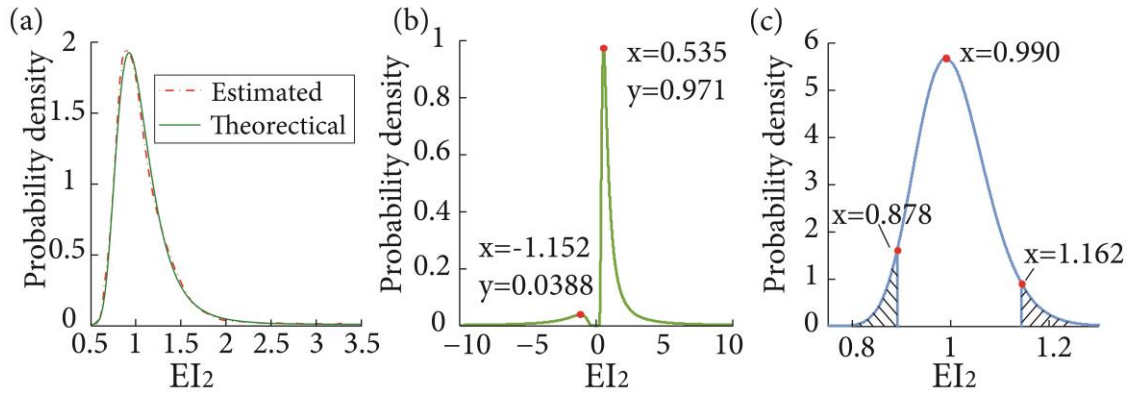

Figure 3-24 Probability density curves for the estimations of EI_2 using (a) set 1 (v_5, v_7 and v_9) with 5% measurement error (theoretical distribution and inferred from data) (b) set 1 (v_5, v_7 and v_9) with 20% measurement error (c) set 3 (w_5, w_9) with 20% measurement error (shaded area for 2.5% and 97.5% percentiles)

Figure 3-25 presents the 95% confidence intervals of the estimations of EI_2 using set 3 under error levels ranging from 0% to 20%. The lower and upper bounds of the confidence interval are the cutting points of the 2.5% regions on the left and right sides of the probability density curve (shaded in Figure 3-24.c). From this figure, it is seen that the bounds of these confidence intervals satisfy a linear relation with the error level. In addition, these intervals are bounded by [1-E_{level}, 1+E_{level}] for each error level.

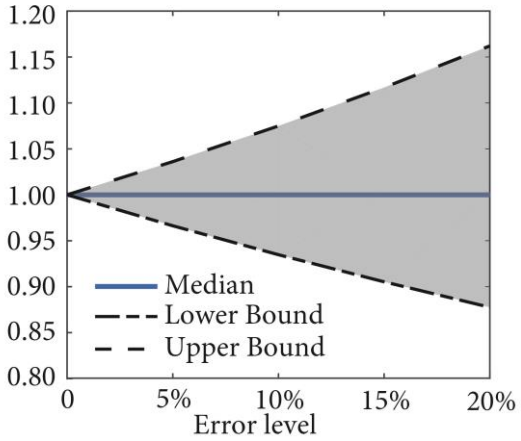

Figure 3-25 Confidence interval of the estimation for EI_2 under different error levels

Figure 3-26 provides the variations of the positive mode, the mean and the Coefficient Of Variation (COV) for the estimations of EI_2 using different sets against different error levels. The median is always one for set 3 at any error level. The mean and the COV are analyzed with the interval [0, 2]. The remarkable consistency between the mode and the mean for set 3 justifies the unbiasedness of the estimations using rotations (Figure

3-26.a). With 20% error, the deviation in the mean is 0.24% and the related COV is 0.046. On the contrary, the deviations in the mean increase rapidly with errors for set 1 and set 2. The positive mode for set 1 is close to zero when the error level is high. This indicates a large COV, as seen in Figure 3-26.b, and a right skewness. When more deflections are used, the positions of the COV curves also become higher.

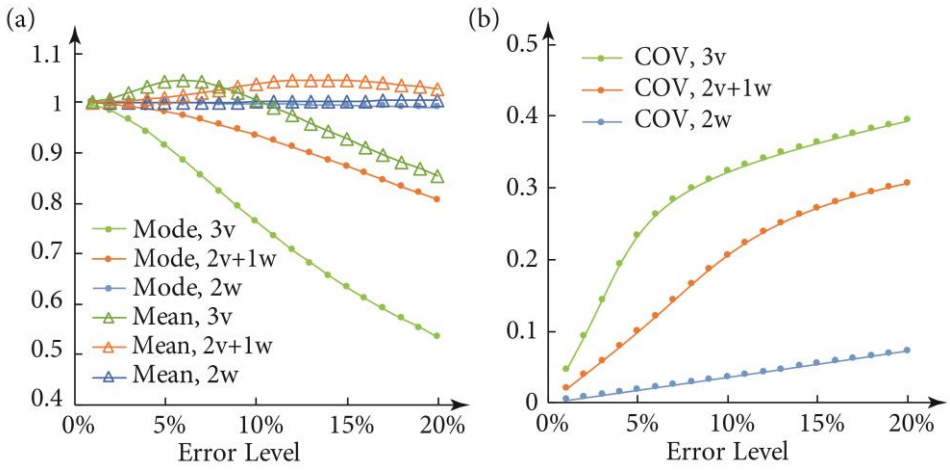

Figure 3-26 For the estimations of EI_2 using different sets (3v for (v_5, v_7 and v_9), 2v+1w for (v_5, v_7, w_9), 2w for (w_5 and w_9)) under error levels of 1%-20%: (a) Mean and mode (b) COV

This analysis shows that: (1) The statistical analysis is capable of analyzing the distribution of the estimations. (2) When the error level is high, the estimations using deflections might be negative and the distribution is severely right-skewed. (3) Unlike the case of using deflections, the estimations using rotations are robust and insensitive to error levels since the confidence intervals of the estimations are well bounded. (4) The higher the number of deflections used in the minimum set, the higher the sensitivity of the estimations to errors.

Example 2: Statistical analysis on a two-story one-bay frame

Similar analysis is carried out in a two-story one-bay frame. The elastic modulus is $3.5\times10^7\ kN/m^2$. The area and inertia of the columns are 0.24 m^2 and $7.2\times10^{-3}\ m^4$ while the area and inertias of the beams are 0.15 m^2 and $3.125\times10^{-3}\ m^4$. The FEM for example 2 is parameterized by bending stiffnesses EI_1-EI_{10} and axial stiffnesses EA_1-EA_{10}, as shown in Figure 3-27.a. A load test of a uniform load of 45 kN/m is carried out on the second story. Assume the target parameter is the bending stiffness EI_9 in the middle part of this story. To identify EI_9, 4 rotations or 5 deflections are required. Without loss of generality, two sets are used for SSI. Set 1 comprises 4 rotations (green) and set 2 comprises 5 deflections (red), see Figure 3-27.a. However, as the analytical expression for EI_9 is not concise, it is not provided. The probability density curves for the estimations of EI_9 for these sets under different error levels

(indicated in the brackets) are presented in Figure 3-27.b. For set 1 (dashed lines), the positive modes always center around 1 and the negative ones are negligible. As the errors increase, the probability density curve for EI_9 estimated from rotations becomes wider and flatter. For 5% error, the mean and the positive mode are 1.025 and 0.957, respectively. However, the estimations using deflections (solid lines) are delicate. The bimodality is observed with a minor 0.2% error. In addition, the positive modes are greatly deviated from 1. The positive modes related to 0.2% error and 1% error are 0.695 and 0.222, respectively.

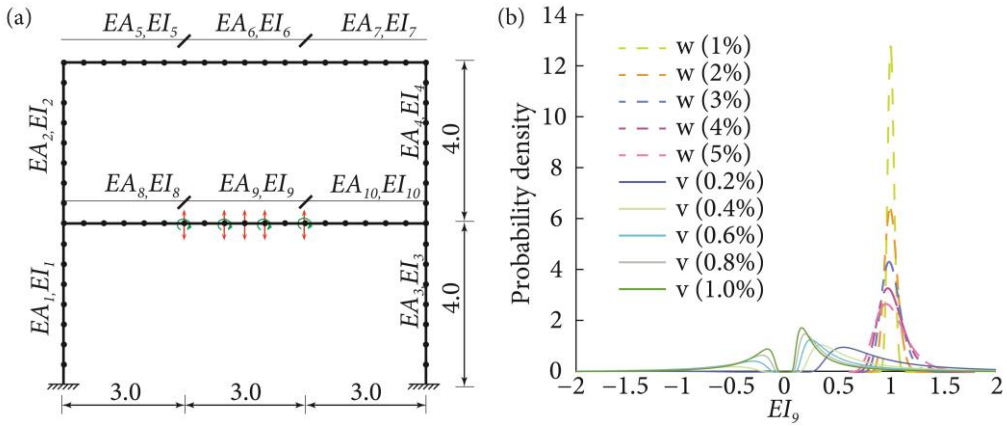

Figure 3-27 (a) FEM for a two-story one-bay frame (arrows denote deflections, arcs denote rotations) (b) The distributions of the estimations using rotations (w) or deflections (v) under different error levels (indicated in the brackets)

This analysis shows that: (1) the estimations using deflections are extremely sensitive to measurement errors in frame structures. (2) Measuring rotations outperforms measuring deflections regarding both the unbiasedness and the extent of variation in the estimations of the target parameter. It should be also pointed out that in frames, measuring rotations might be more practical since finding a reference point to measure deflections is non-trivial.

3.4.4 Different Strategies For Using Redundant Measurements

The statistical analysis applies when the analytical expressions for the target parameters θ are available, i.e. the minimum set for θ is used. It is observed that when the error levels increase, the accuracy of the estimations may not be satisfactory. In order to tackle this issue, a logical solution is to include redundant measurements. In the case of redundant measurements, the system of equations from the observability method is not compatible, (i.e. does not have a solution). In the numerical case, least square method or pseudo inverse can be applied, but no solution satisfies the system rigorously. Four strategies are proposed to use redundant measurements:

(1) Strategy 1: Using the traditional observability method (Nogal et al., 2015) to solve Equation (3-48) that is formulated by redundant measurements. In this case, the

equations cannot be satisfied stringently.

(2) Strategy 2: Derive the compatibility conditions , i.e. the geometrical relations that the nodal displacements should satisfy (J. Lei, Xu, et al., 2018). The deformation shape satisfying these conditions is regarded compatible. Using optimization to minimize the discrepancy between the measured shape and the compatible one. The estimations of the parameters are obtained by providing the compatible displacements in Equation (3-48). In this case, Equation (3-48) is stringently satisfied. However, the acquirement of compatibility conditions in frame structures is non-trivial due to the coupling of axial and bending behaviors.

(3) Strategy 3: Divide the redundant measurement set into several minimum sets. Obtain the estimation of the target parameter by averaging those valid estimations from each minimum set. By valid, it means that the outliers in estimations are detected and removed. Boxplot is a powerful and popular tool in analyzing the distribution and the outliers of data (Tukey 1977). To do so, the first quantile Q_1 and the third quantile Q_3 of the estimations are obtained first. If the estimations are normally distributed, valid estimations should fall into the interval [Q_1-2.7(Q_3-Q_1), Q_3+2.7(Q_3-Q_1)] with a coverage of 99.7%. Hence, values out of this range are invalid and ruled out in this strategy.

(4) Strategy 4: same procedure as strategy 3 but without removing outliers.

Verification for a simply supported bridge

These strategies are applied in the same structure described in section 3.4.4 (Figure 3-23). Assume EI_2 is the target parameter and five rotations (w_5-w_9) are measured. Two error levels, E_{level}=5% and 10%, are studied. For each error level, 2000 samples of measurements are generated by Equation (3-52).

To identify EI_2, two rotations are sufficient. Hence, there are C_5^2=10 minimum sets that are able to identify EI_2. For strategy 4, the final estimation is the average of the 10 estimations from these sets. Table 3-6 presents the statistical summary of the estimations. The first 4 rows are the results for the proposed strategies while the last 10 rows are the results for respective minimum sets.

Great bias in the mean and a large variation is seen for estimations obtained using strategy 1. In the case of strategies 2, 3 and 4, the estimations are unbiased and robust. Note that these estimations are always better than any minimum set. For the minimum sets, the numbers of invalid sets agree well with the COV. Regarding the dispersion in the estimations, the best strategy (strategy 2) is to impose compatibility conditions. Nevertheless, the extents of dispersion related to strategies 3 and 4 are also well controlled. Note that after the outliers are ruled out, the decrease in COV is -12.5% and -17.6% from strategy 4 to strategy 3, respectively, for the error levels of 5% and 10%. A comparison of the probability density curve of strategies 2 and 3 is provided in Figure

3-28.

Table 3-6 Statistical summary of the estimations using different strategies.

Measurements	E_{level}=5%			E_{level}=10%		
	Mean	COV	Invalid sets	Mean	COV	Invalid sets
w_5-w_9 (strategy 1)	0.884	0.154	-	0.703	0.239	-
w_5-w_9 (strategy 2)	1.002	0.011	-	1.004	0.023	-
w_5-w_9 (strategy 3)	0.999	0.014	-	0.999	0.028	-
w_5-w_9 (strategy 4)	1.002	0.016	-	1.006	0.034	-
w_5,w_6	1.002	0.037	13	1.006	0.075	39
w_5,w_7	1.000	0.020	0	1.002	0.040	0
w_5,w_8	1.000	0.017	0	1.001	0.035	0
w_5,w_9	1.001	0.018	0	1.002	0.035	0
w_6,w_7	1.000	0.018	0	1.001	0.036	0
w_6,w_8	1.000	0.019	0	1.001	0.039	0
w_6,w_9	1.001	0.020	0	1.002	0.041	0
w_7,w_8	1.001	0.042	36	1.006	0.086	61
w_7,w_9	1.002	0.034	7	1.006	0.069	22
w_8,w_9	1.009	0.090	370	1.036	0.200	412

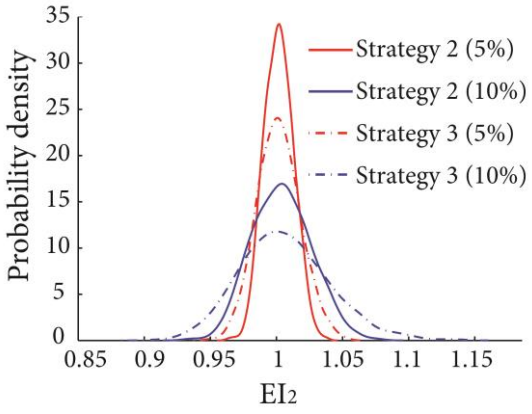

Figure 3-28 The probability density curve of the estimations using strategies 2 (compatibility conditions) and 3 (averaging with outliers ruled out)

As shown by the COV, the dispersion of estimations in strategy 2 is lower than that in

strategy 3. This figure also visualizes the distribution of the estimations. It is seen that for both strategies, the deviations in the estimations are well bounded by the error levels. From this section, it is concluded that in the bridge example: (1) Using redundant measurements without any treatment leads to greatly biased estimations. (2) Using strategies 2-4 leads to result better than only using one minimum set. (3) Imposing compatibility conditions is the best strategy regarding the unbiasedness and the dispersion of the estimations. (4) Averaging the estimations from minimum sets also lead to satisfactory estimations. The estimations can be further improved by ruling out the outliers in the estimations.

Verification for a high-rise frame

As the compatibility method cannot be used for reducing error in frame structures when redundant information is available, the averaging method is going to be tested in a high-rise building studied previously, see Figure 3-29.a (adapted from Figure 12 in (Lozano-Galant et al. 2013)). In that study, the observability of the parameters was studied symbolically while the numerical analysis and the effect of measurement errors were not included. In this paper, the focus is the identification of the bending stiffness of the concrete slab in the middle right of 3^{th} floor. Figure 3-29.b shows the FEM for this part. It is parameterized by three bending stiffnesses EI_9-EI_{11}.The parameterization of the remaining part is the same as that in (Lozano-Galant et al. 2013). The bending stiffness of zones associated with EI_9 and EI_{10} is $1.75\times10^8\ N\cdot m^2$. A damage in the right part of the target floor slab is simulated by a 30% reduction in bending stiffness EI_{11}, i.e. $EI_{11}=1.225\times10^8\ N\cdot m^2$. An overload of 40 kN/m is applied on this floor slab to simulate a static load test. Due to the unsatisfactory result of using deflections (as discussed in section 3.4.4), 10 rotations, (w_{32}, w_{72}, w_{74}, w_{76}, w_{78}, w_{80}, w_{82}, w_{84}, w_{86} and w_{46}), are measured to identify EI_9-EI_{11}. The increments of the displacements due to this load are calculated by direct analysis. Five error levels (1%, 2%, 3%, 4% and 5%) are studied here. For each level, 100 noisy measurement sets are generated using Equation (3-52). To identify EI_9-EI_{11}, two rotations are required for each zone that is related to one bending stiffness, 6 in total. Taking two rotations from (w_{32}, w_{72}, w_{74}, w_{76}), (w_{76}, w_{78}, w_{80}, w_{82}), and (w_{82}, w_{84}, w_{86}, w_{46}), respectively, for EI_9-EI_{11}, (duplicated rotations do not count), leads to 117 minimum sets of 6 rotations. Thus, for each measurement set, 117 estimations are obtained and the outliers in these estimations are ruled out.

Figure 3-29.c presents the error bar plot of the final estimations of EI_9-EI_{11} under different error levels. The centerlines indicate the mean of associated estimations for each set. The vertical error bars represent one standard deviation of uncertainty in the estimations. Hence, the length of these bars indicates the amount of variation in the estimations.

From this figure, it can be concluded that: (1) the estimations are unbiased since the centerline locates at 1. (2) The estimations of EI_{10} always have the least amount of

variation. (3) The increase of variations in the estimations follows a linear relationship with error levels. (4) The sensitivity of the increase of variation with error levels is the lowest for EI_{10}. In fact, the better estimations in EI_{10} is due to the higher curvature of the zones parameterized by EI_{10} than the remaining zones, which agrees with the result in the previous study (J. Lei et al., 2017).

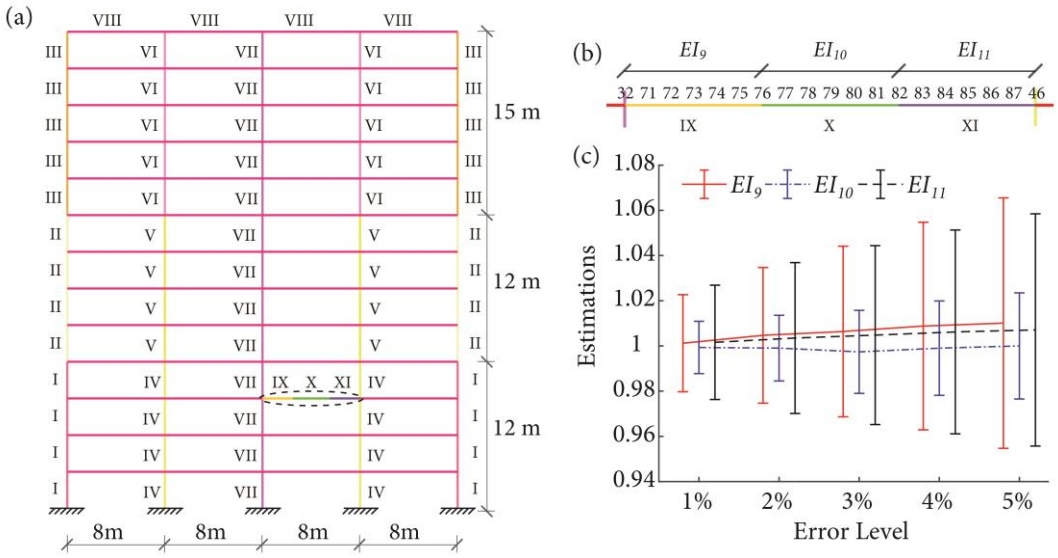

Figure 3-29 (a) The FEM of the high-rise building (adapted from (Jose Antonio Lozano-Galant, Nogal, et al., 2013)) (b) The FEM for the floor slab to be identified. (c) Error bar plot of the estimations of EI_9-EI_{11}.

3.4.5 Conclusions

In this paper, the theoretical advantage of using rotations than deflections is justified with a statistical analysis. To do so, SSI by constrained observability method is used to derive the analytical expressions for the target parameters first. These expressions are obtainable when a minimum set is used. With these expressions and the inverse distribution theory, a procedure for obtaining the distributions of the estimations is proposed for the very first time, which is verified by the comparison with a Monte-Carlo analysis.

The statistical analyses were carried out in a simply supported bridge and a two-story one-bay frame with different measurement sets. In both structures, the distributions of the estimations obtained for those sets only comprised of deflections are very sensitive to the errors. These distributions explain the reason for the biased or even negative estimations when only measuring deflections. In the comparative study of using deflections or rotations for estimating bending stiffnesses, it is justified that using rotations is always less sensitive to measurement errors than using deflections regarding the unbiasedness and the extent of variation in the estimations.

Redundant measurements are expected to improve the accuracy of estimations. Taking account of the theoretical and practical advantages of using rotations, this study proposed four strategies to use redundant rotations in static SSI. In the simply supported bridge example where the compatibility conditions are available, the strategy of using compatibility conditions outperforms the rest. Nevertheless, the performance of strategy 3 (averaging with outliers ruled out) is entirely satisfactory. Furthermore, the strategy 3 can be applied in frame structures where compatibility conditions are not available. In the numerical analysis of the high-rise frame, the satisfactory accuracy and the robust performance achieved by using rotations along with the strategy 3 justify the effectiveness and versatility of the proposed method.

3.5 Structural system identification by Measurement Error-Minimizing Observability Method

Title: Structural system identification by Measurement Error-Minimizing Observability Method

Authors: Jun Lei, José Antonio Lozano-Galant, Dong Xu, José Turmo

Journal: Structural Control and Health Monitoring

Publication: Technical Paper

Submitted: 12-March-2017

Accepted: Under review

DOI: -

Available at:-

3.5.1 Abstract

This paper proposes a method for the finite element model updating using static load tests under the framework of observability analysis. Previous works included measurement errors in the coefficient matrix of equations. This impeded the obtainment of accurate estimations. To deal with this issue, the proposed method relocates the errors and incorporates an optimization procedure to minimize the square sum of these errors. The main advantage of this method is its ability to identify the structural parameters of complex structures where the axial and the bending behavior are coupled, such as inclined beams or frame structures. To illustrate the application of this method, several structures are analyzed. First, the method is validated in a beam-like structure by comparing it with other methods in the literature and then applied to a multi-story frame. The effects of curvatures, of the inclusion of rotation measurements and of the constraints on the range of unidentifiable parameters are investigated.

Keyword: structural system identification; stiffness method; observability method; measurement errors; single loading case;

3.5.2 Introduction

Structural health monitoring has become a powerful tool to help decision making during life cycle of civil and infrastructure systems (Enrique Castillo et al., 2015). As a key component of structural health monitoring, Structural System Identification (SSI) aims to identify the parameters of a mathematical model that links the measured response and the external excitation of a structure. It is commonly assumed that the degradation of structures is reflected in the change of these parameters (Shahsavari et al., 2017).

Regarding the type of excitation, SSI can be classified as static SSI (Bakhtiari-Nejad et al., 2005; Evan C. Bentz & Hoult, 2016; Ghrib, Li, & Wilbur, 2012; Hjelmstad & Shin, 1997; J. Lei, Nogal, et al., 2018; Jose Antonio Lozano-Galant, Nogal, et al., 2013; Masoud Sanayei & Scampoli, 1991; Tomàs, Lozano-Galant, Ramos, & Turmo, 2018; E. Viola & Bocchini, 2007; Erasmo Viola & Bocchini, 2011; Q. Yang & Sun, 2010) or dynamic SSI (Astroza, Nguyen, & Nestorović, 2016; Ghrib & Li, 2017; Huang, Hung, Su, & Wu, 2009; S. S. Jin & Jung, 2016; Z. Li et al., 2017; Marano et al., 2011; Osornio-Rios, Amezquita-Sanchez, Romero-Troncoso, & Garcia-Perez, 2012; Jann N. Yang, Pan, & Lin, 2007; Y. Yang & Yu, 2016; K.-V. Yuen & Kuok, 2011). Numerous algorithms have been developed, e.g. response surface model (S. S. Jin & Jung, 2016), simulated annealing (Astroza et al., 2016), least square estimation (Huang et al., 2009; Jann N. Yang et al., 2007), artificial neural network (Osornio-Rios et al., 2012), genetic algorithm (Marano et al., 2011; E. Viola & Bocchini, 2007). Most of these algorithms are developed for dynamic SSI methods. Compared with static SSI, dynamic SSI has been developed more extensively in the past decades. However, this research is going to focus on static SSI for the following reasons: (1) the physical equations involved with static SSI are only related to the structural stiffness while those involved with dynamic SSI are also related to the mass and the damping of the structure. Hence static SSI are simpler than dynamic SSI. Also, in the majority of dynamic methods, it is common to assume that the damage of structure does not lead to the loss of mass and also the damping of the structure is zero (Q. Yang & Sun, 2010). This might introduce modelling errors in the identification. (2) The solution for measuring static displacements is easier, cheaper and has higher accuracy than those for dynamic SSI (Andreaus et al., 2017). (3) Static method might be significantly more sensitive to local damages while dynamic methods reflect the global and distributed phenomenon of the structure like frequency response (Jenkins et al., 1997).

Regarding the uncertainty of the parameters, SSI methods are of two types: (1) Deterministic methods, which pinpoint a best set of parameters that minimize the discrepancy between the measured response and the one predicted by the parameterized model (Erasmo Viola & Bocchini, 2011), and (2) probabilistic methods, which aim at obtaining the distribution of the parameters. The process of finding the best parameters is mostly done by optimization techniques. The objective of these techniques can be minimizing the discrepancies in the structural response, e.g. forces (Erasmo Viola & Bocchini, 2011), displacements (Masoud Sanayei & Scampoli, 1991), acceleration (Marano et al., 2011), mode shapes and frequencies (Eskew & Jang, 2017). In the case of probabilistic approach, mainly in the Bayesian method, the distributions of the target parameters are obtained by Bayesian inference. Then, the parametric uncertainty can be quantified in the form of probability distribution (Ghrib & Li, 2017; Jiang et al., 2007). Compared to deterministic methods, probabilistic methods are more robust to measurement errors. However, major challenges of these methods (H. Sun & Betti, 2015; K.-V. Yuen & Kuok, 2011) are: (1) the explicit likelihood function is not

available in some cases; (2) the computation burden might be expensive or even impossible despite the existence of an implicit likelihood function; (3) the computation burden increases exponentially with the number of parameters, especially when the model is not globally identifiable. A detailed review of Bayesian methods in dynamic SSI can be found in (K.-V. Yuen & Kuok, 2011).

Observability method (OM) can determine the existence and uniqueness of the solution of linear system of equations when some unknowns in the direct analysis are known in the inverse analysis. This method has been applied in several engineering fields (Enrique Castillo et al., 2007, 2016; Díaz et al., 2016). The SSI by OM under static loads was proposed to identify plane beam element models loaded in its plane (e.g. frames) (Jose Antonio Lozano-Galant, Nogal, et al., 2013). The SSI by OM is a deterministic model-based SSI under controlled static load. With a given measurement set, it is able to determine whether the parameters can be estimated from the measured response, i.e. the observability of the parameters. Hence it is able to prove the existence and uniqueness of the solution (e.g. bending stiffnesses, axial stiffnesses) symbolically. However, the numerical estimations of the unknowns were lacking. Later, the numerical application of this method was developed by (Nogal et al., 2015). In (J. Lei et al., 2017), the parametric equations of the structural parameters were derived explicitly and thus sensitivity analysis on measurement errors was developed. The effect of shear parameter on the SSI of thin-walled structures modelled by Timoshenko beam element was also investigated (Tomàs et al., 2018).

The observability of the structural system depends both on the number and the location of measurements. When the number of measurements is less than the number of parameters, the structural system is not observable. When the number of measurements is greater than or equal to the number of parameters, the system is potentially observable (Hjelmstad & Shin, 1997; J. Lei, Nogal, et al., 2018; Masoud Sanayei & Scampoli, 1991). Specially, measurement sets are defined as *essential sets* (J. Lei, Nogal, et al., 2018) when: (1) they have exactly as many measurements as the number of structural parameters to be estimated; (2) they are able to identify all targeted parameters and the drop of any measurement fails to do so. A systematic approach to find essential sets was proposed in (Jose Antonio Lozano-Galant et al., 2015). This method provides a deep understanding of the physical meaning and the necessity of each measurement. An improvement in finding essential sets is made by retrieving the missing constraints among unknowns in the observability equations (J. Lei, Nogal, et al., 2018). When noise affects measurements, the accuracy of the numerical estimations of parameters based on essential sets may not be satisfactory. Hence, additional measurements should be used to reduce estimation errors and thus *redundant sets* are formed. However, it is verified that the solution for the observability equations with redundant sets given by ordinary least square method is greatly biased (J. Lei, Xu, et al., 2018). To solve this issue, the geometrical relations among the displacements in beam-like structures, referred to compatibility conditions, were obtained analytically by OM via symbolical

approach (J. Lei, Xu, et al., 2018). Then the incompatibility among the displacements due to errors was reduced by imposing these compatibility conditions. Subsequently the parameters are estimated with those compatible displacements. However, when bending behaviors and axial behaviors are coupled, obtaining the compatibility conditions in frames and inclined elements is challenging. Hence, the current solution of static SSI by OM for measurement errors is only available for beam-like structures but not for frame structures. This limits the application of the method in buildings. In this paper, a different formulation of the observability equations is proposed to deal with measurement errors in the static SSI of frame structures. To do so, the measurement errors are separated from the coefficient matrix and moved to the unknowns, forming a new system of observability equations. Then the square sum of all error terms is minimized by an optimization procedure while some nonlinear relations among the unknowns are imposed (J. Lei, Nogal, et al., 2018).

Apart from ensuring the observability of targeted parameters, an additional issue in SSI is the sensor placement that addresses the observability as well as the accuracy of the estimations. In structures of simple geometry or small number of Degrees Of Freedom (DOF), experience or trial and error might be able to handle the task of placing sensors. However, in a complicated structure having many DOFs, determining the optimal sensor placement is a very challenging task. One of the most known and commonly adopted approach for the optimal sensor placement was developed by Kammer (Kammer, 1991). This approach maximizes the information that can be extracted from the measurement by maximizing the norm of the Fisher Information matrix [F] that was constructed from the modal and measurement covariance matrix. Since then, many variants of this method dealing with the sensor placement in SSI were proposed. A Fisher Information matrix for the sensor placement in static SSI can be constructed from the noise variance and the gradient of structural displacements with respect to different structural parameters (Bakhtiari-Nejad et al., 2005). The sensor placement strategy used in this paper is developed based on this Fisher Information matrix.

The major contributions of this study are: (1) a new method is proposed to deal with the static structural system identification of complicated structure where axial and bending behaviors are coupled under the framework of observability method; (2) the difficulty of identifying parameters associated with null curvature zones despite the increase of measurements or inclusion of rotations is illustrated; (3) When only one loading case is available, the effect of imposing different constraints on parameters associated with null curvature zones is investigated regarding the accuracy and dispersion of the estimations of the identifiable parameters.

In the remainder of this paper, section 3.5.3 briefly introduces the static SSI by constrained OM. Then the procedure for the proposed measurement error-minimizing observability method (MEMOM) is illustrated by an academic example. The sensor placement is determined by the Fisher Information matrix together with a genetic

algorithm. In section 3.5.4, the performance of the proposed method is validated in a beam-like structure. The estimations obtained from *essential sets* and *redundant sets* are compared with those obtained by the original method (Nogal et al., 2015) and the compatible OM (J. Lei, Xu, et al., 2018), respectively. In addition, a table summarizing the characteristics of these methods is provided at the end of this section. In section 3.5.5, the effectiveness of the proposed method is verified by the identification of a floor beam in a large frame. Section 3.5.6 summarizes the key findings and concludes the paper.

3.5.3 Methodology

Structural system identification by constrained observability method

Static SSI by Constrained OM imposes constraints on variables when no more parameters can be observed using SSI by OM. The identical part between these two methods is introduced first and their difference is pointed out at the end of this section.

In static SSI by OM, a finite element model (FEM) has to be defined first. The equilibrium equations (3-58) are then established. For 2D beam element models, due to the equilibrium of forces on each node in horizontal, vertical and rotational directions, the number of equations N_{eq} is three times the number of nodes N_n, i.e. $N_{eq}=3N_n$,.

$$[K] \cdot \{\delta\} = \{f\} \tag{3-58}$$

In this system, the global stiffness matrix $[K]$ includes both the geometrical and the mechanical properties of element j (i.e. length L_j, elastic moduli E_j, area A_j and inertia I_j, j=1, 2, …, N_e; where N_e is the number of elements). The displacement vector $\{\delta\}$ includes horizontal displacements u_i, vertical deflections v_i, rotations w_i of node i (i=1, 2, …, N_n; where N_n is the number of nodes). The right-hand side vector $\{f\}$ includes horizontal forces H_i, vertical forces V_i, and moments M_i on node i. Hence, all the variables appearing in the equations are (E_j, A_j, I_j, L_j, u_i, v_i, w_i, H_i, V_i and M_i). The objective of SSI is to identify structural parameters θ (such as axial stiffness E_jA_j or bending stiffness E_jI_j) so as to assess the condition of the structure by the values of θ. To reduce unknowns, these stiffnesses, E_jA_j and E_jI_j are treated as linearized unknowns, EA_j and EI_j, and L_j is usually assumed as known. In addition, during the static test, the controlled static loads are known and some resulting increments of the displacements $\tilde{\delta}$ have to be measured.

These parameters appear in matrix $[K]$ as monomial ratios, such as $\frac{EA_j}{L_j}$, $\frac{EI_j}{L_j^2}$ or $\frac{EI_j}{L_j^3}$. As some elements of vector $\{f\}$ are also unknowns, nonlinearity arises in the system of equations. Hence, the system is linearized by a series of algebraic operations (Jose Antonio Lozano-Galant, Nogal, et al., 2013), as shown in Equation (3-59).

$$[K^*]\cdot\{\delta^*\}=\begin{bmatrix}K_{10}^* & K_{11}^*\\ K_{00}^* & K_{01}^*\end{bmatrix}\begin{Bmatrix}\delta_0^*\\ \delta_1^*\end{Bmatrix}=\begin{Bmatrix}f_1\\ f_0\end{Bmatrix}=\{f\} \tag{3-59}$$

The remaining coefficient matrix $[K^*]$ are composed of constants that are either zero or the powers of the inverse of L_j. Once the loads and the measurements from the static test as well as the boundary conditions of the structure have been defined, it is assumed that a subset $\{\delta_1^*\}$ of $\{\delta^*\}$ and a subset $\{f_1\}$ of $\{f\}$ are known while remaining subset $\{\delta_0^*\}$ of $\{\delta^*\}$ and $\{f_0\}$ of $\{f\}$ are not. To cluster the unknowns together, Equation (3-59) is transformed to Equation (3-60) by static condensation.

$$[B]\cdot\{z\}=\begin{bmatrix}K_{10}^* & 0\\ K_{00}^* & -I\end{bmatrix}\begin{Bmatrix}\delta_0^*\\ f_0\end{Bmatrix}=\begin{Bmatrix}f_1-K_{11}^*\delta_1^*\\ -K_{01}^*\delta_1^*\end{Bmatrix}=\{D\} \tag{3-60}$$

In Equation (3-60), both the coefficient matrix $[B]$ and the right-hand side vector $\{D\}$ are completely known. The coefficient matrix $[B]$ is composed of either zero or monomial ratios of knowns (measured displacements, known stiffnesses and element lengths). Meanwhile, the right-hand side vector $\{D\}$ is composed of the external loads $\{f_1\}$ and the equivalent nodal forces ($K_{11}^*\delta_1^*$ or $K_{01}^*\delta_1^*$). On the other hand, the unknowns z are of two types: (1) node displacements, (u_i, v_i or w_i), or parameters θ, (EA_j or EI_j), or the products of both, (EA_ju_i, EA_jv_i, EA_jw_i, EI_ju_i, EI_jv_i or EI_jw_i); (2) unknown reactions, (H_i, V_i and M_i), at the boundary conditions. When Equation (3-60) has at least one solution, the solution is the sum of a particular solution $\{z_p\}$, and the product of a vector of arbitrary values, $\{\rho\}$, and the null space $[N]$ of the coefficient matrix $[B]$ in Equation (3-60).

$$\{z_g\}=\{z_p\}+[N]\cdot\{\rho\}=\begin{Bmatrix}\delta_0^*\\ f_0\end{Bmatrix}_p+[N]\cdot\{\rho\} \tag{3-61}$$

The particular solution $\{z_p\}$ is the pseudo inverse solution of Equation (3-60). $[N]\cdot\{\rho\}$ is the set of all solutions of the associated homogeneous system of equations (a linear space of solutions, wherein the columns of N are vectorial bases, and the entries of the vector $\{\rho\}$ are arbitrary values functioning as the coefficients of all possible linear combinations). If any row of the null space $[N]$ is composed of only zeros, then the scalar in the same row of the product $[N]\cdot\{\rho\}$will be zero, and thereby the particular solution specifies the unique solution for that parameter. Namely, any unknown associated with a zero row in the null space $[N]$ is observable, i.e. it exists and it is determined and unique. All these observable unknowns are introduced as known in the next step to obtain updated observability equations and thus new parameters might be observed. A step-by-step example is presented in (Jose Antonio Lozano-Galant, Nogal, et al., 2013).

However, treating algebraic relations among variables inappropriately might arise since the products of structural parameters and displacements are regarded as linearized variables (J. Lei, Nogal, et al., 2018). This is to say, the equality between coupled unknowns and the product of the associated components, for instance, $EI_2w_2=EI_2\cdot w_2$, is

missing due to the linearization of the variable EI_2w_2. This linearization enables the application of algebraic techniques that is essential for observability analysis but leads to the loss of information. To deal with this issue, the lacking constraints are imposed by an optimization procedure if some parameters are not observed by the linearized procedure in SSI by OM. In the numerical optimization, the objective function is to minimize the square sum of the residuals (equilibrium forces) of the observability equations from the last recursive step in SSI by OM while forcing the equality between the coupled variable and the product of its components (J. Lei, Nogal, et al., 2018).

Formulation of the system of observability equations by separating the errors

The coefficient matrix of the observability equations (Equation (3-60)) takes in the measurements together with the errors, which is a perturbation to the accurate matrix. Previous study shows that the least square solution of Equation (3-60) is greatly biased even with redundant sets (J. Lei, Xu, et al., 2018). This section proposes a measurement error-minimizing observability method (MEMOM). Measurement errors are separated from the coefficient matrix and then included in the unknown vector so as to eliminate the adverse effect of errors in the coefficient matrix. For illustrative purpose, the necessary procedures to implement the proposed method are demonstrated below by an academic example.

Consider a 10-m simply supported beam. Its FEM has two elements of length L=5m. The boundary conditions are that u_1=v_1=v_3=0. The FEM is parameterized by two bending stiffnesses, EI_1 and EI_2, and two axial stiffnesses, EA_1 and EA_2, as depicted in Figure 3-30.

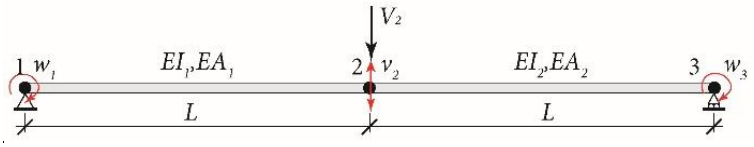

Figure 3-30 A 3-node simply supported beam with measurement set (w_1, v_2 and w_3).

Without loss of generality, it is assumed that a vertical load V_2 is applied at midspan (Node 2) and the increments of displacements (w_1, v_2, and w_3) are measured. The necessary steps to implement the MEMOM are presented below.

Step 1. Introduce the geometry, as well as the known mechanical and geometrical properties and external forces to establish an FEM for the structure. Build the equilibrium equations for this FEM.

The equilibrium equations for this FEM are given in Equation (3-62).

$$\begin{pmatrix} \frac{EA_1}{L} & 0 & 0 & -\frac{EA_1}{L} & 0 & 0 & 0 & 0 & 0 \\ 0 & \frac{12EI_1}{L^3} & \frac{6EI_1}{L^2} & 0 & -\frac{12EI_1}{L^3} & \frac{6EI_1}{L^2} & 0 & 0 & 0 \\ 0 & \frac{6EI_1}{L^2} & \frac{4EI_1}{L} & 0 & -\frac{6EI_1}{L^2} & \frac{2EI_1}{L} & 0 & 0 & 0 \\ -\frac{EA_1}{L} & 0 & 0 & \frac{EA_1+EA_2}{L} & 0 & 0 & -\frac{EA_2}{L} & 0 & 0 \\ 0 & -\frac{12EI_1}{L^3} & -\frac{6EI_1}{L^2} & 0 & \frac{12EI_1}{L^3}+\frac{12EI_2}{L^3} & \frac{6EI_2}{L^2}-\frac{6EI_1}{L^2} & 0 & -\frac{12EI_2}{L^3} & \frac{6EI_2}{L^2} \\ 0 & \frac{6EI_1}{L^2} & \frac{2EI_1}{L} & 0 & \frac{6EI_2}{L^2}-\frac{6EI_1}{L^2} & \frac{4EI_1}{L}+\frac{4EI_2}{L} & 0 & -\frac{6EI_2}{L^2} & \frac{2EI_2}{L} \\ 0 & 0 & 0 & -\frac{EA_2}{L} & 0 & 0 & \frac{EA_2}{L} & 0 & 0 \\ 0 & 0 & 0 & 0 & -\frac{12EI_2}{L^3} & -\frac{6EI_2}{L^2} & 0 & \frac{12EI_2}{L^3} & -\frac{6EI_2}{L^2} \\ 0 & 0 & 0 & 0 & \frac{6EI_2}{L^2} & \frac{2EI_2}{L} & 0 & -\frac{6EI_2}{L^2} & \frac{4EI_2}{L} \end{pmatrix} \begin{pmatrix} u_1 \\ v_1 \\ w_1 \\ u_2 \\ v_2 \\ w_2 \\ u_3 \\ v_3 \\ w_3 \end{pmatrix} = \begin{pmatrix} H_1 \\ V_1 \\ M_1 \\ H_2 \\ V_2 \\ M_2 \\ H_3 \\ V_3 \\ M_3 \end{pmatrix} \tag{3-62}$$

Step 2: Obtain the observability equations $[\boldsymbol{B}] \cdot \{\boldsymbol{z}\} = \{\boldsymbol{D}\}$.

Introduce the boundary conditions into Equation (3-62) and rearrange the equations such that all the unknowns are collected in the new unknown vector $\{z\}$, and both the coefficient matrix $[B]$ and right-hand side vector $\{D\}$ are known, as shown in Equation (3-60).

Without loss of generality, the observability equations related with the measurement set (w_1, v_2 and w_3) are obtained from Equation (3-62) by a series of algebraic operations. In this system of equations, the measurements are absorbed in the coefficient matrix. Provided that error-free measurements are used, this system of equations holds stringently. Denote the error-free displacements by a hat, ^. This relation is demonstrated by Equation (3-63).

$$\begin{pmatrix} 0 & 0 & -\frac{6\hat{v}_2}{L^2} & \frac{4\hat{w}_1}{L} & \frac{2}{L} & 0 & 0 & 0 & 0 & 0 & 0 \\ \frac{2}{L} & -\frac{1}{L} & 0 & 0 & 0 & 0 & 0 & 0 & 0 & 0 & 0 \\ 0 & 0 & \frac{12\hat{v}_2}{L^3} & -\frac{6\hat{w}_1}{L^2} & -\frac{6}{L^2} & \frac{12\hat{v}_2}{L^3} & \frac{6}{L^2} & \frac{6\hat{w}_3}{L^2} & 0 & 0 & 0 \\ 0 & 0 & -\frac{6\hat{v}_2}{L^2} & \frac{2\hat{w}_1}{L} & \frac{4}{L} & \frac{6\hat{v}_2}{L^2} & \frac{4}{L} & \frac{2\hat{w}_3}{L} & 0 & 0 & 0 \\ -\frac{1}{L} & \frac{1}{L} & 0 & 0 & 0 & 0 & 0 & 0 & 0 & 0 & 0 \\ 0 & 0 & 0 & 0 & 0 & \frac{6\hat{v}_2}{L^2} & \frac{2}{L} & \frac{4\hat{w}_3}{L} & 0 & 0 & 0 \\ -\frac{1}{L} & 0 & 0 & 0 & 0 & 0 & 0 & 0 & -1 & 0 & 0 \\ 0 & 0 & -\frac{12\hat{v}_2}{L^3} & \frac{6\hat{w}_1}{L^2} & \frac{6}{L^2} & 0 & 0 & 0 & 0 & -1 & 0 \\ 0 & 0 & 0 & 0 & 0 & -\frac{12\hat{v}_2}{L^3} & -\frac{6}{L^2} & -\frac{6\hat{w}_3}{L^2} & 0 & 0 & -1 \end{pmatrix} \begin{pmatrix} EA_1u_2 \\ EA_2u_3 \\ EI_1 \\ EI_1 \\ EI_1w_2 \\ EI_2 \\ EI_2w_2 \\ EI_2 \\ H_1 \\ V_1 \\ V_3 \end{pmatrix} = \begin{pmatrix} M_1 \\ H_2 \\ V_2 \\ M_2 \\ H_3 \\ M_3 \\ 0 \\ 0 \\ 0 \end{pmatrix} \tag{3-63}$$

Step 3: Include the error terms in the coefficient matrix $[B]$.

In real life, the measurements are always contaminated by errors. These measurements $\tilde{\delta}$ comprise of the error-free displacements $\hat{\delta}$ and the errors ϵ_δ. This relation can be rearranged as Equation (3-64).

$$\hat{\delta} = \tilde{\delta} - \epsilon_\delta \tag{3-64}$$

Replace the error-free displacements $\hat{\delta}$ in the coefficient matrix $[B]$ of Equation (3-63) by the difference of the measured displacements $\tilde{\delta}$ and the measurement errors ϵ_δ, Equation (3-64). The resulting system of equations is given in Equation (3-65).

$$\begin{pmatrix}
0 & 0 & -\frac{6(\tilde{v}_2-\epsilon_{v_2})}{L^2} & \frac{4(\tilde{w}_1-\epsilon_{w_1})}{L} & \frac{2}{L} & 0 & 0 & 0 & 0 & 0 & 0\\
\frac{2}{L} & -\frac{1}{L} & 0 & 0 & 0 & 0 & 0 & 0 & 0 & 0 & 0\\
0 & 0 & \frac{12(\tilde{v}_2-\epsilon_{v_2})}{L^3} & -\frac{6(\tilde{w}_1-\epsilon_{w_1})}{L^2} & -\frac{6}{L^2} & \frac{12(\tilde{v}_2-\epsilon_{v_2})}{L^3} & \frac{6}{L^2} & \frac{6(\tilde{w}_3-\epsilon_{w_3})}{L^2} & 0 & 0 & 0\\
0 & 0 & -\frac{6(\tilde{v}_2-\epsilon_{v_2})}{L^2} & \frac{2(\tilde{w}_1-\epsilon_{w_1})}{L} & \frac{4}{L} & \frac{6(\tilde{v}_2-\epsilon_{v_2})}{L^2} & \frac{4}{L} & \frac{2(\tilde{w}_3-\epsilon_{w_3})}{L} & 0 & 0 & 0\\
-\frac{1}{L} & \frac{1}{L} & 0 & 0 & 0 & 0 & 0 & 0 & 0 & 0 & 0\\
0 & 0 & 0 & 0 & 0 & \frac{6(\tilde{v}_2-\epsilon_{v_2})}{L^2} & \frac{2}{L} & \frac{4(\tilde{w}_3-\epsilon_{w_3})}{L} & 0 & 0 & 0\\
-\frac{1}{L} & 0 & 0 & 0 & 0 & 0 & 0 & 0 & -1 & 0 & 0\\
0 & 0 & -\frac{12(\tilde{v}_2-\epsilon_{v_2})}{L^3} & \frac{6(\tilde{w}_1-\epsilon_{w_1})}{L^2} & \frac{6}{L^2} & 0 & 0 & 0 & 0 & -1 & 0\\
0 & 0 & 0 & 0 & 0 & -\frac{12(\tilde{v}_2-\epsilon_{v_2})}{L^3} & -\frac{6}{L^2} & -\frac{6(\tilde{w}_3-\epsilon_{w_3})}{L^2} & 0 & 0 & -1
\end{pmatrix}
\begin{pmatrix}
EA_1u_2\\ EA_2u_3\\ EI_1\\ EI_1\\ EI_1w_2\\ EI_2\\ EI_2w_2\\ EI_2\\ H_1\\ V_1\\ V_3
\end{pmatrix}
=
\begin{pmatrix}
M_1\\ H_2\\ V_2\\ M_2\\ H_3\\ M_3\\ 0\\ 0\\ 0
\end{pmatrix}
\tag{3-65}$$

Step 4: Obtain the new system of equations including error terms, $\boldsymbol{B_e \cdot z_e = D}$ (Equation (3-66)).

This step is similar to the algebraic techniques used for the linearization of the observability equations. Each column containing $\tilde{\delta}-\epsilon_\delta$ is separated into two columns, where one is related to the error-free displacement $\tilde{\delta}$ and the other is related to the error term ϵ_δ. Subsequently, all the error terms are extracted from the respective columns and are included in the unknown vector. Duplication of unknowns might occur due to these extractions. In the case of duplicated unknowns, the associated columns are merged to compact the system. The final system of equations is presented in Equation (3-66).

$$\begin{pmatrix}
0 & 0 & \frac{4\tilde{w}_1}{L}-\frac{6\tilde{v}_2}{L^2} & \frac{6}{L^2} & \frac{2}{L} & -\frac{4}{L} & 0 & 0 & 0 & 0 & 0 & 0 & 0\\
\frac{2}{L} & -\frac{1}{L} & 0 & 0 & 0 & 0 & 0 & 0 & 0 & 0 & 0 & 0 & 0\\
0 & 0 & \frac{12\tilde{v}_2}{L^3}-\frac{6\tilde{w}_1}{L^2} & -\frac{12}{L^3} & -\frac{6}{L^2} & \frac{6}{L^2} & \frac{12\tilde{v}_2}{L^3}+\frac{6\tilde{w}_3}{L^2} & -\frac{12}{L^3} & \frac{6}{L^2} & -\frac{6}{L^2} & 0 & 0 & 0\\
0 & 0 & \frac{2\tilde{w}_1}{L}-\frac{6\tilde{v}_2}{L^2} & \frac{6}{L^2} & \frac{4}{L} & -\frac{2}{L} & \frac{6\tilde{v}_2}{L^2}+\frac{2\tilde{w}_3}{L} & -\frac{6}{L^2} & \frac{4}{L} & -\frac{2}{L} & 0 & 0 & 0\\
-\frac{1}{L} & \frac{1}{L} & 0 & 0 & 0 & 0 & 0 & 0 & 0 & 0 & 0 & 0 & 0\\
0 & 0 & 0 & 0 & 0 & 0 & \frac{6\tilde{v}_2}{L^2}+\frac{4\tilde{w}_3}{L} & -\frac{6}{L^2} & \frac{2}{L} & -\frac{4}{L} & 0 & 0 & 0\\
-\frac{1}{L} & 0 & 0 & 0 & 0 & 0 & 0 & 0 & 0 & 0 & -1 & 0 & 0\\
0 & 0 & \frac{6\tilde{w}_1}{L^2}-\frac{12\tilde{v}_2}{L^3} & \frac{12}{L^3} & \frac{6}{L^2} & -\frac{6}{L^2} & 0 & 0 & 0 & 0 & 0 & -1 & 0\\
0 & 0 & 0 & 0 & 0 & 0 & -\frac{12\tilde{v}_2}{L^3}-\frac{6\tilde{w}_3}{L^2} & \frac{12}{L^3} & -\frac{6}{L^2} & \frac{6}{L^2} & 0 & 0 & -1
\end{pmatrix}
\begin{pmatrix}
EA_1u_2\\ EA_2u_3\\ EI_1\\ EI_1\epsilon_{v2}\\ EI_1w_2\\ EI_1\epsilon_{w1}\\ EI_2\\ EI_2\epsilon_{v2}\\ EI_2w_2\\ EI_2\epsilon_{w3}\\ H_1\\ V_1\\ V_3
\end{pmatrix}
=
\begin{pmatrix}
M_1\\ H_2\\ V_2\\ M_2\\ H_3\\ M_3\\ 0\\ 0\\ 0
\end{pmatrix}
\tag{3-66}$$

Step 5: **Generate all single unknowns and establish the constraints among coupled unknowns.** Identify all single unknowns in the new unknowns $\{z_e\}$, and the nonlinear constraints among them.

In the unknown vector $\{z_e\}$, there exist three types of unknowns: (1) coupled unknowns: products of structural parameters and unknown displacements or error terms (e.g. EA_1u_2, EI_2w_2 and $EI_1\epsilon_{v_2}$); (2) existing single unknowns, including reactions (e.g. H_1,V_1,V_3) and structural parameters θ (e.g. bending stiffnesses EI_1, EI_2 and axial stiffness EA_1); (3) additional single unknowns that are obtained by the decoupling of those coupled unknowns. These new single unknowns include the unmeasured displacements, (e.g. u_2, u_3 and w_2) and the measurement errors, (e.g. ϵ_{w_1}, ϵ_{v_2} and ϵ_{w_3}). Once different types of unknowns are determined in Equation (3-66), the constraints among these unknowns will be established and used in the optimization in Step 6.

Step 6: **Obtain the final estimation by minimizing Equation (3-67)**. Solve the optimization problem with the objective function Equation (3-67) and the nonlinear constraints obtained in step 5**.**

Despite the inclusion of the constraints (e.g. EI_2w_2=$EI_2 \cdot w_2$) among unknowns, the system of equations to be solved is always underdetermined. As a result, infinite solutions satisfy Equation (3-66). To find the one with physical meaning from these solutions, it is always desirable to select the model minimizing the discrepancy between the measured and the predicted response. Hence, the objective function is to minimize the square sum of the ratios between the error term ϵ_{δ_i} and the associated measurements $\tilde{\delta}_i$, as presented in Equation (3-67). N_m is the number of measured displacements.

$$f(z_e) = \sum_{i=1}^{N_m} \left(\frac{\epsilon_{\delta_i}}{\tilde{\delta}_i} \right)^2 \tag{3-67}$$

In order to let the optimization problem have some desirable properties regarding the convergence, numerical scaling is applied such that the unknowns having widely varying orders of magnitude due to the physical nature are converted to be of similar orders (Gill, Murray, & Wright, 1982). To do so, each column of the coefficient matrix B_e is scaled by the associated nominal values of the unknowns. This scaling does not affect the solution but improve the efficiency of solving the optimization. The initial values for the error terms are zeros while those for the others are ones. No bound is applied to the estimated parameters, unless otherwise stated. Final estimations are obtained by multiplying the scaling factors with the solution from the optimization. All the aforementioned steps to implement the algorithm are summarized in Figure 3-31.

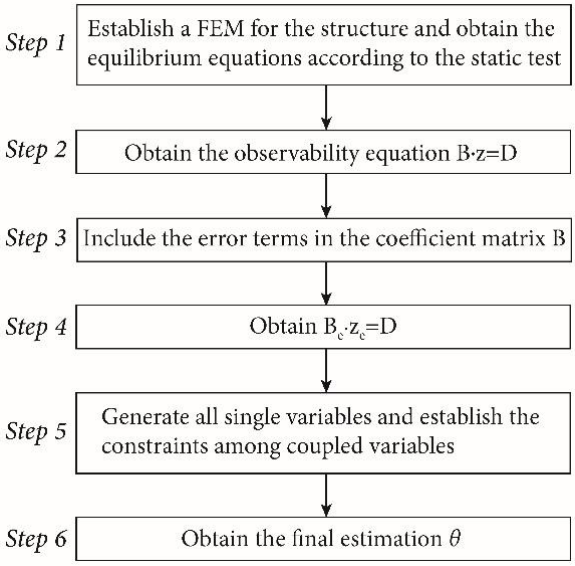

Figure 3-31 Flow chart of the proposed algorithm

Sensor placement

The accuracy of the estimations of structural parameters θ depends on the location of the measurements. In this paper, the Fisher Information matrix $[F]$ is used to select the location of sensors (Bakhtiari-Nejad et al., 2005). For an efficient unbiased estimation of $\hat{\theta}$, the lower bound of the covariance of estimations is given by the inversed Fisher Information matrix $[F^{-1}]$:

$$E\left[(\hat{\theta}-\theta)(\hat{\theta}-\theta)^T\right] \geq F^{-1} \tag{3-68}$$

The Fisher Information matrix $[F(\Theta)]$ contains the information about the values of the parameters θ based on the data from all measured locations (Guo, Ni, & Chen, 2017). Its formulation depends on the sensor location vector $\{\Theta\}$. The calculation of the matrix $[F(\Theta)]$ is shown by Equation (3-69)

$$F(\Theta) = S(\Theta)^T[\Psi_0^2]^{-1}S(\Theta) \tag{3-69}$$

To calculate the Fisher Information matrix $[F(\Theta)]$, the sensitivity matrix $[S(\Theta)]$ for measured DOFs and the noise variance $[\Psi_0^2]$ are required. The matrix $[S(\Theta)]$ is the sensitivity matrix with respect to the sensor location vector $\{\Theta\}$. The vector $\{\Theta\}$ is a $3N_n \times 1$ Boolean vector $\{\Theta\}$. If the i^{th} DOF of the FEM is measured, the associated entry in $\{\Theta\}$ is one, otherwise zero.

Prior to obtain the sensitivity matrix $[S(\Theta)]$ for the measured DOFs, the sensitivity matrix $[S^a]$ for all DOFs is calculated by Equation (3-70).

$$[S^a] = \frac{\partial \delta}{\partial \theta} = \frac{\partial [K(\theta)^{-1} f]}{\partial \theta} = \frac{\partial K(\theta)^{-1}}{\partial \theta} f = -K(\theta)^{-1} \frac{\partial K(\theta)}{\partial \theta} K(\theta)^{-1} f \tag{3-70}$$

The dimension of the sensitivity matrix $[S^q]$ is $3N_n \times N_p$. The element $S^q_{i,j}$, in the i^{th} row and j^{th} column of the matrix $[S^q]$, is the derivative of the i^{th} DOF with respect to the j^{th} parameter. The sensitivity matrix $[S(\Theta)]$ for the measured DOF is the collection of all those rows of $[S^q]$ where Θ_i equals one.

In estimation theory, the minimum variance in the estimations is desired, which means the minimization or maximization of some measures of $[F]$. Different norms of the matrix $[F]$ have been used as the criteria for measuring the goodness of a measurement set regarding the accuracy of the estimations. These norms include the determinant, the trace and the minimum singular value of the matrix $[F]$. In this paper, the problem of sensor placement is formulated as the maximization of the determinant, $det([F])$, of the Fisher information matrix $[F]$. It should be also mentioned that the i^{th} diagonal terms of the inversed matrix $[F^{-1}]$ gives the lower bound of the variance of the estimations of the i^{th} parameter θ_i (Masoud Sanayei, Dicarlo, Rohela, Miller, & Kilmer, 2015). High values in the diagonal elements indicate that the estimations for the associated parameters have a high variation. Parameters of zones that are out of the load path cannot be identified accurately. This is manifested by the large diagonal elements related to these parameters in the inversed matrix $[F^{-1}]$. In this study, the threshold of 0.1 is used to differentiate between the identifiable and the unidentifiable parameters. The parameters associated with diagonal elements of $[F^{-1}]$ that are less than 0.1 might be regarded as identifiable.

The sensor placement is a combinatorial problem whose dimension increases exponentially with the number of possible sensor locations. It is intractable to find the optimal solution by global search. However, some classic metaheuristic algorithms are capable of finding a near-optimal solution of such a problem (Marano et al., 2011). One is the genetic algorithm that is featured by bio-inspired operators such as mutation and crossover and selection. Its application in SSI can be found in (Marano et al., 2011; E. Viola & Bocchini, 2007) . The discrete optimization problem arising from the sensor placement problem here is solved by the *Matlab* function *ga* with the objective function (3-71) and constraints (3-72) and (3-73).

$$\Theta_{\text{opt}} = \max_{\Theta} \det(F) \tag{3-71}$$

Subjected to

$$\sum_{i \in v} \Theta_i = N_{m,v} \quad \text{for any } i \text{ related to vertical deflections } v \tag{3-72}$$

And

$$\sum_{i \in w} \Theta_i = N_{m,w} \quad \text{for any } i \text{ related to rotations } w \tag{3-73}$$

$N_{m,v}$ and $N_{m,w}$ are the numbers of measured deflections and of measured rotations, respectively.

3.5.4 Application in beam-like structures

The observability and the accuracy of estimations for all parameters are always of primary importance. On the one hand, a necessary condition for the observability of all parameters is that the number of measured displacements, N_m, should be no less than the number of parameters, N_p (Jose Antonio Lozano-Galant et al., 2015). With N_p measurements, the observability for all parameters might not be achieved and the accuracy of the estimations might not be satisfactory. Hence, it is intuitive and reasonable to introduce redundant measurements, which is known as redundant sets.

To verify the effectiveness of the proposed method, a simply supported bridge example is analyzed here. Two cases are considered depending on the relation between the number of measured displacements, N_m, and the number of unknown parameters, N_p. Firstly, the performance of the MEMOM and the SSI by OM are compared when essential sets are used. Then, regarding the same structure, the performance of MEMOM and SSI by compatible OM (J. Lei, Xu, et al., 2018) are compared when redundant sets are used. The considered factors include error levels, number of measurements, loading cases.

Equivalence of MEMOM and the original method in case of essential set

Assume an 18-m simply supported bridge with a concentrated load applied at one-third point, as shown in Figure 3-32. The area and inertia of the girder are 0.1 m^2 and 0.015 m^4, respectively and the Young's modulus E is 210 GPa. This structure is discretized into 18 elements each with the length of 1 m. Because the axial behavior of this structure is not excited under this loading case, the identification of axial stiffness is not feasible. The parameterization of this model is shown in Figure 3-32.

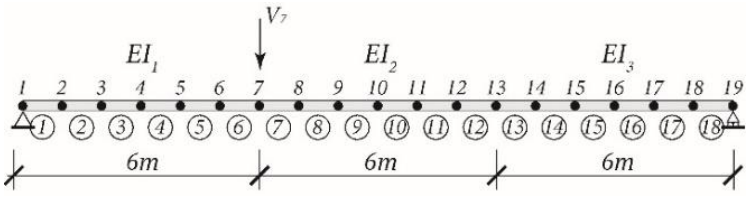

Figure 3-32 A 19-node simply supported beam with three target parameters (bending stiffnesses EI_1-EI_3).

Since the number of parameters, N_p, is three, the essential sets should have three distributed measurements. For each bending stiffness, one displacement from the

elements of that parameter is measured. Specifically, one from {v_2-v_7, w_1-w_7}, {v_7-v_{13}, w_7-w_{13}} and {v_{13}-v_{18}, w_{13}-w_{19}} for EI_1, EI_2 and EI_3, respectively. All potential essential sets are enumerated by taking one measurement from these sets. If duplicated measurements, e.g.w_7 or v_7, are detected, then that set is rejected. This leads to 2314 essential sets. 50 samples are generated for each set with an error level of 5%. One sample for a given measurement set is the collection of associated measurements generated by Equation (3-74).

$$\tilde{\delta} = \delta \cdot (1 + E_{level} \cdot \xi) \tag{3-74}$$

Here, the measurements, $\tilde{\delta}$, are simulated by adding proportional errors to the theoretical values, δ, that are obtained by direct analysis. E_{level} is the error level in measurement and ξ is a random number following normal distribution with mean of zero and standard deviation of 0.5, same as in (J. Lei, Xu, et al., 2018).

Regarding essential sets, it is always possible to find a set of parameters that exactly replicates any value of the measurement, either accurate or noisy measurements. In other words, the objective function (Equation (3-67)) should be exactly zero. With respect to this simply supported bridge, 2314×50=115700 estimations are carried out. For all these estimations, it is found that the estimations from the proposed method are capable of replicating the provided noisy measurements. Hence, it is concluded that the proposed method and SSI by OM lead to the same estimation when essential sets are used. However, as pointed out in (J. Lei et al., 2017), estimations from essential sets might be far from satisfactory.

Comparison of the performance of different methods in a beam-like structure

In order to improve the unsatisfactory estimations from essential sets, redundant sets are used. However, it was observed that the estimations could still be greatly biased. In addition, imposing the compatibility conditions among the displacements can lead to accurate estimations (J. Lei, Xu, et al., 2018). In this section, the performance of the SSI by compatible OM and the MEMOM is compared by a further investigation on the structure depicted in Figure 3-32. The parameterization is still the same with the studied factors being the number of measurements, N_m, and the error levels, $E_{level,}$ and the loading cases.

In the first comparison, the loading case is a vertical load applied at node 7. Three measurement sets are used, including (1) Set 1 (v_3, v_5, v_7, v_9, v_{11}, v_{13}, v_{15} and v_{17}); (2) Set 2 (v_3-v_5, v_7, v_9-v_{11}, v_{13} and v_{15}-v_{17}) and (3) Set 3 (v_2-v_{17}). These sets are not determined by the Fisher Information matrix and are the same as those in (J. Lei, Xu, et al., 2018). The error levels range from 1% to 5%. 2000 samples are generated for each measurement set at all error levels using Equation (3-74). In this paper, all the

estimations are normalized by their real values, unless otherwise stated. To evaluate the performance of different algorithms, Equations (3-75)-(3-77) are used.

$$\hat{\theta}_m = \frac{\sum_{i=1}^{N_s} \hat{\theta}_{i,r}}{N_s} \tag{3-75}$$

$$\hat{\theta}_{sd} = \sqrt{\frac{1}{N_s - 1} \Sigma_{i=1}^{N_s} \left(\hat{\theta}_{i,r} - \hat{\theta}_m\right)^2} \tag{3-76}$$

$$\hat{\theta}_{COV} = \frac{\hat{\theta}_{sd}}{\hat{\theta}_m} \tag{3-77}$$

Here, $\hat{\theta}_{i,r}$ is the estimation (normalized by the real value) of parameter θ using the i^{th} sample. N_s is the number of samples. $\hat{\theta}_m$ is the mean of all the N_s estimations of θ, which measures the accuracy of the estimations. The closer the mean, $\hat{\theta}_m$, to one, the lower the bias. In addition, $\hat{\theta}_{COV}$ describes the variability among all the N_s estimations of θ, which is the ratio of the standard deviation, $\hat{\theta}_{sd}$, and the mean, $\hat{\theta}_m$.The smaller the $\hat{\theta}_{COV}$, the less variation in the estimations of θ.

In this example (Figure 3-32), the target parameters are EI_1-EI_3. A careful examination shows that both methods lead to the same estimations for each measurement set and each error level. The results are presented as the bar graph with error bar in Figure 3-33.a. The bar graph shows the mean of the estimations while the error bar indicates one standard deviation of the estimations.

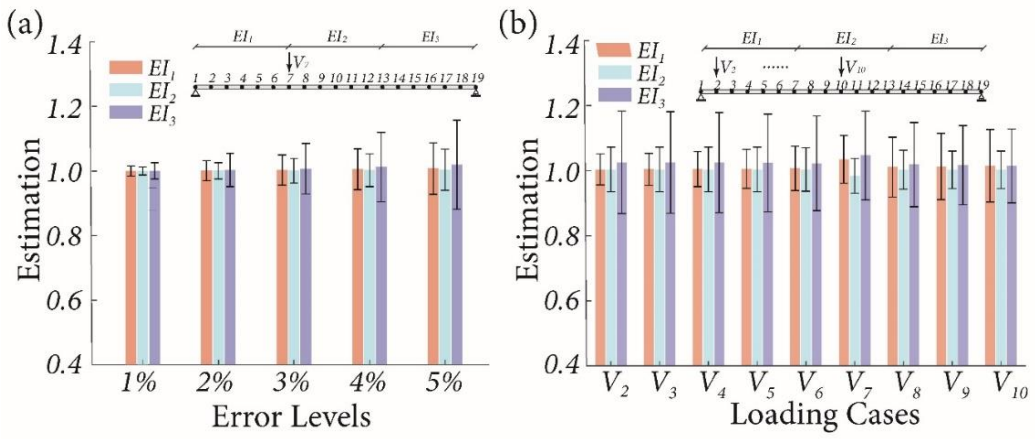

Figure 3-33 Bar graph with error bar for the estimations of EI_1-EI_3: (a) under the loading case of V_7 with different error levels; (2) under different loading cases (V_2-V_{10}) with an error level of 5%.

It should be pointed out that as the load is applied at node 7, the elements associated with EI_1 and EI_2 are more excited than those associated with EI_3. From Figure 3-33.a, it is seen that the standard deviation, which is the length of the error bar, increases much

faster in zones of less excited zones (EI_3). The bias of the estimations of EI_1-EI_3 is small. The worst case is an overestimation of 1.45% in EI_3 with an error level of 5%. However, it should be pointed out that the bias also increases faster in less excited zones.

The performance of the two methods is also compared using different loading cases with set 1 (v_3, v_5, v_7, v_9, v_{11}, v_{13}, v_{15} and v_{17}) and an error level of 5%. The load moves from V_2 through V_{10}, leading to 9 loading cases. Under each loading case, the estimations produced by the proposed method are the same as those obtained via SSI by compatible OM. The results are presented in Figure 3-33.b. When load changes from V_2 to V_{10}, the curvatures for areas associated with EI_1 decreases and the standard deviation of the estimations of EI_1 increase correspondingly. An opposite trend is observed for the parameter EI_3. In addition, the estimations of EI_1 and EI_3 have the same mean and standard deviation when identical curvatures are excited in areas associated with these two parameters in the loading case of V_{10}.

The same performance of the two methods might be due to the fact that the inclusion of the nonlinear constraints among the unknowns in the proposed method implicitly contains the compatibility conditions (the geometrical relations that the displacements should satisfy). Hence, it is concluded that: (1) the proposed method is applicable in beam-like structures and (2) its accuracy is as good as the SSI by compatible OM. For clarity, the difference of the mentioned methods is summarized in Table 3-7.

Table 3-7 Characteristic of different observability method

Method	Applicability	Optimization involved	Nonlinear constraints	Objective function	Sensitive to errors
SSI by OM	Beam-like/ frame	No	-	-	Yes
SSI by constrained OM	Beam-like/ frame	Yes	Yes	Force Residues	Yes
SSI by compatible OM	Beam-like	Yes	No	Displacement Residues	No
SSI by MEMOM	Beam-like/ frame	Yes	Yes	Displacement Residues	No

3.5.5 Application of the proposed method in a frame structure

Due to the coupling of the bending and the axial behavior in frames, obtaining compatibility conditions in such structures is nontrivial. However, the proposed method does not suffer from this limitation. In this section, the effectiveness of the proposed method is verified by the identification of a floor beam (see dashed ellipse in Figure

3-34.a) in a 13-story frame building adapted from (Jose Antonio Lozano-Galant, Nogal, et al., 2013).

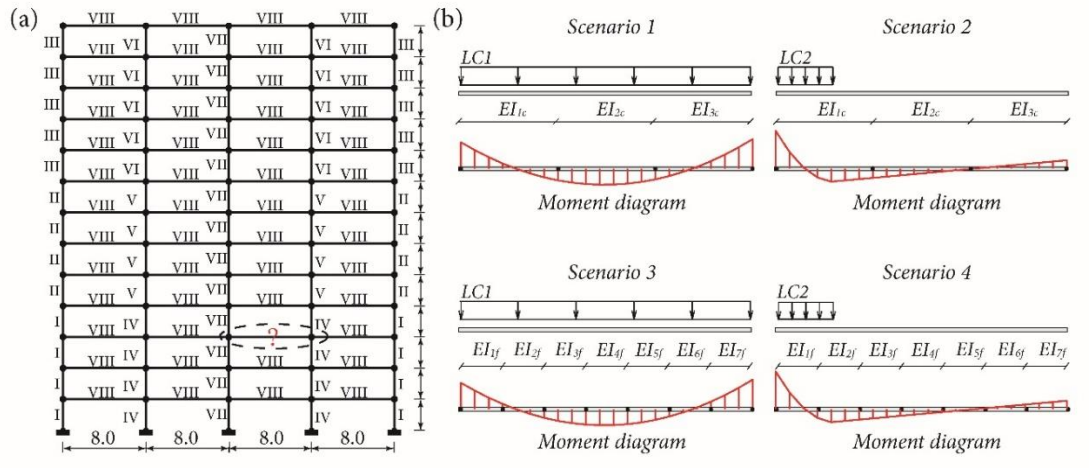

Figure 3-34 (a) Finite element model for the 13-story frame (b) Four scenarios for the identification of the floor beam (different loading cases, parameterizations and moment diagrams)

Damage in structural members that have insignificant contribution to the structural response under the given loading case cannot be accurately identified (Bakhtiari-Nejad et al., 2005). On the one hand, simultaneous identification of all parameters requires a well-designed loading scheme capable of exciting all structural members sufficiently. On the other hand, many sensors are required for data collection. These might not be very feasible in real life for technical and economic reasons. Hence, it is more interesting to identify the parameters of a local area because only a small zone needs to be excited and the number of sensors is significantly reduced. In the following study, the focus is to identify the parameters of a floor beam on 3rd floor using noisy measurements.

The elastic moduli is $3.5\times10^4\ MPa$. Geometrical properties for different elements are provided in Table 3-8. In previous study, measurement errors were not taken into account and the floor beams were assumed to have constant stiffness (the same parameter to be estimated) (Jose Antonio Lozano-Galant, Nogal, et al., 2013). In this study, the real values of the parameters for the target floor beam are the same as those in element type VIII. However, different parameterizations are applied for this beam (Figure 3-34.b) and these parameters are assumed different and are to be estimated. Measurement errors are also included in the numerical analysis.

Parametric studies have been performed trying to evaluate the influence of different factors in the accuracy of the estimations. Firstly, the effect of curvatures in different zones of the floor beam is investigated. Then, the benefit of including rotations in the measurement set is illustrated. Finally, with the aim of identifying the parameters using

only one loading case, different constraints limiting the feasible values of the unidentifiable parameters are compared.

Table 3-8 Geometrical properties for different elements

Element type	Area (m^2)	Inertia (m^4)
I	0.563	0.026
II	0.360	0.011
III	0.250	0.005
IV	0.360	0.011
V	0.250	0.011
VI	0.160	0.002
VII	1.800	5.400
VIII	0.180	0.005

Effect of curvatures

The analyzed floor beam is evenly discretized into 42 elements. To show the effect of curvatures, four scenarios are studied regarding two loading cases and two parameterizations of this floor beam, as presented in Table 3-9 and Figure 3-34.b. The coarse parameterization models the structure with three bending stiffnesses, EI_{1c}-EI_{3c}. Each parameter is related to fourteen elements. The fine parameterization models the structure with seven bending stiffnesses, EI_{1f}-EI_{7f}. Each parameter is related to six elements. The loading case 1 (LC1) is a uniform load of 25kN/m applied along the entire span while the loading case 2 (LC2) is of the same magnitude but only applied on the left four elements (2.667 m). The configuration and the associated moment diagrams are depicted in Figure 3-34.b. Note that the bending behaviors for the zones of EI_{2f} and EI_{6f} under LC1 (scenario 3) are not quite excited. Similar situation is observed for the zones of EI_{4f}-EI_{7f} under LC2 (scenario 4). In scenarios 1 and 2, though the inflection points are included in zones related to EI_{1c} and EI_{3c}, the bending behavior for these zones is still sufficiently excited due to the wide coverage of the zones associated with EI_{1c} and EI_{3c}. It should be noted that the number, the location and the type of measurements affect the result of the estimations. Providing that the number of measurements is three times the number of parameters, $N_m=3N_p$, and at least half of these measurements are composed of deflections, the near-optimal measurement set for each scenario is determined by Fisher Information matrix.

Table 3-9 Description of different scenarios of the continuous beam

Scenarios	Parameterization	Loading case
1	Coarse, three parameters	Uniform load over whole span
2	Coarse, three parameters	Uniform load on the left
3	Fine, seven parameters	Uniform load over whole span
4	Fine, seven parameters	Uniform load on the left

According to the diagonal terms in the associated inversed Fisher Information matrix, EI_{2f} and EI_{6f} in scenario 3 and EI_{5f} -EI_{7f} in scenario 4 cannot be accurately identified. Hence, the absolute constraints of [0, 10] are applied to limit the feasible range of these unidentifiable parameters. 500 samples are generated for each scenario with an error level of 5% using Equation (3-74). The mean and standard deviation are summarized as the bar graph with error bar in Figure 3-35.

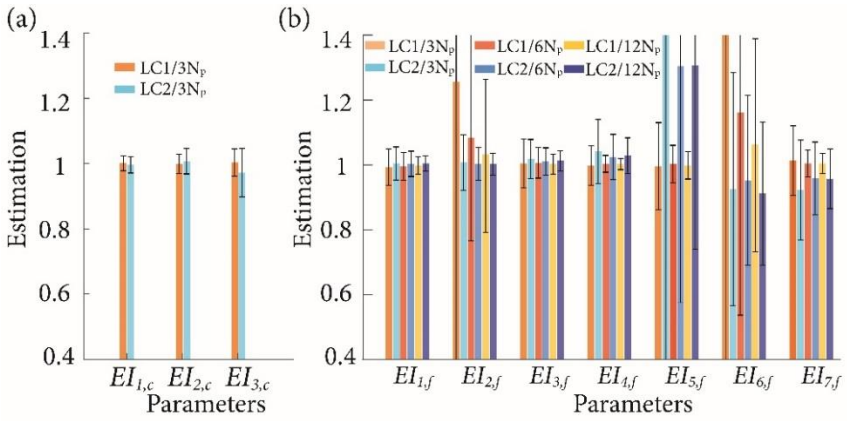

Figure 3-35 The bar graph with error bar for the estimations of parameters in (a) scenarios 1 and 2; (b) scenarios 3 and 4. (The legend indicates the loading case and the number of measurements, respectively. Subscript *f* and c indicate fine and coarse parameterization, respectively. N_p, number of parameters).

When the number of measurements, N_m, is three times the number of parameters, N_p: (1) N_m=9 measurements are sufficient to provide unbiased and robust estimations of EI_{1c}-EI_{3c} in both loading cases. However, larger variations in EI_{2c} and EI_{3c} are observed for LC2 than those for LC1. This is due to the fact that the curvature in zones of EI_{2c} and EI_{3c} is much less excited in LC2 than that in LC1. A slight underestimation of EI_{3c} is also observed in LC2. (2) This phenomenon is more noticeable in Figure 3-35.b. N_m=21 measurements are used to estimate 7 parameters in the fine parameterization. As expected, the estimations of EI_{2f} and EI_{6f} from LC1 have large bias and variations. Note that the bending behavior for zones of EI_{2f} in LC2 are well excited. Comparing

the estimations of EI_{2f} from LC1 and LC2, the latter one is more consistent and less variable. As expected, the estimations of EI_{5f}-EI_{7f} from LC2 are not reliable. (3) Comparing Figure 3-35.a and b, it is seen that the estimations of bending stiffnesses for the coarse parameterization is much better than those for the fine parameterization regarding the unbiasedness and variation under the same loading case.

In order to reduce the large variation and bias in the estimations of the parameters associated with null curvature zones in the case of fine parameterization, other two sets having more measurements are investigated. The first set is to measure the deflection and the rotation every 2 nodes, leading to 42(=$6N_p$) measurements with the deflections at the joint excluded. The second one is to measure the deflection and the rotation of each node, leading to 84(=$12N_p$) measurements with the deflection at the joint excluded. The results are also summarized in Figure 3-35.b. Despite the improvement in all estimations, the standard deviations in the estimations of parameters associated with null curvature zones are still large and thus unreliable.

Type of measurements

It was shown that using rotations had theoretical advantages when estimating the parameters. Wide applications of inclinometers in real engineering practice are also provided (J. Lei, Lozano-Galant, Xu, & Turmo, 2018). The effect of including different number of rotations with a fixed number of measurements on the estimations is studied here. The loading case is LC1 and the parameterization is the fine one, as seen in the scenario 3 in Figure 3-34.b. The number of measurements N_m is 25. The number of rotations varies from 0 to 25, adding up to 26 measurement sets. For each set, the near-optimal measurement set is found by Fisher Information matrix. 500 estimations are obtained for each set using the same setting in previous analysis (Figure 3-35). The result is summarized in Figure 3-36. It is found that using rotations cannot improve the estimations of parameters associated with null curvature zones in this structure. Hence, the results for EI_{2f} and EI_{6f} are not presented.

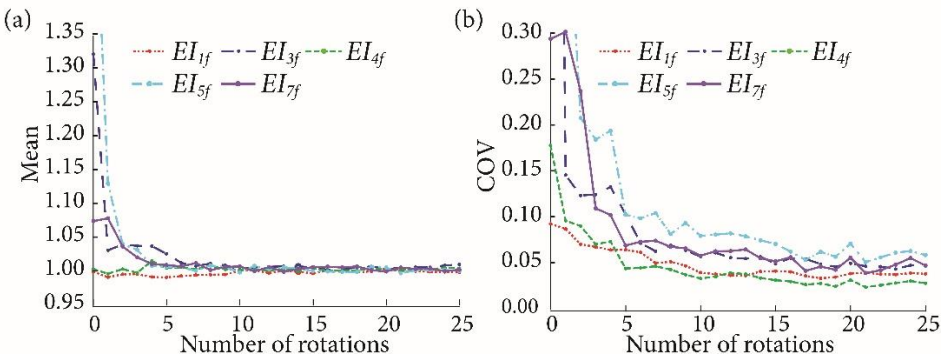

Figure 3-36. Estimation result using different number of rotations: (a) Mean (b) Coefficient Of Variation (COV)

When no rotation is used, the bias in EI_{3f} and EI_{5f} is 32.0% and 64.3%, respectively. The extent of the bias in EI_{3f} and EI_{5f} decreases with the number of rotations. It should be noted that the inclusion of one rotation in the measurements reduces the bias significantly. In addition, the deviations of the mean of the estimations for all parameters are always within 1.0% when the number of rotations exceeds 8. Regarding the COV of the estimations, a gradual decrease is observed when the number of rotations increases from 0 to 17. However, the COVs of the estimations for all parameters do not improve noticeably when more rotations are used.

From this analysis, it is seen that: (1) Compared with using only deflections, the inclusion of rotations in the measurements improves the estimations remarkably with respect to the unbiasedness and the extent of variation; (2) The rate of improvement due to the inclusion of rotations is drastic initially. When the number of rotations reach a certain number, this rate becomes slow, as indicated by the plateau in Figure 3-36b.

Effect of different constraints to limit the value of the estimates in the null curvature zones

The load path by one loading case can hardly cover each part of a local region, as depicted by the moment diagrams in Figure 3-34.b. The parameters for unexcited members may not be accurately identified without using multiple loading cases. This is justified by the observation that either increasing the number of measurements or including rotations cannot improve the estimations for parameters associated with null curvature zones using only one loading case. However, multiple loading cases might be costly, cumbersome and hence not desirable for engineers. Providing that only one loading case is used, it is interesting to limit the feasible ranges of those unidentifiable parameters by imposing different types of constraints during the estimation process. In this section, the effect of these constraints on the unbiasedness and the variation of the estimations for those identifiable parameters are investigated.

In previous study, the absolute constraint that $EI_i \in [0, 10]$ is imposed on unidentifiable parameters, for instance, EI_{2f} and EI_{6f} in LC1. Two types of constraints are studied here. The first type is related to a tight absolute constraint of [0.5, 1.5] on those unidentifiable parameters. The second type is a relative constraint that the parameters for the null curvature zones are between those for adjacent zones. This is to say, $(EI_{2f}\text{-}EI_{1f})$ $(EI_{2f}\text{-}EI_{3f})\leq 0$ and $(EI_{6f}\text{-}EI_{5f})$ $(EI_{6f}\text{-}EI_{7f})\leq 0$. The loading case, the parameterization and the measurement sets are the same as scenario 3 in Figure 3-34.b. It should be pointed out that the following discussions will focus on the results of those identifiable parameters (EI_{1f}, EI_{3f}- EI_{5f}, EI_{7f}) in this scenario.

Under both types of constraints, 500 estimations are carried out for each measurement set using the identical data for the analysis in Figure 3-36. For both types of constraints, the mean and the COVs are summarized in Figure 3-37.a and b, respectively.

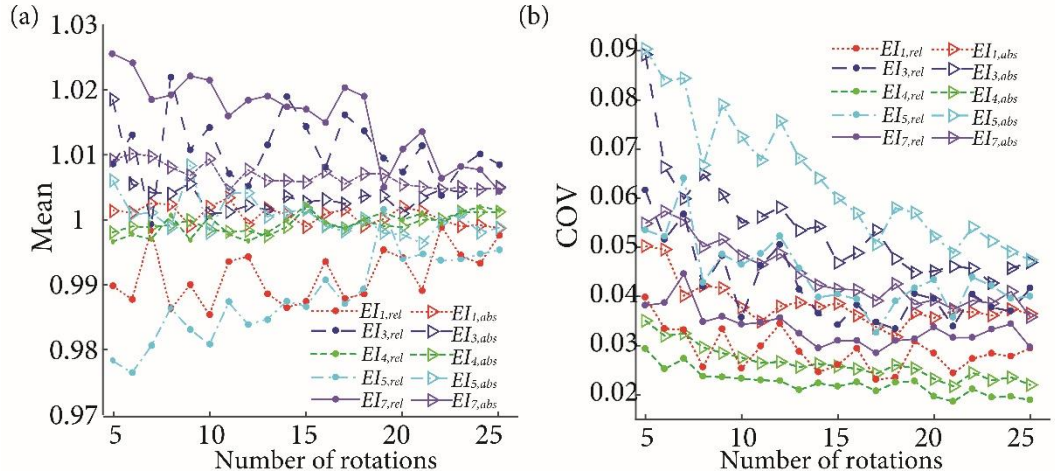

Figure 3-37. Estimations using different number of rotations with the absolute constraint of [0.5, 1.5] (triangle) and the relative constraint (dot): (a) Mean (b) Coefficient Of Variation (COV)

Regarding the tight absolute constraint, the bias and the COVs for EI_{3f} and EI_{5f} are not always satisfactory when the number of rotations used is less than 5. For instance, when 4 rotations are used, the bias in EI_{3f} is 3.5% and the COVs is 0.11. Hence, the results of using less than 5 rotations are not included in this figure. When the number of rotations is equal to or greater than 5: (1) the bias in all identifiable parameters is always less than 1.0%. (2) The bias decreases with the number of rotations. (3) The bias in EI_{3f} is the lowest among the bias for all parameters because the bending behavior of the local zone associated with EI_{3f} is fully excited.

In the case of relative constraints, the bias in EI_{3f} is also the lowest one. However, bias of around 1-2% exists in those estimations for parameters associated with regions adjacent to null curvature zones. In Figure 3-37.a, it is observed that the bias in EI_{1f} and EI_{3f} are very close in magnitude but different in sign. This might be due to the fact that introducing the relative constraints averages the estimations of EI_{1f}, EI_{2f} and EI_{3f}. Similar phenomenon is observed for parameters EI_{5f} and EI_{7f}.

Regarding the variation of the estimations, the COVs for those identifiable parameters can be reduced by both types of constraints. The COVs for EI_{1f}, EI_{3f}-EI_{5f}, EI_{7f} obtained from the tight absolute constraint [0.5, 1.5] are always lower than those respective ones obtained from the constraint [0, 10] for all measurement sets. These COVs drop more significantly when the relative constraint is imposed. The comparison of COVs obtained from the tight absolute constraint and the relative one is depicted in Figure 3-37.b.

The analysis of the comparison between the results obtained from the absolute constraint and the relative constraint shows that: (1) when insufficient rotations are introduced in the measurement set, biased estimations can be obtained despite of the

constraints imposed on the parameters of insufficiently excited zones. (2) When sufficient rotations are introduced, both the tight and the relative constraints can reduce the variations of the estimations for those identifiable parameters where the bending behavior are sufficiently excited. (3) The relative constraint reduces the variations more than the tight absolute constraint at the cost of slight bias.

3.5.6 Conclusion

This paper proposes a Measurement Error-Minimizing Observability Method (MEMOM) for the static structure system identification. For the first time in the literature, to deal with the biasedness in the estimations, those error terms in the coefficient matrix of the observability equations are separated and moved into the unknowns. The resulting equations are solved by minimizing the square sum of the ratios between the error terms and the associated measurements subjected to the nonlinear constraints among the unknowns.

The proposed method is first validated in a beam-like structure with previous methods. In the case of essential sets, the method is capable of exactly replicating any given values of the measurements. In the case of redundant measurements, the proposed method is compared with the SSI by compatible OM regarding different factors, such as the number of measurements, the loading cases and the error levels. The same estimations validate the performance of the proposed method in beam-like structures. The identical estimations of these two methods for beam-like structures might be due to the fact that the geometrical relations among displacements are implicitly imposed by the nonlinear constraints in the proposed method.

In addition, the proposed MEMOM is applicable in frame structures where the SSI by compatible OM is not. In the frame structure, the identification of a local floor beam is investigated regarding the effect of curvatures, the measurement types and the constraint on those unidentifiable parameters. The results indicate that the accuracy of the estimation of a given parameter θ highly depends on the curvature of the zones of parameter θ, which is related to the parameterization and the loading case of the structure. In the case of coarse parameterization, the bending behavior for all zones are sufficiently excited in both loading cases, hence the estimations for all parameters are satisfactory. For the same loading case, the parameters for more excited zones are estimated more accurately than those for less excited zones. In the case of fine parameterization, this situation is even severe. The estimations of the parameters for null curvature zones are greatly biased and variable. The possibility of improving the estimations by including more measurements is investigated. It is found that this means is not efficient in the sense that the estimations for parameters associated with null curvature zones are still unsatisfactory despite plentiful measurements.

To investigate the effect of measurement type, the estimations from 26 measurement sets are evaluated regarding different number of rotations. The analysis of these

simulations shows that the inclusion of rotations in measurements is critical for accurate estimations. As the number of rotations increases, the improvement in the estimations is significant initially but reaches a plateau at a given moment. The inclusion of rotations cannot solve the issue of bad estimations of parameters associated with null curvature zones in frame structures. In addition, providing only one loading case is used, the effect of limiting the feasible range of the estimations for parameters of null curvature zones is studied. It is found that: (1) To obtain unbiased and robust estimations, the inclusion of rotations in the measurement set is necessary despite different types of constraints. (2) The variations for parameters for zones whose curvatures are well excited can be reduced when tight absolute constraints or relative constraints are imposed on the estimations of parameters associated with null curvature zones. (3) The relative constraint reduces the variations more than the tight absolute constraint at the cost of slight bias.

3.6 Structural system identification by Measurement Error-Minimization Observability Method Using Multiple Loading Cases

Title: Structural system identification by Measurement Error-Minimization Observability Method Using Multiple Loading Cases

Authors: Jun Lei, José Antonio Lozano-Galant, Dong Xu, José Turmo

Journal: Structural Control and Health Monitoring

Publication: Technical Paper

Submitted: Draft Version

Accepted: -

DOI: -

Available at:-

3.6.1 Abstract

Evaluating the current condition of existing structures is of primary importance for the safety and due to economic reasons. This can be addressed by Structural System Identification (SSI). A reliable SSI depends on well-designed loading cases and sensor configurations as well as efficient parameter estimation algorithms. Static SSI by Measurement Error-Minimizing Observability Method (MEMOM) is a model-based deterministic static SSI method to estimate structural parameters from static responses. However, this method did not incorporate multiple loading cases. As a result, bending stiffnesses in null curvature zones cannot be satisfactorily identified under one loading case. To solve this issue, the SSI by MEMOM using multiple loading cases is proposed. Observability equations obtained from different loading cases are concatenated simultaneously and an optimization procedure is introduced to obtained the estimations by minimizing the discrepancy between the predicted response and the measured one. Meanwhile, a Genetic-Algorithm (GA)-based Optimal Sensor Placement (OSP) method using the Fisher Information Matrix (FIM)'s determinant as the metric of the goodness of measurement configurations is proposed to handle the OSP problem under multiple loading cases. Two numerical examples, including a 3-span continuous bridge and a 13-story frame, are investigated to validate the applicability of the extended SSI by MEMOM and the GA-based OSP method. Results indicate that the proposed methods are efficient and can be potentially used in practical SSI.

Keyword: structural system identification; stiffness method; observability method; measurement errors; multiple loading case;

3.6.2 Introduction

During the construction and operation stages, infrastructures and civil structure suffer from irreversible deterioration due to various factors such as overloading, concrete cracking, concrete carbonation and corrosion of reinforcement. Consequently, these structures might fail to meet the public requirements regarding the normal use and even safety. It is of primary importance to obtain their current condition to provide the decision-making basis for the follow-up treatment. During the past decades, Structural System Identification (SSI) has emerged as a powerful tool to serve this purpose. The basic principle of SSI is that the change of structural condition is reflected by the change of structural parameters; and can be revealed by the change of structural response.

Regarding the types of external excitation, SSI can be categorized as dynamic SSI (Brownjohn et al., 2008; Papadopoulos & Garcia, 1998; X. Wang et al., 2001) and static SSI (Abdo, 2012; Bakhtiari-Nejad et al., 2005; Banan et al., 1994b, 1994a; J. Lei, Lozano-Galant, et al., 2018; Sheena et al., 1982). As shown by their long history in civil engineering, static load tests provide important information on displacement, rotation and strain, serving as an appropriate alternative and an amendment to visual and dynamic inspections as deflection or strain measurements are relatively easy (Nguyen et al., 2016). However, the majority of SSI research focuses on the dynamic SSI. In dynamic SSI, it is common to assume no damping in the system and that the damage of the structure does not lead to loss of mass (Papadopoulos & Garcia, 1998; X. Wang et al., 2001). These assumptions might introduce modelling error in the parameter estimation. Meanwhile, the modal shapes are sensitive to structural damage but are hard to obtain accurately, especially in stiff structures. On the contrary, the acquisition of accurate frequency is less challenging but frequency is not very sensitive to structural damages (Farrar et al., 1994; Kim et al., 2003). Static response might be more sensitive to local damage while dynamic response provides the overall and distributed information about the structure (Brownjohn et al., 2008). In the static SSI, the basic equations are established on the equilibrium of nodal forces. Neither damping or mass is involved (X. Wang et al., 2001), which makes the static SSI easier than the dynamic SSI. Also, current measurement devices for static tests are cheaper and more accurate than those for dynamic testing (Andreaus et al., 2017; Kourehli, 2017).

Static SSI have been investigated for the purpose of condition assessment. (Sheena et al., 1982) presented a method for improving the analytical stiffness matrix. After measuring a set of Degrees Of Freedom (DOFs), spline functions were used to predict the remaining unmeasured DOFs. Then the difference between the theoretical stiffness matrix and the real one was minimized by adjusting the element properties. (Hajela & Soeiro, 1990a) classified the SSI into three types: equation error approach, output error approach and minimum deviation approach. Both static and eigenmodes of the structure were combined in the damage detection. (Banan et al., 1994a, 1994b) used the iterative optimization method to estimate element properties based on two indices of discrepancy including the Force Error Estimation and the Displacement Error Estimation. (Hjelmstad & Shin, 1997) assumed the baseline values of structure parameters were

known and proposed adaptive parameter grouping algorithm to detect and evaluate structural damage. (Brian J. Walsh & González, 2009) used the cross-entropy method to estimate the structural parameters of a plate structure, given data from a simulated non-destructive static loading test. This method simulated the stiffness of each element with a statistical distribution that was updated by the measurement data. The effect of initial distribution values, structural model, number of readings and sample size was investigated. (Abdo, 2012) studied the relation between the change in static displacement curvature and the damage characteristics (location and severity). This method successfully detected and located damage in beam-like structures. However, mechanical properties of the intact structure were required.

SSI is essentially the application of parameter estimation in structural system. In parameter estimation, the classical observability problem is involved with the observability (existence and uniqueness) of the estimated parameters. The Observability Method (OM) has been applied in static SSI to determine the observability of the structural parameters by checking the null space of the coefficient matrix of observability equations (Jose Antonio Lozano-Galant, Nogal, et al., 2013). These equations are obtained by reconstructing the static equilibrium equations via a series of algebraic operations. (Nogal et al., 2015) proposed SSI by Numerical OM that incorporated a numerical evaluation procedure in the original SSI by OM. In order to identify the minimum measurement sets that are capable of ensuring the observability of all parameters with the least and necessary number of measurements, (Jose Antonio Lozano-Galant et al., 2015) proposed the observability tree method according to the mechanical connection between structural parameters and measurements. (J. Lei, Nogal, et al., 2018) revealed the lacking nonlinear constraints in the observability equations in SSI by NOM and reintroduced these constraints by an optimization procedure. The effect of measurement errors and simulation errors on the accuracy of the estimated parameters using SSI by NOM with minimum sets were investigated in (J. Lei et al., 2017). In order to improve the estimation by using redundant measurements, the SSI by Measurement Error Minimizing Observability Method (MEMOM) was proposed. This method decomposed the measurements $\tilde{\delta}$ contained in the coefficients matrix of observability equations into error-free terms $\hat{\delta}$ and error terms ϵ_{δ}. The error terms were then transferred to the unknown vector. The final estimations were obtained by minimizing the square sum of all the ratios between the error terms ϵ_{δ} and the measurements $\tilde{\delta}$.

The quality of the static SSI result depends on three factors: (1) loading cases that activate the mechanical behavior of the structures to be identified; (2) the number and the spatial location of sensors that ensures the quality of the measurement raw data; and (3) efficient parameter estimation algorithms that exploit the essential information of the structure from the loading cases and the measured response. The damage of structures might be concealed due to the limitation of the load paths (Chen, Zhu, & Chen, 2005; Q. Yang & Sun, 2010). This situation is very significant when only one loading case is used to identify the structure. This agrees with the observation that

accurate estimation of bending structural parameters in null curvature zones is intractable (J. Lei et al., 2017; J. Lei, Xu, et al., 2018). Such zones include those adjacent to the support or near the inflection point of the moment diagram. However, it is inevitable to have null curvature zones in the structure when only one static load test is applied. Alternatively, test data from multiple loading cases can be used in the static SSI.

Apart from the importance of loading cases in the static SSI, the Optimal Sensor Placement (OSP) is also a vital issue. The OSP problem can be formulated as a combinatorial optimization problem aiming at minimizing or maximizing some user-defined objective functions with the sensor location vector being the decision variable. Such objective functions include some norms of the Fisher information matrix. Regarding the formidable dimension of real structures, seeking the OSP is an intractable task by ordinary global search method due to the fact that the solution space is huge and the searching efficiency is low. For a model with n DOFs and N_m sensors, there are C_n^{Nm} possible sensor placement configuration. For instance, the case of 70 DOFs and 20 sensors means 2.0237×10^{63} possible sensor placement configurations. Typically, the combinatorial optimization problem is a non-convex optimization problem. Traditional optimization methods tend to be trapped in the local minimal (maximal) points. Instead of finding the OSP from a global sense, current work for the OSP in static SSI (Masoud Sanayei & Chitra, 2002; Masoud Sanayei, Dicarlo, et al., 2015) adopted the idea of greedy algorithm. This leads to the problem that these methods might make certain choices too early, preventing them from finding the best overall solution later. This is typical for OSP method using greedy algorithm (Bertola, Papadopoulou, Vernay, & Smith, 2017). Another limitation is that these methods cannot specify the number of different types of sensors to be used. They can guarantee the total number of sensors but cannot control the number of inclinometers, strain gauges or deflection gauges.

The objective of this research includes (1) develop the static SSI using multiple loading cases under the framework of OM; (2) propose a systematic method to determine the OSP configuration for static SSI under multiple loading cases.

The organization of the paper is as follows: firstly, the procedure to implement SSI by MEMOM under Multiple loading cases is presented. This starts with the previous method aimed for single loading case. Then a detailed description of how to combine the equations for different loading cases is provided. In section 3.6.4, the property of the FIM and the formulation of the FIM under multiple loading cases are presented. Section 3.6.5 provides some numerical examples to validate the proposed methods. Finally, in section 3.6.6, some conclusions are drawn.

3.6.3 Structural System Identification by Measurement Error Minimizing Observability Method under multiple loading cases

SSI by MEMOM under single loading case

Firstly, a Finite Element Model (FEM) for the target structure is required and its static equilibrium equations should be established.

$$[K]\{\delta\} = \{f\} \tag{3-78}$$

For 2D analysis, the stiffness matrix [K] includes the element length L_j, elastic modulus E_j, area A_j, inertia I_j, shear modulus G_j, torsional stiffness J_j of element j (j=1,2, …, N_e, where N_e is the number of elements). The displacement vector $\{\delta\}$ includes the horizontal deflection u_i, vertical deflection v_i and rotation w_i of node i (i=1,2, …, N_n, where N_n is the number of nodes).

For the sake of simplicity, this paper will focus on the structural mechanism involved with E_jA_j, E_jI_j. Since the main objective of SSI is to assess the condition of the structure, the estimations of axial stiffnesses EA and bending stiffnesses EI are of primary importance. These parameters, $EA_j$and EI_j, are treated as one unknown each to reduce unknowns.

Different unknowns may appear in the same column in the matrix $[K]$. Meanwhile, in controlled static load tests, the magnitude of the external force and the measured responses are known to experimenters. Hence, some elements of the force vector and the displacement vector are known. To distinct the knowns from the unknowns, those known elements are indicated by subscript 1 while those unknown elements are indicated by 0. In order to solve the inverse problem formulated from Equation (3-78), the equilibrium equations are reconstructed as the observability Equation (3-79) using a series of algebraic operations.

$$B \cdot z = \begin{bmatrix} K_{10}^* & 0 \\ K_{00}^* & -I \end{bmatrix} \begin{Bmatrix} \delta_0^* \\ f_0 \end{Bmatrix} = \begin{Bmatrix} f_1 - K_{11}^*\delta_1^* \\ -K_{01}^*\delta_1^* \end{Bmatrix} = D \tag{3-79}$$

In the observability equations, the coefficient matrix $[B]$ contains the measured displacements $\tilde{\delta}$ and the known element length. The unknown vector z is composed of three types of unknowns, including (1) single unknowns, such as bending stiffnesses EI_j, axial stiffnesses EA_j; (2) coupled unknowns, such as EI_jw_i, EI_jv_i; (3) reactions (H_i, V_i, M_i).

Based on the observability equations, the observability (existence and uniqueness) of any unknown in the vector $\{z\}$ can be determined symbolically from the structure of the null space of the coefficient matrix $[B]$. Meanwhile, a particular solution of the observability equation is obtained by least-square methods. The particular solution for those observable unknowns is regarded as the final estimations.

Despite its efficiency in determining the observability of the target parameters, the

overall accuracy of this method is far from satisfactory when measurement errors exist. Some improvements are made to alleviate the adverse effect of measurement errors. For instance, the compatibility conditions (geometrical relations among nodal displacements) in beam-like structures can be obtained from the observability equations and can be used to smooth away the incompatibility induced by measurement errors (J. Lei, Xu, et al., 2018). Also, averaging the estimations from different combinations of rotation measurements is capable of acquiring robust estimations of the target parameters. However, both methods suffer from the limitation in either the structure type or the measurement type. In order to have a more general method, the SSI by MEMOM is proposed. In the observability equations, the measured displacement $\tilde{\delta}$ contained in the coefficient matrix $[B]$ are separated into an error-free term $\hat{\delta}$ and an error term ϵ_δ. Then the error terms ϵ_δ for all measured displacements are transferred to the unknown vector. A new observability equation with measurement errors being included in the unknowns is formulated, as shown by Equation (3-80).

$$[B_e] \cdot \{z_e\} = \{D\} \tag{3-80}$$

In this new observability equation, those measured displacements $\tilde{\delta}$ are included in the matrix $[B_e]$. Compared to the previous unknown $\{z\}$, the new unknown $\{z_e\}$ also contains the error terms ϵ_δ. The Equation (3-80) usually has more unknowns than the number of equations. To solve this underdetermined system, other conditions have to be imposed. The discrepancy between the measured response and the predicted response is minimized by numerical optimization. The objective function is the square sum of the ratios between the error terms and the measured displacements.

SSI by MEMOM under multiple loading case

To make use of multiple loading cases, the observability equations for different loading cases are obtained first. Then the observability equations for different loading cases have to be stacked. The procedure to combine the observability equations in different loading cases is demonstrated in Figure 3-38. In one loading case, the number of equations equals the number of equilibrium N_{eq} on all nodes. As a result, the number of equations in the observability equations for multiple loading cases equals $N_{LC} \times N_{eq}$.

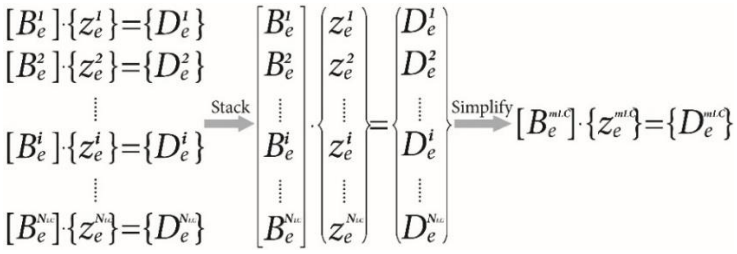

Figure 3-38 Formulation of observability equations for multiple loading cases by stacking (*mLC* means multiple loading cases, N_{LC} is the number of loading cases)

It is assumed that structural parameters do not change due to the static tests and they remain constant along time. In each loading case, the unknowns always include the structural parameters to be estimated. Hence, the concatenated equations contain duplicated variables (structural parameters). This system of equations can be simplified by merging columns that are related with these duplicated variables. In the final observability equations, the unknowns are composed of three types: (1) single unknowns, including structural parameters (bending/axial stiffness), reactions from different loading cases, (2) coupled unknowns, products of structural parameters and unknown displacements or error terms from different loading cases; (3) additional single unknowns that are obtained by the decoupling of those coupled unknowns and are not included in the first type, such as the unmeasured displacements and the error terms.

After obtaining the final observability equations, the structural parameters are estimated by minimizing the square sum of the ratios between the error terms and the measured displacements in all loading cases, as shown in Equation (3-81).

$$f(z_e^{mLC}) = \sum_{i=1}^{N_{LC}} \sum_{j=1}^{N_m} \left(\frac{\epsilon_{\delta_{i,j}}}{\delta_{i,j}} \right)^2 \tag{3-81}$$

Here, N_{LC} is the number of loading cases. N_m is the number measurements in each loading case. $\delta_{i,j}$ is the j^{th} measurement in the i^{th} loading case and $\epsilon_{\delta_{i,j}}$ is the corresponding error term.

The procedure to carry out SSI by MEMOM for multiple loading cases is summarized in Figure 3-39.

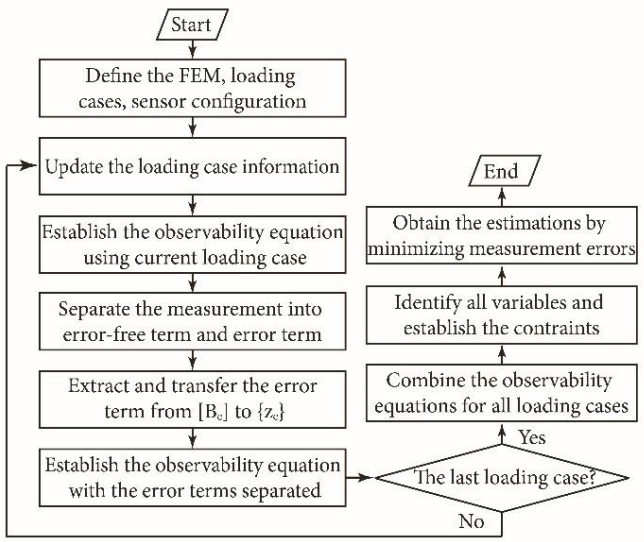

Figure 3-39 Flowchart of the structural system identification by measurement-error minimizing observability method under multiple loading cases.

3.6.4 Genetic Algorithm-based Optimal Sensor Placement

Formulation of FIM under multiple loading cases

The majority of research dealing with sensor placement focuses on the dynamic SSI. Little attention has been paid to the static case. Existing research on the OSP for static SSI is based on the FIM $[F]$ (Masoud Sanayei & Chitra, 2002; Masoud Sanayei, Dicarlo, et al., 2015). The rationale of this sensor placement method is that FIM provides a lower bound estimation of the covariance of the estimated parameters θ, as stated by the Cramer-Rao lower bound (Udwadia, 1994).

$$\mathrm{E}\left[\left(\hat{\theta}-\theta\right)\left(\hat{\theta}-\theta\right)^{\mathrm{T}}\right] \geq [F]^{-1} \tag{3-82}$$

Firstly, the computation of FIM $[F_s]$ under single loading case is given below.

$$[F_s(\Theta)] = [S(\Theta)^T][\Psi_0^2]^{-1}[S(\Theta)] \tag{3-83}$$

The FIM $[F_s]$ is comprised of a sensitivity matrix $[S(\Theta)]$ and a noise variance matrix $[\Psi_0^2]$. The sensitivity matrix $[S(\Theta)]$ describes the effects of the variation of structural parameters on the selected measurements. It has N_m rows and N_p columns, where N_m is the number of measurements and N_p is the number of parameters. The noise variance matrix $[\Psi_0^2]$ of the measurements are typically available to experimenters through instrument calibration, sensor-supplier information and engineering judgement (Bertola et al., 2017; Masoud Sanayei, Dicarlo, et al., 2015). The sensor location vector Θ is a binary vector with the length of N_d, where N_d is the number of DOFs in the model. Each element of the sensor location vector Θ is associated with one DOF. When i^{th} DOF is measured, then Θ_i=1. Otherwise, Θ_i=0. Clearly, the sum of all elements of Θ equals N_d.

To obtain the sensitivity matrix $[S(\Theta)]$ for measured DOF, the sensitivity matrix $[S^a]$ for all DOFs is obtained first, as shown below.

$$[S^a] = \frac{\partial \delta}{\partial \theta} = \frac{\partial [K(\theta)^{-1} f]}{\partial \theta} \tag{3-84}$$

Here, $[K]$ is the stiffness matrix and $\{f\}$ is the load vector.

The matrix form of Equation (3-84) is given in Equation (3-85).

$$[S^a] = \nabla_\theta \delta = \begin{bmatrix} \frac{\partial \delta}{\partial \theta_1} & \cdots & \frac{\partial \delta}{\partial \theta_{N_p}} \end{bmatrix} = \begin{bmatrix} \frac{\partial \delta_1}{\partial \theta_1} & \cdots & \frac{\partial \delta_1}{\partial \theta_{N_p}} \\ \vdots & \ddots & \vdots \\ \frac{\partial \delta_{N_d}}{\partial \theta_1} & \cdots & \frac{\partial \delta_{N_d}}{\partial \theta_{N_p}} \end{bmatrix} \tag{3-85}$$

Since $[K][K^{-1}]=[I]$, the following equation holds.

$$\mathbf{0} = \frac{\partial[K \cdot K^{-1}]}{\partial\theta} = [K] \cdot \frac{\partial[K(\theta)^{-1}]}{\partial\theta} + \frac{\partial[K(\theta)]}{\partial\theta} \cdot [K^{-1}] \tag{3-86}$$

Combining Equation (3-84) and Equation (3-86).

$$[S^a] = \frac{\partial[K(\theta)^{-1}]}{\partial\theta} \cdot f = -[K(\theta)^{-1}] \frac{\partial[K(\theta)]}{\partial\theta} [K(\theta)^{-1}]\{f\} \tag{3-87}$$

The sensitivity matrix $S(\Theta)$ for the selected measurements is obtained by extracting the associated rows of the matrix $[S^a]$ where the corresponding elements of Θ are 1.

(Masoud Sanayei, Dicarlo, et al., 2015) pointed out that the noise variance matrix is semi-definite and thus the Cholesky decomposition can be applied.

$$\Psi_0^2 = [L] \cdot [L^T] \tag{3-88}$$

Substituting Equation (3-88) into Equation (3-83), then:

$$F_s(\Theta) = S(\Theta)^T (L \cdot L^T)^{-1} S(\Theta) = \left(L^{-1} S(\Theta)\right)^T L^{-1} S(\Theta) = \tilde{S}(\Theta)^T \tilde{S}(\Theta) \tag{3-89}$$

The modified sensitivity matrix $\tilde{S}(\Theta)$ incorporates measurement uncertainty into the sensitivity matrix.

With the formulation of FIM under one loading case, the procedure to obtain the FIM for a static load test comprised of N_{LC} loading cases is presented below.

Step 1:For the i^{th} loading case, obtain the sensitivity matrix $[S_i^a]$ (N_d by N_p matrix) for all DOFs according to Equation (3-87) and the lower triangular matrix $[L_i]$ from the noise variance matrix $\left[\Psi_{0,i}^2\right]$. Then the modified sensitivity matrix $[\tilde{S}_i^a]$ for the i^{th} loading case is given by:

$$\left[\tilde{S}_i^a\right] = L_i^{-1} S_i^a \tag{3-90}$$

Step 2: Formulate the modified sensitivity matrix $\left[\tilde{S}_m^a\right]$ for all DOFs under multiple loading cases by combining the modified sensitivity matrix $[\tilde{S}_i^a]$ for different loading cases.

$$\left[\tilde{S}_m^a\right] = \begin{bmatrix} \tilde{S}_1^a \\ \vdots \\ \tilde{S}_{N_{LC}}^a \end{bmatrix} \tag{3-91}$$

Note that the modified sensitivity matrix $[\tilde{S}_a]$ for all loading cases has $N_{LC} \times N_d$ rows and N_p columns.

Step 3: Extracting those rows of the matrix $\left[\tilde{S}_m^a\right]$ where the corresponding DOFs are measured so as to formulate the modified sensitivity matrix $[\tilde{S}_m(\Theta_m)]$ for the selected DOFs under multiple loading cases.

The sensor placement vector Θ_m for multiple loading cases has $N_{LC} \times N_d$ elements. From a practical point of view, it is rational to keep the sensor configuration the same in each loading case so that the cumbersome disassembly and installation of sensors

due to the difference of sensor configurations can be avoided. When the sensor configuration for each loading case is the same, the sensor placement vector Θ_m for multiple loading cases is the N_{LC} times repetition of the sensor placement vector Θ_s for one loading case. Thus the number of unknowns to be optimized is the same as the number of elements in the vector Θ_s, which is N_d. Regarding the computation aspect, this is also beneficial due to the reduction of the search space in the optimization.

Step 4: Calculate the FIM for multiple loading cases, as shown by Equation (3-92).

$$F_m(\Theta_s) = \tilde{S}_m(\Theta_s)^T \tilde{S}_{\mathrm{m}}(\Theta_s) \tag{3-92}$$

Optimal Sensor Placement using Genetic Algorithm

The objective of OSP is to find the best sensor locations to extract as much information from the structural response as possible with a given number of sensors. The OSP for static SSI can be stated as maximizing or minimizing an objective function associated with the static characteristic of the structure, where the optimization variable is the sensor location vector Θ and the constraint is the number of available sensors.

According to the Cramer-Rao lower bound, maximization of some norms of the matrix $[F]$ would yield possible minimum lower bound of the covariance of the estimation θ. Common norms of the matrix $[F]$ include trace, determinant and minimum singular values. (D.-S. Li, Li, & Fritzen, 2012) pointed out that different matrix norms are equivalent in the sense that one norm can be always bounded in a range by another norm with appropriate constant scaling factors. Hence, the determinant of the FIM, $\det([F])$ is adopted as the objective function to judge the goodness of a sensor placement configuration, which is the same as the criterion in current static OSP methods (Bakhtiari-Nejad et al., 2005; Masoud Sanayei & Chitra, 2002; Masoud Sanayei, Dicarlo, et al., 2015). In Sanayei's method, an initial sensor set containing all possible sensor locations (namely DOFs for the FEM) is created first. The determinant of the FIM associated with this initial set is used as a reference value, $\det([F_0])$. Based on the algebraic property of the determinant of matrices, the ratio R_{Di} between the determinant of the FIM, $det([F_{-i}])$, after the removal of the i^{th} DOF in the initial sensor set and the reference value $det([F_0])$, can be determined quantitatively. This ratio R_{Di} is always between [0, 1]. The higher R_{Di}, the less important the measurement of the i^{th} DOF. After getting R_{Di} for all DOFs, the DOF with the highest R_{Di} (lowest importance) is removed from the initial sensor set. Thus a new sensor set is formed. The process of forming new sensor sets and deleting sensor candidates (DOFs) is repeated until the remaining number of sensors in the current set is the same as the number of available sensors. In (Bakhtiari-Nejad et al., 2005), the importance of DOFs is determined in a similar way. However, the best sensor locations are simply chosen as those DOFs with the lowest R_{Di} in the initial sensor set without the process of updating sensor sets. Another difference is that the sensor configurations for different loading cases are selected independently in (Bakhtiari-Nejad et al., 2005).

Consequently, the physical locations of the sensors are not invariant, which leads to additional costs in the disassembly and the installation of sensors. However, the sensor configuration in each loading case is kept constant in (Masoud Sanayei & Chitra, 2002; Masoud Sanayei, Khaloo, et al., 2015). Both methods evaluate the importance of potential sensor locations by checking the decrease in the determinant of FIM after removing one DOF. This kind of evaluation cannot reconsider the previous choices on sensor locations. This is to say, due to the limitation of evaluating the importance of different DOFs in a sequential manner, the joint effect of two or more DOFs on the determinant of FIM cannot be accounted. Also, the number of deflectometers and inclinometers cannot be specified in these methods, only the sum of them. This issue can be solved by biology-inspired algorithms, such as Genetic Algorithm (GA) or particle swarm optimization, artificial bee colony algorithm. In this paper, the GA proposed by (Deep, Singh, Kansal, & Mohan, 2009) is used to solve the combinatorial optimization problem for the OSP. The mathematical formulation of the aforementioned OSP problem for multiple loading cases is given below.

$$\Theta_{opt} = \max_{\Theta} det(F_m(\Theta_s)) \tag{3-93}$$

Subjected to

$$N_{LC} \cdot \sum_{i \in v} \Theta_{s,i} = N_v \quad \Theta_{s,i} \in \{0,1\} \tag{3-94}$$

$$N_{LC} \cdot \sum_{i \in w} \Theta_{s,i} = N_w \quad \Theta_{s,i} \in \{0,1\} \tag{3-95}$$

The GA proposed by (Deep et al., 2009) includes following stages: (1) initialization stage; (2) evaluation stage; (3) selection stage; (4) crossover stage; (5) mutation stage; (6) truncation stage. In GA, a batch of initial solutions is generated randomly at the initialization stage. The batch and each solution are called population and individual, respectively. The evaluation stage assesses the fitness of each individual in the current population and also checks whether the termination criterion is reached or not. Regarding the fitness of individuals, the judging criteria correspond with three cases: (a) feasible solutions always overmatch infeasible ones; (b) among feasible solutions, the one with the best objective function overmatches the others; (c) among infeasible solutions, the one with the lowest constraint violation overmatches the others. The selection, crossover, mutation and truncation stages are carried out repeatedly. The first three stages aim at updating and diversifying the population while the truncation stage aims at satisfying the restriction that each element of the individual should be integer. When one round of these four stages is finished, a new generation of the population is obtained. Subsequently, the evaluation stage is carried out based on this new population. The best individual in this population and its fitness value are recorded and compared with those of the previous population. If the number of generations exceeds the predefined number or the improvement of the fitness value does not exceed a threshold, the algorithm will terminate and the best individual in the last population is determined

as the best solution. For more technical details, please refer to (Deep et al., 2009).

3.6.5 Numerical Examples

Example 1: A 3-span continuous beam

The first example is a $36\,m$ +$54\,m$ +$36\,m$ continuous beam. The FEM and its parameterization are depicted in Figure 3-40. It is assumed that the bending stiffnesses for the first span (EI_1-EI_4), those for the second span (EI_5-EI_{10}) and those for the third span (EI_{11}-EI_{14}) equal to 1.5×10^7 $kN\cdot m^2$, 2.5×10^7 $kN\cdot m^2$ and 1.5×10^7 $kN\cdot m^2$, respectively.

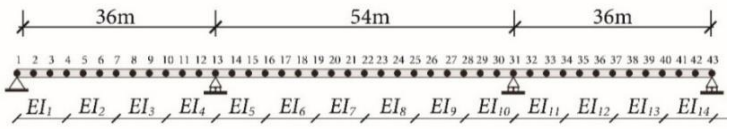

Figure 3-40 Finite element model for the 36m+54m+36m continuous beam

(1) Advantages of using multiple loading cases

Four loading cases are studied here, as shown in Figure 3-41 and

Table 3-10.

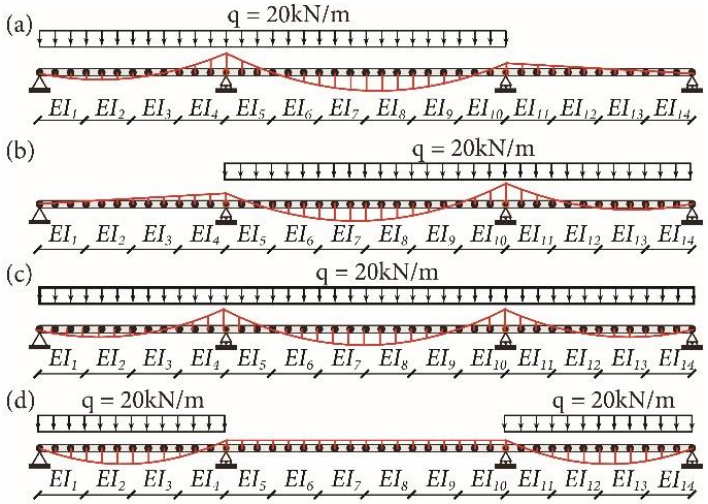

Figure 3-41 Different loading cases:(a) LC1 (b) LC2 (3) LC3 (4) LC4

Table 3-10 Description of the loading cases of the continuous beam

Loading Case	Range	Magnitude	Type
LC1	Span 1+ Span 2	20 kN/m	Uniform
LC2	Span 2+ Span 3	20 kN/m	Uniform
LC3	Span 1+ Span 2+ Span 3	20 kN/m	Uniform
LC4	Span 1+ Span 3	20 kN/m	Uniform

In order to demonstrate the advantage and effectiveness of using multiple loading cases, five scenarios are considered.

Scenario 1: Using 28 deflections and 14 rotations under LC1.

Scenario 2: Using 28 deflections and 14 rotations under LC2.

Scenario 3: Using 28 deflections and 14 rotations under LC3.

Scenario 4: Using 14 deflections and 7 rotations for both LC1 and LC2.

Scenario 5: Using 14 deflections and 7 rotations for both LC3 and LC4.

Due to the existence of null curvature zones, some parameters are not identifiable using only one loading case. This can be judged by the value of the diagonal elements in the inversed FIM, $[F^{-1}]$. For instance, in scenario 1, the bending stiffnesses EI_{10} and EI_{14} cannot be identified. In scenario 2, the bending stiffnesses EI_1 and EI_5 cannot be identified. In scenario 3, all parameters can be identified as all diagonal elements of the associated inversed FIM, $[F^{-1}]$, are smaller than 0.1. However, the extent of variation of EI_3, EI_6, EI_9 and EI_{12} is much higher than that of other parameters. Regarding scenarios 4 and 5, all diagonal elements of the associated inversed FIM are smaller than 0.1. In the optimization, an absolute bound of [0.5, 1.5] is applied on the normalized estimation of all unidentifiable parameters.

For scenarios 1-3, the OSP is determined by the GA-based optimization using one loading case. For scenarios 4 and 5, the OSP is determined by the GA-based optimization using multiple loading cases. For each OSP configuration of the associated scenario, 200 measurement sets are simulated with proportional measurement errors using Equation (3-96).

$$\tilde{\delta} = \delta_r \cdot (1 + E_{level} \cdot \xi) \tag{3-96}$$

The result of the estimations in each scenario is summarized as the box plots in Figure 3-42.

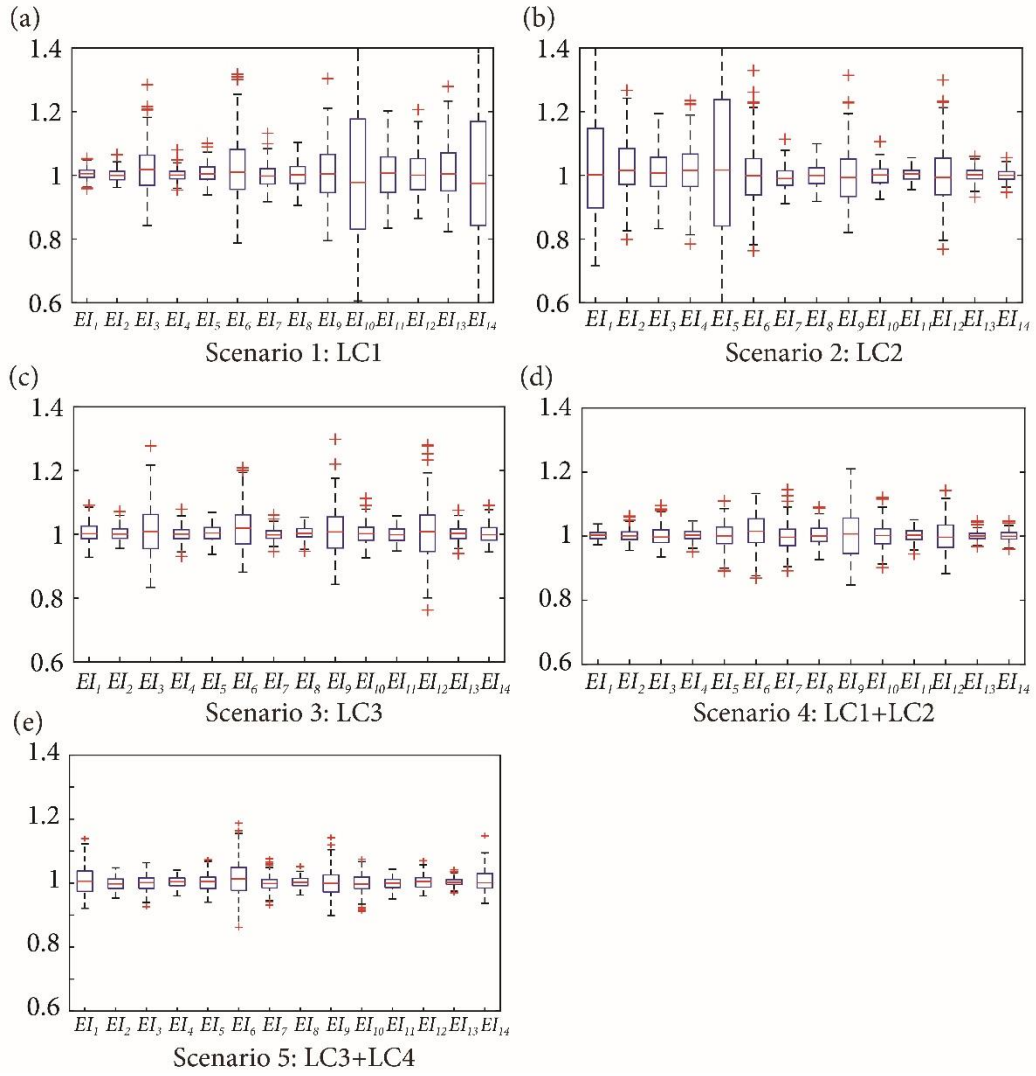

Figure 3-42 boxplot of the 200 estimations for EI_1-EI_{14} in scenarios 1-5

The box plot is a statistical diagram that describes the dispersion of the data without making any assumption of the underlying distribution. The box is composed of three horizontal lines. From the bottom to the top, these lines are associated with the first quartile Q_1, the median Q_2 and the third quartile Q_3 of the data. The longer the box, the larger the dispersion in the data. For the sake of easy comparison between different scenarios, the range of y-axis in Figure 3-42 is set between 0.6 and 1.4. In scenario 1 (Figure 3-42.a), it is seen that the length of the box for EI_{10} and EI_{14} is significantly larger than those of other parameters. This is to say, despite of the absolute bound of [0.5, 1.5] on the normalized values of the estimation of the parameters (EI_{10} and EI_{14}) for null curvature zones, the dispersion of these estimations cannot be reduced. Similar phenomenon is observed for the bending stiffnesses EI_1 and EI_5 in scenario 2 (Figure 3-42.b). In scenario 3, the load is applied the whole structure and the bending behavior of the structure is more excited than the scenarios 1 and 2. Even so, the curvature of the zones adjacent to the inflection points in the moment diagram for LC3

(Figure 3-42.c) is not well excited. As a result, the dispersion in EI_3, EI_6, EI_9 and EI_{12} is comparatively high. The corresponding COVs for these parameters are 0.080, 0.074, 0.071, 0.088, while the highest and the lowest values of the COVs for the remaining parameters are 0.031 and 0.017. Regarding the scenarios using one loading case, the overall accuracy of the estimations for scenario 3 surpass those for scenarios 1 and 2, whereas the dispersion is lower. Hence, the accuracy and the dispersion of the estimations in scenario 3 are set as the reference for further comparison with the results using multiple loading cases.

When multiple loading cases are used, all parameters are identifiable. This is also manifested by the fact that all the diagonal elements of the inversed FIM are always less than 0.1. Hence, no constraint is applied on any parameter during the optimization. A comparison of the COVs for the estimations of all parameters obtained from scenarios 3-5 is depicted in Figure 3-43. The COVs for EI_3, EI_6 and EI_{12} reduce from 0.080, 0.074, 0.088 in scenario 3 (LC3) to 0.031, 0.052, 0.048 in scenario 4 (LC1+LC2), corresponding to reductions of 61%, 30%, 45%. The COVs of EI_9 in scenarios 3 (0.071) and 4 (0.072) does not change much. Regarding the other parameters, the COVs for EI_1, EI_{13}, EI_{14} decrease drastically. On the contrary, the COVs in EI_5, EI_7, EI_8 and EI_{10} increase from 0.026, 0.017, 0.020, 0.031 to 0.038, 0.040, 0.029, 0.038, respectively.

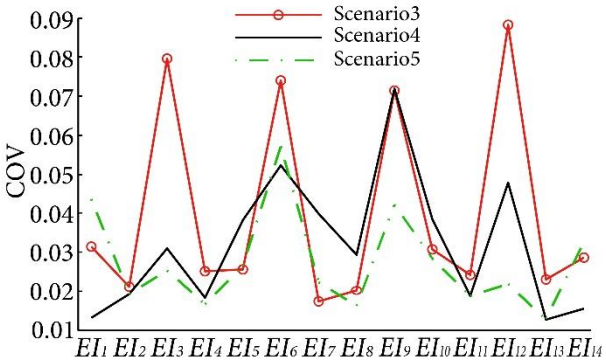

Figure 3-43 comparison of the COVs for the estimations of EI_1-EI_{14}.

In scenario 5, the improvement of the dispersion in the estimations is more significant when compared with scenario 3. The dispersion of all parameters is controlled to an acceptable level. The COVs for the bending stiffnesses associated with null curvature zones, namely EI_3, EI_6, EI_9 and EI_{12} decreased from 0.080, 0.074, 0.071, 0.088 to 0.025, 0.057, 0.042, 0.022, corresponding with reductions of 68%, 23%, 41%, 75%. Despite the increase of COVs in EI_1(38%), EI_7(28%) and EI_{14}(13%), the reductions of the COVs in other parameters are at least 20%.

From the analysis above, it is seen that applying multiple loading cases: (1) the bending stiffnesses associated with null curvature zones in some load cases can be effectively identified by the proposed method; (2) the dispersion in the estimations of bending

stiffnesses in zones where bending behaviors are well excited can be further reduced. (3) The combination of different loading cases has different impact on the accuracy of the estimations.

(2) Effect of the measurement type

In this part, the effect of the number of rotations used in the measurement set is studied. The combination of loading cases 3 and 4 is used here. The total number of measurements is fixed as 21 and the number of rotations varies from 0 to 21, leading to 22 cases. The measurement set for each case is determined by the GA-based OSP. 200 samples for each measurement set are simulated by Equation (3-96). The mean and the COVs of the estimation are summarized in Figure 3-44.

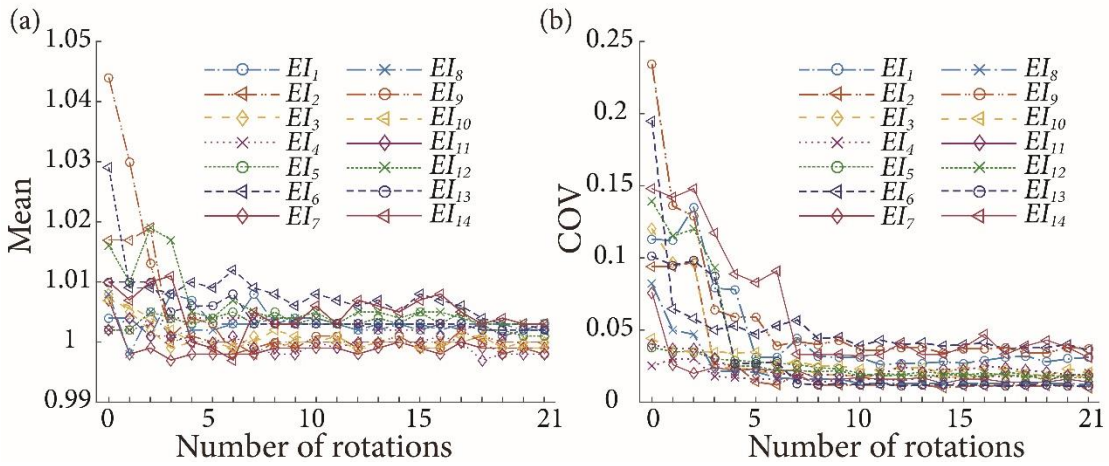

Figure 3-44 The estimations of EI1-EI14 under loading cases 3+4 using different number of rotations : a) Mean b) Coefficient of Variation (COV).

Figure 3-44.a analyzes the effect of the number of rotations on the mean of the estimations of all bending stiffnesses. It is seen that when no rotation is used, overestimation is observed in EI_2(4.4%) and EI_6(2.9%). As the number of rotations starts to increase, the bias in the estimations decreases sharply. The decrease rate is significant initially. When the number of rotations is more than 5, the deviation of the mean of all parameters is within 1%. However, increasing the number of rotations in the measurement set is no longer effective in reducing the bias.

Figure 3-44.b analyzes the effect of the number of rotations on the COVs of the estimations of all bending stiffnesses. When no rotation is used, the COVs for the majority of the bending stiffnesses are very high. Half of these COVs exceed 0.1. As the number of rotations increase, the COVs for all parameters reduces gradually and reach a steady level finally. The reduction is most significant when the number of rotations is less than 4. Take EI_9 for instance, the COV for the estimations is 0.234, 0.136, 0.129, 0.064, 0.059, 0.059 when the number of rotations varies from 0 to 5. When the number of rotations exceeds 7, the reduction of COVs in the estimations by increasing the number of rotations is not significant.

From the analysis above, it is seen that: (1) the measurement type has a great impact on the accuracy of static SSI using multiple loading cases; (2) When no rotation is introduced, non-negligible bias and significant dispersion exist in the estimations of bending stiffnesses; (3) The accuracy and the dispersion of the estimation can be improved by including more rotations.

Example 2: A frame

In a previous study on the identification of a floor beam in a 13-story frame, it was found that the bending stiffnesses of null curvature zones cannot be identified. In this example, those unidentifiable parameters are identified by the SSI by MEMOM using multiple loading cases. Also, the effect of using different number of rotations is studied.

(1) Advantages of using multiple loading cases

Three loading cases are studied here. The magnitude and range of these loading cases are shown in Figure 3-45 and Table 3-11.

Table 3-11 Description of the loading cases of the frame

Loading Case	Range	Magnitude	Type
LC1	Left 3m	20 kN/m	Uniform
LC2	Right 3.8m	20 kN/m	Uniform
LC3	Over the whole span	20 kN/m	Uniform

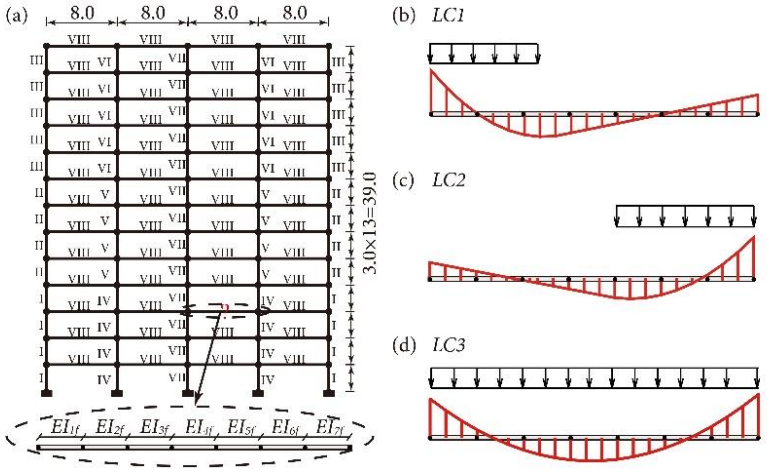

Figure 3-45 (a) Finite element model of the 13-story frame structure with the targeted beam to be identified; (b) loading case 1; (c) loading case 2; (d) loading case 3;

To demonstrate the advantage of using multiple loading cases, four scenarios are

studied.

Scenario 1:Using 34 deflections and 16 rotations under LC1.

Scenario 2: Using 34 deflections and 16 rotations under LC2.

Scenario 3: Using 34 deflections and 16 rotations under LC3.

Scenario 4: Using 17 deflections and 8 rotations for both LC1 and LC2.

The objective is to identify the selected beam depicted in Figure 3-45. During the optimization, the absolute constraints of [0.5, 1.5] are applied on those bending stiffnesses for the null curvature zones. Namely, LC1 (EI_{2f}, EI_{5f}, EI_{6f}), LC2 (EI_{2f}, EI_{3f} EI_{6f}) and LC3 (EI_{2f}, EI_{6f}). When LC1 and LC2 are used jointly, all the diagonal elements of the inversed FIM are lower than 0.1. Hence, all parameters are identifiable and no constraint is applied on them in scenario 4. For scenarios 1-3, the OSP is determined by the GA-based optimization using one loading case. For scenarios 4, the OSP is determined by the GA-based optimization using multiple loading cases. For each OSP configuration of the associated scenario, 200 measurement sets are simulated with an error level of 5%. All the results are summarized in Figure 3-46.

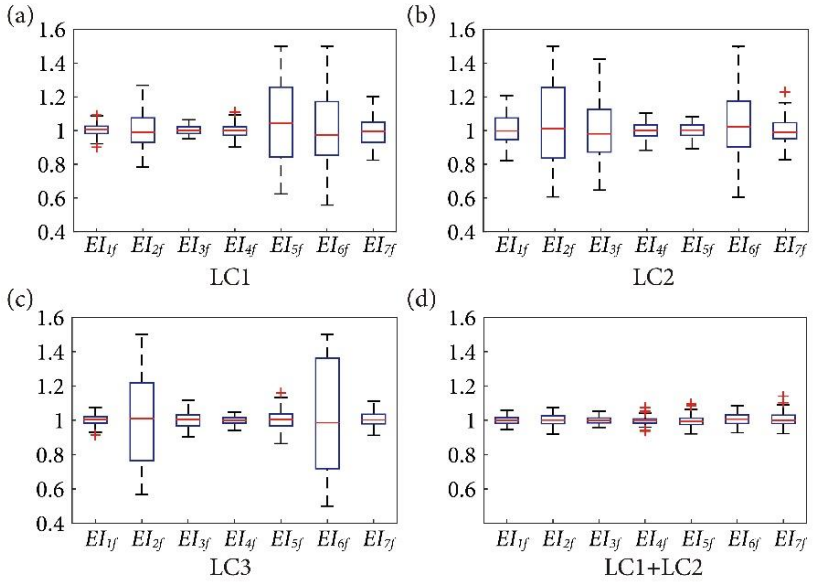

Figure 3-46 Box plots of the estimations of different scenarios:(a) Scenario 1; (b) Scenario 2; (3) Scenario 3; (d) Scenario 4

All the y axes are scaled to [0.4, 1.6] for the sake of an easy comparison between different scenarios. In scenario 1-3 (Figure 3-46.a-c), single loading case is used to obtain the estimations of the bending stiffnesses. The estimations of bending stiffnesses associated with null curvature zones have much larger dispersion (indicated by the length of the box) than other bending stiffnesses. In scenario 4 (Figure 3-46.d), it is seen that the dispersion of all parameters is well controlled when compared with those for scenarios 1-3. In the meanwhile, the dispersion of the estimations of bending

stiffnesses associated with zones of high curvatures is reduced. Regarding the bending stiffnesses EI_{1f}-EI_{7f}, three COVs can be obtained from the estimations in scenarios 1-3. The lowest COVs for EI_{1f}-EI_{7f} in these scenarios are 0.031, 0.098, 0.026, 0.022, 0.042, 0.201, 0.041 while the associated COVs in scenario 4 are 0.024, 0.031, 0.021, 0.023, 0.031, 0.035, 0.039, which means decreases of 22.6%, 68.4%, 19.2%, -4.5%, 26.2%, 82.6%, 4.9%. Despite of the slight increase of COV for EI_{4f}, the overall results are improved.

(2) Effect of the measurement type

Assuming that 25 measurements are used in each loading case, the cases of using 0, 2, 4, 5, 8, 10 rotations are considered. The sensor location for each case is determined by the GA-based OSP and 200 samples are simulated with an error level of 5%. The result is described by Figure 3-47.

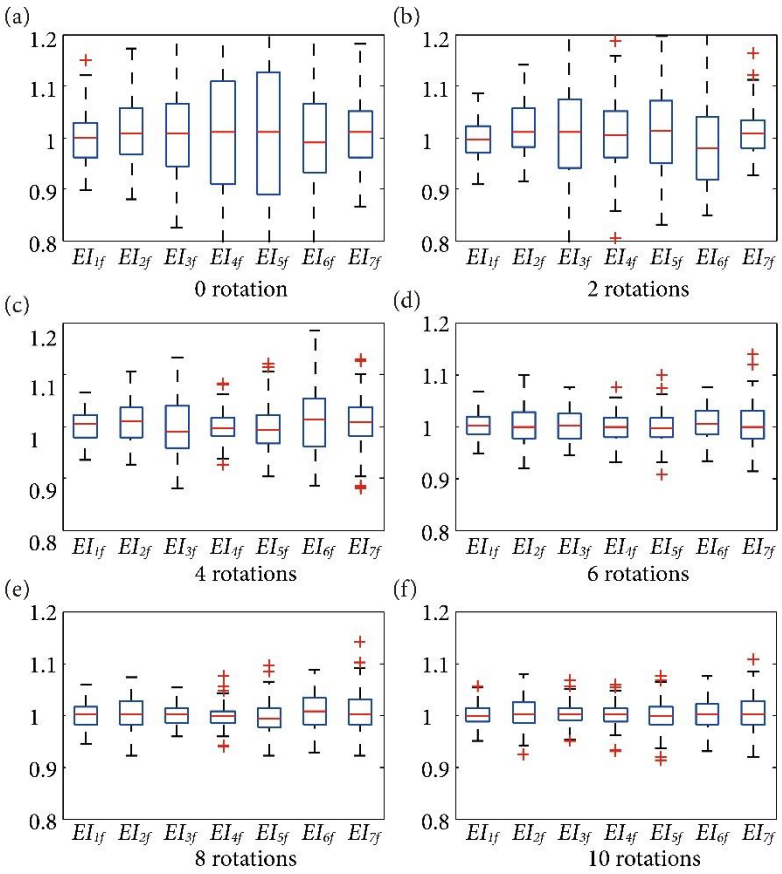

Figure 3-47 Box plot of the estimations of EI_{1f}-EI_{7f} using: (a) 0 rotation; (b) 2 rotations (c) 4 rotations (d) 6 rotations (e) 8 rotations (f) 10 rotations

All the y axes are scaled to [0.8, 1.2]. When only deflections are measured, the upper limit or the lower limit of the box plot for EI_{3f}-EI_{6f} exceeds the range of [0.8, 1.2]. This indicates large dispersions of these estimations. As the number of rotations increases, the dispersions of all parameters reduce gradually. When the number of

rotations is more than 6, the improvement is no longer significant. In the case of using 10 rotations, the bias of the estimations for EI_{1f}-EI_{7f} is always within 0.5%. The associated COVs are 0.020, 0.028, 0.020, 0.020, 0.027, 0.31, 0.034 for the estimations of EI_{1f}-EI_{7f}, which is satisfactory.

The analysis of the effect of measurement type on the frame leads to conclusions similar to those for beam-like structures. In summary: (1) the measurement type has a great impact on the accuracy of static SSI using multiple loading cases; (2) When only deflections are measured, the bias and the dispersion in the estimations are far from acceptable. This can be improved by including rotations in the measurements. (3) The improvement in the bias and the dispersion of estimations is very considerable when rotations are introduced at the beginning. When the number of rotations exceeds a certain level, this improvement becomes no longer significant.

3.6.6 Conclusions

In this paper, the static Structure System Identification (SSI) by Measurement Error-Minimizing Observability Method (MEMOM) under multiple loading cases is presented. For each loading case, the observability equations are obtained first using the OM. Then these equations are concatenated so that the information from multiple loading cases can be addresses by the algorithm simultaneously. The estimations of the parameters are determined by minimizing the square sum of the ratios between the error terms and the measured displacements. The method presented here is an improvement on the SSI by MEMOM under single loading case regarding its ability to identify those parameters in null curvature zones.

In the meanwhile, the OSP problem for the static SSI is formulated as a combinatorial optimization problem with the determinant of the Fisher Information Matrix as the objective function and the sensor location vector as the decision variable. The location of the sensors in each loading case are kept constant to avoid the cumbersome work of the disassembly and the installation of sensors.

To justify the effectiveness of the proposed methods, the numerical examples of a 3-span continuous bridge and a 13-storey frame are investigated using noisy measurements with respect to the loading cases, measurement types. It is seen that: (1) the SSI by MEMOM under multiple loading cases can effectively identify the parameters for regions where structural behaviors may not be sufficiently excited in one loading case. (2) Also, the estimation accuracy and dispersion can be significantly improved in regions where structural behaviors are moderately activated. (3) Measurement type has a great impact on the estimation results. When only deflections are used, the estimations are greatly biased even when multiple loading cases are used. (4) A drastic improvement is observed when rotations are included in the measurements initially. When the number of rotations increases to a certain level, the improvement in the estimations will be no longer noticeable regarding the bias and the dispersion of the estimations.

4 Closure

4.1 Discussion and conclusion

This work presents the study of the Structural System Identification (SSI) using static tests under the framework of Observability Methods (OM).

In the pioneering work of SSI by original OM, a systematic analysis of the effect of measurement errors on the estimation result was lacking. Also, the assumption of linearization of unknowns simplified the process of determining the observability of unknowns. However, this assumption might lead to the omission of some observable unknowns. To this end, different aspects of this topic are addressed to advance the SSI by original OM, which include: (1) the investigation of the effects of measurement errors and simulation errors on the estimations of target parameters using minimum measurement sets (Chapter 3.1); (2) the incorporation of nonlinear constraints to enhance the ability of the original OM to observe unknowns (Chapter 3.2);(3) different strategies to reduce the adverse effect of measurement errors on the estimation accuracy using redundant measurement sets (Chapter 3.3-3.6). Specifically, Chapter 3.3 focuses on imposing compatibility conditions (derived by OM) on the displacements in beam-like structures to remove the incompatible components in the measurements due to errors. Chapter 3.4 investigates the advantages of using rotations as measurements in SSI and proposes a practical and effective way of using rotations for SSI with the aim of obtaining low bias and dispersion in the estimations. Chapter 3.5 formulates the observability equations in a different way so that the measurement errors are separated from the coefficient matrix. The best estimations of parameters are determined as the set of solution that minimizes the discrepancy between the predicted response and the measured one. In the meanwhile, the combinatorial optimization problem arising from the optimal sensor placement problem for static SSI is solved by a genetic-algorithm, with the determinant of Fisher Information Matrix (FIM) being the objective function.

The main conclusions are summarized below:

(1) In the SSI by original OM, the observability equations are obtained by transforming the equilibrium equations. Then, the observability of unknowns is determined by inspecting the structure of the null space of the coefficient matrix of the observability equations. The application of this linear algebraic operation implicitly admits that the unknowns are linear, which might not be true because nonlinear constraints exist among the unknowns. The proposed SSI by Constrained OM (COM) appends the nonlinear constraints among the unknowns to the SSI by original OM via optimization technique. The analysis of numerical examples shows that the SSI by COM achieves a significant improvement by observing parameters that are omitted by the SSI by original OM. The SSI by COM exploits the information in the measurements more effectively than the original method.

(2) When the minimum set is used, the loading cases are of primary importance for the accurate estimation of the target parameters. The estimations of parameters representing the regions near null curvature zones (supports or inflection points of the moment diagram) are much worse than those representing other regions regarding the accuracy and the dispersion of the estimations. The higher the extent of curvature excitation in the zones to be identified, the lower the sensitivity of the parameter estimations to the measurement errors. In order to tackle the adverse effect of null curvature, it is recommended to use sufficient loading cases for SSI. Meanwhile, the numerical simulations with random errors in all measurements and the analytical results show that using rotations for SSI is much better than the case of using deflections in respect of the sensitivity of the parameter estimations to the measurement errors.

(3) Redundant measurement sets are used to improve estimation accuracy when measurement errors exists. However, the result given by the SSI by original OM leads to underestimated and dispersed estimations. To alleviate the adverse effect of measurement errors, the compatibility conditions among all displacements in beam-like structures are derived through OM. By imposing the compatibility conditions in the measurement with optimization techniques, the adverse effect of measurement errors are mitigated and the final parameter estimations are obtained. The numerical analysis shows that when the curvature of the zones increases, the bias and the dispersion of the corresponding parameter estimations will decrease and that the selected loading case should excite the curvature of the region of interest. The dispersion of the parameter estimations varies linearly with the error level. For the curvature-excited region, the parameter estimation accuracy is insensitive to changes in the error level. With respect to the bias and dispersion of parameter estimations, the accuracy of parameters representing zones of null curvature decreases faster with the increase of error levels than the accuracy of parameters representing zones of high curvature.

(4) The theoretical distribution of the target parameters can be acquired by the analytical expressions of these parameters and the inverse distribution theory. Based on the numerical analysis of a beam-like structure and a frame structure, the statistical properties of the distribution of the target parameters using different types of measurements (rotations, deflections) are obtained and compared. The result justifies the advantages of using rotations by comparing the sensitivity of the estimations to measurement errors. Four different strategies to use rotations as measurements are proposed and studied. It is recommended to divide the redundant rotation measurements into multiple minimum sets and obtain the respective estimations from each of these minimum sets. The final estimations are determined as the average of these estimations with the outliers being removed by the box-plot technique.

(5) Using SSI by Measurement Error-Minimizing Observability Method (MEMOM), adopting more measurements or including rotation measurements can improve the estimations result of all parameters. However, the accuracy and the dispersion of

those parameters in null curvatures are still unsatisfactory. Combining multiple loading cases with SSI by MEMOM can accurately identify the parameters of such regions. Meanwhile, the estimations of those parameters that belong to regions where curvatures are excited are also improved.

(6) In the case of using single loading case, the effect of using relative or absolute constraints on the unidentifiable parameters is investigated regarding the unbiasedness and dispersion of the estimations. When the number of rotations is insufficient, the estimations are always biased despite the type of constraints applied on those unidentifiable parameters. When the number of rotations is sufficient, both type of constraints can reduce the dispersion of the estimations; The relative constraints reduces dispersion more effectively than the absolute constraint, but at the cost of slightly higher biases.

(7) In either single or multiple loading cases, the inclusion of rotation measurements can significantly reduce the biases and the dispersion of the parameter estimations. The extent of improvement by including rotations is very significant initially. After the number of rotations increases to a certain level, further increase of rotations will no longer improve the estimation results.

(8) Under single or multiple loading cases, the optimal sensor placement method using Fisher Information Matrix and genetic algorithm can be efficiently adopted to design reliable sensor configurations. This establishes a sound foundation for the subsequent estimations of the target parameters and provides the guideline for non-destructive static test set-up.

4.2 Summary of related work and publications

This work has led to the following published papers:

1. Jun Lei, José Antonio Lozano-Galant, María Nogal, Dong Xu, José Turmo, Analysis of measurement and simulation errors in structural system identification by observability techniques, Structural Control and Health Monitoring,
2. Jun Lei, María Nogal, José Antonio Lozano-Galant, Dong Xu, José Turmo, Constrained observability method in static structural system identification, Structural Control and Health Monitoring
3. Jun Lei, Dong Xu, José Turmo, Static structural system identification for beam-like structures using compatibility conditions, Structural Control and Health Monitoring

And the following under review or under preparation papers:

1. Jun Lei, José Antonio Lozano-Galant, María Nogal, Dong Xu, José Turmo, Robust Static Structural System Identification Using Rotations, Structural Control and Health Monitoring
2. Jun Lei, José Antonio Lozano-Galant, Dong Xu, José Turmo, Structural system identification by Measurement Error-Minimizing Observability Method, Structural

Control and Health Monitoring

3. Jun Lei, José Antonio Lozano-Galant, Dong Xu, José Turmo, Structural system identification by Measurement Error-Minimization Observability Method Using Multiple Loading Cases, Structural Control and Health Monitoring

4.3 Further research

The future research line of this work might be summarized as follows:

(1) Experimental verification

The proposed methods in this work are verified by numerical simulations. The measurement errors are simulated by adding proportional errors that follow normal distributions. However, measurement errors might not be proportional in real life. Meanwhile, modelling errors, such as inaccurate description of boundary conditions, linearization of nonlinear structural behavior, are not incorporated in current methods. To assure the application of the proposed methods, experimental verification is indispensable.

(2) Improving the computational efficiency using substructure technique.

The number of target parameters controls the scale of the SSI problem. As the number of parameters increases, the search space of the optimization or the sampling algorithm increases exponentially, which is directly linked with the computational difficulty. In large structures, it usually contains a large number of parameters. The SSI of such structures could be formidable. Substructure techniques can isolate the interested regions to be identified and thus reduce the number of unknown parameters. For this reason, the incorporation of substructure techniques will be studied in the future.

(3) Incorporate dynamic test information.

Static SSI methods are better at reflecting local damages of structures than dynamic SSI methods. However, it is not as effective as dynamic methods in reflecting the global features of structures. Static and dynamic information from non-destructive tests should be combined regarding the acquisition of both global and local features of structures.

(4) A systematic method to design the loading cases

Sufficient excitation of the structural behavior is one of most important factors for the accurate estimation of corresponding parameters. As shown by the current work, loading case combinations also affect the estimation accuracy and dispersion. However, this work only explores the optimal sensor placement problem for static case. The loading cases are selected in an empirical way. Quantitative metric for evaluating the goodness of single or multiple loading cases is lacking. Further research on the systematic method for designing loading cases is needed.

5 References

Abdo, M. A.-B. (2012). Parametric study of using only static response in structural damage detection. *Engineering Structures*, *34*, 124–131.

Abur, A., & Exposito, A. G. (2004). *Power system state estimation: theory and implementation*. Boca Raton, FL: CRC press.

Agarwal, S., Kachroo, P., & Contreras, S. (2016). A Dynamic Network Modeling-Based Approach for Traffic Observability Problem. *IEEE Transactions on Intelligent Transportation Systems*, *17*(4), 1168–1178.

Alves, V., Cury, A., Roitman, N., Magluta, C., & Cremona, C. (2015). Structural modification assessment using supervised learning methods applied to vibration data. *Engineering Structures*, *99*, 439–448.

American Society of Civil Engineers. (2013). *Structural Identification of Constructed Systems*. (F. N. Çatbaş, T. Kijewski-Correa, & A. E. Aktan, Eds.), *American Society of Civil Engineers*. Reston, VA: American Society of Civil Engineers.

Amezquita-Sanchez, J. P., & Adeli, H. (2015). Synchrosqueezed wavelet transform-fractality model for locating, detecting, and quantifying damage in smart highrise building structures. *Smart Materials and Structures*, *24*(6), 065034.

Amezquita-Sanchez, J. P., & Adeli, H. (2016). Signal Processing Techniques for Vibration-Based Health Monitoring of Smart Structures. *Archives of Computational Methods in Engineering*, *23*(1), 1–15.

Andreaus, U., Baragatti, P., Casini, P., & Iacoviello, D. (2017). Experimental damage evaluation of open and fatigue cracks of multi-cracked beams by using wavelet transform of static response via image analysis. *Structural Control and Health Monitoring*, *24*(4), 1–16.

Astroza, R., Nguyen, L. T., & Nestorović, T. (2016). Finite element model updating using simulated annealing hybridized with unscented Kalman filter. *Computers and Structures*, *177*, 176–191.

Atamturktur, S., Hemez, F. M., & Laman, J. A. (2012). Uncertainty quantification in model verification and validation as applied to large scale historic masonry monuments. *Engineering Structures*, *43*, 221–234.

Au, S. K., Ni, Y. C., Zhang, F. L., & Lam, H. F. (2012). Full-scale dynamic testing and modal identification of a coupled floor slab system. *Engineering Structures*, *37*, 167–178.

Bakhary, N., Hao, H., & Deeks, A. J. (2007). Damage detection using artificial neural network with consideration of uncertainties. *Engineering Structures*, *29*(11), 2806–2815.

Bakhtiari-Nejad, F., Rahai, A., & Esfandiari, A. (2005). A structural damage detection method using static noisy data. *Engineering Structures*, *27*(12 SPEC. ISS.), 1784–1793.

Banan, M. R., Banan, M. R., & Hjelmstad, K. D. (1994a). Parameter Estimation of Structures from Static Response. I. Computational Aspects. *Journal of Structural Engineering*, *120*(11), 3243–3258.

Banan, M. R., Banan, M. R., & Hjelmstad, K. D. (1994b). Parameter Estimation of Structures from Static Response. II: Numerical Simulation Studies. *Journal of Structural Engineering*, *120*(11), 3259–3283.

Bao, C., Hao, H., & Li, Z. (2013). Vibration-based structural health monitoring of offshore pipelines: numerical and experimental study. *Structural Control and Health Monitoring*, *20*(5), 769–788.

Beck, J. L., & Au, S.-K. (2002). Bayesian Updating of Structural Models and Reliability using Markov Chain Monte Carlo Simulation. *Journal of Engineering Mechanics*, *128*(4), 380–391.

Beck, J. L., & Katafygiotis, L. S. (1998). Updating Models and Their Uncertainties. I: Bayesian Statistical Framework. *Journal of Engineering Mechanics*, *124*(4), 455–461.

Beck, J. L., & Yuen, K. (2004). Model Selection Using Response Measurements: Bayesian Probabilistic Approach. *Journal of Engineering Mechanics*, *130. No. 2*(February), 192–203.

Behmanesh, I., & Moaveni, B. (2015). Probabilistic identification of simulated damage on the Dowling Hall footbridge through Bayesian finite element model updating. *Structural Control and Health Monitoring*, *22*(3), 463–483.

Bell, E., Lefebvre, P., & Sanayei, M. (2013). Objective Load Rating of a Steel-Girder Bridge Using Structural Modeling and Health Monitoring. *Journal of Structural Engineering*, (October), 1771–1779.

Bellino, A., Garibaldi, L., Marchesiello, S., & Fasana, A. (2010). Damage detection in beam-like structures by using the PCA-method. In *Proceedings of the 5th European Workshop - Structural Health Monitoring 2010*.

Bertola, N. J., Papadopoulou, M., Vernay, D., & Smith, I. F. C. (2017). Optimal multi-type sensor placement for structural identification by static-load testing. *Sensors (Switzerland)*, *17*(12).

Bighamian, R., & Mirdamadi, H. R. (2013). Input/output system identification of simultaneous mass/stiffness damage assessment using discrete-time pulse responses, differential evolution algorithm, and equivalent virtual damped SDOF. *Structural Control and Health Monitoring*, *20*(4), 576–592.

Boumechra, N. (2017). Damage detection in beam and truss structures by the inverse analysis of the static response due to moving loads. *Structural Control and*

Health Monitoring, *24*(10), 1–10.

Breuer, P., Chmielewski, T., Górski, P., Konopka, E., & Tarczyński, L. (2015). Monitoring horizontal displacements in a vertical profile of a tall industrial chimney using Global Positioning System technology for detecting dynamic characteristics. *Structural Control and Health Monitoring*, *22*(7), 1002–1023.

Brincker, R., & Ventura, C. E. (2015). *Introduction to operational modal analysis*. Chichester, UK: John Wiley & Sons.

Brownjohn, J., Fujino, Y., Inaudi, D., & Wu, Z. (2008). Structural Identification of Constructed Systems: Experimental Considerations. *ASCE Structures Congress*, 1–13.

Caddemi, S., & Greco, A. (2006). The influence of instrumental errors on the static identification of damage parameters for elastic beams. *Computers & Structures*, *84*(26–27), 1696–1708.

Caglayan, B. O., Ozakgul, K., & Tezer, O. (2012). Assessment of a concrete arch bridge using static and dynamic load tests. *Structural Engineering & Mechanics*, *41*(1), 83–94.

Caro, E., Arévalo, I., García-Martos, C., & Conejo, A. J. (2013). Power system observability via optimization. *Electric Power Systems Research*, *104*, 207–215.

Carpentier, P., & Cohen, G. (2007). State estimation and leak detection in water distribution networks. *Civil Engineering Systems*, *8*(4), 247–257.

Castillo, E., Conejo, A. J., Eva Pruneda, R., & Solares, C. (2007). Observability in linear systems of equations and inequalities: Applications. *Computers and Operations Research*, *34*(6 SPEC. ISS.), 1708–1720.

Castillo, E., Conejo, A. J., Menéndez, J. M., & Jiménez, P. (2008). The observability problem in traffic network models. *Computer-Aided Civil and Infrastructure Engineering*, *23*(3), 208–222.

Castillo, E., Conejo, A. J., Pruneda, R. E., & Solares, C. (2005). State estimation observability based on the null space of the measurement jacobian matrix. *IEEE Transactions on Power Systems*, *20*(3), 1656–1658.

Castillo, E., Jimenez, P., Menendez, J. M., & Conejo, A. J. (2008). The Observability Problem in Traffic Models: Algebraic and Topological Methods. *IEEE Transactions on Intelligent Transportation Systems*, *9*(2), 275–287.

Castillo, E., Lozano-Galant, J. A., Nogal, M., & Turmo, J. (2015). New tool to help decision making in civil engineering. *Journal of Civil Engineering and Management*, *21*(6), 689–697.

Castillo, E., Nogal, M., Lozano-Galant, J. A., & Turmo, J. (2016). Solving Some Special Cases of Monomial Ratio Equations Appearing Frequently in Physical and Engineering Problems. *Mathematical Problems in Engineering*, *2016*, 25.

Castillo, E., Nogal, M., Rivas, A., & Sánchez-Cambronero, S. (2013). Observability of traffic networks. Optimal location of counting and scanning devices. *Transportmetrica B: Transport Dynamics*, *1*(1), 68–102.

Catbas, F. N., Gokce, H. B., & Gul, M. (2012). Nonparametric analysis of structural health monitoring data for identification and localization of changes: Concept, lab, and real-life studies. *Structural Health Monitoring: An International Journal*, *11*(5), 613–626.

Chang, M., & Pakzad, S. N. (2014). Optimal Sensor Placement for Modal Identification of Bridge Systems Considering Number of Sensing Nodes. *Journal of Bridge Engineering*, *19*(6), 04014019.

Chang, Y., & Huang, H. (2014). Parametric Identification of Complex Bridge Structure using Substructure Approach. *IABSE Symposium Report*, *102*(5), 3086–3091.

Chen, X. Z., Zhu, H. P., & Chen, C. Y. (2005). Structural damage identification using test static data based on grey system theory. *Journal of Zhejiang University Science*, *6A*(8), 790–796.

Cheung, S. H., & Beck, J. L. (2010). Calculation of Posterior Probabilities for Bayesian Model Class Assessment and Averaging from Posterior Samples Based on Dynamic System Data. *Computer-Aided Civil and Infrastructure Engineering*, *25*(5), 304–321.

Chisari, C., Bedon, C., & Amadio, C. (2015). Dynamic and static identification of base-isolated bridges using Genetic Algorithms. *Engineering Structures*, *102*, 80–92.

Choi, I.-Y., Lee, J. S., Choi, E., & Cho, H.-N. (2004). Development of elastic damage load theorem for damage detection in a statically determinate beam. *Computers & Structures*, *82*(29), 2483–2492.

Deep, K., Singh, K. P., Kansal, M. L., & Mohan, C. (2009). A real coded genetic algorithm for solving integer and mixed integer optimization problems. *Applied Mathematics and Computation*, *212*(2), 505–518.

Díaz, S., González, J., & Mínguez, R. (2016). Observability Analysis in Water Transport Networks: Algebraic Approach. *Journal of Water Resources Planning and Management*, *142*(4), 04015071.

Doebling, S. W. S., Farrar, C. R. C., Prime, M. B. M., & Shevitz, D. W. D. (1996). Damage identification and health monitoring of structural and mechanical systems from changes in their vibration characteristics: a literature review. *Shock & Vibration Digest*, *30*(11), 2043–2049.

Dowling, J., Obrien, E. J., & González, A. (2012). Adaptation of Cross Entropy optimisation to a dynamic Bridge WIM calibration problem. *Engineering Structures*, *44*, 13–22.

Eskew, E. L., & Jang, S. (2017). Remaining stiffness estimation of buildings using incomplete measurements. *Structural Control and Health Monitoring*, p. e1899.

Evan C. Bentz, & Hoult, N. A. (2016). Bridge model updating using distributed sensor data. *ICE Proceedings*, *170*(1), 1–13.

Ewins, D. J. (1984). *Modal testing : theory and practice*. Research Studies Press.

Facchini, L., Betti, M., & Biagini, P. (2014). Neural network based modal identification of structural systems through output-only measurement. *Computers & Structures*, *138*, 183–194.

Farrar, C. R., Baker, W. E., Bell, T. M., Cone, K. M., Darling, T. W., Duffey, T. A., … Migliori, A. (1994). *Dynamic characterization and damage detection in the I-40 bridge over the Rio Grande*. *Puerto Rico Health Sciences Journal* (Vol. 24).

Feng, D., Feng, M. Q., Beskhyroun, S., Wegner, L. D., Sparling, B. F., Feng, D., & Feng, M. Q. (2016). Vision-based multipoint displacement measurement for structural health monitoring. *Structural Control and Health Monitoring*, *23*(5), 876–890.

Feng, D., Sun, H., & Feng, M. Q. (2015). Simultaneous identification of bridge structural parameters and vehicle loads. *Computers & Structures*, *157*(May), 76–88.

Foti, D., Gattulli, V., & Potenza, F. (2014). Output-only identification and model updating by dynamic testing in unfavorable conditions of a seismically damaged building. *Computer-Aided Civil and Infrastructure Engineering*, *29*(9), 659–675.

Garcia-Palencia, A. J., Santini-Bell, E., Sipple, J. D., & Sanayei, M. (2015). Structural model updating of an in-service bridge using dynamic data. *Structural Control and Health Monitoring*, *22*(10), 1265–1281.

Geoffrey, B., & Mark, A. (2011). *Alkali-Aggregate Reaction and Structural Damage to Concrete: Engineering Assessment, Repair and Management*. boca raton: CRC Press.

Ghrib, F., & Li, L. (2017). An adaptive filtering-based solution for the Bayesian modal identification formulation. *Journal of Civil Structural Health Monitoring*, *7*(1), 1–13.

Ghrib, F., Li, L., & Wilbur, P. (2012). Damage Identification of Euler –Bernoulli Beams using static response. *Journal of Engineering Mechanics*, *138*(5), 405–415.

Gill, P. E., Murray, W., & Wright, M. (1982). *Practical optimization*. London: Academic Press.

González, A., Covián, E., Casero, M., & Cooper, J. (2013). Experimental Testing of a Cross-Entropy Algorithm to Detect Damage. *Key Engineering Materials*, *569–*

570, 1170–1177.

Guo, Y. L., Ni, Y. Q., & Chen, S. K. (2017). Optimal sensor placement for damage detection of bridges subject to ship collision. *Structural Control and Health Monitoring*, *24*(9), 1–16.

Ha, D. W., Park, H. S., Choi, S. W., & Kim, Y. (2013). A wireless MEMS-based inclinometer sensor node for structural health monitoring. *Sensors*, *13*(12), 16090–16104.

Hà, N. V., & Golinval, J. C. (2010). Localization and quantification of damage in beam-like structures using sensitivities of principal component analysis results. *Mechanical Systems and Signal Processing*, *24*(6), 1831–1843.

Habtour, E., Cole, D. P., Riddick, J. C., Weiss, V., Robeson, M., Sridharan, R., & Dasgupta, A. (2016, December). Detection of fatigue damage precursor using a nonlinear vibration approach. *Structural Control and Health Monitoring*, pp. 1442–1463.

Hajela, P., & Soeiro, F. J. (1990a). Recent developments in damage detection based on system identification methods. *Structural Optimization*, *2*(1), 1–10.

Hajela, P., & Soeiro, F. J. (1990b). Structural damage detection based on static and modal analysis. *AIAA Journal*, *28*(6), 1110–1115.

He, R. S., & Hwang, S. F. (2006). Damage detection by an adaptive real-parameter simulated annealing genetic algorithm. *Computers and Structures*, *84*(31–32), 2231–2243.

He, X., Yang, X., & Zhao, L. (2014). New Method for High-Speed Railway Bridge Dynamic Deflection Measurement. *Journal of Bridge Engineering*, *19*(7), 05014004.

Heal, K. M., Hansen, M. L., Rickard, K. M., & Incorporation, M. (1998). *Maple V : learning guide* (3rd ed.). Springer,.

Hjelmstad, K. D., & Shin, S. (1997). Damage Detection and Assessment of Structures from Static Response. *Journal of Engineering Mechanics*, *123*(6), 568–576.

Huang, C. S., Hung, S. L., Su, W. C., & Wu, C. L. (2009). Identification of time-variant modal parameters using time-varying autoregressive with exogenous input and low-order polynomial function. *Computer-Aided Civil and Infrastructure Engineering*, *24*(7), 470–491.

Isidori, D., Concettoni, E., Cristalli, C., Soria, L., & Lenci, S. (2016). Proof of concept of the structural health monitoring of framed structures by a novel combined experimental and theoretical approach. *Structural Control and Health Monitoring*, *23*(5), 802–824.

Issa, M. A., & Shahawy, M. A. (1993). Dynamic and static tests of prestressed concrete girder bridges in Florida. *Structural Research Center, MS*, *80*.

Jenkins, C. H., Kjerengtroen, L., & Oestensen, H. (1997). Sensitivity of Parameter Changes in Structural Damage Detection. *Shock and Vibration*, *4*(1), 27–37.

Jeong, M., Choi, J.-H., & Koh, B.-H. (2013). Performance evaluation of modified genetic and swarm-based optimization algorithms in damage identification problem. *Structural Control and Health Monitoring*, *20*(6), 878–889.

Jiang, X., & Adeli, H. (2005). Dynamic wavelet neural network for nonlinear identification of highrise buildings. *Computer-Aided Civil and Infrastructure Engineering*, *20*(5), 316–330.

Jiang, X., & Adeli, H. (2007). Pseudospectra, MUSIC, and dynamic wavelet neural network for damage detection of highrise buildings. *International Journal for Numerical Methods in Engineering*, *71*(5), 606–629.

Jiang, X., Mahadevan, S., & Adeli, H. (2007). Bayesian wavelet packet denoising for structural system identification. *Structural Control and Health Monitoring*, *14*(2), 333–356.

Jin, H., Xia, J., & Wang, Y. (2015). Optimal sensor placement for space modal identification of crane structures based on an improved harmony search algorithm. *Journal of Zhejiang University SCIENCE A*, *16*(6), 464–477.

Jin, S. S., & Jung, H. J. (2016). Sequential surrogate modeling for efficient finite element model updating. *Computers and Structures*, *168*, 30–45.

Johnson, N. L., Kotz, S., & Balakrishnan, N. (1994). *Continuous Univariate Distributions.* (2nd ed., Vol. 1). New Jersey: Wiley.

Kammer, D. C. (1991). Sensor Placement for On-Orbit Modal Identification and Correlation of Large Space Structures. *Journal of Guidance, Control, and Dynamics*, *14(2)*(August), 251–259.

Kao, C. Y., & Loh, C. H. (2013). Monitoring of long-term static deformation data of Fei-Tsui arch dam using artificial neural network-based approaches. *Structural Control and Health Monitoring*, *20*(3), 282–303.

Karabeliov, K., Cuéllar, P., Baeßler, M., & Rücker, W. (2015). System identification of inverse, multimodal and nonlinear problems using evolutionary computing – Application to a pile structure supported on nonlinear springs. *Engineering Structures*, *101*, 609–620.

Khuc, T., & Catbas, F. N. (2017). Completely contactless structural health monitoring of real-life structures using cameras and computer vision. *Structural Control and Health Monitoring*, *24*(1), e1852.

Kim, J.-T., Ryu, Y.-S., Cho, H.-M., & Stubbs, N. (2003). Damage identification in beam-type structures: frequency-based method vs mode-shape-based method. *Engineering Structures*, *25*(1), 57–67.

Kourehli, S. S. (2017). Plate-like structures damage detection based on static response

and static strain energy using gaussian process regression (GPR). *Inverse Problems in Science and Engineering*, *5977*(November), 1–16.

Kroese, D. P., & Chan, J. C. C. (2014). *Matlab Primer* (2015b ed.). Springer New York.

Ku, C. J., Tamura, Y., Yoshida, A., Miyake, K., & Chou, L. S. (2013). Output-only modal parameter identification for force-embedded acceleration data in the presence of harmonic and white noise excitations. *Wind and Structures, An International Journal*, *16*(2), 157–178.

Lakshmi, K., Rao, A. R. M., & Gopalakrishnan, N. (2017). Singular spectrum analysis combined with ARMAX model for structural damage detection. *Structural Control and Health Monitoring*, *24*(9), e1960.

Lee, J.-J., Ho, H.-N., & Lee, J.-H. (2012). A vision-based dynamic rotational angle measurement system for large civil structures. *Sensors*, *12*(6), 7326–36.

Lei, J., Lozano-Galant, J. A., Nogal, M., Xu, D., & Turmo, J. (2017). Analysis of measurement and simulation errors in structural system identification by observability techniques. *Structural Control and Health Monitoring*, *24*(6), 1–21.

Lei, J., Lozano-Galant, J. A., Xu, D., & Turmo, J. (2018). Robust Static Structural System Identification Using Rotations. *Structural Control and Health Monitoring*, (Under Review).

Lei, J., Nogal, M., Lozano-Galant, J. A., Xu, D., & Turmo, J. (2018). Constrained observability method in static structural system identification. *Structural Control and Health Monitoring*, *25*(1), 2040e.

Lei, J., Xu, D., & Turmo, J. (2018). Static structural system identification for beam-like structures using compatibility conditions. *Structural Control and Health Monitoring*, *25*(1), e2062.

Lei, Y., Liu, C., & Liu, L. J. (2014). Identification of multistory shear buildings under unknown earthquake excitation using partial output measurements: numerical and experimental studies. *Structural Control and Health Monitoring*, *21*(5), 774–783.

Li, D.-S., Li, H.-N., & Fritzen, C.-P. (2012). Load dependent sensor placement method: Theory and experimental validation. *Mechanical Systems and Signal Processing*, *31*, 217–227.

Li, R., Mita, A., & Zhou, J. (2013). Symbolization-based differential evolution strategy for identification of structural parameters. *Structural Control and Health Monitoring*, *20*(10), 1255–1270.

Li, S., & WU, Z. (2005). Structural identification using static macro-strain measurements from long-gage fiber optic sensors. *Journal of Applied Mechanics*, *8*, 943–949.

Li, Z., Park, H. S., & Adeli, H. (2017). New method for modal identification of super high-rise building structures using discretized synchrosqueezed wavelet and Hilbert transforms. *Structural Design of Tall and Special Buildings*, *26*(3), e1312.

Liu, P., & Chian, C. (1997). Parametric Identification of Truss Structures USING STATIC STRAINS. *Journal of Structural Engineering*, *123*(July), 927–933.

Liu, T., Yang, B., & Zhang, Q. (2017). Health Monitoring System Developed for Tianjin 117 High-Rise Building. *Journal of Aerospace Engineering*, *30*(2), 1–13.

Liu, X., Escamilla-Ambrosio, P. J., & Lieven, N. A. J. (2009). Extended Kalman filtering for the detection of damage in linear mechanical structures. *Journal of Sound and Vibration*, *325*(4–5), 1023–1046.

Lozano-Galant, J. A., Dong, X., Payá-Zaforteza, I., & Turmo, J. (2013). Direct simulation of the tensioning process of cable-stayed bridges. *Computers & Structures*, *121*, 64–75.

Lozano-Galant, J. A., Nogal, M., Castillo, E., & Turmo, J. (2013). Application of observability techniques to structural system identification. *Computer-Aided Civil and Infrastructure Engineering*, *28*(6), 434–450.

Lozano-Galant, J. A., Nogal, M., Paya-Zaforteza, I., & Turmo, J. (2014). Structural system identification of cable-stayed bridges with observability techniques. *Structure and Infrastructure Engineering*, *10*(11), 1331–1344.

Lozano-Galant, J. A., Nogal, M., Turmo, J., & Castillo, E. (2015). Selection of measurement sets in static structural identification of bridges using observability trees. *Computers and Concrete*, *15*(5), 771–794.

Lozano-Galant, J. A., & Turmo, J. (2014). An algorithm for simulation of concrete cable-stayed bridges built on temporary supports and considering time dependent effects. *Engineering Structures*, *79*, 341–353.

Lü, C., Liu, W., Zhang, Y., & Zhao, H. (2012). Experimental estimating deflection of a simple beam bridge model using grating eddy current sensors. *Sensors (Basel, Switzerland)*, *12*(8), 9987–10000.

Malings, C., & Pozzi, M. (2016). Conditional entropy and value of information metrics for optimal sensing in infrastructure systems. *Structural Safety*, *60*, 77–90.

Marano, G. C., Quaranta, G., & Monti, G. (2011). Modified Genetic Algorithm for the Dynamic Identification of Structural Systems Using Incomplete Measurements. *Computer-Aided Civil and Infrastructure Engineering*, *26*(2), 92–110.

Marefat, M. S., Ghahremani-Gargary, E., & Ataei, S. (2004). Load test of a plain concrete arch railway bridge of 20-m span. *Construction and Building Materials*, *18*(9), 661–667.

Mariani, S., & Ghisi, A. (2007). Unscented Kalman filtering for nonlinear structural dynamics. *Nonlinear Dynamics*, *49*(1–2), 131–150.

Mei, L., Mita, A., & Zhou, J. (2016). An improved substructural damage detection approach of shear structure based on ARMAX model residual. *Structural Control and Health Monitoring*, *23*(2), 218–236.

Monti, G., Quaranta, G., & Marano, G. (2009). Genetic-algorithm-based strategies for dynamic identification of nonlinear systems with noise-corrupted response. *Journal of Computing in Civil …*, *24*(April), 173–188.

Mukhopadhyay, S., Lus, H., & Betti, R. (2015). Structural identification with incomplete instrumentation and global identifiability requirements under base excitation. *Structural Control and Health Monitoring*, *22*(7), 1024–1047.

Mukhopadhyay, S., Luş, H., & Betti, R. (2014). Modal parameter based structural identification using input-output data: Minimal instrumentation and global identifiability issues. *Mechanical Systems and Signal Processing*, *45*(2), 283–301.

Muto, M., & Beck, J. L. (2008). Bayesian Updating and Model Class Selection for Hysteretic Structural Models Using Stochastic Simulation. *Journal of Vibration and Control*, *14*(1–2), 7–34.

Nagar, A. K., & Powell, R. S. (2000). Observability Analysis of Water Distribution Systems Under Parametric and Measurement Uncertainty. In *Building Partnerships* (Vol. 104, pp. 1–10). Reston, VA: American Society of Civil Engineers.

Nguyen, V. H., Schommer, S., Maas, S., & Zürbes, A. (2016). Static load testing with temperature compensation for structural health monitoring of bridges. *Engineering Structures*, *127*, 700–718.

Ni, Y.-C., Lu, X.-L., & Lu, W.-S. (2016). Field dynamic test and Bayesian modal identification of a special structure - the Palms Together Dagoba. *Structural Control and Health Monitoring*, *23*(5), 838–856.

Nocedal, J., & Wright, S. J. (2006). *Numerical optimization*. *Springer series in operations research*. NEW York: Springer Science & Business Media.

Nogal, M., Lozano-Galant, J. A., Turmo, J., & Castillo, E. (2015). Numerical damage identification of structures by observability techniques based on static loading tests. *Structure and Infrastructure Engineering*, *12*(9), 1216–1227.

Okada, R., Nakata, N., SPENCER Jr, B. F., Kasai, K., & Kim, S. B. (2006). Rational polynomial approximation modelling for analysis of structures with VE dampers. *Journal of Earthquake Engineering*, *10*(01), 97–125.

Omenzetter, P., & Butt, F. (2016). Updating of an instrumented building model considering amplitude dependence of dynamic resonant properties extracted from seismic response records. *Structural Control and Health Monitoring*, *23*(4),

598–620.

Ortiz, O., Téllez, J., Burgos, F. J., Patrón, A., Reyes, E., Robles, V., … Ruiz-Sandoval, M. E. (2008). Load capacity assessment of “Antonio Dovali Jaime” bridge using static and dynamic tests. In *Tailor made concrete structures* (p. 85). Taylor & Francis Group London.

Osornio-Rios, R. A., Amezquita-Sanchez, J. P., Romero-Troncoso, R. J., & Garcia-Perez, A. (2012). MUSIC-ANN Analysis for Locating Structural Damages in a Truss-Type Structure by Means of Vibrations, *27*(9), 687–698.

Pan, J., & Wang, R. (2005). Nonlinear Observability in the Structural Dynamic Identification. *Proceedings of SPIE*, *5765*(2003), 1045–1052.

Papadopoulos, L., & Garcia, E. (1998). Structural damage identification - A probabilistic approach. *AIAA Journal*, *36*(11), 2137–2145.

Papadopoulos, L., & Garcia, E. (2001). Probabilistic Finite Element Model Updating Using Random Variable Theory. *AIAA Journal*, *39*(1), 193–195.

Park, H. S., Shin, Y., Choi, S. W., & Kim, Y. (2013). An integrative structural health monitoring system for the local/global responses of a large-scale irregular building under construction. *Sensors*, *13*(7), 9085–9103.

Pruneda, R. E., Solares, C., Conejo, A. J., & Castillo, E. (2010). An efficient algebraic approach to observability analysis in state estimation. *Electric Power Systems Research*, *80*(3), 277–286.

Raich, A. M., & Liszkai, T. R. (2012). Multi-objective optimization of sensor and excitation layouts for frequency response function-based structural damage identification. *Computer-Aided Civil and Infrastructure Engineering*, *27*(2), 95–117.

Robert-Nicoud, Y., Raphael, B., Burdet, O., & Smith, I. F. C. (2005). Model identification of bridges using measurement data. *Computer-Aided Civil and Infrastructure Engineering*, *20*(2), 118–131.

Rucka, M. (2011). Damage detection in beams using wavelet transform on higher vibration modes. *Journal of Theoretical and Applied Mechanics*.

Sahin, M., & Shenoi, R. A. (2003). Quantification and localisation of damage in beam-like structures by using artificial neural networks with experimental validation. *Engineering Structures*, *25*(14), 1785–1802.

Sanayei, M. (1986). *Identification of Structural Element Stiffnesses from Incomplete Static Test Data*. University of California.

Sanayei, M., Arya, B., Santini, E. M., & Wadia-Fascetti, S. (2001). Significance of Modeling Error in Structural Parameter Estimation. *Computer-Aided Civil and Infrastructure Engineering*, *16*(1), 12–27.

Sanayei, M., & Chitra, J. (2002). Sensor placement for parameter estimation of

structures using fisher information matrix. *Applications of Advanced Technologies in Transportation*, (617), 386–393.

Sanayei, M., Dicarlo, C. J., Rohela, P., Miller, E. L., & Kilmer, M. E. (2015). Sensor Placement using Fisher Information Matrix for Robust Finite Element Model Updating. *Life Cycle Reliability and Safety Engineering*, *4*(2), 28–39.

Sanayei, M., Imbaro, G. R., McClain, J. A. S., & Brown, L. C. (1997). Structural Model Updating Using Experimental Static Measurements. *Journal of Structural Engineering*, *123*(6), 792–798.

Sanayei, M., Khaloo, A., Gul, M., & Necati Catbas, F. (2015). Automated finite element model updating of a scale bridge model using measured static and modal test data. *Engineering Structures*, *102*, 66–79.

Sanayei, M., McClain, J. A. S., & Wadia-Fascetti, S. (1999). Parameter Estimation Incorporating Modal Data and Boundary Conditions. *Journal of Structural Engineering*, *125*(9), 1048–1055.

Sanayei, M., McClain, J. A. S., Wadia-Fascetti, S., & Santini, E. M. (1999). Parameter estimation incorporating modal data and boundary conditions. *Journal of Structural Engineering*, *125*, 1048–1055.

Sanayei, M., Onipede, O., Babu, S. R., & Babuj, S. R. (1992). Selection of noisy measurement locations for error reduction in static parameter identification. *AIAA Journal*, *30*(9), 2299–2309.

Sanayei, M., & Saletnik, M. J. (1996a). Parameter estimation of structures from static strain measurements. 1: Formulation. *Journal of Structural Engineering*, *122*(5), 555–562.

Sanayei, M., & Saletnik, M. J. (1996b). Parameter estimation of structures from static strain measurements. Part 2: Error sensitivity analysis. *Journal of Structural Engineering*, *122*(5), 563–572.

Sanayei, M., & Scampoli, S. F. (1991). Structural Element Stiffness Identification from Static Test Data. *Journal of Engineering Mechanics*, *117*(5), 1021–1036.

Santos, J. P., Crémona, C., Calado, L., Silveira, P., & Orcesi, A. D. (2015). On-line unsupervised detection of early damage. *Structural Control and Health Monitoring*, *23*(7), 1047–1069.

Serhat Erdogan, Y., Necati Catbas, F., & Gundes Bakir, P. (2014). Structural identification (St-Id) using finite element models for optimum sensor configuration and uncertainty quantification. *Finite Elements in Analysis and Design*, *81*, 1–13.

Shahsavari, V., Chouinard, L., & Bastien, J. (2017). Wavelet-based analysis of mode shapes for statistical detection and localization of damage in beams using likelihood ratio test. *Engineering Structures*, *132*, 494–507.

Sheena, Z., Unger, A., & Zalmanovich, A. (1982). Theoretical stiffness matrix correction by using static test results. *Israel Journal of Technology*, *20*, 245–253.

Sirca, G. F., & Adeli, H. (2012). System identification in structural engineering. *Scientia Iranica*, *19*(6), 1355–1364.

Su, J. Z., Xia, Y., Chen, L., Zhao, X., Zhang, Q. L., Xu, Y. L., … Chen, A. R. (2013). Long-term structural performance monitoring system for the Shanghai Tower. *Journal of Civil Structural Health Monitoring*, *3*(1), 49–61.

Su, W. C., Huang, C. S., Chen, C. H., Liu, C. Y., Huang, H. C., & Le, Q. T. (2014). Identifying the Modal Parameters of a Structure from Ambient Vibration Data via the Stationary Wavelet Packet. *Computer-Aided Civil and Infrastructure Engineering*, *29*(10), 738–757.

Sun, H., & Betti, R. (2015). A hybrid optimization algorithm with Bayesian inference for probabilistic model updating. *Computer-Aided Civil and Infrastructure Engineering*, *30*(8), 602–619.

Sun, H., & Büyüköztürk, O. (2015). Optimal sensor placement in structural health monitoring using discrete optimization. *Smart Materials and Structures*, *24*(12), 125034.

Sun, H., Feng, D., Liu, Y., & Feng, M. Q. (2015). Statistical Regularization for Identification of Structural Parameters and External Loadings Using State Space Models. *Computer-Aided Civil and Infrastructure Engineering*, *30*(11), 843–858.

Sun, Z., Nagayama, T., & Fujino, Y. (2016). Minimizing noise effect in curvature-based damage detection. *Journal of Civil Structural Health Monitoring*, *6*(2), 255–264.

Sun, Z., Zou, Z., & Zhang, Y. (2017). Utilization of structural health monitoring in long-span bridges: Case studies. *Structural Control and Health Monitoring*, e1979.

Terlaje, A., & Truman, K. (2007). Parameter Identification and Damage Detection Using Structural Optimization and Static Response Data. *Advances in Structural Engineering*, *10*(6), 607–621.

Tomàs, D., Lozano-Galant, J. A., Ramos, G., & Turmo, J. (2018). Structural system identification of thin web bridges by observability techniques considering shear deformation. *Thin-Walled Structures*, *123*(November 2017), 282–293.

Trinh, T. N., & Koh, C. G. (2012). An improved substructural identification strategy for large structural systems. *Structural Control and Health Monitoring*, *19*(8), 686–700.

Udwadia, F. E. (1994). Methodology for Optimum Sensor Locations for Parameter Identification in Dynamic Systems. *Journal of Engineering Mechanics*, *120*(2), 368–390.

Viola, E., & Bocchini, P. (2007). Identification of damaged bars in three-dimensional redundant truss structures by means of genetic algorithms. *Key Engineering Materials*, *348–349*, 229–232.

Viola, E., & Bocchini, P. (2011). Non-destructive parametric system identification and damage detection in truss structures by static tests. *Structure and Infrastructure Engineering*, *9*(November 2014), 1–19.

Walsh, B. J., & González, A. (2009). Assessment of the Condition of a Beam Using a Static Loading Test. *Damage Assessment of Structures Viii*, *413–414*, 269–276.

Walsh, B. J., González, A., & Cantero, D. (2014). Application of the Cross-Entropy Method to Estimate Stiffness Distribution in Plate-Type Structures. In *The Tenth International Conference on Computational Structures Technology, CST2010, Valencia, Spain, 14-17 September, 2010*. Civil-Comp Press. Retrieved from http://www.ctresources.info/ccp/paper.html?id=5758

Wang, C., Huang, C., & Chen, C. (2011). Damage Assessment of Beam By a Quasi-Static Moving Vehicular Load. *Advances in Adaptive Data Analysis*, *3*(4), 417–445.

Wang, L., Yang, Z., & Waters, T. P. (2010). Structural damage detection using cross correlation functions of vibration response. *Journal of Sound and Vibration*, *329*(24), 5070–5086.

Wang, S. (2014). Model updating and parameters estimation incorporating flexible joints and boundary conditions. *Inverse Problems in Science and Engineering*, *22*(5), 727–745.

Wang, X., Hu, N., Fukunaga, H., & Yao, Z. H. (2001). Structural damage identification using static test data and changes in frequencies. *Engineering Structures*, *23*(6), 610–621.

Wang, Z., & Chen, G. (2013). A moving-window least squares fitting method for crack detection and rigidity identification of multispan bridges. *Structural Control and Health Monitoring*, *20*(3), 387–404.

Wolfram, S. (1999). *The MATHEMATICA ® Book* (4th ed.). Cambridge University Press.

Xin, F., Guoqiang, L., & Jing, Z. (2005). State the of art of statistical identification for structural health diagnosis in civil engineering. *Earthquake Engineering and Engineering Vibration*, *25*(2), 105–113.

Yan, G. (2014). A particle filter method for damage location in plate-like structures by using Lamb waves. *Structural Control and Health Monitoring*, *21*(6), 847–867.

Yang, J. N., Pan, S., & Lin, S. (2007). Least-Squares Estimation with Unknown Excitations for Damage Identification of Structures. *Journal of Engineering Mechanics*, *133*(1), 12–21.

Yang, J. N., Pan, S. W., & Lin, S. L. (2007). Least-squares estimation with unknown excitations for damage identification of structures. *Journal of Engineering Mechanics-Asce*, *133*(1), 12–21.

Yang, Q., & Sun, B. (2010). Structural damage localization and quantification using static test data. *Structural Health Monitoring*, *10*(4), 381–389.

Yang, Y., & Yu, X. B. (2016). Image analyses for video-based remote structure vibration monitoring system. *Frontiers of Structural and Civil Engineering*, *10*(1), 12–21.

Yao, R., & Pakzad, S. N. (2012). Autoregressive statistical pattern recognition algorithms for damage detection in civil structures. *Mechanical Systems and Signal Processing*, *31*, 355–368.

Yuen, K.-V., & Kuok, S.-C. (2011). Bayesian Methods for Updating Dynamic Models. *Applied Mechanics Reviews*, *64*(1), 010802.

Yuen, K.-V. V., & Katafygiotis, L. S. (2006). Substructure Identification and Health Monitoring Using Noisy Response Measurements Only. *Computer-Aided Civil and Infrastructure Engineering*, *21*(4), 280–291.

Zhang, F.-L., Ni, Y.-C., & Lam, H.-F. (2017). Bayesian structural model updating using ambient vibration data collected by multiple setups. *Structural Control and Health Monitoring*, *24*(12), e2023.

Zhang, F. L., Xiong, H. B., Shi, W. X., & Ou, X. (2016). Structural health monitoring of Shanghai Tower during different stages using a Bayesian approach. *Structural Control and Health Monitoring*, *23*(11), 1366–1384.

Zhang, M., Beer, M., & Koh, C. (2012). Interval Analysis for System Identification of Linear MDOF Structures in the Presence of Modeling Errors. *Journal of Engineering Mechanics*, *138*(11), 1326–1338.

Zhang, M., & Schmidt, R. (2015). Study on an auto-correlation-function-based damage index: Sensitivity analysis and structural damage detection. *Journal of Sound and Vibration*, *359*, 195–214.

Zhang, W., Sun, L. M., & Sun, S. W. (2017). Bridge-Deflection Estimation through Inclinometer Data Considering Structural Damages. *Journal of Bridge Engineering*, *22*(2), 04016117.

Zong, Z. (2012). A review of structural damage identification methods based on the finite element model validation. *China Civil Engineering Journal*, *45*(8), 121–130.